Two-scale modeling of filled-elastomer mechanics

Two-scale modeling of filled-elastomer mechanics

Two-scale modeling of filled-elastomer mechanics

PROEFSCHRIFT

ter verkrijging van de graad van doctor aan de Technische
Universiteit Eindhoven, op gezag van de rector magnificus
prof.dr.ir. F.P.T. Baaijens, voor een commissie aangewezen door
het College voor Promoties, in het openbaar te verdedigen op
dinsdag 20 september 2016 om 16:00 uur

door

Mykhailo Semkiv

geboren te Ivano-Frankivsk, Oekraine

Dit proefschrift is goedgekeurd door de promotoren en de samenstelling van de promotiecommissie is als volgt:

voorzitter: prof.dr. L.P.H. de Goey
1^e promotor: prof.dr.ir. P.D. Anderson
copromotor(en): dr.sc.nat. M. Hütter
leden: dr. P. Ilg (University of Reading)
prof. dr. D.R. Long (CNRS/Solvay Lyon)
prof. dr. ir. P. Onck (University of Groningen)
prof. dr. T.A. Tervoort (ETH Zurich)
prof. dr. J.J.M. Slot

Contents

Summary

Two-scale modeling of filled-elastomer mechanics

In tire manufacturing, hard nanoparticles are dispersed in an elastomer matrix to improve the mechanical properties of the tire. Due to the filler particles, the resulting nanocomposite shows behavior unknown to the unfilled elastomer, namely the prominent Payne effect (significant decrease of elastic modulus under large-amplitude oscillatory shear deformation), the Mullins effect (after cessation of a strong imposed deformation, the elastic modulus increases again with waiting time), and a significantly increased fracture energy. These phenomena have their origin in the existence of immobilized matrix material around the filler particles, i.e. so-called glassy layers, as supported by experimental (e.g. Nuclear Magnetic Resonance) and numerical (Molecular Dynamics and Monte Carlo simulations) studies. Specifically, at high enough filler volume fraction, the glassy layers of different particles may overlap, resulting in so-called glassy bridges and in turn in the formation of a glassy network that permeates the rubbery matrix, which eventually gives rise to the nanocomposite-specific mechanical behavior. Several modeling approaches in the literature mostly rely on representative volume elements with large numbers of particles, which renders these approaches prohibitively expensive for macroscopic inhomogeneous deformations. To alleviate this problem, the main goal of this thesis is:

"Formulation of an efficient two-scale model that effectively describes the transient nonlinear mechanical behavior of silica-filled elastomers in terms of microstructural processes".

To formulate a dynamic model that accounts for two levels of description, as well as for the mutual coupling between them, an abstract procedure is required. In this thesis, non-equilibrium thermodynamics is used to that end, specifically the General Equation for the Non-Equilibrium Reversible-Irreversible Coupling (GENERIC) framework. This results in a set of evolution equations, which couples macroscopic degrees of freedom (the momentum density, the temperature or entropy, and the deformation gradient) with the evolution of the microstructure. The latter is represented by a representative (neighboring) particle-pair only, since the most essential contribution of the particle-level dynamics to the macroscopic response originates from the interaction of neighboring particles. The main benefits of using the GENERIC framework are the formulation of the effect of macroscopic deformation on the microstructure dynamics (macro $\rightarrow$ micro coupling), as well as the specification of the constitutive relation for the macroscopic stress tensor as affected by the filler-particle arrangement (micro $\rightarrow$ macro coupling).

While the above model for describing the nonlinear viscoelastic material behavior works

well on relatively short time periods, it has however limited validity on long time periods. This is because the matrix material around the filler particles, being in a glassy state, shows physical aging over time, which results in an increasing value of the elastic modulus, i.e., in the Mullins effect. Before accounting for physical aging of the glassy bridges in the two-scale model, the aging of bulk glassy polymers is studied from a non-equilibrium thermodynamics perspective. To that end, the concept of kinetic and configurational subsystems from the literature is employed and extended, that allows for describing the relaxation/equilibration of different structural features on different time-scales. So doing, both physical aging and mechanical rejuvenation are described. As an aside, it is found that in such systems the stress tensor can be of hypo- rather than hyperelastic nature. After studying the physical aging of bulk glassy polymers, the two-scale nanocomposite model is extended in order to account for the physical aging of the glassy bridges.

Finally, the microscale (particle-level) component of the two-scale nanocomposite model is translated from a Fokker-Planck equation into stochastic differential equations, and then implemented into a Brownian Dynamics type simulation scheme. Under imposed large-amplitude oscillatory shear deformation, the nonlinearity of the viscoelastic mechanical behavior is examined numerically. Specifically, it is found that (i) the proposed two-scale model shows the well-known Payne and Mullins effects, and (ii) the representative-pair concept is an adequate representation of the many-particle system at small and moderate deformation amplitudes.

In conclusion, the main achievements of this PhD study can be summarized as follows:

- A highly efficient and thermodynamically sound two-scale model is developed for describing the nonlinear viscoelastic behavior of elastomers filled with hard nanoparticles, leading to the well-known Payne and Mullins effects based on microscopic principles.

- Comparison with many-particle simulations in the literature show that the representative-pair concept developed in this thesis represents an adequate simplification, particularly at small and moderate strain amplitudes.

- The benefit of using the proposed representative-pair model rather than its many-particle counterpart lies in the significant lowering of the computation time by several orders of magnitude. This makes the representative-pair model suitable for RVE-based calculations in macroscopically inhomogeneous FEM-calculations.

Chapter 1

Introduction

1.1 Background and motivation

Composite materials have already been widely used in the past and especially nowadays they become even more popular, due to their better performance as compared to the individual constituents, under specific conditions [1]. Speaking about the composites, which usually consist of a matrix (e.g. clay, fluid, thermoset or elastomer) supplemented by some second constituent, the latter one consists of small filler particles that get ever smaller in size as the technology progress (see Fig. 1.1). In particular elastomers, being reinforced with nano-meter sized silica particles, shows a wide range of interesting mechanical phenomena under different kinds of loading and is used in modern tire manufacturing, where adhesion (grip on the road), internal losses (rolling resistance), and wear resistance are important. While carbon black is the most common filler for tire applications, in recent time, hard silica particles become increasingly more popular. This is due to the better dispersion of silica particles in the elastomer matrix than conventional carbon black fillers, which in turn helps to tailor the mechanical properties and thereby improve tire performance.

Due to the nanometer-sized filler particles, from a mechanical perspective the resulting composite (in the following also called nanocomposite) shows behavior unknown

$$\sim 10^{-1}\text{m} \qquad \sim 10^{-4}\text{m} \qquad \sim 10^{-8}\text{m}$$
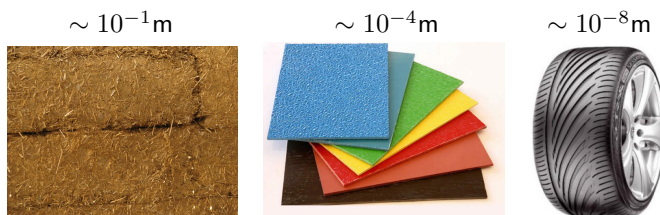
Figure 1.1: Decreasing of a structure length scale: building blocks made of clay and straw; plastic sheets reinforced by glass fibers; car tire, i.e., elastomer filled with nanoparticles; the length scales refer to the size of the fillers (Figures are taken from: http://ecobum.io.ua/s101521/glina, http://besthomeskitchen.com/glass-fibre-reinforced-plastic-wall-house.html, http://adaptivestrategies.com).

(a)   (b)
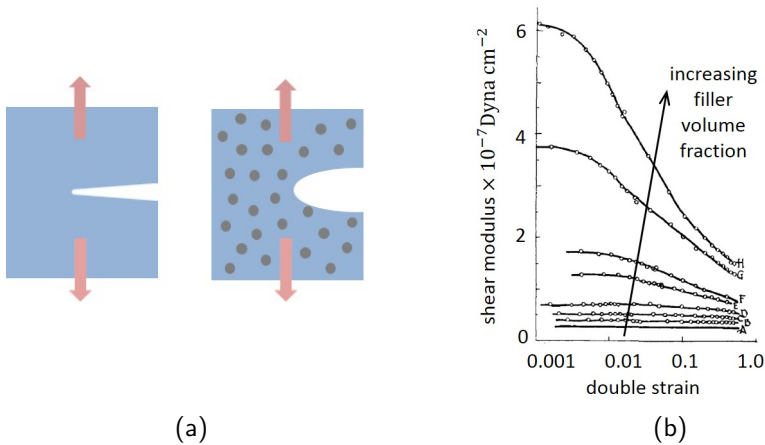
Figure 1.2: (a) Mechanical behavior of unfilled and filled elastomers: Crack propagation in an unfilled and in a filled elastomer; for the latter, the crack tip is more round and significantly more energy is required to propagate the crack. (b) Payne effect: Decrease of storage modulus with increasing deformation amplitude (Fig. 1.2 (b) is adapted from [2]).

to unfilled elastomers. First, a significant dissipative component can be observed in the crack-propagation behavior, in contrast to purely elastic for unfilled elastomers (see Fig. 1.2 (a)). Second, due to particle interaction, the value of effective shear modulus is substantially higher than the shear modulus of pure elastomers. However, under large amplitude oscillatory deformation, the prominent Payne effect takes place (Fig. 1.2 (b)), i.e. a significant decrease of elastic modulus under large-amplitude oscillatory shear deformation with increasing deformation amplitude [2]. In addition, after cessation of a strong imposed deformation, the elastic modulus increases again slowly with waiting time, which is called the Mullins effect [3–6]. These phenomena have their origin in the underline microstructure, i.e. on the level of the nanoparticles.

The discussion above motivate us to formulate an adequate thermodynamic model, that equally accounts for both the macroscopic and the microscopic aspects (see Fig. 1.3) as well as their mutual interaction, in order to mimic the main effects inherent to filled elastomers. The need for considering explicitly the microstructure relates to the notion that the above described phenomena originate from the micro-mechanics on the level of the filler-particles.

1.2 From microscopic thermomechanics to macroscopic behavior

The variety of physical effects, mentioned in the previous section (e.g. nonlinear viscoelastic response, Payne and Mullins effects) can be explained qualitatively by assuming the
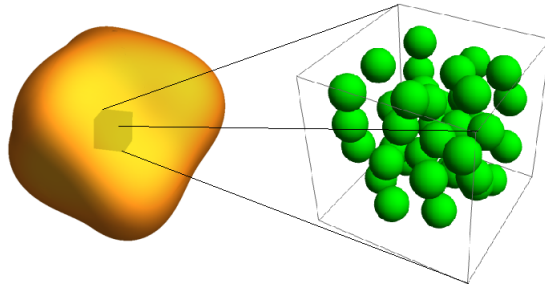
Figure 1.3: Two-scale nature of filled elastomers, accounting for both macroscopic scale (e.g., due to an interest in inhomogeneous deformation) and microscopic scale (filler particle-level to account for particle-particle and particle-matrix interactions).

existence of glassy layers of matrix material around the filler particles[1]. In this assumption, of key importance are the dynamical properties of the matrix material in the vicinity of particle surfaces, as they have been probed experimentally, e.g. by NMR [8]. More recently, model systems have been studied with well-dispersed spherical silica particles with a diameter of about 50 nm and typical distance between the particles of about 20 nm [9,10]. By studying the mechanical properties of the samples as functions of frequency and temperature, it was shown [9, 10] that the dynamical properties are altered as compared to those of the pure elastomer (see Fig. 1.2 (a)). The interpretation proposed is that the presence of (particle-matrix) interfaces, if there is perfect adhesion between the matrix and the filler particle (in reality this is achieved by adding so-called compatibilizing agents; shown in Fig. 1.4 (b)), results in an immobilization of matrix material and thus in an increase in the glass transition temperature T_g of the close to the filler particle surface. This increase of T_g can be described equivalently by a glassy layer around the filler, given by the region in which the local T_g is larger than the actual temperature T. If the glassy layers of different particles do not overlap, the effect on reinforcement is essentially geometrical. The increase in the elastic modulus can be quantitatively explained by an increase in the effective filler volume fraction due to the presence of the glassy layer. Upon lowering the temperature and/or increasing the volume fraction of particles, the glassy layers of adjacent particles overlap, leading to so-called glassy bridges. This happens at temperatures close to $T_\mathrm{g,b} + (10 - 15)\mathsf{K}$ for the samples considered in [9, 10] (where $T_\mathrm{g,b}$ is the glass transition temperature of the elastomer in the bulk), resulting in large reinforcement up to about 100 times. In the case that so-called glassy bridges are formed between adjacent particles, the phenomenology of the resulting particle interaction can be related to the mechanical behavior of bulk glassy polymers [11–13]. Correspondingly, the strength of a glassy bridge depends on both temperature and applied load. In other words, the behavior of bulk polymer glasses is helpful to rationalize typical effects in hard particle-filled elastomer nanocomposites. Because the entire nanocomposite material can be seen as a purely elastic soft matrix supplemented with a hard viscoelastic glassy net-

---

[1]Largely reproduced from the introduction of [7].
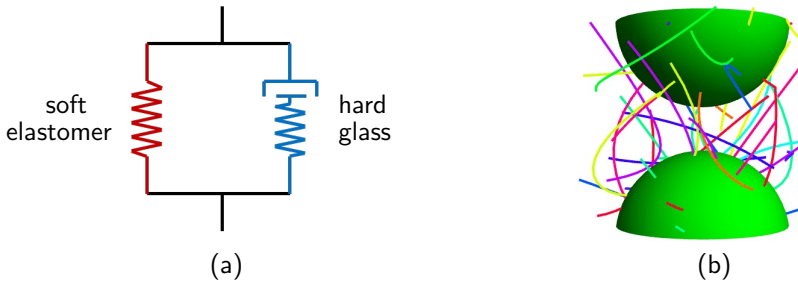
Figure 1.4: (a) Schematic mechanical model of a filled elastomer: Soft elastic elastomer matrix permeated by a hard viscoelastic glassy network. (b) Silica-particles in an elastomer matrix.

work, the viscoelastic (and therefore dissipative) nature of it is evident. Specifically, the yielding of glassy bridges under applied load macroscopically leads to a decrease in the storage modulus, i.e. the Payne effect, shown in Fig. 1.2 (b) [2]. Furthermore, after cessation of a strong deformation, the inter-particle glassy material may age physically, eventually leading to the Mullins effect on the macroscopic scale [3–6].

The mechanical behavior of elastomers filled with hard nanoparticles has been studied extensively and from different perspectives. Among the numerical approaches, one can point out molecular dynamics (MD) and Monte Carlo simulation techniques. For example in [14, 15], MD simulations have been performed of thin films of noncross-linked polymer melts confined between substrates. In both studies, the simulations revealed a decrease in mobility close to the substrate and an increase in the thickness-averaged glass transition temperature upon decreasing the substrate spacing; these results corroborate the existence of glassy layers close to the substrate. On coarser scales, an extensive study of filled (either carbon black or silica particles) elastomers from the microscopic perspective was made in [16–19], where the authors developed a numerical scheme akin to the dissipative particle dynamics (DPD) technique. This concept proved to be key for appropriately simulating [17–19] various nonlinear effects of filled elastomers, e.g., the Payne effect [2] and the Mullins effect [5, 6]. The disadvantage in those works however, is that the numerical approach is expensive in terms of computational time, especially for macroscopically inhomogeneous systems. Furthermore, a multi-level finite element method (MLFEM) simulation for heterogeneous polymeric systems has been employed to study specifically polymeric matrices with either voids or filled with rubber inclusions [20–23].

An analytical approach to describe filled elastomers is given in [24–26], where concepts from fractal geometry were applied. In [24], colloidal carbon black or silica aggregates were considered as fractal objects, since their structures have scale invariance. These authors have established power-law relationships between stress and elongation of filled systems, with an exponent that depends on the fractal dimension. A broad and detailed overview on the filled system is given in [25] and [26], where the viscoelastic properties of filled elastomers were considered. A power law between elastic modulus and filler volume fraction has been established [25], and a constitutive micro-mechanical model of stress softening of filled elastomers was developed, up to large imposed strain [26].

1.3   Scope of the thesis

In this thesis, we aim to develop a highly effective analytical model for describing the mechanics of hard-particle filled elastomers. In particular, in order to explicitly account for microscopic dynamics, a two-scale model is set up, where two levels of description, i.e. macroscopic and microscopic. It is clear that both of these levels must be coupled mutually and concurrently: An applied macroscopically imposed deformation changes the particle positions, leading to interparticle forces, which in turn translates on the macroscopic level into a particle-related contribution to the stress tensor. Since the system is far from equilibrium and of a two-scale nature, certain guidelines must be used and fundamental principles be respected when formulating the model. In this work, nonequilibrium thermodynamics is employed to that end, particularly the General Equation for the Non-Equilibrium Reversible-Irreversible Coupling (GENERIC) [27–29].

In Chapter 2, *"Concurrent two-scale model for the viscoelastic behavior of elastomers filled with hard nanoparticles"*, a two-scale model is formulated in terms of (i) the evolution equations of macroscopic variables (i.e. momentum density, temperature, and total deformation gradient) and a microstructural variable, and (ii) a constitutive relation for the stress tensor. Moreover, this model is analyzed numerically under large amplitude oscillatory deformations, to study the nonlinear elasto-viscoplastic behavior, specifically the Payne effect.

In Chapter 3, *"Modeling aging and mechanical rejuvenation of amorphous solids"*, we have studied and formulated the model of the elasto-viscoplasticity with a focus on the effect of physical aging and mechanical rejuvenation of bulk amorphous material is modeled. This model is based on the concept of two thermal (kinetic and configurational) subsystems, akin to the approaches using an effective (also known as fictive or configurational) temperature, to describe in a compact form the slow glassy dynamics as well as the far-from-equilibrium distribution of states.

In Chapter 4, *"Two-subsystem thermodynamics for the mechanics of aging amorphous solids"*, the model proposed in Chapter 3 is extended to account also for nontrivial coupling of the two thermal subsystems in the reversible dynamics. In order to examine possible choices for that coupling in more detail, the two-subsystem model derived in Chapter 4 is compared in detail with other models in the literature.

In Chapter 5, *"Two-scale model for the Mullins effect in elastomers filled with hard nanoparticles"*, the nanocomposite model derived in Chapter 2 is combined with the bulk aging model in Chapter 3, 4, to be able to model the physical aging of the glassy bridges, which in turn leads to the Mullins effect.

Finally, in Chapter 6, *"Conclusions and discussion"*, the main conclusions are drawn, and recommendations for further research are given.

Chapter 2

Concurrent two-scale model for the viscoelastic behavior of elastomers filled with hard nano-particles

Abstract

A dynamic two-scale model is developed for describing the mechanical behavior of elastomers filled with hard nano-particles. Using nonequilibrium thermodynamics, a closed system of evolution equations is derived, coupling continuum mechanics with a fine-scale description on the level of filler particles. So doing, a constitutive stress-strain relation emerges that is applicable to transient situations. In addition to the number density of filler particles, the particle arrangement is captured by the distribution of the difference vector between two representative interacting particles, which makes this model efficient in comparison to many-particle models. The two-particle model presented here is analyzed numerically in oscillatory deformation, for two purposes. First, the nonlinearity of the model is studied in detail, in terms of the Payne effect, that compares favorably with the literature. And second, the two-particle model is compared with a corresponding many-particle model in the literature.

2.1   Introduction

Composite materials are widely used nowadays, and particularly polymer nanocomposites are studied intensely (see, e.g. [1]). Adequate modeling tools can be helpful to further excel the current developments. For example in tire applications, where adhesion (grip), internal losses (rolling resistance), and wear are important, having a sound rationalization of the behavior of the nanocomposite is essential for further tailoring. While carbon black is the most common filler for tire applications, in recent time, hard silica particles become increasingly popular. This is due to the better dispersion of silica particles than conventional carbon black fillers, which in turn helps to improve tire performance. In this chapter, we address the modeling of the mechanical behavior of elastomers filled with hard nanoparticles. Our main focus is on the effect of the nanoparticles themselves, rather than on the effect of clusters and aggregates. Therefore, silica-filled elastomer nanocomposites (in the sequel simply called "nanocomposite" to emphasize the role of the microstructure) serve as a prototype example for the approach presented here.

   For the description of the mechanical behavior of nanocomposites, adequate modeling is cumbersome. This is due to the intricate phenomena on the level of the nanosized filler particles that lead to the reinforcement effect on the macroscopic engineering scale (see, e.g. [1]). A feature of particular interest in this chapter is the following. While the elastomeric matrix can to a good approximation be described by the theory of elasticity [30–32], filling the elastomer with hard silica-particles adds significant dissipative contributions to the material behavior. Although filled elastomers have been studied for many years, the physical origin of these significant dissipative effects was not understood until recently. Key are the dynamical properties in the vicinity of interfaces, as they have been probed by studies such as NMR in [8]. More recently, model systems have been studied with well-dispersed spherical silica particles with a diameter of about 50 nm and typical distance between the particles of about 20 nm [9, 10]. By studying the mechanical properties of the samples as functions of frequency and temperature, it was shown [9, 10] that the dynamical properties are modified as compared to those of the pure elastomer. The interpretation proposed is that the presence of interfaces, if the interaction between the polymer and the substrate is sufficiently strong, results in an immobilization and thus in an increase of the glass transition temperature T_{g} of the polymer matrix close to the interface. This increase of T_{g} can be described equivalently by a glassy layer around the filler, given by the region in which T_{g} is larger than the actual temperature T. If the glassy layers of different particles do not overlap, the effect on reinforcement (defined as the ratio between the modulus of the filled sample and that of the unfilled sample) is essentially geometrical: the increase of the elastic modulus can be quantitatively explained by an increase of the effective filler volume fraction due to the presence of the glassy layer. Upon lowering the temperature, the thickness of the glassy layer increases to the point that the glassy layers overlap, leading to so-called "glassy bridges". This happens at temperatures close to $T_{\mathrm{g,b}} + (10 - 15)\mathrm{K}$ in the considered samples (where $T_{\mathrm{g,b}}$ is the glass transition temperature of the elastomer in the bulk), resulting in very high reinforcement up to about 100, depending on the filler volume fraction. In the case that so-called "glassy bridges" are formed between adjacent particles, the phenomenology of the resulting particle interaction can be described similar to that of bulk glassy polymers [11–13]. Correspondingly, the strength of a glassy bridge depends on both tem-

perature and applied load. In other words, the behavior of bulk polymer glasses is helpful to rationalize typical effects in nanocomposites. Particularly, the yielding of glassy bridges under applied load macroscopically leads to decreasing the elastic modulus G', i.e., the Payne effect [2]. Furthermore, inter-particle glassy material may also age physically after cessation of large-amplitude oscillatory deformation, leading to the Mullins effect [5, 6].

Many efforts have been made to investigate the properties and mechanical behavior of silica-filled nanocomposites. Among the numerical approaches, both Molecular Dynamics (MD) and Monte Carlo (MC) simulation techniques have been performed on the smallest scales. For example in [14, 15], MD simulations have been performed of thin films of noncross-linked polymer melts confined between substrates. In both studies, the simulations revealed a decrease of mobility close to the substrate and an increase of the thickness-averaged glass transition temperature upon decreasing the substrate spacing; these results corroborate the existence of glassy layers close to the substrate. In [33], the properties of a polystyrene matrix filled with nanoparticles were investigated by coarse-grained MC sampling, and a substantial segmental ordering close to the particle surface was found. On coarser scales, the very broad study of filled (either carbon black or silica particles) elastomers from the microscopic perspective was made in [16–19], where the authors developed a numerical scheme akin to Dissipative Particle Dynamics (DPD) technique. The dynamics of the filler particles has been studied, taking into account soft spring forces, representative of the rubbery matrix, and temporary hard spring forces, representative of the transient network of glassy bridges. The essential idea in their approach is that each glassy bridge has got a finite lifetime that depends on the local glass transition temperature, which in turn is affected by the particle distance and the local load (i.e. the life-time is changing in the course of time). This concept proved to be key for appropriately simulating [17–19] various non-linear effects of filled elastomers, e.g. the Payne effect [2] and the Mullins effect [5, 6]. On the other hand, fully macroscopic numerical approaches, based on providing a Multi-Level Finite Element Method (MLFEM) simulation for heterogeneous polymeric systems, have been employed to study specifically polymeric matrices with either voids or filled with rubber inclusions [20–23]. There, a homogenization method has been proposed to account for the large deformation of viscoelastic media, considering both microscopic and macroscopic levels, and implemented to MLFEM afterwards.

An analytical approach to describe filled systems is given in [24–26], where concepts from fractal geometry were applied. In [24], colloidal carbon black or silica aggregates were considered as fractal objects, since their structures have scale invariance. These authors have established power-law relationships between stress and elongation of filled systems, with an exponent that depends on the fractal dimension. A broad and detailed overview on the filled system is given in [25] and [26], where the viscoelastic properties of filled elastomers were considered. A power-law between elastic modulus and filler volume fraction has been established [25], and a constitutive micro-mechanical model of stress softening of filled elastomers was developed, up to large imposed strain [26].

In this chapter, our main goal is to develop a two-scale model that describes the mechanics of silica-filled elastomers. Particularly, we strive to explicitly account for the mutual coupling of the macroscopic engineering scale with the underlying filler-particle scale. Since transient effects are hallmarks of filled elastomer mechanics, our approach should establish the coupling of both levels also in transient situations. Finally, the ap-

proach should be applicable to studying macroscopically inhomogeneous deformation, in order to enable studies of wear and tear experiments. This last criterion in combination with the requirement for dynamics asks for alternatives to the approaches mentioned in the previous paragraphs. The work of Long et al. [17–19] discussed above shows the significance of the local glass transition temperature and dynamics that depend on the local structure and load, and this complexity helps to understand why until recently no mechanical (visco-plastic) model were able to satisfactorily explain and reproduce mechanical properties of these systems, and in particular their dissipative properties. However, since their model considers a many-particle system to obtain the effective constitutive behavior (at each macroscopic material point), it is computationally rather demanding. Therefore, the aim of this chapter is to propose a drastically simplified description of the model developed in [17–19] and to combine that with macroscopic elasto-viscoplasticity (e.g., see [32, 34]) in a thermodynamically consistent manner.

Before we start, let us give a word about notation used in this chapter. Throughout the entire chapter, Latin indices i, j, k, ... denote components of a set of dynamical variables, while Greek indices α, β, γ, ... are used for the Cartesian components of vectors and tensors. Einstein's summation convention is used for indices that occur twice. Furthermore, subscripts α and (α, β) imply contraction with any vector A_α and any matrix $A_{\alpha\beta}$ multiplied from the left, respectively, while subscripts γ and (γ, ε) imply contraction with the vector A_γ and matrix $A_{\gamma\varepsilon}$ multiplied from the right, respectively. Finally, it is pointed out that boundary terms are neglected throughout the entire chapter. This simplification is justified because this chapter is concerned with modeling bulk material properties, in terms of local evolution equations. It is therefore implicitly assumed that the boundary does not affect the dynamics in the inside over a distance (apart from the fact that any bulk dynamics must obviously be supplemented with proper boundary conditions when a numerical solution is sought-after). For completeness, it is mentioned that systems that interact with the environment have been studied earlier, e.g., [35, 36].

The chapter is organized as follows. In Sec. 2.2, the GENERIC formalism of nonequilibrium thermodynamics is introduced, and in Sec. 2.3 this technique is applied to filled systems in order to formulate evolution equations and constitutive relations. The general two-scale model is summarized in Sec. 2.3.5. In Sec. 2.4, specific exemplary choices are made to concretize the model and translate it into stochastic differential equations that are amendable to numerical simulations. In Sec. 2.5, the model is solved numerically for a concrete example-nanocomposite under oscillatory deformation. Specifically, the two-particle model presented here is compared with the corresponding many-particle model developed in [17–19], and the Payne effect is examined. The chapter closes with a conclusion, Sec. 2.6.

2.2   Methods: nonequilibrium thermodynamics

As a guideline for developing the two-scale model, nonequilibrium thermodynamics is used. In the end of nineties, the framework called General Equation for the Non-Equilibrium Reversible-Irreversible Coupling formalism (GENERIC) has been developed, which is used to describe closed nonequilibrium systems [27–29]. This method has two important advantages over other nonequilibrium thermodynamics techniques. First, it is useful for

setting up multi-scale models. And second, GENERIC provides a concrete procedure for connecting different levels of description, i.e., for coarse graining.

The first step in setting-up the GENERIC for a concrete system is to specify a set of dynamic variables, denoted by $\boldsymbol{\mathcal{X}}$. The time evolution equation is then written as

$$\partial_t \boldsymbol{\mathcal{X}} = \partial_t \boldsymbol{\mathcal{X}}|_{\text{rev}} + \partial_t \boldsymbol{\mathcal{X}}|_{\text{irr}} \,, \tag{2.1}$$

with

$$\partial_t \boldsymbol{\mathcal{X}}|_{\text{rev}} = \boldsymbol{\mathcal{L}}[\boldsymbol{\mathcal{X}}] \odot \frac{\delta E[\boldsymbol{\mathcal{X}}]}{\delta \boldsymbol{\mathcal{X}}} \,, \qquad \partial_t \boldsymbol{\mathcal{X}}|_{\text{irr}} = \boldsymbol{\mathcal{M}}[\boldsymbol{\mathcal{X}}] \odot \frac{\delta S[\boldsymbol{\mathcal{X}}]}{\delta \boldsymbol{\mathcal{X}}} \,. \tag{2.2}$$

The derivatives of the energy E and entropy S, that both are functionals of the dynamical variables $\boldsymbol{\mathcal{X}}$, drive the reversible $\partial_t \boldsymbol{\mathcal{X}}|_{\text{rev}}$ and irreversible $\partial_t \boldsymbol{\mathcal{X}}|_{\text{irr}}$ dynamics, respectively, through the Poisson operator $\boldsymbol{\mathcal{L}}$ and the friction matrix $\boldsymbol{\mathcal{M}}$, which in general also depend on $\boldsymbol{\mathcal{X}}$. The symbol $\odot$ means not only summations over discrete indices but may also include integration over continuous variables; this issue will be discussed in the next section when applying the GENERIC. The operator $\delta/\delta \boldsymbol{\mathcal{X}}$ represents functional rather than partial derivatives.

The Poisson operator is equivalent to a Poisson bracket $\{\,,\,\}$, and the friction matrix is associated with a dissipative bracket $[\,,\,]$,

$$\{A, B\} = \frac{\delta A}{\delta \boldsymbol{\mathcal{X}}} \odot \boldsymbol{\mathcal{L}} \odot \frac{\delta B}{\delta \boldsymbol{\mathcal{X}}} \,, \qquad [A, B] = \frac{\delta A}{\delta \boldsymbol{\mathcal{X}}} \odot \boldsymbol{\mathcal{M}} \odot \frac{\delta B}{\delta \boldsymbol{\mathcal{X}}} \,, \tag{2.3}$$

for two arbitrary functionals A and B. The Poisson operator and the friction matrix must satisfy a number of conditions. First, there are the degeneracy conditions. Namely, the functional derivative of the entropy lies in the null space of the Poisson operator $\boldsymbol{\mathcal{L}}$, and the functional derivative of the energy lies in the null space of the dissipative matrix $\boldsymbol{\mathcal{M}}$,

$$\boldsymbol{\mathcal{L}} \odot \frac{\delta S}{\delta \boldsymbol{\mathcal{X}}} = 0 \quad \Leftrightarrow \quad \{A, S\} = 0 \,, \quad \forall A \,, \tag{2.4a}$$

$$\boldsymbol{\mathcal{M}} \odot \frac{\delta E}{\delta \boldsymbol{\mathcal{X}}} = 0 \quad \Leftrightarrow \quad [A, E] = 0 \,, \quad \forall A \,. \tag{2.4b}$$

As a second set of conditions, $\boldsymbol{\mathcal{L}}$ must be anti-symmetric, whereas $\boldsymbol{\mathcal{M}}$ is positive semi-definite and Onsager-Casimir symmetric

$$\boldsymbol{\mathcal{L}} = -\boldsymbol{\mathcal{L}}^* \quad \Leftrightarrow \quad \{A, B\} = -\{B, A\} \,, \qquad \forall A, B, \tag{2.5a}$$

$$\boldsymbol{\mathcal{M}} = \boldsymbol{\mathcal{M}}^* \quad \Leftrightarrow \quad [A, B] = [B, A] \,, \qquad \forall A, B, \tag{2.5b}$$

$$\boldsymbol{\mathcal{M}} \geq 0 \quad \Leftrightarrow \quad [A, A] \geq 0, \qquad \forall A, \tag{2.5c}$$

where the sign $*$ denotes the adjoint operator. The final condition is that the Poisson operator must satisfy the Jacobi identity (see pp. 14–16 in [29]),

$$\{A, \{B, C\}\} + \{B, \{C, A\}\} + \{C, \{A, B\}\} = 0 \,, \tag{2.6}$$

In (2.5b), only Onsager-symmetry (usual symmetry) is mentioned for simplicity. In Sec. 2.3.4, Casimir-symmetric (antisymmetric) contributions will be discussed.

for all functionals A, B and C of the variable $\mathcal{X}$. It is pointed out that, rigorously speaking, the conditions (2.4)–(2.6) on the operators $\mathcal{L}$ and $\mathcal{M}$ must be checked in terms of the corresponding brackets, $\{\ ,\ \}$ and $[\ ,\ ]$, respectively. In the model formulation in Sec. 2.3 and in Sec. 5.2, these brackets are integrals, and the verification of the conditions (2.4)–(2.6) involves integrations by parts. As explained in Sec. 2.1, due to our interest in bulk material behavior, one may neglect the boundary terms that arise as a result of the integrations by parts.

Using the above conditions, one can show that the reversible dynamics $\partial_t\mathcal{X}|_{\mathrm{rev}}$ possesses the Hamiltonian structure, while the irreversible dynamics $\partial_t\mathcal{X}|_{\mathrm{irr}}$ is a generalization of the Ginzburg-Landau equation. Furthermore, the above stringent conditions (2.4)–(2.6) imply the desired energy conservation and nonnegative entropy production,

$$\dot{E} = 0\ , \qquad \dot{S} \geq 0\,. \tag{2.7}$$

For more details about the GENERIC framework, the reader is referred to [29].

The time evolution equation (2.1) for $\mathcal{X}$ contains a reversible contribution, $\partial_t\mathcal{X}|_{\mathrm{rev}}$, and an irreversible part, $\partial_t\mathcal{X}|_{\mathrm{irr}}$. Usually, reversibility means invariance upon time reversal, $t \mapsto -t$. However, in this study, it is rather a split between contributions related to affine deformation, that will be captured by $\mathcal{L}\odot(\delta E/\delta\mathcal{X})$, and others, that will be captured by $\mathcal{M}\odot(\delta S/\delta\mathcal{X})$. We will come back to the difference between the time-reversibility-split and the affine-nonaffine-split in Sec. 2.3.4.

2.3 Modeling the viscoelastic behavior of silica-filled elastomers

2.3.1 Choice of variables

The envisioned two-scale model should carry the following features. First, the model should account for macroscopic continuum mechanics in order to allow for the description of macroscopically inhomogeneous deformations. Second, the effects of the nanofillers are to be included in such a way that the understanding of the nanofiller-dynamics developed in [17–19] (e.g., the relevance of glassy bridges) can be incorporated, i.e., new dynamic "microscale" variables must be included. And third, the model should properly couple the two levels, not only in stationary but also in transient situations.

While the mechanical behavior of the nanocomposite as a whole is viscoelastic, as evidenced by experimental data for the storage and loss moduli, we choose in this study to distinguish between the matrix and the filler particle contributions. In terms of variables, separate descriptors are used to quantify the state of the elastomer matrix and that of the network of particles connected by glassy bridges, respectively. The elastomer matrix is considered as purely elastic with a low modulus, while the stiff network has viscoelastic, i.e., rate-dependent, behavior with a high elastic modulus and relaxation processes due to the transient nature of the glassy bridges.

It has been shown [32, 34] that macroscopic finite-strain nonisothermal elasticity and visco-plasticity can in principle be formulated within the GENERIC framework. Here, we make use of these earlier efforts to design a properly adjusted model for describing silica-filled nanocomposites. To describe the macroscopic finite-deformation elasticity of
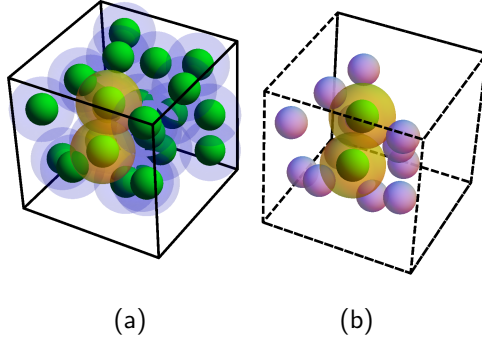
Figure 2.1: (a) System of many particles (green) with glassy layers around them (grey), and a representative particle-pair highlighted in yellow. (b) In the representative particle-pair model, only two particles are considered explicitly (green with yellow layer), while the other surrounding particles are taken into account only implicitly (see text for details).
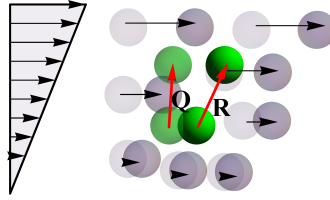
Figure 2.2: Representative particle-pair under applied shear deformation. Imposed deformation moves the particle configuration from an initial state (light green and gray) to another state (green and dark gray).

the elastomer matrix in an Eulerian setting, we choose the momentum density $\boldsymbol{m}(\boldsymbol{r})$, the absolute temperature $T(\boldsymbol{r})$, and the total deformation gradient $\boldsymbol{F}(\boldsymbol{r})$. The vector $\boldsymbol{r}$ is a macroscopic position vector. The velocity field can be obtained from the momentum density as $\boldsymbol{v} = \boldsymbol{m}/\rho$, where mass density, ρ, can be derived from the deformation gradient, namely

$$\rho = \rho_0/\det\boldsymbol{F}\,, \tag{2.8}$$

where ρ_0 denotes the mass density in the undeformed state.

In addition to the variables described above, another variable must be incorporated on the level of the filler particles to account for the effect of glassy bridges adequately. For that, we take inspiration from the many-particle model developed in [17–19], in which several force contributions are included between filler particles, e.g., a force contribution to the glassy bridges (see left box in Fig. 2.1). However, for reasons discussed in the Introduction, we are here looking for a drastic simplification of that model. Particularly, rather than studying a collection of many particles, we consider a representative particle-pair only (see right box in Fig. 2.1), since the mechanics of the glassy-bridge network

roots in these nearest-neighbor interactions.

The representative particle pair is characterized as follows. The current separation vector between the two particles shall be denoted by $\boldsymbol{R}$. For the further arguments in this paragraph, we concentrate on the glassy-bridge network, neglecting other effects of the matrix material. If deformation is imposed on the entire nanocomposite, the glassy-bridge network will deform, and with it also the representative pair. If the imposed deformation is so rapid that the glassy bridges can not relax (i.e., yield), then we expect that the network will return to its original state upon rapid unloading, due to the interactions between all particles. However, considering only a single representative pair, this restoring mechanism will not occur automatically. To nevertheless allow for the restoring toward the unloaded state to occur, we include another vector $\boldsymbol{Q}$, which describes the particle separation vector in the unloaded state. Therefore, upon rapid loading and unloading, the 'reference' $\boldsymbol{Q}$ will stay constant, while the actual state $\boldsymbol{R}$ departs from $\boldsymbol{Q}$ upon loading and is pulled toward $\boldsymbol{Q}$ upon unloading. If, however, the loading happens at a rate on which the glassy bridges can yield, unloading will not lead to the original state. We will capture this by setting-up $\boldsymbol{Q}$-dynamics that is of pure relaxational form toward $\boldsymbol{R}$. So, for example in a step-strain experiment, $\boldsymbol{R}$ immediately attains the new actual conformation, while $\boldsymbol{Q}$ slowly relaxes toward $\boldsymbol{R}$ by re-shaping the glassy network. This implies that (i) the force experienced in the deformed state will decrease with time (since $\boldsymbol{Q}$ relaxes toward $\boldsymbol{R}$), and (ii) upon sudden unloading during this relaxation process the actual $\boldsymbol{R}$ does not relax to its original state, but rather to the new, relaxed state $\boldsymbol{Q}$.

The use of the particle-based vectors $\boldsymbol{R}$ and $\boldsymbol{Q}$ is akin to, in the continuum setting, the multiplicative decomposition of the total deformation gradient $\boldsymbol{F}$ into elastic $\boldsymbol{F}^{\mathrm{e}}$ and plastic $\boldsymbol{F}^{\mathrm{p}}$ parts, respectively, $\boldsymbol{F} = \boldsymbol{F}^{\mathrm{e}} \cdot \boldsymbol{F}^{\mathrm{p}}$ [37]. To illustrate this analogy, let us denote the particle separation vector in the undeformed state by $\boldsymbol{Q}_0$. We then can say $\boldsymbol{R} = \boldsymbol{F} \cdot \boldsymbol{Q}_0$ and $\boldsymbol{Q} = \boldsymbol{F}^{\mathrm{p}} \cdot \boldsymbol{Q}_0$, which leads to the following intuitive relations. First, the dynamics of the unloaded state $\boldsymbol{Q}$ is related to the dynamics of the plastic deformation gradient $\boldsymbol{F}^{\mathrm{p}}$, which is of purely irreversible origin. And second, the difference $\boldsymbol{R} - \boldsymbol{Q}$ is related to the elastic deformation gradient, namely $\boldsymbol{R} - \boldsymbol{Q} = (\boldsymbol{F}^{\mathrm{e}} - \boldsymbol{1}) \cdot \boldsymbol{F}^{\mathrm{p}} \cdot \boldsymbol{Q}_0$. Since, in the absence of strain hardening and related effects, $\boldsymbol{F}^{\mathrm{e}} - \boldsymbol{1}$ is known to be the origin of elastic stresses, so is $\boldsymbol{R} - \boldsymbol{Q}$ the origin of the structural restoring force. This implies that the force for the particle-separation vector depends on $\boldsymbol{R}$ and $\boldsymbol{Q}$ only through the difference $\boldsymbol{R} - \boldsymbol{Q}$. It must be noted that the strength of that particle-level restoring force depends on the connectivity in the entire glassy-bridge network. However, since we consider only a representative particle-pair, such connectivity information is not available explicitly, but can enter in the representative-pair idea only through an appropriate choice of the force strength. This aspect of the model is discussed in detail in Sec. 2.4.1 and in A.4.

For practical purposes, it is easier to consider the statistical distribution function p of the vectors $\boldsymbol{R}$ and $\boldsymbol{Q}$ as dynamic variable rather than the vectors themselves, $p(\boldsymbol{r}, \boldsymbol{R}, \boldsymbol{Q})$, which depends on the macroscopic position $\boldsymbol{r}$. To be more precise, p is the product of the (normalized to unity) probability distribution function of $\boldsymbol{R}$ and $\boldsymbol{Q}$, denoted by $\tilde{p}$, and the number density of particle pairs, n,

$$p(\boldsymbol{r}, \boldsymbol{R}, \boldsymbol{Q}) = n(\boldsymbol{r})\,\tilde{p}(\boldsymbol{r}, \boldsymbol{R}, \boldsymbol{Q}) \ , \tag{2.9}$$

Note that the primary meaning of $\boldsymbol{R}$ is to represent the actual particle separation vector, which may also imply nonaffine deformations. The relation $\boldsymbol{R} = \boldsymbol{F} \cdot \boldsymbol{Q}_0$ is used here only for illustrative purposes. This issue is further discussed in Sec. 2.3.4.2.

where n, using the normalization of $\tilde{p}$, is given by

$$n(\boldsymbol{r}) = \int_{\mathcal{Q}^2} p\left(\boldsymbol{r}, \boldsymbol{R}, \boldsymbol{Q}\right) \mathrm{d}^3 \boldsymbol{R}\, \mathrm{d}^3 \boldsymbol{Q}\,. \tag{2.10}$$

The integral is performed over the set $\mathcal{Q}^2$, that is a Cartesian product of two subsets of Euclidean space, i.e. $\mathcal{Q}^2 \subset \mathbb{R}^3 \times \mathbb{R}^3$. It should be noted that $\tilde{p}(\ldots, \boldsymbol{R}, \ldots)$ is closely related to the pair-correlation function and hence in principle can be measured experimentally, since it is the Fourier-transform of the structure factor. However, in contrast to the pair-correlation function, we are here rather looking at the first peak only, since we are interested in representative pairs with glassy bridges, i.e. nearest-neighbor arrangements.

While the use of the distribution function $\tilde{p}$ seems in close analogy to usual practice in polymer kinetic theory [38, 39], it should be emphasized that the concept of a variable to quantify the unloaded state, $\boldsymbol{Q}$, is quite different. In polymer kinetic theory, an entire polymer chain can be represented by a single end-to-end vector. This end-to-end vector of the polymer chain, $\boldsymbol{R}$, is not only affected by the imposed deformation, but it also enters into an entropic spring force, $\mathbf{f}_S(\boldsymbol{R})$. For purely statistical reasons, i.e. maximization of the configurational entropy, that force drives the polymer toward the spherically symmetric coil-conformation, which is achieved for $\mathbf{f}_S(\boldsymbol{R}) = \boldsymbol{0}$ at $\boldsymbol{R} = \boldsymbol{0}$. Therefore, in these systems there is no need for an additional variable to denote the unloaded state. The situation is quite different for the case of nanocomposites discussed in this chapter. The current position separation vector $\boldsymbol{R}$ of the representative pair reacts immediately to imposed deformation, however, this vector does not carry enough information for the elastic restoring to take place upon unloading. For a representative pair in the nanocomposite, the force balance is achieved not by $\boldsymbol{R}$ going to zero, but rather by $\boldsymbol{R}$ approaching the previous unloaded state, $\boldsymbol{Q}$.

In summary, according to GENERIC, in a Eulerian setting, the set of independent state variables is

$$\boldsymbol{\mathcal{X}} = (\boldsymbol{m}(\boldsymbol{r}),\, T(\boldsymbol{r}),\, \boldsymbol{F}(\boldsymbol{r}),\, p(\boldsymbol{r}, \boldsymbol{R}, \boldsymbol{Q}))\,, \tag{2.11}$$

where $\boldsymbol{r} \in \Omega$, $\left(\Omega \subset \mathbb{R}^3\right)$, and $\boldsymbol{R}, \boldsymbol{Q} \in \mathcal{Q}$, $\left(\mathcal{Q} \subset \mathbb{R}^3\right)$. For later convenience, we introduce the variable $\boldsymbol{\xi}$,

$$\boldsymbol{\xi} = \{\boldsymbol{R}, \boldsymbol{Q}\}\,, \tag{2.12}$$

called internal configuration.

2.3.2   Generating functionals: energy and entropy

For the specification of the total energy E and entropy S, we refrain from making explicit choices since this is (i) not required at this point, and (ii) would disguise the structure of the equations. Let us consider the system occupy an area $\mathcal{B}$ $\left(\boldsymbol{r} \in \Omega,\, \boldsymbol{\xi} \in \mathcal{Q}^2\right)$. It is reasonable to only make the following ansatz for the energy and entropy,

$$E[\boldsymbol{\mathcal{X}}] = \int_{\Omega} \frac{\boldsymbol{m}^2}{2\rho}\, \mathrm{d}^3 \boldsymbol{r} + U[T, \boldsymbol{F}, p]\,, \tag{2.13a}$$

$$S[\boldsymbol{\mathcal{X}}] = S[T, \boldsymbol{F}, p]\,, \tag{2.13b}$$

with internal energy functional $U[T, \boldsymbol{F}, p]$ and entropy functional $S[T, \boldsymbol{F}, p]$. In other words, we have only explicitly split off the kinetic contribution, while leaving the remaining contributions as general as possible.

The functional derivatives of the energy and entropy with respect to the dynamical variable $\boldsymbol{\mathcal{X}}$ are given by

$$\frac{\delta E}{\delta \boldsymbol{\mathcal{X}}} = \begin{pmatrix} \boldsymbol{v} \\ \dfrac{\delta U}{\delta T} \\ \dfrac{\delta U}{\delta \boldsymbol{F}} - \dfrac{\boldsymbol{v}^2}{2}\, \rho_{,\boldsymbol{F}} \\ \dfrac{\delta U}{\delta p} \end{pmatrix}, \qquad \frac{\delta S}{\delta \boldsymbol{\mathcal{X}}} = \begin{pmatrix} \boldsymbol{0} \\ \dfrac{\delta S}{\delta T} \\ \dfrac{\delta S}{\delta \boldsymbol{F}} \\ \dfrac{\delta S}{\delta p} \end{pmatrix}, \tag{2.14}$$

with $\boldsymbol{v} = \boldsymbol{m}/\rho$ for the velocity, $\rho_{,\boldsymbol{F}} = -\rho\, \boldsymbol{F}^{-\top}$, and $\boldsymbol{F}^{-\top}$ the transpose of $\boldsymbol{F}^{-1}$. For the partial derivatives, we use the notation $f_{,\boldsymbol{F}} \equiv \partial f / \partial \boldsymbol{F}$. The functionals U and S will be concretized in Sec. 2.4.

2.3.3   Reversible dynamics: Poisson operator $\mathcal{L}$

The reversible part of the $\boldsymbol{\mathcal{X}}$-evolution equation is presented by the equation $(2.2)_1$. For specification of the Poisson operator, we note that in continuum mechanics the term reversible deformation is synonymous with affine deformation, which is the basics of finite-deformation elasticity theory [31, 32, 40]. In an Eulerian setting, each evolution equation must contain convective terms, i.e., a contribution proportional to the velocity field $\boldsymbol{v}$. Since the $\boldsymbol{m}$-derivative of energy,

$$\delta E / \delta \boldsymbol{m} = \boldsymbol{v}\,, \tag{2.15}$$

is the macroscopic velocity field and $\boldsymbol{m}$ is the first variable in the set (2.11), one may use the first column of the Poisson operator to represent exactly those convective terms. In addition to the macroscopic convective terms, the momentum balance equation must contain the divergence of the stress tensor, and therefore the first row (i.e., the transpose of the first column) of the Poisson operator should reproduce that contribution. On the particle level, reversible dynamics for the structural variable, $p(\boldsymbol{r}, \boldsymbol{\xi})$, occurs due to the dynamics of $\boldsymbol{R}$, which we assume to be deformed affinely with a macroscopic flow field $\boldsymbol{v}$. To study this in detail, let us consider two particles, given by their position vectors $\boldsymbol{R}_1$, $\boldsymbol{R}_2$ respectively. If both particle positions are following the flow field $\boldsymbol{v}$, and if we assume that the particles are rather close to each other compared to the characteristic length-scale for $\boldsymbol{v}$-variations, one finds for the evolution of the connector vector $\boldsymbol{R} = \boldsymbol{R}_1 - \boldsymbol{R}_2$

$$\dot{R}_\gamma = \left[\nabla^r_\mu v_\gamma \right] R_\mu\,. \tag{2.16}$$

This result is completely analogous to the dumbbell model in complex fluids and it is already formulated within the GENERIC framework (see pp. 134-136 in [29]). We note that the variable $\boldsymbol{Q}$ is irrelevant at this point, since it has relaxational dynamics only.

Since the considered particle pair must be representative, it must follow the macroscopic imposed deformation. A mismatch between the imposed deformation and the deformation of the representative particle pair would imply that the particle network gets detached from the elastomer matrix.

To concretize the above arguments in terms of specific forms for the elements of $\mathcal{L}$, one can make use of earlier results for finite-strain elasticity [32], together with the dumbbell model in complex fluids [29], formulated both within the GENERIC framework. So doing, the Poisson operator assumes the form

$$
\boldsymbol{\mathcal{L}}[\boldsymbol{\mathcal{X}}] = \begin{pmatrix}
\mathcal{L}^{(mm)}(\boldsymbol{r}) & \mathcal{L}^{(mT)}(\boldsymbol{r}) & \mathcal{L}^{(mF)}(\boldsymbol{r}) & \mathcal{L}^{(mp)}(\boldsymbol{r}, \boldsymbol{\xi}') \\
\mathcal{L}^{(Tm)}(\boldsymbol{r}) & 0 & 0 & 0 \\
\mathcal{L}^{(Fm)}(\boldsymbol{r}) & 0 & 0 & 0 \\
\mathcal{L}^{(pm)}(\boldsymbol{r}, \boldsymbol{\xi}) & 0 & 0 & 0
\end{pmatrix}.
\tag{2.17}
$$

The elements $\mathcal{L}^{(mm)}(\boldsymbol{r})$, $\mathcal{L}^{(Fm)}(\boldsymbol{r})$, and $\mathcal{L}^{(pm)}(\boldsymbol{r}, \boldsymbol{\xi})$ are a direct consequence of the (known) kinematics of affine deformation [29,32]. The elements $\mathcal{L}^{(mF)}(\boldsymbol{r})$ and $\mathcal{L}^{(mp)}(\boldsymbol{r}, \boldsymbol{\xi}')$ follow due to the anti-symmetry property (2.5a) of the Poisson operator. $\mathcal{L}^{(mT)}(\boldsymbol{r})$ can then be obtained from the degeneracy condition (2.4a), and again using the anti-symmetry property (2.5a) leads to $\mathcal{L}^{(Tm)}(\boldsymbol{r})$. All elements being determined (see A.1 for the explicit expressions), the Jacobi-identity (2.6) can be verified by a lengthy, but straight-forward calculation. For further details on the calculation of the elements of $\mathcal{L}$, the reader is referred to A.1.

The construction of the Poisson operator is thus complete. Calculating $\boldsymbol{\mathcal{L}} \odot (\delta E / \delta \boldsymbol{r})$ with the explicit forms (A.2, A.3, A.7, A.8) for the Poisson operator, and (2.14) for the energy derivatives, one obtains the following reversible contributions to the evolution equations,

$$
\partial_t m_\alpha|_{\mathsf{rev}} = -\nabla_\gamma^r (m_\alpha v_\gamma) + \nabla_\gamma^r \hat{\sigma}_{\alpha\gamma} ,
\tag{2.18a}
$$

$$
\partial_t T|_{\mathsf{rev}} = -v_\gamma (\nabla_\gamma^r T) + \left(\frac{\delta U}{\delta T} \right)^{-1} \hat{\sigma}_{\gamma\varepsilon}^S (\nabla_\varepsilon^r v_\gamma) ,
\tag{2.18b}
$$

$$
\partial_t F_{\alpha\beta}|_{\mathsf{rev}} = -v_\mu (\nabla_\mu^r F_{\alpha\beta}) + F_{\mu\beta} (\nabla_\mu^r v_\alpha) ,
\tag{2.18c}
$$

$$
\partial_t p|_{\mathsf{rev}} = -\nabla_\gamma^r (v_\gamma p) - \nabla_\gamma^R ((\nabla_\mu^r v_\gamma) R_\mu p) ,
\tag{2.18d}
$$

where $\hat{\sigma}_{\alpha\gamma}$ and $\hat{\sigma}_{\alpha\gamma}^S$ are given by the following relations

$$
\hat{\sigma}_{\alpha\gamma} = \left(a - \int_{\mathcal{Q}^2} p \frac{\delta A}{\delta p} \mathrm{d}^6 \boldsymbol{\xi} \right) \delta_{\alpha\gamma} + \frac{\delta A}{\delta F_{\alpha\mu}} F_{\gamma\mu} + \int_{\mathcal{Q}^2} p R_\gamma \left(\nabla_\alpha^R \frac{\delta A}{\delta p} \right) \mathrm{d}^6 \boldsymbol{\xi} ,
\tag{2.19a}
$$

$$
\hat{\sigma}_{\alpha\gamma}^S = -\Theta \left[\left(s - \int_{\mathcal{Q}^2} p \frac{\delta S}{\delta p} \mathrm{d}^6 \boldsymbol{\xi} \right) \delta_{\alpha\gamma} + \frac{\delta S}{\delta F_{\alpha\mu}} F_{\gamma\mu} + \int_{\mathcal{Q}^2} p R_\gamma \left(\nabla_\alpha^R \frac{\delta S}{\delta p} \right) \mathrm{d}^6 \boldsymbol{\xi} \right] .
\tag{2.19b}
$$

It should be noted that $\hat{\sigma}_{\alpha\gamma}$ and $\hat{\sigma}_{\alpha\gamma}^S$ have a form closely related to the stress tensor and its entropic part, respectively. However, the complete form for the stress tensor expression might be calculated only after including the irreversible parts of evolution equations as well (particularly, see Sec. 2.3.4.2). In the relations above, and in the sequel, the abbreviations

$$
\frac{\delta A}{\delta F_{\gamma\varepsilon}} \equiv \frac{\delta U}{\delta F_{\gamma\varepsilon}} - \Theta \frac{\delta S}{\delta F_{\gamma\varepsilon}} ,
\tag{2.20a}
$$

$$
\frac{\delta A}{\delta p} \equiv \frac{\delta U}{\delta p} - \Theta \frac{\delta S}{\delta p} ,
\tag{2.20b}
$$

$$
a \equiv u - \Theta s,
\tag{2.20c}
$$

are used, with

$$\Theta \equiv \frac{\delta U}{\delta T} \left(\frac{\delta S}{\delta T} \right)^{-1}. \tag{2.21}$$

Note that Θ has the dimension of temperature, and if E and S derive from a Helmholtz free energy, then $\Theta = T$.

2.3.4   Irreversible dynamics: friction matrix $\mathcal{M}$

In this section, the irreversible contribution to the evolution equations, namely the equation $(2.2)_2$, is constructed. This is the place where one implements the viscoelastic glassy-bridge dynamics, which will be discussed in Sec. 2.3.4.1. However, there is an additional irreversible contribution. It has to do with the fact that instead of a many-particle system we only consider a representative particle-pair, which brings about non-affine deformation effects, as will be analyzed in Sec. 2.3.4.2. It is noted that all the conditions for the friction matrix discussed in Sec. 2.2 are linear in $\mathcal{M}$. Therefore, if one writes the friction matrix as a sum of two contributions,

$$\mathcal{M} = \bar{\mathcal{M}} + \tilde{\mathcal{M}}, \tag{2.22}$$

and if both contributions satisfy all GENERIC conditions independently, then also the sum $\mathcal{M}$ satisfies all conditions. In the following, $\bar{\mathcal{M}}$ stands for the glassy-bridge dynamics, i.e. the relaxation of Q toward R, and $\tilde{\mathcal{M}}$ represents nonaffine deformation of R. It will turn out that $\bar{\mathcal{M}}$ is symmetric and positive semi-definite, while $\tilde{\mathcal{M}}$ is antisymmetric.

Heat conduction is not described in this work, since its GENERIC-formulation has already been given in [29] and several other papers.

2.3.4.1   Dissipative matrix $\bar{\mathcal{M}}$

By analyzing many examples of dissipative dynamics in the literature, a split of the dissipative matrix $\bar{\mathcal{M}}$ in the following way has been proposed [41],

$$\bar{\mathcal{M}} = \mathcal{C} \odot \mathcal{D} \odot \mathcal{C}^*, \tag{2.23}$$

which is essential to establish a link [29] to linear irreversible thermodynamics [42]. In that factorization, the matrix $\mathcal{D}$ contains all dynamic material information (e.g relaxation times, viscosity, thermal conductivity), while the operator $\mathcal{C}$ represents the so-called mechanical part. It has been noted that

$$\mathcal{C}^* \odot \frac{\delta E}{\delta \boldsymbol{\mathcal{X}}} = \boldsymbol{0} \tag{2.24}$$

is a useful condition to construct $\mathcal{C}^*$, and hence $\mathcal{C}$. Not only is the degeneracy condition $\bar{\mathcal{M}} \odot \delta E/\delta \boldsymbol{\mathcal{X}} = \boldsymbol{0}$ automatically satisfied, but also it has been found that the thermodynamic driving forces $\mathcal{F}$ for the dissipative processes can be written in the form

$$\mathcal{F} = \mathcal{C}^* \odot \frac{\delta S}{\delta \boldsymbol{\mathcal{X}}}. \tag{2.25}$$

The corresponding thermodynamic fluxes $\boldsymbol{\mathcal{J}}$ are then given by

$$\boldsymbol{\mathcal{J}} = \boldsymbol{\mathcal{D}} \odot \boldsymbol{\mathcal{F}} = \boldsymbol{\mathcal{D}} \odot \boldsymbol{\mathcal{C}}^* \odot \frac{\delta S}{\delta \boldsymbol{\mathcal{X}}} \,. \tag{2.26}$$

In other words, $\boldsymbol{\mathcal{C}}^*$ translates the entropy gradient into the thermodynamic driving forces (2.25), while $\boldsymbol{\mathcal{C}}$ determines how the thermodynamic fluxes $\boldsymbol{\mathcal{J}}$ enters the evolution equations,

$$\partial_t \boldsymbol{\mathcal{X}}|_{\mathrm{irr}} = \boldsymbol{\mathcal{C}} \cdot \boldsymbol{\mathcal{J}} \,. \tag{2.27}$$

By requiring

$$\boldsymbol{\mathcal{D}} = \boldsymbol{\mathcal{D}}^* \,, \tag{2.28a}$$

$$\boldsymbol{\mathcal{D}} \geq \boldsymbol{0}, \tag{2.28b}$$

the symmetry and positive semi-definitness of the matrix $\bar{\boldsymbol{\mathcal{M}}}$ are guaranteed.

It has been explained in Sec. 2.3 that the glassy bridges yield under applied load, and thus rate-dependent effects come into play. As discussed, this is to be described by a relaxation process of $\boldsymbol{Q}$ toward $\boldsymbol{R}$. Since this $\boldsymbol{Q}$-dynamics occurs in three dimensions, $\boldsymbol{\mathcal{D}}$ will be a 3×3-matrix. In view of (2.27), $\boldsymbol{\mathcal{C}}$ therefore maps a 3-vector $\boldsymbol{\mathcal{J}}$ onto the irreversible contributions $\partial_t \boldsymbol{\mathcal{X}}|_{\mathrm{irr}}$. While the detailed derivation of $\boldsymbol{\mathcal{C}}$ is described in A.2, the main steps are summarized here. The $\boldsymbol{Q}$-relaxation leads to no contributions to the evolution equations of the momentum density $\boldsymbol{m}$ and the total deformation gradient $\boldsymbol{F}$, which implies that some rows in $\boldsymbol{\mathcal{C}}$ vanish. For the other elements, the p- and T-related rows, one proceeds as follows. Due to the conservation of probability in $\boldsymbol{\xi}$-space and the number density of representative particle-pairs, the evolution equation of the variable p is that of a density of a conserved quantity, and therefore

$$\partial_t p|_{\mathrm{relax}} = -\nabla_\gamma^Q \mathcal{J}_\gamma \,, \tag{2.29}$$

for the relaxation dynamics of the glassy bridge captured in $\mathcal{J}_\gamma$. The form (2.29) can be used to determine the p-component of $\boldsymbol{\mathcal{C}}$, $\boldsymbol{\mathcal{C}}^{(p)}$, and due to the symmetry condition (2.5b) follows $\boldsymbol{\mathcal{C}}^{*(p)}$. That latter result combined with the degeneracy condition (2.4b) results in $\boldsymbol{\mathcal{C}}^{*(T)}$, and again with (2.5b) one obtains $\boldsymbol{\mathcal{C}}^{(T)}$. Collecting all contributions and using (2.25)-(2.27), one finds in addition to the p-dynamics (2.29) the evolution equation for the temperature,

$$\partial_t T|_{\mathrm{relax}} = -\left(\frac{\delta U}{\delta T}\right)^{-1} \int_{\mathcal{Q}^2} \left(\nabla_\gamma^Q \frac{\delta U}{\delta p}\right) \mathcal{J}_\gamma \, \mathrm{d}^6 \boldsymbol{\xi} \,, \tag{2.30}$$

with the current related to the driving force according to (2.26) with a yet unspecified matrix $\boldsymbol{\mathcal{D}}$. For the driving force (2.25) for $\boldsymbol{Q}$-relaxation, one obtains

$$\mathcal{F}_\alpha = -\frac{1}{\Theta} \left(\nabla_\alpha^Q \frac{\delta A}{\delta p}\right) \,, \tag{2.31}$$

which in turn enters the constitutive relation for the flux, (2.26),

$$\mathcal{J}_\gamma = \int_{\mathcal{Q}^2} \mathcal{D}_{\gamma\mu} \, \mathcal{F}'_\mu \mathrm{d}^6 \boldsymbol{\xi}' , \tag{2.32}$$

with a yet unspecified 3×3-diffusion matrix that depends on both $\boldsymbol{\xi}$ and $\boldsymbol{\xi}'$.

2.3.4.2   Antisymmetric contribution $\tilde{\mathcal{M}}$

It has been discussed in Sec. 2.3 that the force to restore the structure to the unloaded state must depend on the difference $\boldsymbol{R} - \boldsymbol{Q}$. If this force was derived from a potential, Φ, it means that the potential will depend on $|\boldsymbol{R} - \boldsymbol{Q}|$. The ramifications for the dynamics discussed up to this point are the following. In the momentum balance (2.18a), the quantity $\hat{\boldsymbol{\sigma}}$ plays the role of the stress tensor. In the last contribution to $\hat{\boldsymbol{\sigma}}$ in (2.19a), $\delta A/\delta p$ is to be identified with the restoring potential Φ (see also Sec. 2.4). If the latter depends on $\boldsymbol{R}$ and $\boldsymbol{Q}$ only through $|\boldsymbol{R} - \boldsymbol{Q}|$, this implies that $\nabla^R \Phi$ is parallel to $\boldsymbol{R} - \boldsymbol{Q}$, and hence $\hat{\boldsymbol{\sigma}}$ is in general not symmetric. This is problematic since the related torques result in an unwanted rotation of the system.

   While in a many-particle system (e.g., [17, 18]) torques may arise locally in small clusters of particles, they may cancel out when summing up the contributions of all interacting particles. However, in the approach presented in this work, we are actually considering a single representative-pair, therefore no such cancellation of non-symmetric contributions is possible. Since for silica-filled elastomers there is no reason for expecting a non-symmetric stress tensor, the cancellation of torques needs to be included explicitly in the model. The Poisson operator is representative of affine deformation; see Appendix B in [29]. However, as shown in Sec. 2.3.3, implementing affine deformation automatically results in a non-symmetric stress tensor, due to the rigid connection between the dynamics (2.16, 2.18d) and the expression for $\hat{\boldsymbol{\sigma}}$. As a result, any modification of the model to arrive at a symmetric stress tensor must be implemented through the irreversible dynamics in (2.1). However, since this contribution to the dynamics is related to the kinematics and thus must not be dissipative, we look for an antisymmetric contribution $\tilde{\mathcal{M}}$ in (2.22), i.e. $\dot{S}|_\sim = (\delta S/\delta \boldsymbol{\mathcal{X}}) \odot \tilde{\mathcal{M}} \odot (\delta S/\delta \boldsymbol{\mathcal{X}}) = 0$. As a matter of fact, a rather analogous case of non-affine kinetics is known in the field of complex fluids, for which the Gordon-Schowalter derivative is used (see [43–45], or pp. 119 - 120 in [29] for details), representing the relative slippage of mesoscopic objects relative to the rotational components of the macroscopic background deformation.

   The guiding principle for constructing $\tilde{\mathcal{M}}$ is the elimination of the antisymmetric contribution in the stress tensor. Following the above discussion and in analogy to pp. 119 - 120 in [29], the antisymmetric $\tilde{\mathcal{M}}$ can be calculated, using the conditions of degeneracy (2.4b) and anti-symmetry (2.5b) for $\tilde{\mathcal{M}}$, see A.2 for details. The resulting modifications of the model arising from the non-affine contribution can be written in the form

$$\partial_t \, m_\alpha|_{\text{non-a}} = \nabla^r_\gamma \hat{\sigma}_{\text{non-a } \alpha\gamma}, \tag{2.33a}$$

$$\partial_t \, T|_{\text{non-a}} = \left(\frac{\delta U}{\delta T} \right)^{-1} \hat{\sigma}^S_{\text{non-a } \gamma\varepsilon} \left(\nabla^r_\varepsilon v_\gamma \right), \tag{2.33b}$$

$$\partial_t \, p|_{\text{non-a}} = -\nabla^R_\gamma \left(\frac{1}{2} \Big[\left(\nabla^r_\gamma v_\mu \right) - \left(\nabla^r_\mu v_\gamma \right) \Big] R_\mu p \right), \tag{2.33c}$$

with

$$\hat{\sigma}_{\text{non-a } \alpha\gamma} = \frac{1}{2} \int_{\mathcal{Q}^2} p \left(R_\alpha \nabla^R_\gamma - R_\gamma \nabla^R_\alpha \right) \frac{\delta A}{\delta p} \mathrm{d}^6 \boldsymbol{\xi}, \tag{2.34a}$$

$$\hat{\sigma}^S_{\text{non-a } \alpha\gamma} = \frac{1}{2} \int_{\mathcal{Q}^2} p \left(R_\alpha \nabla^R_\gamma - R_\gamma \nabla^R_\alpha \right) \left(-\Theta \frac{\delta S}{\delta p} \right) \mathrm{d}^6 \boldsymbol{\xi}. \tag{2.34b}$$

Both of these stress-like expressions are antisymmetric. This underlines that the rotational part in the flow field, see (2.33c), goes hand in hand with the antisymmetric stress contributions, (2.34), which approves the assumption made further above. The ramifications will be more explicit when summarizing all components of the model.

2.3.5   Summary of the model

The complete model is obtained by combining the reversible dynamics, described in Sec. 2.3.3 and the irreversible contributions, discussed in Sec. 2.3.4. Adding up the contributions (2.18), (2.29), (2.30), and (2.33) leads to

$$\partial_t\, m_\alpha = -\,\nabla_\gamma^r\,(m_\alpha v_\gamma) + \nabla_\gamma^r\,\sigma_{\alpha\gamma}\,, \tag{2.35a}$$

$$\partial_t\, T = -\,v_\gamma\,(\nabla_\gamma^r\, T) + \left(\frac{\delta U}{\delta T}\right)^{-1}\left(\sigma_{\gamma\varepsilon}^S\,(\nabla_\varepsilon^r v_\gamma) - \int_{\mathcal{Q}^2}\mathcal{J}_\gamma\nabla_\gamma^Q\frac{\delta U}{\delta p}\,\mathrm{d}^6\boldsymbol{\xi}\right)\,, \tag{2.35b}$$

$$\partial_t\, F_{\alpha\beta} = -\,v_\mu\,(\nabla_\mu^r\, F_{\alpha\beta}) + F_{\mu\beta}\,(\nabla_\mu^r v_\alpha)\,, \tag{2.35c}$$

$$\partial_t\, p = -\,\nabla_\gamma^r\,(v_\gamma p) - \nabla_\gamma^R\big([\nabla_\mu^r v_\gamma]^{\mathsf{sym}}R_\mu\, p\big) - \nabla_\gamma^Q\,\mathcal{J}_\gamma\,, \tag{2.35d}$$

with the symmetric part of a matrix $\mathbf{A}^{\mathsf{sym}} = (\mathbf{A} + \mathbf{A}^\top)/2$. The constitutive relations for the total stress tensor $\boldsymbol{\sigma}$ and its entropic part $\boldsymbol{\sigma}^S$ are given by

$$\sigma_{\alpha\gamma} = \left(a - \int_{\mathcal{Q}^2}p\frac{\delta A}{\delta p}\mathrm{d}^6\boldsymbol{\xi}\right)\delta_{\alpha\gamma} + \frac{\delta A}{\delta F_{\alpha\mu}}F_{\gamma\mu} + \int_{\mathcal{Q}^2}p\left[R_\gamma\left(\nabla_\alpha^R\frac{\delta A}{\delta p}\right)\right]^{\mathsf{sym}}\mathrm{d}^6\boldsymbol{\xi}\,, \tag{2.36a}$$

$$\sigma_{\alpha\gamma}^S = -\,\Theta\left(\left(s - \int_{\mathcal{Q}^2}p\frac{\delta S}{\delta p}\mathrm{d}^6\boldsymbol{\xi}\right)\delta_{\alpha\gamma} + \frac{\delta S}{\delta F_{\alpha\mu}}F_{\gamma\mu} + \int_{\mathcal{Q}^2}p\left[R_\gamma\left(\nabla_\alpha^R\frac{\delta S}{\delta p}\right)\right]^{\mathsf{sym}}\mathrm{d}^6\boldsymbol{\xi}\right)\,. \tag{2.36b}$$

It can be shown [32] that both the total and the entropic stress tensor expressions are symmetric, since the internal energy U and entropy S may depend on the deformation gradient $\boldsymbol{F}$ only via right Cauchy-Green strain tensor, $\mathbf{C} = \boldsymbol{F}^\top\cdot\boldsymbol{F}$. Furthermore, the additive form of the stress tensor expression (i.e. the elastomer-matrix contribution plus the particle contribution) is similar to the Eindhoven Glassy Polymer (EGP) model [46, 47]. While the matrix-contribution, similar to the EGP-spring-element, allows to mimic even neo-Hookean material behavior, the glassy-network contribution corresponds to the phenomenological non-linear Maxwell-element in the EGP-model. The irreversible p-current density is given by (2.32) and (2.31),

$$\mathcal{J}_\gamma = \int_{\mathcal{Q}^2}\mathcal{D}_{\gamma\mu}\frac{1}{\Theta}\left(-\nabla_\mu^{Q'}\frac{\delta A}{\delta p'}\right)\mathrm{d}^6\boldsymbol{\xi}'\,, \tag{2.37}$$

where the 3×3-diffusion matrix depends on both $\boldsymbol{\xi}$ and $\boldsymbol{\xi}'$.

The above model makes the concurrent two-way coupling of the macroscopic scale and the particle level evident. The macroscopic flow field v_α affects the particle level p. This drives the particle arrangement away from the equilibrium state, which in turn results in nonequilibrium forces on the particle level. These forces are felt on the macroscopic scale by way of the constitutive relation for the stress tensor. In effect, one thus obtains the constitutive behavior of the nanocomposites, relating the stress to the deformation. For

specific applications, the model is completed by specification of the functionals of internal energy U and entropy S, and diffusion tensor $\boldsymbol{\mathcal{D}}$, which is illustrated in the following section.

We close the general model development by reminding the reader that the model presented above is substantially different from common practice in polymer kinetic theory [29, 38, 39]. As discussed in Sec. 2.3.1, modeling filled elastomers in the representative-pair setting requires the concept of an unloaded state, $\boldsymbol{Q}$, which is unknown to polymer kinetic theory. As a consequence, the irreversible but non-dissipative contributions to the dynamics in relation to the symmetrization of the stress tensor are absent in common polymer kinetic theory.

2.4   Specific system realization

To make the above model (2.35–2.37) system specific, choices need to be made for the internal energy functional $U[T, \boldsymbol{F}, p]$, and entropy functional $S[T, \boldsymbol{F}, p]$, and the diffusion matrix $\boldsymbol{\mathcal{D}}(T, \boldsymbol{F}, p)$.

2.4.1   Energy and entropy

For illustration purposes, rather than out of necessity, we assume that both U and S can be split additively into contributions related to (i) the elastomer matrix and (ii) the particle configuration. For the potential Φ that accounts for the glassy-bridge interactions discussed earlier in Sec. 2.3.4, we use a Hookean spring potential,

$$\Phi(\boldsymbol{\xi}) = \frac{1}{2} k \left(\boldsymbol{R} - \boldsymbol{Q}\right)^2 , \tag{2.38}$$

with spring constant k. Since the modulus of a glassy polymer depends on temperature (see Ch. 13 in [48]), the same holds for the spring constant, and in turn for the potential Φ in (2.38). Since Φ plays the role of a Helmholtz free energy (per particle pair), its temperature dependence implies that it decomposes into energetic and entropic parts,

$$\Phi = \Phi^E + \Phi^S , \tag{2.39}$$

with

$$\Phi^E = \Phi - T(\partial \Phi / \partial T), \qquad \Phi^S = T(\partial \Phi / \partial T) , \tag{2.40}$$

respectively. This split of Φ is reflected in the expressions for the functionals of internal energy and entropy (see also p.135 in [29]),

$$U = \int_\Omega u_{\mathsf{em}}(T, \boldsymbol{F}) \, \mathrm{d}^3\boldsymbol{r} + \int_\Omega \int_{\mathcal{Q}^2} p \, \Phi^E \, \mathrm{d}^3\boldsymbol{r} \, \mathrm{d}^6\boldsymbol{\xi} , \tag{2.41a}$$

$$S = \int_\Omega s_{\mathsf{em}}(T, \boldsymbol{F}) \, \mathrm{d}^3\boldsymbol{r} - \int_\Omega \int_{\mathcal{Q}^2} p \left[\frac{\Phi^S}{T} + k_{\mathsf{B}} \ln p\right] \mathrm{d}^3\boldsymbol{r} \, \mathrm{d}^6\boldsymbol{\xi} , \tag{2.41b}$$

where the subscript "em" denotes the contributions of the pure elastomer matrix. The symbol k_{B} stands for the Boltzmann constant, and the related contribution to the entropy

is of statistical origin [49,50]. For details on this entropy contribution, the reader is referred to A.3. As far as the contributions due to the elastomer matrix are concerned, u_{em} and s_{em}, we note that the modulus of an elastomer (in its rubbery state, i.e. above T_g) is influenced by temperature, most often approximated by a linear T-dependence (see Ch. 13 in [48]). Therefore, a split of the Helmholtz free energy density a_{em} analogous to (2.40) can be used,

$$u_{em} = a_{em} - T(\partial a_{em}/\partial T)\,, \qquad s_{em} = -(\partial a_{em}/\partial T)\,, \tag{2.42}$$

for the energetic and entropic contributions, respectively, which yields

$$a_{em} = u_{em} - T s_{em}\,. \tag{2.43}$$

For the example in this section, the Helmholtz free energy for compressible neo-Hookean systems is used [51],

$$a_{em} = \frac{G_{em}}{2}\left(I_1 - 3 - 2\ln J\right) + \frac{\kappa_{em}}{2}(\ln J)^2\,, \tag{2.44}$$

with shear modulus G_{em}, bulk modulus κ_{em}, $I_1 = \mathrm{tr}(\boldsymbol{F}^{\mathrm{T}} \cdot \boldsymbol{F})$ and $J = \det \boldsymbol{F}$.

It is noted that by virtue of the expressions for U and S in (2.41) and the splits (2.40) and (2.42), the quantity Θ (2.21) simplifies to $\Theta = T$. Furthermore, $\delta A/\delta p$ used in the flux (2.37) and the stress tensor (2.36a) becomes $\delta A/\delta p = \Phi + k_{\mathrm{B}}T(\ln p + 1)$, while the stress tensor itself assumes the form

$$
\begin{aligned}
\sigma_{\alpha\gamma} =\ & (a_{em} + \kappa_{em}\ln J - 2n k_{\mathrm{B}}T)\,\delta_{\alpha\gamma} \\
& + G_{em}\,(B_{\alpha\gamma} - \delta_{\alpha\gamma}) + \int_{\mathcal{Q}^2} p\left[R_\gamma(\nabla^R_\alpha \Phi)\right]^{\mathsf{sym}} \mathrm{d}^6\boldsymbol{\xi}\,,
\end{aligned} \tag{2.45}
$$

with n defined in (2.10), the left Cauchy-Green strain tensor $B_{\alpha\gamma} = F_{\alpha\nu}F_{\gamma\nu}$, and Φ given by (2.38). Apart from the isotropic contributions, the term proportional to the shear modulus G is typical for neo-Hookean materials. Most interesting is the last contribution in (2.45). It corresponds to known stress tensor expressions in statistical mechanics [52–54] and in polymer kinetic theory [29, 38, 39], a.k.a. Kramers-Kirkwood expression. However, the major difference consists in the potential Φ. One should recall that for the filled elastomers discussed here, the potential Φ depends not only on the current state $\boldsymbol{R}$, but also on a unloaded state $\boldsymbol{Q}$, e.g. according to (2.38).

As it was already mentioned in Sec. 2.3.1, the spring constant k needs to account for the collective effect of all the neighboring particles in order to mimic properly, in the representative particle-pair setting, the restoring mechanism as the glassy-spring network is deformed. If an effective particle-pair is defined by a surface-to-surface separation smaller than half the particle diameter d, the spring constant can be approximated by (see A.4),

$$k = \frac{\pi d}{\sqrt[3]{\phi}\,(8\phi - 1)}\,G_{\mathrm{comp}}\,, \tag{2.46}$$

with G_{comp} the shear modulus of the nanocomposite. G_{comp} depends on the volume fraction ϕ, and might be determined experimentally; e.g. from [17], one gets $G_{\mathrm{comp}} = \{4, 10, 50\}\mathrm{MPa}$ for $\phi = \{0.2, 0.3, 0.4\}$. The values for the number density of particle pairs n (see A.4) and for the resulting spring constant k as a function of volume fraction ϕ are given in Table 2.1.

2.4.2 Dynamics

Since the material has no inherent anisotropy, it is reasonable to assume that the relaxation of the glassy bridges, $\mathcal{J}$, occurs along the direction of the thermodynamic driving force $\mathcal{F}$. According to (2.32), this implies that $\mathcal{D}$ is a multiple of the unity tensor. Furthermore, we assume for illustrative purposes that the probability current $\mathcal{J}(\boldsymbol{\xi})$ depends on the driving force $\mathcal{F}(\boldsymbol{\xi}')$ only for $\boldsymbol{\xi}' = \boldsymbol{\xi}$. One can thus write

$$\mathcal{D}_{\gamma\mu} = \delta(\boldsymbol{R} - \boldsymbol{R}')\,\delta(\boldsymbol{Q} - \boldsymbol{Q}')\,\frac{\Theta\,p}{\zeta}\,\delta_{\gamma\mu}\,, \tag{2.47}$$

with a friction coefficient $\zeta > 0$. Without loss of generality, the positive factors Θ and p have been introduced for later convenience.

  The assumptions made for the energy and entropy (2.41), the glassy-spring potential (2.38), and the diffusion matrix (2.47) render the evolution equation (2.35d, 2.37) into the form

$$\begin{aligned}
\partial_t\,p = &-\nabla_\gamma^r\,(v_\gamma p) - \nabla_\gamma^R\big([\nabla_\mu^r v_\gamma]^{\mathsf{sym}} R_\mu\,p\big) - \nabla_\gamma^Q\left(\frac{k}{\zeta}\,p\,(R_\gamma - Q_\gamma)\right)\\
&-\nabla_\gamma^Q\left[p\,\nabla_\gamma^Q\left(\frac{k_{\mathsf{B}}\Theta}{\zeta}\right)\right] + \nabla_\gamma^Q\nabla_\gamma^Q\left[\frac{k_{\mathsf{B}}\Theta}{\zeta}\,p\right].
\end{aligned} \tag{2.48}$$

This Fokker-Planck equation can be translated into an equivalent set of stochastic differential equations [39],

$$\mathrm{d}\,R_\gamma = [\nabla_\mu^r v_\gamma]^{\mathsf{sym}}\,R_\mu\,\mathrm{d}t\,, \tag{2.49a}$$

$$\mathrm{d}\,Q_\gamma = -\frac{k}{\zeta}\,(Q_\gamma - R_\gamma)\,\mathrm{d}t + \nabla_\gamma^Q\left(\frac{k_{\mathsf{B}}\Theta}{\zeta}\right)\mathrm{d}t + \sqrt{\frac{2k_{\mathsf{B}}\Theta}{\zeta}}\,\mathrm{d}W_{\mathsf{t}\gamma}\,, \tag{2.49b}$$

which will be used for the numerical simulations in Sec. 2.5. The last term in (2.49b) represents the fluctuating Brownian contributions, that adds stochasticity to the $\boldsymbol{Q}$-dynamics. The symbol $\mathrm{d}\mathbf{W}_t$ stands for increments in Wiener processes, with average and variance,

$$\langle\mathrm{d}\,W_{t\alpha}\rangle = 0 \quad\text{and}\quad \langle\mathrm{d}\,W_{t\alpha}\mathrm{d}W_{t'\beta}\rangle = \delta_{\alpha\beta}\,\delta_{tt'}\,\mathrm{d}t, \tag{2.50}$$

respectively. In other words $\mathrm{d}\mathbf{W}_t$ represents white noise, being uncorrelated in time.

2.4.3 Relaxation of glassy bridges

In the dynamic model (2.49), the occurrence of a relaxation time τ for the $\boldsymbol{Q}$-dynamics is evident, with

$$\tau = \frac{\zeta}{k}\,. \tag{2.51}$$

This relaxation time contains all the information about the temperature- and load-dependence of the glassy-bridge dynamics. In the following, we will discuss a possible choice for the relaxation time τ, which for given spring constant k will imply a specific choice for the friction coefficient ζ.

To determine the dependence of the relaxation time τ on temperature and loading, we refer to [17–19]. In that study, the concept of a local glass-transition temperature is invoked (see also Sec. 2.1). If the matrix material adheres well to the filler-particle surface, the elastomer chain segments have decreased mobility the closer they are located to the particle, which is captured by a (local) glass-transition temperature that increases towards the filler-particle surface. It was proposed in [9, 10] that the glass transition temperature $T_g(z)$ at distance z from a particle is given by $T_g(z) = T_{g,b}(1 + \beta/z)$, which could fit their results well over a 100 K temperature range. Based on the relation for $T_g(z)$, the thickness of the glassy layer z_{th} at temperature T can be estimated by $T_g(z_{th}) = T$, i.e., $z_{th} = \beta T_{g,b}/(T - T_{g,b})$. The divergence in $T_g(z)$ is purely formal, since the physics which lead to this relation [55, 56] has a natural cut-off at short distance of about 2 nm. The corresponding increase of the glass transition temperature, about $100\mathrm{K}$ at 2 nm in their system, corresponds to the increase of T_g measured in [10], either in mechanical experiments or by using NMR. Further support of the glassy-layer picture has been given in [57–59], where glassy volume fractions have been measured for model samples using DSC, which were consistent with NMR and mechanical measurements.

If two particles are separated by a surface-to-surface separation of z, the most mobile chain segments are located in the middle, which will dominate the relative motion of the two particles. This relative motion of the two particles is influenced by the local glass-transition temperature T_g in the middle, that in general not only depends on the distance z but also on the local load Σ_{loc} [17, 18],

$$T_g(z, \Sigma_{loc}) = T_{g,b}\left(1 + \frac{\beta}{z}\right) - \frac{\Sigma_{loc}}{K}, \tag{2.52}$$

where $T_{g,b}$ is the bulk glass transition temperature of the pure elastomer, β and K are material parameters. K relates the yield stress σ_y to the temperature below T_g by $\sigma_y = K(T_g - T)$, and is a physically measurable quantity. The dependence of T_g on Σ_{loc} mimics the plasticization of the glassy bridge upon loading, which resembles the well-known plasticization/yielding of bulk polymer glasses upon loading [60, 61] . The change in T_g due to the presence of fillers and local load is relevant for the α-relaxation time described by the Williams-Landel-Ferry (WLF) law,

$$\ln\left(\frac{\tau_\alpha(z, \Sigma_{loc})}{\tau_g}\right) = \ln\left(\frac{\tau_{WLF}(T - T_g(z, \Sigma_{loc}))}{\tau_g}\right) = -\frac{C_1(T - T_g(z, \Sigma_{loc}))}{C_2 + (T - T_g(z, \Sigma_{loc}))}, \tag{2.53}$$

where C_1 and C_2 are the WLF parameters specific to the polymer, and τ_g represents the relaxation time at $T = T_g$.

In the context of the model presented in this chapter, one can incorporate the approach of [17, 18] by using the identifications $\tau = \tau_\alpha$ (i.e., $\zeta = k\,\tau_\alpha$), and

$$z = |\boldsymbol{R}| - d, \tag{2.54}$$

with d the particle diameter. As for the quantity Σ_{loc}, it has been identified in [17,18] with the absolute value of the glassy-bridge force. In contrast, modeling of bulk polymer glasses suggests to identify Σ_{loc} with the stress [61]. However, in our setting of a representative pair, the stress as such in between the two particles is not well defined. Since resemblance

to the concept of stress is nevertheless desirable, the following choice has been made in analogy to established von Mises J_2-plasticity, e.g., [62, 63],

$$\Sigma_{\mathrm{loc}} = \sqrt{|I_2|} \, , \tag{2.55}$$

with the second invariant $I_2 = (1/2)[(\mathrm{tr}\boldsymbol{\Sigma})^2 - \mathrm{tr}(\boldsymbol{\Sigma} \cdot \boldsymbol{\Sigma})]$ of

$$\boldsymbol{\Sigma}_{\mathrm{loc}} = \left[\boldsymbol{R} \, \nabla^R \Phi_{\mathrm{t}} \right]^{\mathrm{sym}} \, , \tag{2.56}$$

inspired by the stress-tensor expression (2.45). The $\boldsymbol{\Sigma}_{\mathrm{loc}}$ in (2.56) should account for all stress contributions, and therefore Φ_{t} should include not only the glassy-bridge contribution Φ in (2.38) but also an elastomer matrix contribution, denoted by Φ_{em}. In principle, the elastomer behavior is captured in our approach in a continuum sense rather than on the particle level (see e.g. (2.41) and (2.45)), however, for the sake of a meaningful definition of $\boldsymbol{\Sigma}_{\mathrm{loc}}$ one may recast it on the particle level into the form $\Phi_{\mathrm{em}}(\boldsymbol{\xi}) = \frac{1}{2} k_{\mathrm{em}} \left(\boldsymbol{R} - \boldsymbol{Q}_0 \right)^2$, analogous to the procedure outlined in A.4, with k_{em} the spring constant representing the elastomer matrix. Since the elastomer matrix does not yield but is purely elastic, the corresponding strain energy depends on the difference between the current state $\boldsymbol{R}$ and $\boldsymbol{Q}_0$, the initial unloaded state.

It is noted that the description given above with a load-dependent relaxation time closely resembles the modeling of viscoplastic behavior in bulk polymers [61, 64]. Particularly, yielding comes about by the strongly nonlinear dependence of the relaxation time on the applied load, and hence the use of a classical yield criterion [62, 63] is not required. However, in comparison to modeling bulk polymers in the post-yield regime, see e.g. [46, 47], the model in this chapter is different. First, strain softening, being connected with physical aging, is not in the scope of the presented work. And second, the particles in the two-particle model should always remain neighbors, which limits the applicability of this model to the deformation regimes where strain hardening becomes relevant (about 30% and higher [46]).

2.5   Simulation of oscillatory deformation

2.5.1   Simulation setup

Using all the system specifications of Sec. 2.4, the dynamics (2.49) is solved numerically (see [39]) to determine the stress-response (2.45) upon imposed oscillatory deformation, under isothermal conditions, i.e., constant T.

The initial particle configuration for each trajectory corresponds to an unloaded configuration, $\boldsymbol{R} = \boldsymbol{Q}$, with $\boldsymbol{R}$ being isotropically distributed. The length $R = |\boldsymbol{R}|$ was sampled from a narrow distribution of the form $w(R) \propto (d - \langle R \rangle)^2 - (R - \langle R \rangle)^2$ for $R \in [d, 2\langle R \rangle - d]$. This distribution has mean $\langle R \rangle = d/\sqrt[3]{\phi} = \{3.42, 2.99, 2.71\} \cdot 10^{-8}\mathrm{m}$ and standard deviation $\sqrt{\langle R^2 \rangle - \langle R \rangle^2} = (\langle R \rangle - d)/\sqrt{5} = \{6.4, 4.4, 3.2\} \cdot 10^{-9}\mathrm{m}$ for volume fractions $\phi = \{0.2, 0.3, 0.4\}$. The representative particle-pair is then subjected to a simple oscillatory shear deformation. This is realized by imposing a velocity field of the form $\boldsymbol{v} = (v_1, v_2, v_3)$ with components $v_1(x_2, t) = \dot{\gamma}(t)x_2$ and $v_2 \equiv v_3 \equiv 0$. The time-dependent imposed deformation is sinusoidal,

$$\gamma(t) = \gamma_0 \sin(\omega t), \tag{2.57}$$

with amplitude γ_0 and angular frequency ω.

The parameters used are listed in Table 2.1 and are the same as the ones considered in [17–19], which is representative of a filled elastomer consisting of silica particles dispersed in a poly(ethyl acrylate) matrix. All these parameters can be related to physical parameters, as explained in [17]. In particular, the value we chose for the parameter $\beta = 0.8$ nm, which sets the amplitude of the T_g-shift in the vicinity of the fillers, has been considered in [17], and corresponds to that measured experimentally in [9, 10]. The only parameter that is slightly adapted from the many-particle simulations in [17–19] to our two-particle model is the stress-sensitivity K in (2.52). In [17], K is determined such that, when imposing an oscillatory strain with amplitude 0.1 and rate $0.1\mathrm{s}^{-1}$, the stress-induced shift of the glass-transition temperature is $100\mathrm{K}$ at the maximum strain, which would result in $K = 1.2 \cdot 10^{-20} \mathrm{J~K}^{-1}$. However, in order to get better agreement between our model and the results in [19] (see further below), it was advantageous to choose the value $K = 2 \cdot 10^{-20} \mathrm{J~K}^{-1}$. In the simulations, the stress-induced shift in the glass transition temperature (2.52) has been limited to ≤ 200 K, since above that value the system is already plasticized (see also [18]). Finally, for numerical reasons, the range of the relaxation time (2.53) has been limited to $0.01 \mathrm{~s} \leq \tau_\alpha \leq 100 \mathrm{~s}$ [19].

To express the frequency relative to an internal rate of relaxation, it is below presented in terms of $\omega \cdot \langle \tau_\alpha^\mathrm{init} \rangle$, where $\langle \tau_\alpha^\mathrm{init} \rangle$ represents the α-relaxation time of the initial configuration, averaged over all trajectories. Specifically, for the simulations presented below, $\langle \tau_\alpha^\mathrm{init} \rangle = \{1.16, 1.87, 3.83\} \cdot 10^{-1}\mathrm{s}$ for volume fractions $\phi = \{0.2, 0.3, 0.4\}$.

Table 2.1: Parameters of the model. The range of values for k and n correspond to the different volume fractions studied, $\phi = \{0.2, 0.3, 0.4\}$.

parameter	symbol	physical value
particle diameter	d	$2 \cdot 10^{-8}$ m
number density of pairs	n	$\{1.43, 5.01, 10.5\} \cdot 10^{22}$ m^{-3}
bulk glass transition temperature	$T_\mathrm{g,b}$	213 K
relaxation time	τ_g	100 s
temperature of the experiment	T	263 K
distance-sensitivity parameter	β	$8 \cdot 10^{-10}$ m
stress-sensitivity parameter	K	$2 \cdot 10^{-20}$ J K^{-1}
glassy spring constant	k	$\{0.72, 0.67, 1.94\}$ N/m
elastomer spring constant	k_em	$k_{\phi=0.4}/100$ (see [19])
WLF-constants	C_1, C_2	$12.8, \quad 34$ K
shear modulus elastomer	G_em	10^6 Pa

2.5.2   Effect of deformation amplitude

The stress-strain curves for small- and large-amplitude oscillatory deformation are shown in Fig. 2.3 and Fig. 2.4, respectively. For small amplitude (Fig. 2.3), for the slow deformation rate (solid line), the stress-strain curve has a substantial viscous component, leading to hysteresis and thus dissipation, while for increasing deformation rate the hysteresis
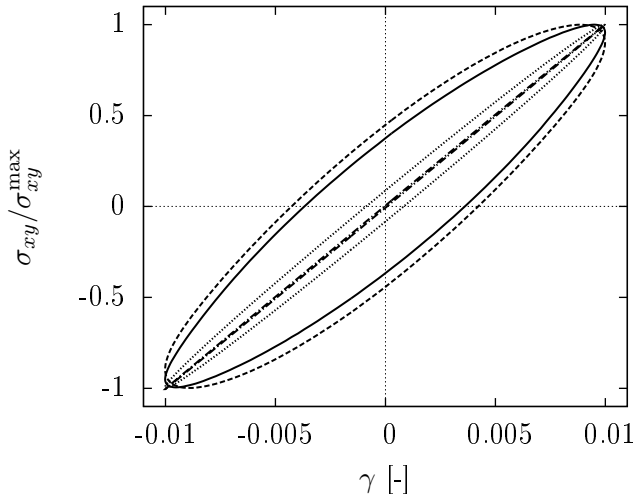
Figure 2.3: Lissajous-Bowditch plot: Shear stress σ_{xy}, normalized to its maximum value $\sigma_{xy}^{\max}$, vs. strain γ, for amplitude $\gamma_0 = 0.01$ at volume fraction $\phi = 0.4$. The simulation has been performed for different frequencies, namely $\omega \langle \tau_\alpha^{\mathrm{init}} \rangle = 3.83$ (solid line, with $\sigma_{xy}^{\max} = 1.26 \cdot 10^5 \mathrm{Pa}$), $\omega \langle \tau_\alpha^{\mathrm{init}} \rangle = 38.3$ (dashed line, with $\sigma_{xy}^{\max} = 1.80 \cdot 10^5 \mathrm{Pa}$), $\omega \langle \tau_\alpha^{\mathrm{init}} \rangle = 383$ (dotted line, with $\sigma_{xy}^{\max} = 2.61 \cdot 10^5 \mathrm{Pa}$), and $\omega \langle \tau_\alpha^{\mathrm{init}} \rangle = 3830$ (dash-dotted line, with $\sigma_{xy}^{\max} = 2.62 \cdot 10^5 \mathrm{Pa}$).

diminishes until almost pure (linear) elastic behavior is recovered (dash-dotted line). Such kind of behavior is typical for a linear viscoelasticity.

The above results suggest that the material responds elastically if the applied rate of deformation is fast with respect to the rate of structural re-arrangements. In contrast, the material responds viscous-like if the applied rate of deformation is slow with respect to the rate of structural re-arrangements. This argument is straightforward in the case that the internal time scale does not depend on the imposed load, and leads to linear viscoelastic behavior. However, the discussion in the previous section has shown that the internal time scale in the case of filled elastomers, i.e. of the glassy bridges, depends strongly on the applied load. This will lead thus to a nonlinear material response. While elliptic curves in a Lissajous-Bowditch plot are a hallmark of linear viscoelasticity, it is observed upon increasing the deformation amplitude (e.g. $\gamma_0 = 0.2$) that the stress-strain curves are significantly nonelliptic in shape, see Fig. 2.4. However, even in the nonlinear case, increasing the frequency leads to a narrowing of the loop in the Lissajous-Bowditch plot, meaning that the behavior becomes more elastic.

2.5.3   Measure of the nonlinearity. Payne effect

Nonlinear effects have been observed in Fig. 2.4, where large amplitude oscillatory shear (LAOS) deformation is imposed, resulting in a nonelliptical stress-strain curve. To quantify
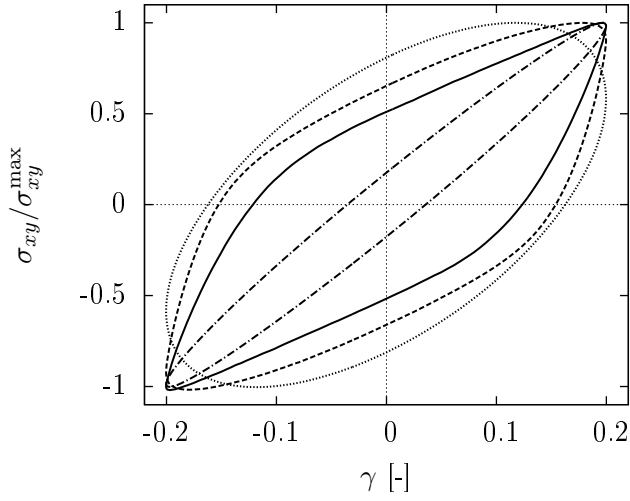
Figure 2.4: Lissajous-Bowditch plot: Shear stress σ_{xy}, normalized to its maximum value $\sigma_{xy}^{\max}$, vs. strain γ, for amplitude $\gamma_0 = 0.2$ at volume fraction $\phi = 0.4$. The simulation has been performed for different frequencies, namely $\omega \langle \tau_\alpha^{\text{init}} \rangle = 0.1915$ (solid line, with $\sigma_{xy}^{\max} = 4.81 \cdot 10^5 \text{Pa}$), $\omega \langle \tau_\alpha^{\text{init}} \rangle = 1.915$ (dashed line, with $\sigma_{xy}^{\max} = 5.89 \cdot 10^5 \text{Pa}$), $\omega \langle \tau_\alpha^{\text{init}} \rangle = 19.15$ (dotted line, with $\sigma_{xy}^{\max} = 2.36 \cdot 10^6 \text{Pa}$), and $\omega \langle \tau_\alpha^{\text{init}} \rangle = 191.5$ (dash-dotted line, with $\sigma_{xy}^{\max} = 5.18 \cdot 10^6 \text{Pa}$).
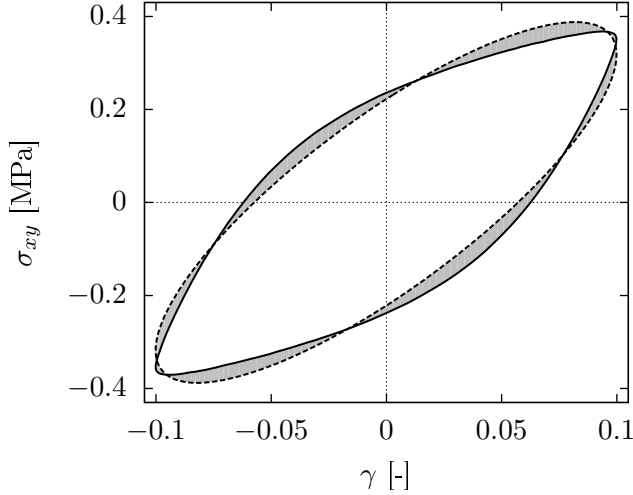
Figure 2.5: Best-fit elliptical approximation (dashed curve) for a nonlinear stress response (solid curve).

the nonlinearity, i.e. nonellipticity, two approaches are considered. For a given deformation $\gamma(t)$ (2.57), the stress response obtained from the simulation is denoted by $\sigma_{\mathsf{data}}(t)$. One can then attempt to represent this data-set by a the common linear viscoelastic relation $\sigma_{\mathsf{fit}}(t) = \gamma_0 \left[G'(\omega) \sin(\omega t) + G''(\omega) \cos(\omega t) \right]$. An optimal representation (see Fig. 2.5 for an example) can be defined as the specific choice for the parameters $G'(\omega)$ and $G''(\omega)$ that minimizes the (dimensionless) functional

$$N = \frac{\int_0^{2\pi/\omega} \left[\sigma_{\mathsf{data}}(t) - \sigma_{\mathsf{fit}}(t) \right]^2 \mathrm{d}t}{\int_0^{2\pi/\omega} \sigma_{\mathsf{data}}^2(t) \mathrm{d}t}. \tag{2.58}$$

The quality of the resulting best-fit can then be quantified by the corresponding value of N. Note that $N = 0$ for linear viscoelasticity.

A different way to quantify the nonlinearity in the system was developed in [65], and extended in [66, 67]. In the latter, two different elastic moduli and two different viscosities have been defined based on the Lissajous-Bowditch plot [66, 67],

$$G'_M = \left. \frac{\mathrm{d}\sigma}{\mathrm{d}\gamma} \right|_{\gamma=0}, \qquad G'_L = \left. \frac{\sigma}{\gamma} \right|_{\gamma=\pm\gamma_0}, \tag{2.59a}$$

$$\eta'_M = \left. \frac{\mathrm{d}\sigma}{\mathrm{d}\dot{\gamma}} \right|_{\dot{\gamma}=0}, \qquad \eta'_L = \left. \frac{\sigma}{\dot{\gamma}} \right|_{\dot{\gamma}=\pm\omega\gamma_0}, \tag{2.59b}$$
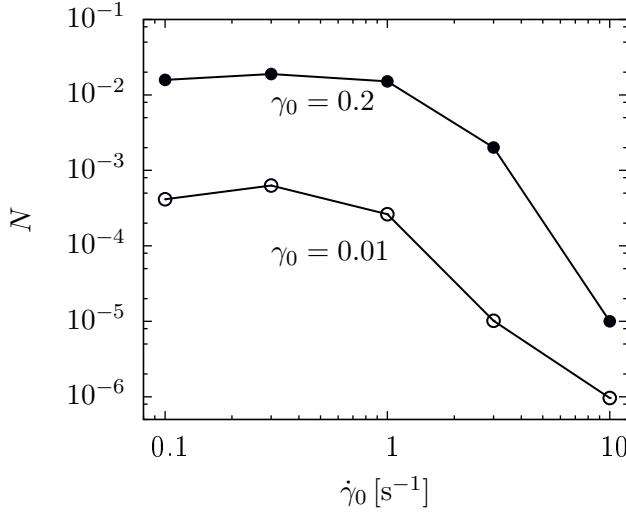
Figure 2.6: Quantification of nonlinearity: Parameter N defined in (2.58), for $\phi = 0.4$.

which in turn are used to define two dimensionless indexes of nonlinearity [66,67],

$$S_S \equiv \frac{G'_L - G'_M}{G'_L}, \tag{2.60a}$$

$$S_T \equiv \frac{\eta'_L - \eta'_M}{\eta'_L}. \tag{2.60b}$$

For linear viscoelasticity, both $G'_M = G'_L$ and $\eta'_M = \eta'_L$, and therefore $S_S = S_T = 0$. The parameters S_S and S_T can hence be used as a dimensionless quantification of the significance of non-linear effects. While the quantity N tells directly how the stress-strain curve differs from the elliptical shape (i.e. from linear viscoelasticity), $S_S > 0$ corresponds to strain stiffening, and $S_S < 0$ stands for strain softening [66]. Furthermore, $S_T > 0$ represents intracycle shear thickening, and $S_T < 0$ intracycle shear thinning [66].

In Fig. 2.6 and Fig. 2.7, the nonlinearity of the mechanical response of the model is presented in terms of the parameters N defined in (2.58), as well as S_S and S_T defined in (2.60). At fixed strain-amplitude γ_0, the nonlinearity parameter N decreases by two orders of magnitude upon increasing the deformation rate by two orders of magnitude. The quantities S_S and S_T also show the same overall trend, with decreasing nonellipticity with increasing deformation rate, however with significantly more scatter than for N. While the modulus-based quantity S_S shows a strong dependence on the deformation rate, the viscosity-based S_T does not permit such a conclusion.

A prominent effect of the nonlinear viscoelastic response of filled elastomers is the Payne effect, i.e., the dependence of G' and G'' on the amplitude of the applied deformation. For a quantitative evaluation of this effect in the present model, the ratios G'_M/G'_0 and G'_L/G'_0 are employed, where G'_M, G'_L are the tangential and secant moduli defined
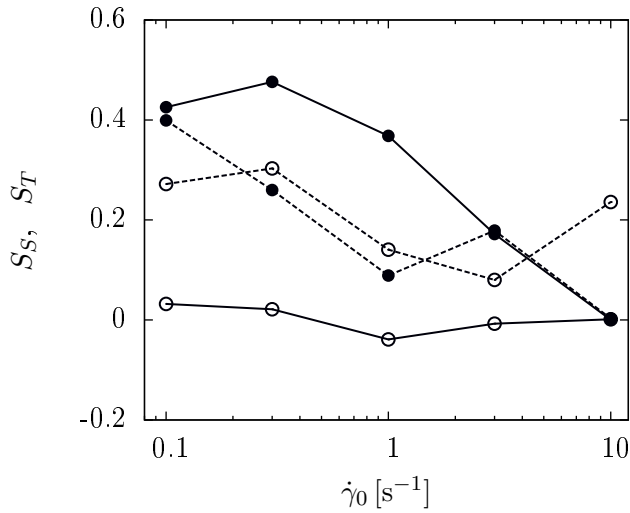
Figure 2.7: Quantification of nonlinearity: Parameters S_S (solid line) and S_T (dashed line) defined in (2.60), for $\phi = 0.4$. Open symbols stand for a strain amplitude of $\gamma_0 = 0.01$, and filled symbols for $\gamma_0 = 0.2$.
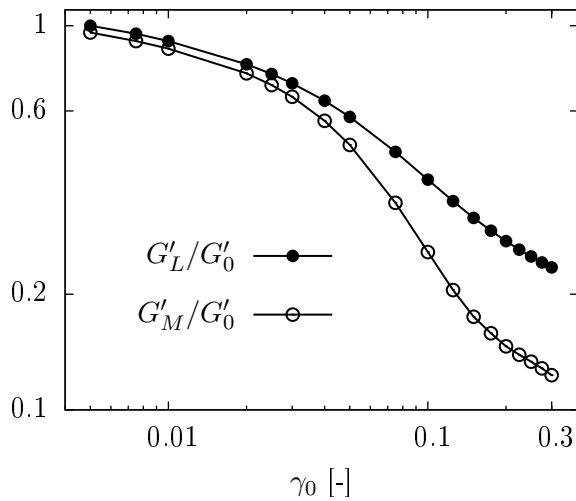
Figure 2.8: Quantification of nonlinearity: Payne effect. Ratios G'_M/G'_0 and G'_L/G'_0 vs. strain amplitude at frequency $\omega = 1\,\mathrm{s}^{-1}$ and volume fraction $\phi = 0.4$, where G'_0 is the shear modulus in a linear regime ($G'_0 = 8.84$ MPa for $\gamma_0 = 0.005$).

in (2.59a), respectively, and G_0' is a shear modulus at small amplitude (linear regime), in this particular case for $\gamma_0 = 0.005$, leading to Fig. 2.8. For both definitions, there is a decrease with increasing deformation amplitude, where the decrease is stronger for the tangent-based G_M'/G_0' than for the secant-based G_L'/G_0'. However, the trend of both curves agrees qualitatively with the original work of Payne [2] and also corresponds closely to the results of the many-particle model [18, 19]. The mechanism leading to the Payne effect in this model can be summarized as follows: An applied macroscopic deformation induces local inter-particle stresses, that in turn reduce the effective inter-particle glass transition temperature (see expression (2.52)), thereby lowering the local relaxation time. This implies that the ability of the micro-structure to relax (part of) the imposed load is increased, which is then observed as the Payne effect. The fact that the Payne effect is qualitatively reproduced underlines that the most essential aspects of the filled elastomer are appropriately represented in the model.

2.5.4   Comparison to many-particle simulations [19]

As stated in the Introduction 2.1, the goal of this chapter is to design a two-scale model to describe the main effects in filled elastomers, however it should be more compact than the many-particle approach in [17–19]. The above detailed discussion of system specification and parameter estimation makes clear that the model presented in this chapter is closely related to the one in [17–19]. Correspondingly, the simulation results discussed above are analogous to the ones in [17–19]. Nevertheless, it is also clear that the reduction from a many-particle system to a representative particle-pair, this chapter, comes at a price.

   The model comparison is performed on the basis of the mechanical response under oscillatory deformation $\gamma(t)$ in (2.57). The simulations are performed using the parameters in Table 2.1. The only exception is that for this comparison $\beta = 0.4$ nm is used, in agreement with the specific value used in Fig. 15 in [19]. The results of the comparison can be seen in Fig. 2.9 and Fig. 2.10. At moderate strains, the agreement with the many-particle approach is rather satisfactory, keeping in mind the drastic simplification of our model. The most apparent difference between the many-particle and two-particle models is the behavior in the outer strain-regions. In the many-particle model, the stress-strain curves show strain hardening at large amplitudes of deformation. It has been argued that this is due to the particle heterogeneity (see [19] for details). Naturally, this is an effect that is not accounted for in our effective particle-pair approach, and therefore this is a short-coming that is inherent to the substantial reduction in model complexity.

2.6   Conclusions

In this chapter, a two-scale model was developed for describing the mechanical behavior of hard-particle filled elastomers, in agreement within nonequilibrium thermodynamics principles, specifically the General Equation for the Non-Equilibrium Reversible-Irreversible Coupling (GENERIC). The two scales considered are on the one hand the macroscopic scale on which mechanical tests are performed, and on the other hand the scale of the filler particles, specifically the glassy-bridge network. So doing, the intricate mechanical behavior of these composites can be captured by a mutual coupling of both scales. This results
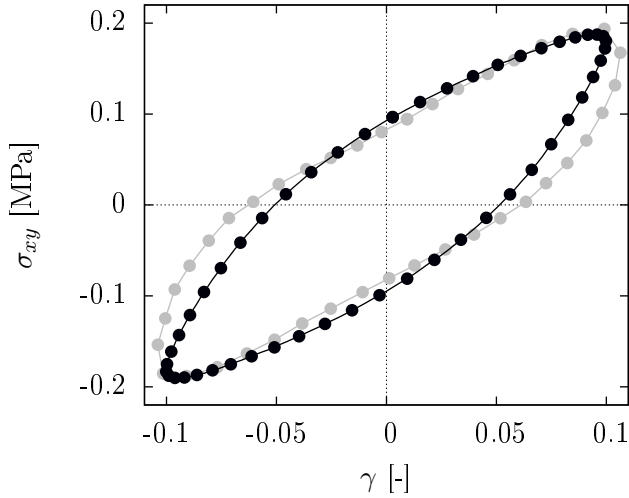
Figure 2.9: Lissajous-Bowditch plot: Shear stress σ_{xy} vs. strain γ. Comparison of two-particle model in this chapter (black) with many-particle model (grey) in [19] (see Fig. 15 therein), at $\gamma_0 = 0.1$.
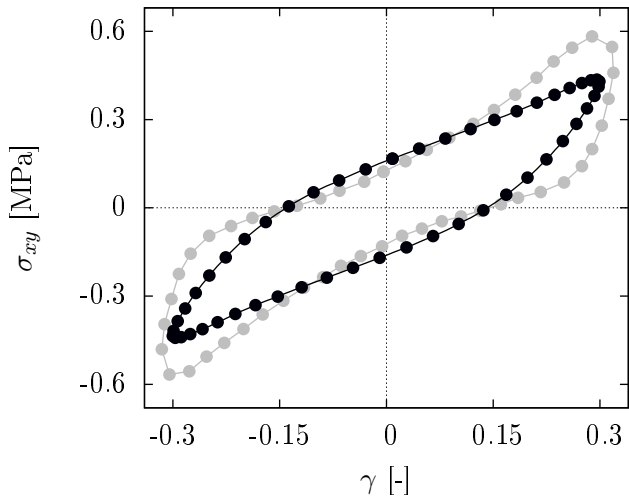
Figure 2.10: Lissajous-Bowditch plot: Shear stress σ_{xy} vs. strain γ. Comparison of two-particle model in this chapter (black) with many-particle model (grey) in [19] (see Fig. 15 therein), at $\gamma_0 = 0.3$.

in the set of concurrent evolution equations (for the momentum density, the temperature, the total macroscopic deformation gradient and the structural variable), supplemented by the constitutive relation for the stress tensor, which is summarized in Sec. 2.3.5. The presented model can be applied to hard-particle filled elastomer systems with not too low particle volume fraction, i.e. in the presence of a glassy-bridge network.

The proposed two-scale model has been solved numerically for macroscopically homogeneous oscillatory deformation, for both small and large amplitude. Of specific interest is the large-amplitude oscillatory test (LAOS). Under LAOS for strain amplitudes approximately equal or higher than 0.1, the glassy bridges between the particles yield. This results in a dramatic decrease of the effective elastic modulus, G', in literature known as the Payne effect [2], and is related to the stress-dependence of the glassy-bridge relaxation time. The nonlinearity of the mechanical response has been quantified and discussed in Sec. 2.5.3. The numerical results compare favorably with the literature.

Similar effects as modeled in this two-particle model have also been accounted for in the many-particle approach in [17–19]. While the general features of the stress-strain response of both models agree, there are also marked differences, as shown in Sec. 2.5.4. Namely, at high strains, it has been argued in [19] that the heterogeneity in particle arrangement leads to strain hardening. Such effects are not present in the two-particle approach taken here. More detailed comparisons between the two approaches will be done in the future, also in relation to the Mullin's effect (see below). However, it is already clear now, that both approaches have their benefits, depending on application. On the one hand, if one is interested in the material behavior in a macroscopically homogeneous sample, one may choose for using the many-particle approach, since it captures the many-particle aspects more appropriately. On the other hand, if one is interested in studying a macroscopically inhomogeneous situation, one would need to solve in each volume element the many-particle simulation to express the stress state in terms of the deformation (history). One can anticipate that this is computationally too costly, and alternatives must be sought. A possible solution is to use the two-particle approach developed here, which is computationally substantially more efficient than the many-particle model, and simplifies the calculation in each volume element of the stress in terms of the deformation. This might open the way towards two-scale modeling of inhomogeneous phenomena such as wear and tear, of hard-particle filled elastomers.

In future work, the model presented here will be extended to describe also the Mullins effect [5,6], i.e., the recovery of the effective elastic modulus with increasing waiting time after application of strong deformation. It seems that the origin of this recovery behavior roots in the physical aging of the glassy bridges, akin to the physical aging of bulk glassy polymers. Therefore, the proper modeling of the Mullins effect will substantially benefit from modeling efforts to describe physical aging in bulk glassy polymers, e.g. as described in the Eindhoven Glassy Polymer (EGP) model [46,47].

Chapter 3

Modeling aging and mechanical rejuvenation of amorphous solids

Abstract

The elasto-viscoplasticity of amorphous solids is modeled, with a focus on the effects of physical aging and mechanical rejuvenation. Using nonequilibrium thermodynamics, the concept of kinetic and configurational subsystems has been employed. The Hamiltonian structure of reversible dynamics is exploited to derive a constitutive relation for the stress tensor. Furthermore, it is demonstrated that accounting for mechanical rejuvenation results in a modification of the driving force for viscoplastic flow.

3.1   Introduction

Amorphous solids, i.e. glasses, show behavior that is unknown to their crystalline coun-
terparts. Particularly, glasses age slowly over time accompanied by corresponding changes
in the physical properties (see e.g. [68]). A discussion of the main effects of physical
aging (leaving aside chemical aging, which shall not be discussed in this study) for poly-
mer glasses can be found in [69]. Most prominent features in polymer glasses concern
the behavior under deformation. Upon loading a glassy polymer, an initially elastic re-
sponse is followed by a gradual but rather pronounced transition to yielding, which upon
further loading is followed by strain-softening and finally strain-hardening (see e.g. [13]).
The more aged the specimen, the higher the yield stress [70]. However, the subsequent
strain-softening leads to a stress value that is independent of the initial age of the sample,
which is the reason for calling strain-softening also mechanical rejuvenation, as it erases
the effect of aging [13, 71, 72].

To model physical aging and mechanical rejuvenation of glassy systems, the concept of
internal state variables has been employed (see e.g. [73]). A frequently used internal state
variable is the fictive temperature introduced in [74], also referred to as configurational or
effective temperature [75–80]. This concept is based on the notion that, in the (potential)
energy landscape, there are kinetic/vibrational degrees of freedom that relax rather rapidly
(by intra-basin dynamics) as compared to the configurational degrees of freedom that
relax on significantly longer time scales (by inter-basin transitions) [81–88], which has
also been employed in atomistic simulations (see e.g. [89]). A choice different from the
configurational temperature to phenomenologically describe the effect of aging on the
yielding kinetics has been made in [13, 46, 90].

The goal of this chapter is to derive a closed model to describe the effect of aging on
the yielding kinetics and mechanical rejuvenation, using nonequilibrium thermodynamics in
the form of the General Equation for the Non-Equilibrium Reversible-Irreversible Coupling
(GENERIC) [27–29] (Sec. 2.2). Earlier efforts in finite-deformation non-isothermal elasto-
viscoplasticity [32, 34, 91] are extended by using the concept of kinetic and configurational
subsystems (Sec. 3.2). However, in contrast to the literature, (i) the GENERIC imposes
more constraints on the model formulation, e.g. Hamiltonian reversible dynamics and
the degeneracy conditions, and (ii) we allow for more general thermodynamics of the
entire system. Finally, the relation with experimental findings on aging and rejuvenation
is discussed (Sec. 3.3).

Before we start, let us comment about the notation. Greek indices are used for
Cartesian components, and Einstein's summation convention is used for indices that occur
twice. Furthermore, with respect to operators, subscripts α and (α, β) imply contraction
with any vector A_α and any matrix $A_{\alpha\beta}$ multiplied from the left, respectively, while
subscripts γ and (γ, ε) imply contraction with the vector A_γ and matrix $A_{\gamma\varepsilon}$ multiplied
from the right, respectively. Finally, the quantity $f_{,\mathcal{X}_i}$ stands for the partial derivative of a
function f with respect to the variable $\mathcal{X}_i$. Unless stated otherwise, it is tacitly assumed
that this derivative is taken at constant $\boldsymbol{\mathcal{X}} \setminus \mathcal{X}_i$, with $\boldsymbol{\mathcal{X}} = (\boldsymbol{m}, s, \eta, \boldsymbol{F}^{\mathrm{e}})$.

3.2   Model formulation with kinetic and configurational subsystems

3.2.1   Set of variables and generating functionals

In [32, 34], finite-deformation non-isothermal elasto-viscoplasticity, without strain harden-
ing, has been described in an Eulerian (i.e. spatial) setting, in terms of the momentum
density $\boldsymbol{m}$, the temperature T, and the elastic part of the deformation gradient $\boldsymbol{F}^{\mathrm{e}}$, while
in [91] the temperature variable has been replaced by the internal energy e_{t}. Since, in
this chapter we are interested in a formulation with both a kinetic and a configurational
subsystem, the extension to two temperatures or energies seems obvious, however, the
technical steps will be unnecessarily complicated. Instead, we choose to describe the ki-
netic and configurational subsystems by their respective entropy densities, s and η, which
has been discussed also in [77, 79, 80, 85, 87]. In summary, the set of variables is thus given
by $\boldsymbol{\mathcal{X}} = (\boldsymbol{m}, s, \eta, \boldsymbol{F}^{\mathrm{e}})$.

In terms of the complete set of variables $\boldsymbol{\mathcal{X}}$, the energy and entropy can be written in
the form

$$E = \int \left(\frac{\boldsymbol{m} \cdot \boldsymbol{m}}{2\rho} + e_{\mathrm{t}}(s, \eta, \boldsymbol{F}^{\mathrm{e}}) \right) d^3 r \,, \qquad S = \int (s + \eta) \, d^3 r \,, \tag{3.1}$$

with $s + \eta$ the total entropy density [82]. The mass density is given by $\rho = \rho_0 / \det \boldsymbol{F}^{\mathrm{e}}$
(with ρ_0 the mass density in the undeformed state), which implies the assumption that
the non-elastic deformation is isochoric (see further below), i.e. $\det \boldsymbol{F}^{\mathrm{e}} = \det \boldsymbol{F}$ with $\boldsymbol{F}$
the total deformation gradient. The gradient of energy and entropy are then given by

$$\frac{\delta E}{\delta \boldsymbol{\mathcal{X}}} = \begin{pmatrix} v_\gamma \\ T \\ \theta \\ -\frac{v_\mu v_\mu}{2} \rho_{,F^{\mathrm{e}}_{\gamma\varepsilon}} + e_{\mathrm{t},F^{\mathrm{e}}_{\gamma\varepsilon}} \end{pmatrix} \,, \qquad \frac{\delta S}{\delta \boldsymbol{\mathcal{X}}} = \begin{pmatrix} 0 \\ 1 \\ 1 \\ 0 \end{pmatrix} \,, \tag{3.2}$$

with velocity $v_\gamma = m_\gamma / \rho$, $\rho_{,F^{\mathrm{e}}_{\gamma\varepsilon}} = -\rho F^{\mathrm{e},-1}_{\varepsilon\gamma}$, and where we have introduced the abbrevi-
ations

$$T = e_{\mathrm{t},s} \,, \qquad \theta = e_{\mathrm{t},\eta} \,, \tag{3.3}$$

which in the following are called kinetic and configurational temperatures, respectively
[74–80, 82].

3.2.2   Reversible dynamics

According to $(2.2)_1$, the reversible dynamics involves the Poisson operator $\boldsymbol{\mathcal{L}}$. Departing
from [32], and bearing in mind that the total entropy consists of the two contributions s
and η, we propose the generalization

$$\boldsymbol{\mathcal{L}} = \begin{pmatrix} -\nabla_\gamma m_\alpha - m_\gamma \nabla_\alpha & -s\nabla_\alpha & -\eta\nabla_\alpha & (\nabla_\alpha F^{\mathrm{e}}_{\gamma\varepsilon}) + \nabla_\mu F^{\mathrm{e}}_{\mu\varepsilon}\delta_{\alpha\gamma} \\ -\nabla_\gamma s & 0 & 0 & 0 \\ -\nabla_\gamma \eta & 0 & 0 & 0 \\ -(\nabla_\gamma F^{\mathrm{e}}_{\alpha\beta}) + F^{\mathrm{e}}_{\mu\beta}\nabla_\mu \delta_{\alpha\gamma} & 0 & 0 & 0 \end{pmatrix} \,. \tag{3.4}$$

It can be shown that this Poisson operator satisfies all the necessary conditions (2.4a), (2.5a) and (2.6), including the Jacobi identity. Using the gradient of energy $(3.2)_1$, the reversible contributions to the evolution equations, $(2.2)_1$, become

$$
\begin{aligned}
\partial_t m_\alpha|_{\text{rev}} &= -\nabla_\gamma (m_\alpha v_\gamma) + \nabla_\gamma \sigma_{\alpha\gamma}, \\
\partial_t s|_{\text{rev}} &= -\nabla_\gamma (s\, v_\gamma), \\
\partial_t \eta|_{\text{rev}} &= -\nabla_\gamma (\eta\, v_\gamma), \\
\partial_t F^{\text{e}}_{\alpha\beta}|_{\text{rev}} &= -v_\gamma(\nabla_\gamma F^{\text{e}}_{\alpha\beta}) + (\nabla_\mu v_\alpha) F^{\text{e}}_{\mu\beta},
\end{aligned}
\tag{3.5}
$$

with the Cauchy stress tensor defined by

$$
\sigma_{\alpha\gamma} = (e_{\text{t}} - Ts - \theta\eta)\, \delta_{\alpha\gamma} + e_{\text{t}, F^{\text{e}}_{\alpha\varepsilon}}\, F^{\text{e}}_{\gamma\varepsilon} = \rho\, \hat{e}_{\text{t}, F^{\text{e}}_{\alpha\varepsilon}}\big|_{\hat{s},\hat{\eta}}\, F^{\text{e}}_{\gamma\varepsilon},
\tag{3.6}
$$

with the abbreviation $\hat{f} = f/\rho$ for any quantity f.

A possible limitation of the ansatz (3.4) might be that the entropy densities s and η do not interact due to reversible dynamics, as evidenced in $(3.5)_2$ and $(3.5)_3$. It is in principle possible to add reversible terms to the evolution equations of the partial entropy densities s and η in such a way that the total entropy density stays unaffected. However, such additional terms must satisfy the rather stringent Jacobi identity (2.6), which will impose certain restrictions on the admissible additional terms. Furthermore, by adding such terms to the reversible dynamics of the partial entropy densities, this implies adding certain terms in the first column (in the corresponding rows) of the Poisson operator (3.4). Due to the anti-symmetry of the Poisson operator, this means that there will be additional terms on the first row of the Poisson operator, which in turn leads finally to a modification of the right-hand side of the momentum evolution equation $(3.5)_1$, most likely in the form of a modified stress tensor expression (3.6). Requirements on the abstract form of the constitutive relation for the stress tensor can therefore also be employed (e.g. hyperelasticity, in contrast to hypoelasticity [92]) to restrict the possible exchange terms between the partial entropy densities s and η.

3.2.3   Irreversible dynamics

Based on the analysis of many dissipative models in the literature, the following split of the friction matrix has been proposed [41],

$$
\boldsymbol{\mathcal{M}} = \boldsymbol{\mathcal{C}}\boldsymbol{\mathcal{R}}\boldsymbol{\mathcal{C}}^{\text{T}}.
\tag{3.7}
$$

With this split, the link between the GENERIC and linear irreversible thermodynamics [42] can be established [29]. In (3.7), $\boldsymbol{\mathcal{R}}$ is a symmetric ($\boldsymbol{\mathcal{R}}^{\text{T}} = \boldsymbol{\mathcal{R}}$) and positive semi-definite ($\boldsymbol{\mathcal{R}} \geq 0$) operator that contains all dynamic material information (e.g relaxation times, viscosity, thermal conductivity), while the operator $\boldsymbol{\mathcal{C}}$ represents the so-called mechanical part. In practical applications, the operator $\boldsymbol{\mathcal{C}}$ is determined by $\boldsymbol{\mathcal{C}}^{\text{T}}(\delta E/\delta \boldsymbol{\mathcal{X}}) = 0$, which implies the degeneracy condition (2.4b), and by the requirement that the combination $\boldsymbol{\mathcal{F}} = \boldsymbol{\mathcal{C}}^{\text{T}}(\delta S/\delta \boldsymbol{\mathcal{X}})$ represents the thermodynamic driving forces for the irreversible processes. These, in turn, induce the thermodynamic fluxes, $\boldsymbol{\mathcal{J}} = \boldsymbol{\mathcal{R}}\boldsymbol{\mathcal{F}}$, which enter the irreversible dynamics $(2.2)_2$ in the form $\partial_t \boldsymbol{\mathcal{X}}|_{\text{irr}} = \boldsymbol{\mathcal{C}}\boldsymbol{\mathcal{J}}$.

For the specific case discussed in this chapter, the irreversible processes include heat conduction in each of the two subsystems (kinetic and configurational), exchange between

the two subsystems, and viscoplastic deformation. In view of the driving forces for these processes [29, 34, 42], and using the gradient of energy $(3.2)_1$, one can write

$$
\boldsymbol{\mathcal{C}}^{\mathrm{T}} = \begin{pmatrix}
0 & \nabla_\alpha \frac{1}{T} & 0 & 0 \\
0 & 0 & \nabla_\alpha \frac{1}{\theta} & 0 \\
0 & \frac{1}{T} & -\frac{1}{\theta} & 0 \\
0 & -\frac{\psi}{T} P_{\alpha\beta\mu\nu}\, e_{\mathrm{t},F^{\mathrm{e}}_{\mu\nu}} & -\frac{(1-\psi)}{\theta} P_{\alpha\beta\mu\nu}\, e_{\mathrm{t},F^{\mathrm{e}}_{\mu\nu}} & P_{\alpha\beta\gamma\varepsilon}
\end{pmatrix}, \tag{3.8}
$$

with an arbitrary function ψ of the variables $\boldsymbol{\mathcal{X}}$, and the projection [34]

$$
P_{\alpha\beta\gamma\varepsilon} = \delta_{\alpha\gamma}\delta_{\beta\varepsilon} - \frac{1}{3} F^{\mathrm{e},-1}_{\beta\alpha} F^{\mathrm{e}}_{\gamma\varepsilon}, \tag{3.9}
$$

with $P_{\alpha\beta\gamma\varepsilon} P_{\gamma\varepsilon\mu\nu} = P_{\alpha\beta\mu\nu}$. Using $P_{\alpha\beta\gamma\varepsilon}\rho_{,F^{\mathrm{e}}_{\gamma\varepsilon}} = 0$, the above choice guarantees that $\boldsymbol{\mathcal{C}}^{\mathrm{T}}(\delta E/\delta \boldsymbol{\mathcal{X}}) = 0$. Furthermore, the thermodynamic driving forces $\boldsymbol{\mathcal{F}}$ assume the form

$$
\boldsymbol{\mathcal{F}} = \boldsymbol{\mathcal{C}}^{\mathrm{T}}(\delta S/\delta \boldsymbol{\mathcal{X}}) = \begin{pmatrix}
\nabla_\alpha \frac{1}{T} \\
\nabla_\alpha \frac{1}{\theta} \\
\frac{1}{T} - \frac{1}{\theta} \\
-\left(\frac{\psi}{T} + \frac{(1-\psi)}{\theta}\right) P_{\alpha\beta\mu\nu}\, e_{\mathrm{t},F^{\mathrm{e}}_{\mu\nu}}
\end{pmatrix}, \tag{3.10}
$$

i.e., there are four driving forces, $\boldsymbol{\mathcal{F}} = (\boldsymbol{\mathcal{F}}^s, \boldsymbol{\mathcal{F}}^\eta, \boldsymbol{\mathcal{F}}^\Delta, \boldsymbol{\mathcal{F}}^{F^{\mathrm{e}}})$. Correspondingly, the thermodynamic fluxes, $\boldsymbol{\mathcal{J}} = \boldsymbol{\mathcal{R}}\boldsymbol{\mathcal{F}}$, will also contain four contributions, $\boldsymbol{\mathcal{J}} = (\boldsymbol{\mathcal{J}}^s, \boldsymbol{\mathcal{J}}^\eta, \boldsymbol{\mathcal{J}}^\Delta, \boldsymbol{\mathcal{J}}^{F^{\mathrm{e}}})$, representative of heat conduction in each of the two subsystems and heat exchange between them, and viscoplastic deformation. Calculating the adjoint of $\boldsymbol{\mathcal{C}}^{\mathrm{T}}$,

$$
\boldsymbol{\mathcal{C}} = \begin{pmatrix}
0 & 0 & 0 & 0 \\
-\frac{1}{T}\nabla_\gamma & 0 & \frac{1}{T} & -\frac{\psi}{T} P_{\gamma\varepsilon\mu\nu}\, e_{\mathrm{t},F^{\mathrm{e}}_{\mu\nu}} \\
0 & -\frac{1}{\theta}\nabla_\gamma & -\frac{1}{\theta} & -\frac{(1-\psi)}{\theta} P_{\gamma\varepsilon\mu\nu}\, e_{\mathrm{t},F^{\mathrm{e}}_{\mu\nu}} \\
0 & 0 & 0 & P_{\gamma\varepsilon\alpha\beta}
\end{pmatrix}, \tag{3.11}
$$

the fluxes $\boldsymbol{\mathcal{J}}$ translate into irreversible dynamics by way of $\partial_t \boldsymbol{\mathcal{X}}|_{\mathrm{irr}} = \boldsymbol{\mathcal{C}}\boldsymbol{\mathcal{J}}$,

$$
\begin{aligned}
\partial_t m_\alpha|_{\mathrm{irr}} &= 0, \\
\partial_t s|_{\mathrm{irr}} &= -\frac{1}{T}\nabla_\gamma \mathcal{J}^s_\gamma + \frac{1}{T}\mathcal{J}^\Delta - \frac{\psi}{T} P_{\gamma\varepsilon\mu\nu}\, e_{\mathrm{t},F^{\mathrm{e}}_{\mu\nu}} \mathcal{J}^{F^{\mathrm{e}}}_{\gamma\varepsilon}, \\
\partial_t \eta|_{\mathrm{irr}} &= -\frac{1}{\theta}\nabla_\gamma \mathcal{J}^\eta_\gamma - \frac{1}{\theta}\mathcal{J}^\Delta - \frac{(1-\psi)}{\theta} P_{\gamma\varepsilon\mu\nu}\, e_{\mathrm{t},F^{\mathrm{e}}_{\mu\nu}} \mathcal{J}^{F^{\mathrm{e}}}_{\gamma\varepsilon}, \\
\partial_t F^{\mathrm{e}}_{\alpha\beta}|_{\mathrm{irr}} &= P_{\gamma\varepsilon\alpha\beta}\mathcal{J}^{F^{\mathrm{e}}}_{\gamma\varepsilon}.
\end{aligned} \tag{3.12}
$$

This highlights the physical interpretation of $\boldsymbol{\mathcal{J}}^s$ and $\boldsymbol{\mathcal{J}}^\eta$ as heat fluxes in the two thermal subsystems, respectively, of $\boldsymbol{\mathcal{J}}^\Delta$ as the subsystem heat exchange, and of $\boldsymbol{\mathcal{J}}^{F^{\mathrm{e}}}$ as being related to the viscoplastic deformation rate.

For the fluxes $\boldsymbol{\mathcal{J}}$, constitutive relations must be formulated. To start, we use the decomposition $\boldsymbol{\mathcal{R}} = \boldsymbol{\mathcal{R}}^{\mathrm{h}} + \boldsymbol{\mathcal{R}}^{\mathrm{x}} + \boldsymbol{\mathcal{R}}^{\mathrm{p}}$, with contributions representative of heat conduction ("h"), exchange between the kinetic and configurational subsystems ("x"), and viscoplastic deformation ("p"). Proper force-flux relations for intra-subsystem heat conduction

can be established by [29, 42]

$$\mathcal{R}^{\mathrm{h}} = \begin{pmatrix} T^2 \lambda_{\alpha\gamma}^s & Q_{\alpha\gamma} & 0 & 0 \\ Q_{\gamma\alpha} & \theta^2 \lambda_{\alpha\gamma}^{\eta} & 0 & 0 \\ 0 & 0 & 0 & 0 \\ 0 & 0 & 0 & 0 \end{pmatrix}. \tag{3.13}$$

with the requirement that both $\boldsymbol{\lambda}^s$ and $\boldsymbol{\lambda}^{\eta}$ must be symmetric and positive semi-definite. Neglecting the cross-coupling coefficients, $\boldsymbol{Q} = 0$, one obtains for the heat fluxes

$$\mathcal{J}_{\alpha}^{s,\mathrm{h}} = -\lambda_{\alpha\gamma}^s \nabla_{\gamma} T, \qquad \mathcal{J}_{\alpha}^{\eta,\mathrm{h}} = -\lambda_{\alpha\gamma}^{\eta} \nabla_{\gamma} \theta, \tag{3.14}$$

while $\mathcal{J}^{\Delta,\mathrm{h}} = 0$ and $\mathcal{J}^{F^{\mathrm{e}},\mathrm{h}} = 0$. Furthermore, for the heat exchange between kinetic and configurational subsystems we choose (see [42] for the comparable case of two discrete coupled systems),

$$\mathcal{R}^{\mathrm{x}} = \begin{pmatrix} 0 & 0 & 0 & 0 \\ 0 & 0 & 0 & 0 \\ 0 & 0 & \mu^{\mathrm{x}} & 0 \\ 0 & 0 & 0 & 0 \end{pmatrix}, \tag{3.15}$$

with $\mu^{\mathrm{x}} \geq 0$, which leads to the corresponding flux

$$\mathcal{J}^{\Delta,\mathrm{x}} = \mu^{\mathrm{x}} \left(\frac{1}{T} - \frac{1}{\theta} \right), \tag{3.16}$$

while $\mathcal{J}^{s,\mathrm{x}} = 0$, $\mathcal{J}^{\eta,\mathrm{x}} = 0$, and $\mathcal{J}^{F^{\mathrm{e}},\mathrm{x}} = 0$.

We now turn to the formulation of the viscoplastic flow rule. The driving force $\mathcal{F}^{F^{\mathrm{e}}}$ in (3.10) contains a contribution that is proportional to $1/T - 1/\theta$. Since this latter combination is equal to $\mathcal{F}^{\Delta}$ in (3.10), it might be necessary to combine both $\mathcal{F}^{F^{\mathrm{e}}}$ and $\mathcal{F}^{\Delta}$ into the actual driving force for viscoplastic deformation. Therefore, we choose (see also [34])

$$\mathcal{R}^{\mathrm{p}} = \begin{pmatrix} 0 \\ 0 \\ \Omega_{\nu\mu} \\ \delta_{\alpha\nu} F_{\mu\beta}^{\mathrm{e}} \end{pmatrix} \Lambda_{\nu\mu\varrho\lambda} \begin{pmatrix} 0 \\ 0 \\ \Omega_{\varrho\lambda} \\ \delta_{\varrho\gamma} F_{\lambda\varepsilon}^{\mathrm{e}} \end{pmatrix}, \tag{3.17}$$

where for later convenience we assume that the coupling $\Omega_{\alpha\beta}$ is traceless, $\Omega_{\mu\mu} = 0$. The symmetry of $\mathcal{R}$ requires $\Lambda_{\nu\mu\varrho\lambda} = \Lambda_{\varrho\lambda\nu\mu}$, and furthermore we impose $\Lambda_{\mu\nu\varrho\lambda} = \Lambda_{\nu\mu\varrho\lambda} = \Lambda_{\nu\mu\lambda\varrho}$. For the fluxes related to viscoplastic deformation one obtains

$$\mathcal{J}^{\Delta,\mathrm{p}} = -D_{\mu\nu}^{\mathrm{p}} \Omega_{\mu\nu}, \qquad \mathcal{J}_{\alpha\beta}^{F^{\mathrm{e}},\mathrm{p}} = -D_{\alpha\mu}^{\mathrm{p}} F_{\mu\beta}^{\mathrm{e}}, \tag{3.18}$$

with the definition

$$D_{\alpha\beta}^{\mathrm{p}} = \Lambda_{\alpha\beta\varrho\lambda} \Sigma_{\varrho\lambda}^{\mathrm{d}}, \quad \text{with} \quad \Sigma_{\varrho\lambda}^{\mathrm{d}} = \left(\left(\frac{\psi}{T} + \frac{(1-\psi)}{\theta} \right) \sigma_{\varrho\lambda}^{\mathrm{d}} - \left(\frac{1}{T} - \frac{1}{\theta} \right) \Omega_{\varrho\lambda} \right), \tag{3.19}$$

where the superscript "d" denotes the deviatoric (i.e., trace-free) part of a tensor $A_{\alpha\beta}$, $A_{\alpha\beta}^{\mathrm{d}} = A_{\alpha\beta} - (A_{\mu\mu}/3)\delta_{\alpha\beta}$. For the other flux contributions based on (3.17) one finds $\mathcal{J}^{s,\mathrm{p}} = 0$ and $\mathcal{J}^{\eta,\mathrm{p}} = 0$.

For the three dissipative effects discussed above, the question arises whether the corresponding force-flux relations are or should be coupled. In the above treatment, it is assumed that the force-flux relation for heat conduction ("h") is not directly coupled to the force-flux relations for heat exchange ("x") and viscoplastic flow ("p"), implying that the latter two are not significantly affected by spatial inhomogeneities in the temperatures. However, the heat exchange ("x") and viscoplastic effects ("p") are mutually coupled through a (non-zero) choice for the tensor $\Omega_{\alpha\beta}$.

3.2.4   Complete dynamic model

The full set of evolution equations (2.1) is obtained by combining the reversible (3.5) and irreversible (3.12) contributions. Using the constitutive relations for the heat transfer (3.16) and the viscoplastic flow (3.18), one finds

$$\partial_t m_\alpha = -\nabla_\gamma\left(m_\alpha v_\gamma\right) + \nabla_\gamma \sigma_{\alpha\gamma}\,, \tag{3.20}$$

$$\partial_t s = -\nabla_\gamma\left(s\,v_\gamma\right) - \frac{1}{T}\nabla_\gamma \mathcal{J}_\gamma^{s,\mathrm{h}} + \frac{1}{T}\mu^{\mathrm{x}}\left(\frac{1}{T} - \frac{1}{\theta}\right)$$

$$+\quad \frac{1}{T}\left(-\Omega_{\mu\nu} + \psi\sigma_{\mu\nu}^{\mathrm{d}}\right)D_{\mu\nu}^{\mathrm{p,d}}\,, \tag{3.21}$$

$$\partial_t \eta = -\nabla_\gamma\left(\eta\,v_\gamma\right) - \frac{1}{\theta}\nabla_\gamma \mathcal{J}_\gamma^{\eta,\mathrm{h}} - \frac{1}{\theta}\mu^{\mathrm{x}}\left(\frac{1}{T} - \frac{1}{\theta}\right)$$

$$+\quad \frac{1}{\theta}\left(\Omega_{\mu\nu} + (1-\psi)\sigma_{\mu\nu}^{\mathrm{d}}\right)D_{\mu\nu}^{\mathrm{p,d}}\,, \tag{3.22}$$

$$\partial_t F_{\alpha\beta}^{\mathrm{e}} = -v_\gamma(\nabla_\gamma F_{\alpha\beta}^{\mathrm{e}}) + \left((\nabla_\mu v_\alpha) - D_{\alpha\mu}^{\mathrm{p,d}}\right)F_{\mu\beta}^{\mathrm{e}}\,, \tag{3.23}$$

with stress tensor $\sigma_{\alpha\gamma}$ defined in (3.6), heat fluxes $\mathcal{J}_\gamma^{s,\mathrm{h}}$ and $\mathcal{J}_\gamma^{\eta,\mathrm{h}}$ given by (3.14), and the traceless plastic strain rate tensor $D_{\alpha\mu}^{\mathrm{p,d}}$, which is the deviatoric part of (3.19). Note that $D_{\alpha\mu}^{\mathrm{p,d}}$ being traceless a posteriori justifies the assumption that $\det \boldsymbol{F}^{\mathrm{e}} = \det \boldsymbol{F}$, and thus for the mass density $\rho = \rho_0/\det \boldsymbol{F}^{\mathrm{e}}$, as discussed in Sec. 3.2.1. For practical applications, the model is completed by making constitutive choices for the internal energy e_t, function ψ, thermal conductivity tensors $\lambda_{\alpha\gamma}^s$ and $\lambda_{\alpha\gamma}^\eta$, heat transfer coefficient μ^{x}, (stress-) relaxation tensor $\Lambda_{\alpha\beta\gamma\varepsilon}$, and the tensor $\Omega_{\alpha\gamma}$, in terms of the system variables $\boldsymbol{\mathcal{X}}$.

While the choice of s and η as dynamic variables for the kinetic and configurational subsystems is convenient from a fundamental modeling viewpoint, practical applications give a preference to formulate the model (3.20)–(3.23) in terms of temperatures, (3.3). There are two main consequences of this change of variables for the above model. First, the stress tensor (3.6) can be cast into the form

$$\sigma_{\alpha\beta} = \rho\,\hat{a}_{,F_{\alpha\varepsilon}^{\mathrm{e}}}\big|_{T,\theta}\,F_{\beta\varepsilon}^{\mathrm{e}} = \sigma_{\alpha\beta}^{e_\mathrm{t}} + \sigma_{\alpha\beta}^{s} + \sigma_{\alpha\beta}^{\eta}\,, \tag{3.24}$$

with $\hat{a} = a/\rho$, and the Helmholtz free energy per unit volume $a = a(T,\theta,\boldsymbol{F}^{\mathrm{e}})$. The latter is the Legendre transform of the internal energy density $e_\mathrm{t} = e_\mathrm{t}(s,\eta,\boldsymbol{F}^{\mathrm{e}})$ [82],

$$a = e_\mathrm{t} - Ts - \theta\eta\,, \tag{3.25}$$

and gives rise to three stress tensor contributions,

$$\sigma^{e_t}_{\alpha\beta} = \rho\,\hat{e}_{t,F^e_{\alpha\varepsilon}}\big|_{T,\theta}\,F^e_{\beta\varepsilon}\,, \tag{3.26}$$

$$\sigma^{s}_{\alpha\beta} = -T\rho\,\hat{s}_{,F^e_{\alpha\varepsilon}}\big|_{T,\theta}\,F^e_{\beta\varepsilon}\,, \tag{3.27}$$

$$\sigma^{\eta}_{\alpha\beta} = -\theta\rho\,\hat{\eta}_{,F^e_{\alpha\varepsilon}}\big|_{T,\theta}\,F^e_{\beta\varepsilon}\,. \tag{3.28}$$

The second major consequence of the change of variables is that the evolutions equations for s and η are replaced by evolution equations for T and θ. Specifically, it can be shown that

$$D_t T = T^{-1}T_{,s}\left(\sigma^{s}_{\alpha\gamma}\nabla_\gamma v_\alpha + T\mathring{s}\right) + \theta^{-1}T_{,\eta}\left(\sigma^{\eta}_{\alpha\gamma}\nabla_\gamma v_\alpha + \theta\mathring{\eta}\right)\,, \tag{3.29}$$

$$D_t \theta = T^{-1}\theta_{,s}\left(\sigma^{s}_{\alpha\gamma}\nabla_\gamma v_\alpha + T\mathring{s}\right) + \theta^{-1}\theta_{,\eta}\left(\sigma^{\eta}_{\alpha\gamma}\nabla_\gamma v_\alpha + \theta\mathring{\eta}\right)\,, \tag{3.30}$$

with $D_t = \partial_t + v_\gamma\nabla_\gamma$ the material (substantial) time derivative, and with the irreversible contributions

$$\begin{aligned}T\mathring{s} &= -\nabla_\gamma\mathcal{J}^{s,h}_\gamma + \mu^x\left(\tfrac{1}{T}-\tfrac{1}{\theta}\right) + \left(\psi\sigma^d_{\mu\nu} - \Omega_{\mu\nu} - \sigma^{s,d}_{\mu\nu}\right)D^p_{\mu\nu}\,,\\ \theta\mathring{\eta} &= -\nabla_\gamma\mathcal{J}^{\eta,h}_\gamma - \mu^x\left(\tfrac{1}{T}-\tfrac{1}{\theta}\right) + \left((1-\psi)\sigma^d_{\mu\nu} + \Omega_{\mu\nu} - \sigma^{\eta,d}_{\mu\nu}\right)D^p_{\mu\nu}\,.\end{aligned} \tag{3.31}$$

Note that the prefactors on the right hand side of (3.29) and (3.30) are generalizations of inverse heat capacities. For example, in the absence of the configurational subsystem (η,θ), $T^{-1}T_{,s}$ reduces to $1/c_v$ with the standard isochoric heat capacity $c_v = Ts_{,T}|_{\boldsymbol{F}^e}$.

In conclusion, when working with the temperatures instead of the entropy densities, the relevant set of equations is given by the dynamics (3.20), (3.23), (3.29), (3.30) with (3.31), with stress tensor $\sigma_{\alpha\gamma}$ (3.24)–(3.28), heat fluxes $\mathcal{J}^{s,h}_\gamma$ and $\mathcal{J}^{\eta,h}_\gamma$ (3.14), and the traceless plastic strain rate tensor $D^{p,d}_{\alpha\mu}$, which is the deviatoric part of (3.19).

3.3   Summary and discussion

The GENERIC framework of nonequilibrium thermodynamics has been used to formulate a model to describe the elasto-viscoplastic deformation of glasses, using the concept of kinetic and configurational subsystems to capture aging as well as mechanical rejuvenation. The closed model has been formulated, with as few assumptions as possible (see comment at the end of Sec. 3.2.2), both in terms of the entropy densities s and η, and in terms of the corresponding temperatures, T and θ.

The evolution equation for the configurational temperature θ, (3.30) with (3.31)$_2$, corresponds to the dynamics discussed in [75, 77, 79, 80]. Particularly, it contains the relaxation of θ towards the kinetic temperature T, which is representative of the aging process towards the equilibrium state $\theta = T$, and accounts for both inter-subsystem and intra-subsystem heat flow. Furthermore, θ is influenced (mechanically rejuvenated) by viscoplastic deformation. In [79], no restriction is made on how the dissipation due to viscoplastic deformation splits onto the kinetic and configurational subsystems. In our case, in analogy, tuning of this split is achieved by the quantities ψ and $\Omega_{\alpha\beta}$, see (3.31). It is pointed out that in contrast to common procedure in the literature, e.g. [77,79,80], we do not assume an additive split of the thermodynamic potential (e_t or a, respectively) into

subsystem contributions, where the latter may not depend on the thermodynamic variable of the other subsystem. We believe that such an assumption would be useful for practical applications, but not for the general model development. Note, that as a consequence of our more general ansatz, the cross-coupling quantity $T_{,\eta} = e_{\mathrm{t},s,\eta} = \theta_{,s}$ is in general non-zero and leads to a nontrivial coupling of the T- and θ-evolution equations (3.29) and (3.30). Finally, we have demonstrated that accounting for mechanical rejuvenation results in a modification of the driving force $(3.19)_2$ for viscoplastic flow, as compared to [34].

For illustration purposes, we consider the above model for homogeneous deformation and constant kinetic temperature T, $D_t T = 0$, to mimic isothermal conditions in an experiment. To proceed, one observes in the evolution equation (3.23) that $D^{\mathrm{p,d}}_{\alpha\mu}$ is the plastic strain rate tensor, and (3.19) shows that this is driven by $\Sigma^{\mathrm{d}}_{\varrho\lambda}$. In modeling glassy polymers, the driving force of glassy polymers (whether aged or rejuvenated) is commonly assumed as $\sigma^{\mathrm{d}}_{\varrho\lambda}$, and therefore it is reasonable to assume that $\Omega_{\varrho\lambda} = \omega\,\sigma^{\mathrm{d}}_{\varrho\lambda}$, with ω a yet unspecified function. This simplifies the above model significantly, since $\Omega_{\varrho\lambda}$ and ψ only appear in the combination $\psi\sigma^{\mathrm{d}}_{\varrho\lambda} - \Omega_{\varrho\lambda} \equiv \zeta\,\sigma^{\mathrm{d}}_{\varrho\lambda}$ with $\zeta \equiv \psi - \omega$. With this, and assuming isotropic material behavior, $\Lambda_{\alpha\beta\varrho\lambda} = \Lambda(\delta_{\alpha\varrho}\delta_{\beta\lambda} + \delta_{\beta\varrho}\delta_{\alpha\lambda})/2$ with $\Lambda \geq 0$, one obtains from (3.19)

$$D^{\mathrm{p,d}}_{\alpha\mu} = D^{\mathrm{p}}_{\alpha\mu} = \Lambda\left(\frac{1}{\theta} + \left(\frac{1}{T} - \frac{1}{\theta}\right)\zeta\right)\sigma^{\mathrm{d}}_{\alpha\mu} \equiv \Lambda'\sigma^{\mathrm{d}}_{\alpha\mu}\,, \tag{3.32}$$

where Λ' depends on a scalar equivalent-stress measure σ_{eq} (see further below), T, and θ. Furthermore, one can use (3.29) with $D_t T = 0$ to re-write (3.30) in the form

$$\begin{aligned} D_t\theta &= \theta^{-1}\left(\theta_{,\eta} - \frac{\theta_{,s}T_{,\eta}}{T_{,s}}\right)\left(\sigma^{\eta}_{\alpha\gamma}\nabla_\gamma v_\alpha - \mu^{\mathrm{x}}\left(\frac{1}{T} - \frac{1}{\theta}\right)\right. \\ &+ \left.\left((1-\zeta)\sigma^{\mathrm{d}}_{\mu\nu} - \sigma^{\eta,\mathrm{d}}_{\mu\nu}\right)D^{\mathrm{p}}_{\mu\nu}\right). \end{aligned} \tag{3.33}$$

Note in this equation that $\theta_{,s} = e_{\mathrm{t},\eta,s} = T_{,\eta}$, which represents a non-trivial coupling of the kinetic and configurational subsystems through the potential e_{t}.

The above simplified model (3.23) with (3.32) and (3.33) is now studied for two scenarios. First, let us consider a sample that is aged under quiescent conditions, for a certain aging time t_{a}. Using (3.33) with $\nabla_\gamma v_\alpha = 0$ and $D^{\mathrm{p}}_{\mu\nu} = 0$, this leads to a certain value for configurational temperature value, $\theta(t_{\mathrm{a}})$, which obviously depends on the choice for the function $\mu^{\mathrm{x}}(\boldsymbol{\mathcal{X}})$. This aged sample is then deformed at a certain imposed $\nabla_\mu v_\alpha$. At the yield point, the imposed deformation is balanced by the plastic strain rate tensor, $D_{\alpha\mu} = D^{\mathrm{p,d}}_{\alpha\mu}$ [93], with symmetric strain rate tensor $D_{\alpha\mu} = (\nabla_\mu v_\alpha)^{\mathrm{sym}}$. Using the common definitions for the equivalent strain rate $\dot{\gamma}_{\mathrm{eq}} = \sqrt{2D_{\mu\nu}D_{\nu\mu}}$ [94] and the equivalent stress $\sigma_{\mathrm{eq}} = \sqrt{\sigma^{\mathrm{d}}_{\mu\nu}\sigma^{\mathrm{d}}_{\nu\mu}/2}$ [62] for isotropic materials, one obtains from (3.32),

$$\dot{\gamma}_{\mathrm{eq}} = 2\Lambda'(\sigma_{\mathrm{eq}}, T, \theta; \zeta)\,\sigma_{\mathrm{eq}}\,, \tag{3.34}$$

where it has been assumed that all kinetics (Λ', and also μ^{x} below) depends on $\boldsymbol{F}^{\mathrm{e}}$ by way of σ_{eq}, and usually Λ' depends strongly on σ_{eq} (cf. Eyring viscosity [61]). Eq. (3.34) can

be used to obtain the yield stress $\sigma_{\mathrm{y}} = \sigma_{\mathrm{eq}}(\dot{\gamma}_{\mathrm{eq}}, T, \theta; \zeta)$. At common deformation rates and due to the small amount of plastic deformation prior to reaching the yield point, it is reasonable to use in (3.34) the value $\theta(t_{\mathrm{a}})$ prior to mechanical deformation, and thus one obtains a relation between the yield stress σ_{y} and the aging time t_{a}. This predicted relation depends on the constitutive choices for both $\mu^{\mathrm{x}}(\sigma_{\mathrm{eq}}, T, \theta)$ and $\Lambda'(\sigma_{\mathrm{eq}}, T, \theta; \zeta)$, and thus a comparison with experimental data for the effect of aging on the yield stress [13, 70] puts a constraint on possible choices for μ^{x} and Λ'.

The second case of interest is that of deforming a sample at constant (equivalent) strain rate beyond its yield point until strain-softening is completed, i.e., until the sample is completely mechanically rejuvenated. Experiments show [13, 71, 72] that this state of the material is independent of the initial age (value of θ) of the sample. In the absence of strain-hardening, this situation is a steady state characterized by $D_{\alpha\mu} = D_{\alpha\mu}^{\mathrm{p,d}}$, and $D_t\theta = 0$. Using these two conditions, the θ-equation (3.33) together with (3.32) reduces to the condition

$$\mu^{\mathrm{x}} \left(\frac{1}{T} - \frac{1}{\theta} \right) = 2(1 - \zeta)\Lambda'\sigma_{\mathrm{eq}}^2 . \tag{3.35}$$

The coupled equations (3.34) and (3.35) can be solved for given temperature T and rate of deformation $\dot{\gamma}_{\mathrm{eq}}$, to obtain the stationary values of the configurational temperature θ and the yield stress $\sigma_{\mathrm{y}} = \sigma_{\mathrm{eq}}$. If this solution is reached out of the full dynamics, and if the steady state solution of (3.34) and (3.35) is indeed unique, one has shown that the steady state is independent of the initial age. Requiring [79] that the rejuvenated value for θ is independent of the applied rate of deformation, $\dot{\gamma}_{\mathrm{eq}}$, puts an additional condition on the constitutive choices for $\mu^{\mathrm{x}}(\sigma_{\mathrm{eq}}, T, \theta)$ and $\Lambda'(\sigma_{\mathrm{eq}}, T, \theta; \zeta)$. This will be discussed in an upcoming publication in more detail.

With respect to the applicability of the approach in this chapter to different material classes, the following two comments are made. First, as far as the distinction of glasses into strong and fragile is concerned [95, 96], this distinction is primarily based on how the viscosity (i.e. internal timescale) depends on temperature. In our approach, this can be specified by an appropriate choice of the kinetic tensor $\Lambda_{\alpha\beta\gamma\varepsilon}$. Any dependence of $\Lambda_{\alpha\beta\gamma\varepsilon}$ on the system variables is admissible, as long as $\Lambda_{\alpha\beta\gamma\varepsilon}$ is symmetric and positive semi-definite. In other words, our current treatment is not restricted to either strong or fragile glasses. As a second point, one might wonder about how the exchange between the kinetic (s) and configurational (η) entropy densities might depend on the type of material. For example, entropy exchange mechanisms could be rather different for metallic (i.e. low-molecular) glasses and polymeric (i.e. high-molecular) glasses. Such differences in exchange mechanisms could be accounted for in our approach e.g. by the choice of the reversible exchange terms (see end of Sec. 3.2.2) and by the choice of the tensor $\Omega_{\alpha\beta}$ (see end of Sec. 3.2.3).

For future work, an in-depth comparison with various approaches in the literature for the thermomechanics of aging glasses is desirable, in order to potentially achieve a unification of approaches, and to make the actual modeling choices more apparent and comparable. In particular, a comparison with the internal-state variable approach in [73], efforts based on configurational (effective) temperature [75–80], and the aging-parameter model in [13, 46, 90] is of interest.

Chapter 4

Two-subsystem thermodynamics for the mechanics of aging amorphous solids

Abstract

The effect of physical aging on the mechanics of amorphous solids as well as mechanical rejuvenation are modeled with nonequilibrium thermodynamics, using the concept of two thermal subsystems, namely a kinetic and a configurational one. Earlier work (Semkiv and Hütter, J. Non-Equilib. Thermodyn. 41(2) (2016), 79–88) is extended to account for a fully general coupling of the two thermal subsystems. This coupling gives rise to hypoelastic-type contributions in the expression for the Cauchy stress tensor, that reduces to the more common hyperelastic case for sufficiently long aging. The general model, particularly the reversible and irreversible couplings between the thermal subsystems, is compared in detail with models in the literature (Boyce *et al.*, Mech. Mater. 7 (1988), 15–33; Buckley *et al.*, J. Mech. Phys. Solids 52 (2004), 2355–2377; Klompen *et al.*, Macromolecules 38 (2005), 6997–7008; Kamrin and Bouchbinder, J. Mech. Phys. Solids 73 (2014), 269–288; Xiao and Nguyen, J. Mech. Phys. Solids 82 (2015), 62–81). It is found that only for the case of Kamrin and Bouchbinder (J. Mech. Phys. Solids 73 (2014), 269–288) there is a nontrivial coupling between the thermal subsystems in the reversible dynamics, for which the Jacobi identity is automatically satisfied. Moreover, in their work as well as in Boyce *et al.* (Mech. Mater. 7 (1988), 15–33), viscoplastic deformation is driven by the deviatoric part of the Cauchy stress tensor, while for Buckley *et al.* (J. Mech. Phys. Solids 52 (2004), 2355–2377) and Xiao and Nguyen (J. Mech. Phys. Solids 82 (2015), 62–81) this is not the case.

4.1   Introduction

The mechanical properties of solids often depend on the way they are produced. For example, in the case of semi-crystalline polymers, the processing conditions determine the crystal structure, which in turn affects, e.g., the yield stress. Also in amorphous solids, i.e., structural glasses, the mechanical properties depend on processing, most prominently on the cooling rate. The difference of amorphous to (semi)crystalline solids is that amorphous solids typically show ongoing changes over extended periods of time. This is because the amorphous solids, being rapidly quenched to temperatures below their glass transition temperature, are manifestly in a nonequilibrium glassy state. While the kinetics in that state is extraordinarily slow, the system still evolves towards lower energy states. With this dynamics, called aging, changes in physical properties of the material can be observed over time. A comprehensive overview over the main physical effects due to aging dynamics in the case of polymers is given in [68, 69]. In particular, the effect of physical aging on the mechanical behavior of glassy polymers has been studied in [11, 13, 46, 70, 90]. The effects of physical aging can (to some extent) be reversed by the application of a significant non-elastic deformation, which coined the term of mechanical rejuvenation [72].

The formal description of aging dynamics often is based on a concept of internal state variables [11], particularly in the form of configurational temperature, first proposed by Tool [74], and then used intensively, e.g. in [75–80, 97]. According to this concept, the amorphous solid is described by two, rather than one, thermal degrees of freedom, namely a kinetic and a configurational one. Generally, the character of these two thermal degrees of freedom is either that of temperature, entropy density, or internal energy density, respectively. While the kinetic (vibrational) degree of freedom accounts for intra-basin thermodynamics, the configurational one describes the inter-basin thermodynamics [81–88]. Models have been developed for the evolution of the kinetic and configurational thermal degrees of freedom [75–80], as well as constitutive expressions have been formulated for a stress tensor and for a plastic flow-rule for the mechanical deformation of aging solids. However, in these models the mutual interaction of the kinetic and configurational subsystems is in general incomplete, as discussed in the sequel of this chapter, and leaves room for further investigation and generalization.

In a recent publication [97], a closed-form dynamic model for the elasto-viscoplastic deformation of aging amorphous solids has been developed, according to nonequilibrium thermodynamic principles and making use of a kinetic and a configurational entropy density. Next to evolution equations for the thermal and mechanical degrees of freedom, constitutive relations for the stress tensor as well as for the plastic flow-rule have been formulated. As elaborated in detail in [97], the split of the energy dissipated by the viscoplastic deformation into the kinetic and configurational thermal subsystems is non-unique from a thermodynamics perspective. It has also been observed that the choice for that split significantly affects the driving force for plastic flow. All this concerns the irreversible dynamics of the model. With respect to the reversible dynamics, no coupling of the kinetic and configurational subsystems, namely the respective entropy densities, has been considered so far.

The main goal of this chapter is, in view of these lessons learned from the irreversible

---

In the presented chapter, only physical aging is discussed, while chemical aging is neglected.

dynamics, to systematically explore the possibilities for letting the kinetic and configurational subsystems interact non-trivially also through the reversible contributions to the dynamics, and to study the ramifications of doing so.

The chapter is organized as follows. The model for the elasto-viscoplastic behaviour of aging amorphous solids is developed (Sec. 4.2), specifically including the nontrivial reversible coupling between the kinetic and configurational degrees of freedom. This general model is then compared in detail with other approaches in the literature, i.e. [11, 46, 75, 79, 80] (Sec. 4.3), before drawing conclusions (Sec. 4.4).

Before starting with the main content, some general comments about the notation used in this chapter. Greek indices are used for Cartesian components, and Einstein's summation convention is used for indices that occur twice. Furthermore, with respect to operators, subscripts α and (α, β) imply contraction with any vector A_α and any tensor $A_{\alpha\beta}$ multiplied from the left, respectively, while subscripts γ and (γ, ε) imply contraction with the vector A_γ and tensor $A_{\gamma\varepsilon}$ multiplied from the right, respectively. With respect to partial derivatives, the quantity $f_{,\mathcal{X}_i}$ stands for the partial derivative of a function f with respect to the variable $\mathcal{X}_i$. Unless stated otherwise, it is tacitly assumed that this derivative is taken at constant $\mathcal{X} \setminus \mathcal{X}_i$, with $\mathcal{X} = (\boldsymbol{m}, s, \eta, \boldsymbol{F}^{\mathrm{e}})$. Finally, $A_{\alpha\beta}^{\mathrm{d}}$ denotes the deviatoric part of the tensor $A_{\alpha\beta}$, i.e., $A_{\alpha\beta}^{\mathrm{d}} \equiv A_{\alpha\beta} - (A_{\mu\mu}/3)\delta_{\alpha\beta}$.

4.2 Dynamic model with general coupling between kinetic and configurational subsystems

4.2.1 Set of variables, and generating functionals

The first step in the model formulation concerns the specification of meaningful dynamic variables, for which evolution equations are sought. To that end, we depart from our earlier results [97], where the elasto-viscoplastic behavior of amorphous materials was studied, with a focus on the effects of physical aging and mechanical rejuvenation. In that work, the set of variables in an Eulerian (i.e. spatial) setting consisted of the momentum density $\boldsymbol{m}$, the elastic part of the deformation gradient, $\boldsymbol{F}^{\mathrm{e}}$, and the entropy densities (per unit volume) of the kinetic- and configurational-subsystems, s and η, respectively. In summary, the complete set of dynamic variables, which shall also be used in this chapter, is thus given by $\mathcal{X} = \{\boldsymbol{m}, s, \eta, \boldsymbol{F}^{\mathrm{e}}\}$.

It should be noted that the case of a single entropy density is equivalent to what has been studied in [32, 34] for describing finite-deformation non-isothermal elasto-viscoplasticity. However, in order to account for the effect of physical aging, also called structural relaxation, a split of that thermal degree of freedom into its kinetic and configurational contributions is considered, in analogy to [77, 79, 80, 85, 87]. While from a practical (interpretation) point of view one might be tempted to use two temperatures instead of two (partial) entropies, this would result in unnecessary technical complications, which would rather disguise the essence of the two-subsystem approach. Therefore, it has been decided on purpose in this chapter to consider the kinetic and configurational subsystem entropies as fundamental variables.

In view of the set of variables $\mathcal{X}$, it is convenient to write the energy and entropy in

the form

$$E = \int \left(\frac{\boldsymbol{m} \cdot \boldsymbol{m}}{2\rho} + e_{\mathrm{t}}(s, \eta, \boldsymbol{F}^{\mathrm{e}}) \right) d^3 \boldsymbol{r} \,, \tag{4.1}$$

$$S = \int s_{\mathrm{t}}(s, \eta) \, d^3 \boldsymbol{r} \,, \tag{4.2}$$

with

$$s_{\mathrm{t}} = s + \eta \tag{4.3}$$

the total entropy density [82]. Specifically, the energy is split into its macroscopic kinetic energy and internal energy parts. The mass density is given by $\rho = \rho_0 / \det \boldsymbol{F}^{\mathrm{e}}$, with ρ_0 the mass density in the undeformed state, in which it is tacitly assumed that all volumetric change is elastic in origin (see further below), i.e. $\det \boldsymbol{F}^{\mathrm{e}} = \det \boldsymbol{F}$ with $\boldsymbol{F}$ the total deformation gradient. Based on (4.1)–(4.2), the functional derivatives become

$$\frac{\delta E}{\delta \boldsymbol{\mathcal{X}}} = \begin{pmatrix} v_\gamma \\ T \\ \theta \\ -\frac{v_\mu v_\mu}{2} \rho_{,F^{\mathrm{e}}_{\gamma\varepsilon}} + e_{\mathrm{t},F^{\mathrm{e}}_{\gamma\varepsilon}} \end{pmatrix}, \tag{4.4}$$

$$\frac{\delta S}{\delta \boldsymbol{\mathcal{X}}} = \begin{pmatrix} 0 \\ 1 \\ 1 \\ 0 \end{pmatrix}, \tag{4.5}$$

with velocity $v_\gamma = m_\gamma / \rho$, and with $\rho_{,F^{\mathrm{e}}_{\gamma\varepsilon}} = -\rho F^{\mathrm{e},-1}_{\varepsilon\gamma}$. Furthermore, we have introduced the kinetic (T) and configurational (θ) temperatures, respectively, according to

$$T = e_{\mathrm{t},s} \,, \tag{4.6}$$
$$\theta = e_{\mathrm{t},\eta} \,, \tag{4.7}$$

which have also been used frequently in the literature for modeling the two-subsystem thermodynamics [74–80, 82].

4.2.2   Reversible dynamics

In order to specify the reversible dynamics $(2.2)_1$, a choice needs to be made for the Poisson operator $\boldsymbol{\mathcal{L}}$. To that end, we depart from our earlier results [97], where the evolution equation for $\boldsymbol{\mathcal{X}}$ has been formulated. In that earlier model, there is no reversible exchange between the subsystem entropy densities s and η, since they evolve simply according to $\partial_t s|_{\mathrm{rev}} = -\nabla_\gamma (s v_\gamma)$ and $\partial_t \eta|_{\mathrm{rev}} = -\nabla_\gamma (\eta v_\gamma)$. However, one can imagine that in general there is a coupling between the kinetic and configurational degrees of freedom during an imposed (macroscopically affine) deformation. In the language of the potential energy landscape, this would mean that when deforming the system, changes in the intra-basin and the inter-basin distributions would result that are non-trivially coupled. It is thus of interest to examine the possibility of a coupling between the subsystem entropy densities upon (reversible) deformation. While the evolution equation for the

total entropy density, $\partial_t s_t|_{\text{rev}} = -\nabla_\gamma(s_t v_\gamma)$, will be unaltered, specifically the possibility of an exchange term between s and η is sought.

Since the coupling between s and η relates to the macroscopic velocity field $\boldsymbol{v}$ and in view of (4.4), it seems natural to incorporate an exchange between s and η via the first column of $\boldsymbol{\mathcal{L}}$. It is thus suggested that the Poisson operator in [97] is modified in its first column and, due to the anti-symmetry condition (2.5a), also in the first row, namely [97]

$$\boldsymbol{\mathcal{L}} = \begin{pmatrix} \mathcal{L}^{(mm)}_{\alpha\gamma} & \mathcal{L}^{(ms)}_\alpha & \mathcal{L}^{(m\eta)}_\alpha & \mathcal{L}^{(mF)}_{\alpha\gamma\varepsilon} \\ \mathcal{L}^{(sm)}_\gamma & 0 & 0 & 0 \\ \mathcal{L}^{(\eta m)}_\gamma & 0 & 0 & 0 \\ \mathcal{L}^{(Fm)}_{\alpha\beta\gamma} & 0 & 0 & 0 \end{pmatrix}, \tag{4.8}$$

with the following operators

$$\mathcal{L}^{(mm)}_{\alpha\gamma} \equiv -\nabla_\gamma m_\alpha - m_\gamma \nabla_\alpha, \tag{4.9}$$

$$\mathcal{L}^{(ms)}_\alpha \equiv -s\nabla_\alpha - \nabla_\mu Y_{\alpha\mu}, \tag{4.10}$$

$$\mathcal{L}^{(m\eta)}_\alpha \equiv -\eta\nabla_\alpha + \nabla_\mu Y_{\alpha\mu}, \tag{4.11}$$

$$\mathcal{L}^{(mF)}_{\alpha\gamma\varepsilon} \equiv (\nabla_\alpha F^{\text{e}}_{\gamma\varepsilon}) + \nabla_\mu F^{\text{e}}_{\mu\varepsilon}\delta_{\alpha\gamma}, \tag{4.12}$$

$$\mathcal{L}^{(sm)}_\gamma \equiv -\nabla_\gamma s - Y_{\gamma\mu}\nabla_\mu, \tag{4.13}$$

$$\mathcal{L}^{(\eta m)}_\gamma \equiv -\nabla_\gamma \eta + Y_{\gamma\mu}\nabla_\mu, \tag{4.14}$$

$$\mathcal{L}^{(Fm)}_{\alpha\beta\gamma} \equiv -(\nabla_\gamma F^{\text{e}}_{\alpha\beta}) + F^{\text{e}}_{\mu\beta}\nabla_\mu\delta_{\alpha\gamma}. \tag{4.15}$$

The $\boldsymbol{Y}$-related contributions in the first column represent the exchange between the subsystem entropies, since the reversible contributions to their evolution (2.2)$_1$ with Poisson operator (4.8) and energy gradient (4.4) becomes

$$\partial_t s|_{\text{rev}} = -\nabla_\gamma(sv_\gamma) - Y_{\gamma\mu}(\nabla_\mu v_\gamma), \tag{4.16}$$

$$\partial_t \eta|_{\text{rev}} = -\nabla_\gamma(\eta v_\gamma) + Y_{\gamma\mu}(\nabla_\mu v_\gamma). \tag{4.17}$$

The exchange term is proportional to the velocity gradient, i.e., homogeneous (bulk) translations do not lead to any entropy exchange, as required. This serves as a posteriori explanation of the structure of the $\boldsymbol{Y}$-related contributions in the first column of (4.8). Due to the anti-symmetry condition (2.5a), the $\boldsymbol{Y}$-related contributions in the first row of (4.8) can be derived. For this Poisson operator, also the evolution equations for the momentum density and for the elastic part of the deformation gradient can be determined according to (2.5a) with Poisson operator (4.8) and energy gradient (4.4),

$$\partial_t m_\alpha|_{\text{rev}} = -\nabla_\gamma(m_\alpha v_\gamma) + \nabla_\gamma \sigma_{\alpha\gamma}, \tag{4.18}$$

$$\partial_t F^{\text{e}}_{\alpha\beta}|_{\text{rev}} = -v_\gamma(\nabla_\gamma F^{\text{e}}_{\alpha\beta}) + (\nabla_\mu v_\alpha)F^{\text{e}}_{\mu\beta}, \tag{4.19}$$

which is as expected. However, it should be noted that the Cauchy stress tensor contains a contribution related to the exchange tensor $\boldsymbol{Y}$,

$$\sigma_{\alpha\gamma} = (e_t - Ts - \theta\eta)\delta_{\alpha\gamma} + e_{t,F^{\text{e}}_{\alpha\varepsilon}}F^{\text{e}}_{\gamma\varepsilon} + (\theta - T)Y_{\alpha\gamma} \tag{4.20}$$

$$= \rho\,\hat{e}_{t,F^{\text{e}}_{\alpha\varepsilon}}\big|_{\hat{s},\hat{\eta}}\,F^{\text{e}}_{\gamma\varepsilon} + (\theta - T)Y_{\alpha\gamma}, \tag{4.21}$$

with the abbreviation $\hat{f} = f/\rho$ for any quantity f. This implies that the Cauchy stress tensor carries a signature of the entropy exchange, however, (4.20) suggests that this contribution vanishes as the system tends to thermal equilibrium, $T \simeq \theta$. This issue will be discussed below in more detail. If the system is not in thermal equilibrium, the stress tensor is not simply related to the derivative of the thermodynamic potential with respect to deformation (i.e. hyperelastic type), but rather it contains also another contribution, akin to hypoelasticity [92].

As far as the conditions (2.4a), (2.5a) and (2.6) are concerned, it is clear from the above that the anti-symmetry condition (2.5a) is satisfied by construction. Furthermore, it can be shown readily that the degeneracy condition (2.4a) is fulfilled. One can thus concentrate on the Jacobi identity (2.6), which puts a constraint on the tensor $Y_{\alpha\beta}$, namely

$$
\left(\hat{Y}_{\gamma\beta} \delta_{\alpha\delta} - \hat{Y}_{\alpha\delta} \delta_{\gamma\beta} \right) \ + \ \left(\hat{Y}_{\gamma\delta} \frac{\partial \hat{Y}_{\alpha\beta}}{\partial \hat{\eta}} \bigg|_{\hat{s}_{\mathrm{t}}, \boldsymbol{F}^{\mathrm{e}}} - \hat{Y}_{\alpha\beta} \frac{\partial \hat{Y}_{\gamma\delta}}{\partial \hat{\eta}} \bigg|_{\hat{s}_{\mathrm{t}}, \boldsymbol{F}^{\mathrm{e}}} \right)
$$
$$
+ \ \left(\frac{\partial \hat{Y}_{\alpha\beta}}{\partial F^{\mathrm{e}}_{\gamma\varepsilon}} \bigg|_{\hat{s}_{\mathrm{t}}, \hat{\eta}} F^{\mathrm{e}}_{\delta\varepsilon} - \frac{\partial \hat{Y}_{\gamma\delta}}{\partial F^{\mathrm{e}}_{\alpha\varepsilon}} \bigg|_{\hat{s}_{\mathrm{t}}, \hat{\eta}} F^{\mathrm{e}}_{\beta\varepsilon} \right) = 0 \,. \qquad (4.22)
$$

For technical convenience, in all partial derivatives in relation to the Jacobi calculation here, $\hat{s}_{\mathrm{t}}$ is used as a thermal variable rather than $\hat{s}$, together with $\hat{\eta}$. To proceed, it is noted that the requirement of a symmetric stress tensor implies that also $Y_{\alpha\beta}$ is symmetric. Therefore, one can write

$$
\hat{Y}_{\alpha\beta} = F^{\mathrm{e}}_{\alpha\gamma} \hat{\bar{Y}}_{\gamma\delta} F^{\mathrm{e}}_{\beta\delta} \,, \qquad (4.23)
$$

with a symmetric tensor $\hat{\bar{Y}}_{\alpha\beta}$. Note that this factorization (4.23) is without loss of generality, as long as $F^{\mathrm{e}}_{\alpha\beta}$ is invertible. Inserting this factorization into (4.22), one obtains

$$
\left(\hat{\bar{Y}}_{\alpha\beta} \frac{\partial \hat{\bar{Y}}_{\gamma\delta}}{\partial \hat{\eta}} \bigg|_{\hat{s}_{\mathrm{t}}, \boldsymbol{F}^{\mathrm{e}}} - \hat{\bar{Y}}_{\gamma\delta} \frac{\partial \hat{\bar{Y}}_{\alpha\beta}}{\partial \hat{\eta}} \bigg|_{\hat{s}_{\mathrm{t}}, \boldsymbol{F}^{\mathrm{e}}} \right)
$$
$$
+ \ \left(F^{\mathrm{e},-1}_{\alpha\varepsilon} \frac{\partial \hat{\bar{Y}}_{\gamma\delta}}{\partial F^{\mathrm{e}}_{\varepsilon\beta}} \bigg|_{\hat{s}_{\mathrm{t}}, \hat{\eta}} - F^{\mathrm{e},-1}_{\gamma\varepsilon} \frac{\partial \hat{\bar{Y}}_{\alpha\beta}}{\partial F^{\mathrm{e}}_{\varepsilon\delta}} \bigg|_{\hat{s}_{\mathrm{t}}, \hat{\eta}} \right) = 0 \,. \qquad (4.24)
$$

While this condition (4.24) holds in full generality, we now proceed to discuss it by making two assumptions, for the purpose of illustration. The first assumption is that $\hat{\bar{Y}}_{\alpha\beta}$ depends on $F^{\mathrm{e}}_{\mu\nu}$ only through the right Cauchy-Green strain tensor $C^{\mathrm{e}}_{\gamma\delta} = F^{\mathrm{e}}_{\mu\gamma} F^{\mathrm{e}}_{\mu\delta}$. Making use of the general relation $\partial g / \partial F^{\mathrm{e}}_{\alpha\beta} = 2 F^{\mathrm{e}}_{\alpha\gamma} (\partial g / \partial C^{\mathrm{e}}_{\gamma\beta})$ for any function g of the right Cauchy-Green strain tensor, the condition (4.24) turns into

$$
\left(\hat{\bar{Y}}_{\alpha\beta} \frac{\partial \hat{\bar{Y}}_{\gamma\delta}}{\partial \hat{\eta}} \bigg|_{\hat{s}_{\mathrm{t}}, \boldsymbol{C}^{\mathrm{e}}} - \hat{\bar{Y}}_{\gamma\delta} \frac{\partial \hat{\bar{Y}}_{\alpha\beta}}{\partial \hat{\eta}} \bigg|_{\hat{s}_{\mathrm{t}}, \boldsymbol{C}^{\mathrm{e}}} \right) + 2 \left(\frac{\partial \hat{\bar{Y}}_{\gamma\delta}}{\partial C^{\mathrm{e}}_{\alpha\beta}} \bigg|_{\hat{s}_{\mathrm{t}}, \hat{\eta}} - \frac{\partial \hat{\bar{Y}}_{\alpha\beta}}{\partial C^{\mathrm{e}}_{\gamma\delta}} \bigg|_{\hat{s}_{\mathrm{t}}, \hat{\eta}} \right) = 0 \,. \qquad (4.25)
$$

The second assumption concerns the tensorial character of $\hat{\bar{Y}}_{\alpha\beta}$. Particularly, it is assumed that $\hat{\bar{Y}}_{\alpha\beta}$ is of quasi-potential form, i.e. $\hat{\bar{Y}}_{\alpha\beta} = (1/y_1)(\partial y_2 / \partial C^{\mathrm{e}}_{\alpha\beta})|_{\hat{s}_{\mathrm{t}}, \hat{\eta}}$ with y_1 and y_2

two scalar-valued functions of the variables $\hat{s}_{\mathrm{t}}$, $\hat{\eta}$, and $\boldsymbol{C}^{\mathrm{e}}$. Doing so, the condition (4.25) becomes

$$
\left.\frac{\partial y_2}{\partial C^{\mathrm{e}}_{\alpha\beta}}\right|_{\hat{s}_{\mathrm{t}},\hat{\eta}} \left.\frac{\partial}{\partial C^{\mathrm{e}}_{\gamma\delta}}\right|_{\hat{s}_{\mathrm{t}},\hat{\eta}} \left(\left.\frac{\partial y_2}{\partial\hat{\eta}}\right|_{\hat{s}_{\mathrm{t}},\boldsymbol{C}^{\mathrm{e}}} + 2y_1 \right)
$$
$$
= \left.\frac{\partial y_2}{\partial C^{\mathrm{e}}_{\gamma\delta}}\right|_{\hat{s}_{\mathrm{t}},\hat{\eta}} \left.\frac{\partial}{\partial C^{\mathrm{e}}_{\alpha\beta}}\right|_{\hat{s}_{\mathrm{t}},\hat{\eta}} \left(\left.\frac{\partial y_2}{\partial\hat{\eta}}\right|_{\hat{s}_{\mathrm{t}},\boldsymbol{C}^{\mathrm{e}}} + 2y_1 \right) . \tag{4.26}
$$

This condition can be processed further if the functions y_1 and y_2 depend on $\boldsymbol{C}^{\mathrm{e}}$ only through the three invariants $J_1 = \mathrm{tr}\boldsymbol{C}^{\mathrm{e}}$, $J_2 = \ln\det\boldsymbol{C}^{\mathrm{e}}$, and $J_3 = -\mathrm{tr}\boldsymbol{C}^{\mathrm{e},-1}$ of $\boldsymbol{C}^{\mathrm{e}}$, that have the useful property $\partial J_k/\partial\boldsymbol{C}^{\mathrm{e}} = \boldsymbol{C}^{\mathrm{e},1-k}$ [29, 98]. In this case, the non-trivial part of condition (4.26) can be cast into the form

$$
\left.\frac{\partial y_2}{\partial J_k}\right|_{\hat{s}_{\mathrm{t}},\hat{\eta},\bar{J}_k} \left.\frac{\partial}{\partial J_l}\right|_{\hat{s}_{\mathrm{t}},\hat{\eta},\bar{J}_l} \left(\left.\frac{\partial y_2}{\partial\hat{\eta}}\right|_{\hat{s}_{\mathrm{t}},\boldsymbol{J}} + 2y_1 \right)
$$
$$
= \left.\frac{\partial y_2}{\partial J_l}\right|_{\hat{s}_{\mathrm{t}},\hat{\eta},\bar{J}_l} \left.\frac{\partial}{\partial J_k}\right|_{\hat{s}_{\mathrm{t}},\hat{\eta},\bar{J}_k} \left(\left.\frac{\partial y_2}{\partial\hat{\eta}}\right|_{\hat{s}_{\mathrm{t}},\boldsymbol{J}} + 2y_1 \right) , \quad \text{for all } k \neq l , \tag{4.27}
$$

with $\boldsymbol{J} = (J_1, J_2, J_3)$ and $\bar{J}_k = \boldsymbol{J} \setminus J_k$.

It is straightforward to show that (4.27) is indeed a non-trivial condition. For example for $y_1 \equiv 1$, one concludes from (4.27) that only if y_2 depends only on a single invariant J_k (e.g. on $\det\boldsymbol{C}^{\mathrm{e}}$, by way of $\rho = \rho_0/\sqrt{\det\boldsymbol{C}^{\mathrm{e}}}$, which implies $Y_{\alpha\beta} \propto \delta_{\alpha\beta}$), the Jacobi identity is trivially satisfied. In contrast, if y_2 depends on more than one of the invariants of $\boldsymbol{C}^{\mathrm{e}}$, the Jacobi identity puts a constraint on the function y_2. It is mentioned that another example where the Jacobi identity imposes non-trivial constraints on the dynamics has been discussed in the context of complex fluids [29, 98].

This elaboration of the implications of the Jacobi identity on the choice of the tensor $\boldsymbol{Y}$ is concluded by a comment about the stress tensor. Using the representation (4.23), if $\hat{\boldsymbol{Y}}$ is of quasi-potential form, and if $\hat{e}_{\mathrm{t}}$ depends on $\boldsymbol{F}^{\mathrm{e}}$ only through $\boldsymbol{C}^{\mathrm{e}}$, the stress tensor (4.20) can be written as

$$
\sigma_{\alpha\beta} = \rho F^{\mathrm{e}}_{\alpha\gamma} \left(2\hat{e}_{\mathrm{t},C^{\mathrm{e}}_{\gamma\delta}}\Big|_{\hat{s},\hat{\eta}} + \frac{\theta - T}{y_1} \, y_{2,C^{\mathrm{e}}_{\gamma\delta}}\Big|_{\hat{s},\hat{\eta}} \right) F^{\mathrm{e}}_{\beta\delta} . \tag{4.28}
$$

It is important to note that $(\theta - T)/y_1$ is in general a function of $\boldsymbol{C}^{\mathrm{e}}$, $\hat{s}$, and $\hat{\eta}$, also by virtue of the definitions (4.6)–(4.7). Therefore, the expression in the parenthesis in (4.28) can not always be written as the $C^{\mathrm{e}}_{\gamma\delta}$-derivative of a potential.

4.2.3 Irreversible dynamics

The irreversible dynamics, due to $(2.2)_2$, involves the friction matrix $\boldsymbol{\mathcal{M}}$ and is driven by the entropy gradient $\delta S/\delta\boldsymbol{\mathcal{X}}$. While the previous section explained in detail how to account for entropy-exchange due to reversible dynamics, it is pointed out that entropy-exchange due to irreversible dynamics has been accounted for already in [97]. For this reason, only the main results about the irreversible dynamics are summarized here as far as

they are relevant for this chapter, while the reader interested in the full details is referred to [97].

Four different irreversible processes are accounted for in this model. These are specifically: heat conduction in each of two thermal subsystems (kinetic and configurational), heat exchange between the subsystems, and viscoplastic deformation. Correspondingly, for each of these four processes, the are thermodynamic fluxes, namely $\mathcal{J}^s$ and $\mathcal{J}^\eta$ for the bulk subsystem heat fluxes, $\mathcal{J}^\Delta$ for the subsystem exchange heat flux, and $\mathcal{J}^{F^e}$ for the viscoplastic deformation, related to the irreversible dynamics of $\boldsymbol{F}^e$. It has been shown earlier that these thermodynamic fluxes result in irreversible dynamics of $\boldsymbol{\mathcal{X}}$, according to $(2.2)_2$, of the form [97]

$$\partial_t m_\alpha|_{\text{irr}} = 0\,, \tag{4.29}$$

$$\partial_t s|_{\text{irr}} = -\frac{1}{T}\nabla_\gamma \mathcal{J}_\gamma^s + \frac{1}{T}\mathcal{J}^\Delta - \frac{\psi}{T}P_{\gamma\varepsilon\mu\nu}e_{\text{t},F_{\mu\nu}^e}\mathcal{J}_{\gamma\varepsilon}^{F^e}\,, \tag{4.30}$$

$$\partial_t \eta|_{\text{irr}} = -\frac{1}{\theta}\nabla_\gamma \mathcal{J}_\gamma^\eta - \frac{1}{\theta}\mathcal{J}^\Delta - \frac{(1-\psi)}{\theta}P_{\gamma\varepsilon\mu\nu}e_{\text{t},F_{\mu\nu}^e}\mathcal{J}_{\gamma\varepsilon}^{F^e}\,, \tag{4.31}$$

$$\partial_t F_{\alpha\beta}^e|_{\text{irr}} = P_{\gamma\varepsilon\alpha\beta}\mathcal{J}_{\gamma\varepsilon}^{F^e}\,, \tag{4.32}$$

which satisfies the degeneracy condition (2.4b). The parameter ψ defines how the dissipation caused by viscoplastic deformation is distributed among the kinetic and configurational entropies. The tensor $P_{\gamma\varepsilon\alpha\beta}$ is a projection defined by $P_{\gamma\varepsilon\alpha\beta} = \delta_{\alpha\gamma}\delta_{\beta\varepsilon} - (1/3)F_{\varepsilon\gamma}^{e,-1}F_{\alpha\beta}^e$ to ensure that the viscoplastic change to $\boldsymbol{F}^e$ is indeed isochoric [34].

The evolution equations (4.29)–(4.32) highlight the physics of thermodynamic fluxes, for which the constitutive expressions are required in order to complete the model formulation. Specifying suitable constitutive relations for these thermodynamic fluxes (see [97] for details), the irreversible contributions to the evolution equation can be written in the form

$$\partial_t m_\alpha|_{\text{irr}} = 0\,, \tag{4.33}$$

$$\partial_t s|_{\text{irr}} = -\frac{1}{T}\nabla_\gamma\left(-\lambda_{\gamma\delta}^s\nabla_\delta T\right) + \frac{1}{T}\mu^{\text{x}}\left(\frac{1}{T}-\frac{1}{\theta}\right) - \frac{1}{T}Z_{\mu\nu}D_{\mu\nu}^{\text{p,d}}\,, \tag{4.34}$$

$$\partial_t \eta|_{\text{irr}} = -\frac{1}{\theta}\nabla_\gamma\left(-\lambda_{\gamma\delta}^\eta\nabla_\delta\theta\right) - \frac{1}{\theta}\mu^{\text{x}}\left(\frac{1}{T}-\frac{1}{\theta}\right)$$
$$+ \frac{1}{\theta}\left(Z_{\mu\nu} + \left[e_{\text{t},F_{\mu\varepsilon}^e}F_{\nu\varepsilon}^e\right]^{\text{d}}\right)D_{\mu\nu}^{\text{p,d}}\,, \tag{4.35}$$

$$\partial_t F_{\alpha\beta}^e|_{\text{irr}} = -D_{\alpha\mu}^{\text{p,d}}F_{\mu\beta}^e\,. \tag{4.36}$$

The thermal conductivities for the two subsystems are denoted by $\boldsymbol{\lambda}^s$ and $\boldsymbol{\lambda}^\eta$, both of which must be symmetric and positive semi-definite to ensure the conditions (2.5b) and (2.5c). Similarly, the quantity μ^{x}, which describes the heat transfer between the two subsystems, must be non-negative. The quantity $D_{\alpha\beta}^{\text{p,d}}$ is the deviatoric part of

$$D_{\alpha\beta}^{\text{p}} = \Lambda_{\alpha\beta\gamma\delta}\Sigma_{\gamma\delta}^{\text{d}}\,, \tag{4.37}$$

driven by the stress-like quantity

$$\Sigma_{\gamma\delta}^{\text{d}} = \frac{1}{\theta}[e_{\text{t},F_{\gamma\varepsilon}^e}F_{\delta\varepsilon}^e]^{\text{d}} - \left(\frac{1}{T}-\frac{1}{\theta}\right)Z_{\gamma\delta}\,. \tag{4.38}$$

The fact that $\Sigma_{\gamma\delta}^{\mathrm{d}}$ is deviatoric implies that also $Z_{\gamma\delta}$ must be a traceless tensor, which is tacitly used throughout this chapter. In order to comply with the condition for symmetry (2.5b), the tensor $\Lambda_{\alpha\beta\gamma\delta}$ must be symmetric, i.e., $\Lambda_{\alpha\beta\gamma\delta} = \Lambda_{\gamma\delta\alpha\beta}$, and furthermore we impose $\Lambda_{\alpha\beta\gamma\delta} = \Lambda_{\beta\alpha\gamma\delta} = \Lambda_{\beta\alpha\delta\gamma}$; the positive semi-definiteness condition (2.5c) is guaranteed by requiring $A_{\alpha\beta}\Lambda_{\alpha\beta\gamma\delta}A_{\gamma\delta} \geq 0$ for any tensor $A_{\alpha\beta}$. Based on the evolution equation (4.36) it can be concluded that $D_{\alpha\beta}^{\mathrm{p,d}}$ stands for the plastic strain-rate tensor.

The quantity $Z_{\mu\nu}$ (which contains the effect of ψ discussed earlier) in the evolution equations for the kinetic and configurational entropy densities, (4.34) and (4.35), describes the split of the dissipation due to viscoplastic deformation among the two (partial) entropies. While the specification of this split is the main purpose of $Z_{\mu\nu}$, it is worthy to note that nonequilibrium thermodynamics (i.e. the conditions (2.4b), (2.5b) and (2.5c)) requires that $Z_{\mu\nu}$ also occurs in the driving force for viscoplastic deformation $\Sigma_{\varrho\lambda}^{\mathrm{d}}$, see (4.38).

4.2.4 Complete dynamic model, and its temperature and energy reformulations

Combining the results of the previous subsections, the complete set of evolution equations, (2.1) together with (2.2), one finds

$$\partial_t m_\alpha = -\nabla_\gamma (m_\alpha v_\gamma) + \nabla_\gamma \sigma_{\alpha\gamma}, \tag{4.39}$$

$$\partial_t s = -\nabla_\gamma (s\, v_\gamma) - Y_{\gamma\mu} (\nabla_\mu v_\gamma) - \frac{1}{T}\nabla_\gamma \left(-\lambda_{\gamma\delta}^s \nabla_\delta T\right)$$
$$+ \frac{1}{T}\mu^{\mathrm{x}} \left(\frac{1}{T} - \frac{1}{\theta}\right) - \frac{1}{T} Z_{\mu\nu} D_{\mu\nu}^{\mathrm{p,d}}, \tag{4.40}$$

$$\partial_t \eta = -\nabla_\gamma (\eta\, v_\gamma) + Y_{\gamma\mu} (\nabla_\mu v_\gamma) - \frac{1}{\theta}\nabla_\gamma \left(-\lambda_{\gamma\delta}^\eta \nabla_\delta \theta\right)$$
$$- \frac{1}{\theta}\mu^{\mathrm{x}} \left(\frac{1}{T} - \frac{1}{\theta}\right) + \frac{1}{\theta} \left(Z_{\mu\nu} + \left[e_{\mathrm{t},F_{\mu\varepsilon}^{\mathrm{e}}} F_{\nu\varepsilon}^{\mathrm{e}}\right]^{\mathrm{d}}\right) D_{\mu\nu}^{\mathrm{p,d}}, \tag{4.41}$$

$$\partial_t F_{\alpha\beta}^{\mathrm{e}} = -v_\gamma (\nabla_\gamma F_{\alpha\beta}^{\mathrm{e}}) + \left((\nabla_\mu v_\alpha) - D_{\alpha\mu}^{\mathrm{p,d}}\right) F_{\mu\beta}^{\mathrm{e}}, \tag{4.42}$$

with the Cauchy stress tensor $\sigma_{\alpha\gamma}$ given by (4.20), and the traceless plastic strain rate tensor $D_{\alpha\mu}^{\mathrm{p,d}}$, which is the deviatoric part of (4.37), with driving force (4.38). The fact that the plastic strain-rate tensor is traceless serves, in hindsight, as a justification of the assumption that the viscoplastic deformation is isochoric, and therefore one can indeed use $\rho = \rho_0/\det \boldsymbol{F}^{\mathrm{e}}$ for the mass density, as discussed in Sec. 4.2.1.

To make the proposed model suitable for practical applications, constitutive choices need to be made for the static aspects (namely e_{t}), for the transport/relaxation coefficients (namely $\lambda_{\alpha\gamma}^s$, $\lambda_{\alpha\gamma}^\eta$, μ^{x}, and $\Lambda_{\alpha\beta\gamma\varepsilon}$), and for the quantities that regulate the exchange and coupling between the thermodynamic subsystems (namely $Y_{\alpha\beta}$ and $Z_{\alpha\beta}$), in terms of the system variables $\boldsymbol{\mathcal{X}}$. Particularly, $Y_{\alpha\beta}$ and $Z_{\alpha\beta}$ are of interest in this chapter, and will be discussed in the following section in more detail, when comparing our model with other models in the literature.

Similar to [97], to simplify the comparison with the literature, it is useful to transition from the entropy densities s and η as dynamic variables to other two equivalent variables, for example the temperatures, (4.6)–(4.7). There are two main consequences of this

change of variables for the above model. First, the stress tensor (4.20) can be expressed in terms of the Helmholtz free energy per unit volume $a = a(T, \theta, \boldsymbol{F}^{\mathrm{e}})$, which is the Legendre transform of the internal energy density $e_{\mathrm{t}} = e_{\mathrm{t}}(s, \eta, \boldsymbol{F}^{\mathrm{e}})$ [82]. If in addition a split of the internal energy e_{t} into its kinetic (e) and configurational (ϵ) parts, analogous to (4.3),

$$e_{\mathrm{t}} = e + \epsilon\,, \tag{4.43}$$

is introduced for later convenience, one finds for the Helmholtz free energy

$$a = e + \epsilon - Ts - \theta\eta\,. \tag{4.44}$$

With this, it can be shown that the stress tensor (4.20) can be written in the form

$$
\begin{aligned}
\sigma_{\alpha\beta} &= \rho\,\hat{a}_{,F^{\mathrm{e}}_{\alpha\varepsilon}}\big|_{T,\theta}\,F^{\mathrm{e}}_{\beta\varepsilon} + (\theta - T)Y_{\alpha\beta} \\
&= \sigma^{e}_{\alpha\beta} + \sigma^{\epsilon}_{\alpha\beta} + \sigma^{s}_{\alpha\beta} + \sigma^{\eta}_{\alpha\beta} + \sigma^{[s\eta]s}_{\alpha\beta} + \sigma^{[s\eta]\eta}_{\alpha\beta}\,,
\end{aligned}
\tag{4.45}
$$

with $\hat{a} = a/\rho$, and the six stress tensor contributions defined by

$$
\begin{array}{ll}
\sigma^{e}_{\alpha\beta} = \rho\,\hat{e}_{,F^{\mathrm{e}}_{\alpha\varepsilon}}\big|_{T,\theta}\,F^{\mathrm{e}}_{\beta\varepsilon}\,, & \sigma^{\epsilon}_{\alpha\beta} = \rho\,\hat{\epsilon}_{,F^{\mathrm{e}}_{\alpha\varepsilon}}\big|_{T,\theta}\,F^{\mathrm{e}}_{\beta\varepsilon}\,, \tag{4.46}
\end{array}
$$

$$
\begin{array}{ll}
\sigma^{s}_{\alpha\beta} = -T\rho\,\hat{s}_{,F^{\mathrm{e}}_{\alpha\varepsilon}}\big|_{T,\theta}\,F^{\mathrm{e}}_{\beta\varepsilon}\,, & \sigma^{\eta}_{\alpha\beta} = -\theta\rho\,\hat{\eta}_{,F^{\mathrm{e}}_{\alpha\varepsilon}}\big|_{T,\theta}\,F^{\mathrm{e}}_{\beta\varepsilon}\,, \tag{4.47}
\end{array}
$$

$$
\begin{array}{ll}
\sigma^{[s\eta]s}_{\alpha\beta} = -TY_{\alpha\beta}\,, & \sigma^{[s\eta]\eta}_{\alpha\beta} = \theta Y_{\alpha\beta}\,. \tag{4.48}
\end{array}
$$

The second major consequence of the transition $(s, \eta) \to (T, \theta)$ is the replacement of (4.40) and (4.41) by evolution equations for the two temperatures. Specifically, it can be shown that

$$
\begin{aligned}
D_t T &= T^{-1}T_{,s}\left[\left(\sigma^{s}_{\alpha\gamma} + \sigma^{[s\eta]s}_{\alpha\gamma}\right)\nabla_\gamma v_\alpha + T\mathring{s}\right] \\
&+ \theta^{-1}T_{,\eta}\left[\left(\sigma^{\eta}_{\alpha\gamma} + \sigma^{[s\eta]\eta}_{\alpha\gamma}\right)\nabla_\gamma v_\alpha + \theta\mathring{\eta}\right]\,,
\end{aligned}
\tag{4.49}
$$

$$
\begin{aligned}
D_t \theta &= T^{-1}\theta_{,s}\left[\left(\sigma^{s}_{\alpha\gamma} + \sigma^{[s\eta]s}_{\alpha\gamma}\right)\nabla_\gamma v_\alpha + T\mathring{s}\right] \\
&+ \theta^{-1}\theta_{,\eta}\left[\left(\sigma^{\eta}_{\alpha\gamma} + \sigma^{[s\eta]\eta}_{\alpha\gamma}\right)\nabla_\gamma v_\alpha + \theta\mathring{\eta}\right]\,,
\end{aligned}
\tag{4.50}
$$

with $D_t = \partial_t + v_\gamma\nabla_\gamma$ the material (substantial) time-derivative, and with the irreversible contributions

$$
T\mathring{s} = -\nabla_\gamma\mathcal{J}^{s,\mathrm{h}}_\gamma + \mu^{\mathrm{x}}\left(\frac{1}{T} - \frac{1}{\theta}\right) + \left(-Z_{\mu\nu} - \sigma^{s,\mathrm{d}}_{\mu\nu}\right)D^{\mathrm{p},\mathrm{d}}_{\mu\nu}\,,
\tag{4.51}
$$

$$
\theta\mathring{\eta} = -\nabla_\gamma\mathcal{J}^{\eta,\mathrm{h}}_\gamma - \mu^{\mathrm{x}}\left(\frac{1}{T} - \frac{1}{\theta}\right) + \left(Z_{\mu\nu} + \sigma^{e,\mathrm{d}}_{\mu\nu} + \sigma^{\epsilon,\mathrm{d}}_{\mu\nu} + \sigma^{s,\mathrm{d}}_{\mu\nu}\right)D^{\mathrm{p},\mathrm{d}}_{\mu\nu}\,.
\tag{4.52}
$$

The driving force for viscoplastic deformation, (4.38), can be re-written with the aid of the relation

$$
\left[e_{\mathrm{t},F^{\mathrm{e}}_{\alpha\varepsilon}}\big|_{s,\eta}\,F^{\mathrm{e}}_{\beta\varepsilon}\right]^{\mathrm{d}} = \sigma^{e,\mathrm{d}}_{\alpha\beta} + \sigma^{\epsilon,\mathrm{d}}_{\alpha\beta} + \sigma^{s,\mathrm{d}}_{\alpha\beta} + \sigma^{\eta,\mathrm{d}}_{\alpha\beta}\,.
\tag{4.53}
$$

Finally, it is noted that the prefactors on the right hand side of (4.49) and (4.50) are generalizations of inverse heat capacities.

Instead of replacing the entropy densities by the two temperatures, one could also think of other replacements. In view of the literature, it is useful to consider instead the energy densities (per unit mass) of the kinetic and configurational subsystems, $\hat{e}$ and $\hat{\epsilon}$ respectively. From the above, it can be shown that the evolution equations for the partial energy densities become

$$
\begin{aligned}
\rho D_t \hat{e} &= T^{-1} \left. \hat{e}_{,\hat{s}} \right|_{\hat{\eta}, \boldsymbol{F}^{\mathrm{e}}} \left[\left(\sigma^s_{\gamma\mu} + \sigma^{[s\eta]s}_{\gamma\mu} \right) (\nabla_\mu v_\gamma) + T\mathring{s} \right] \\
&+ \theta^{-1} \left. \hat{e}_{,\hat{\eta}} \right|_{\hat{s}, \boldsymbol{F}^{\mathrm{e}}} \left[\left(\sigma^\eta_{\gamma\mu} + \sigma^{[s\eta]\eta}_{\gamma\mu} \right) (\nabla_\mu v_\gamma) + \theta\mathring{\eta} \right] \\
&+ \sigma^e_{\mu\nu} \left(\mathrm{D}_t F^{\mathrm{e}}_{\mu\varepsilon} \right) F^{\mathrm{e},-1}_{\varepsilon\nu} , \quad\quad (4.54)
\end{aligned}
$$

$$
\begin{aligned}
\rho D_t \hat{\epsilon} &= T^{-1} \left. \hat{\epsilon}_{,\hat{s}} \right|_{\hat{\eta}, \boldsymbol{F}^{\mathrm{e}}} \left[\left(\sigma^s_{\gamma\mu} + \sigma^{[s\eta]s}_{\gamma\mu} \right) (\nabla_\mu v_\gamma) + T\mathring{s} \right] \\
&+ \theta^{-1} \left. \hat{\epsilon}_{,\hat{\eta}} \right|_{\hat{s}, \boldsymbol{F}^{\mathrm{e}}} \left[\left(\sigma^\eta_{\gamma\mu} + \sigma^{[s\eta]\eta}_{\gamma\mu} \right) (\nabla_\mu v_\gamma) + \theta\mathring{\eta} \right] \\
&+ \sigma^\epsilon_{\mu\nu} \left(\mathrm{D}_t F^{\mathrm{e}}_{\mu\varepsilon} \right) F^{\mathrm{e},-1}_{\varepsilon\nu} . \quad\quad (4.55)
\end{aligned}
$$

This completes the formulation of the model for physical aging and mechanical rejuvenation of glasses using subsystem entropies, and of alternative formulations of it in terms of other variables for the kinetic and configurational subsystems, namely temperatures or kinetic energies.

4.3   Discussion: Comparison with the literature

In Sec. 4.2, we have presented a general model to describe physical aging and mechanical rejuvenation of amorphous solids, by considering the evolution of two (rather than one) thermal degrees of freedom, i.e. kinetic and configurational entropies, or the corresponding temperatures or internal energies, respectively. In particular, as shown in (4.40) and (4.41), these entropies are coupled non-trivially in the reversible dynamics through the tensor-valued function $Y_{\alpha\beta}$, while the distribution of dissipated energy (due to viscoplastic deformation) between the two thermal subsystems is controlled by another tensor-valued function, $Z_{\alpha\beta}$, in the irreversible dynamics. In this section, the model developed in Sec. 4.2 is compared with approaches in the literature, with the particular goal to learn about the common choices made for the quantities $Y_{\alpha\beta}$ and $Z_{\alpha\beta}$. In this comparison that follows below, the models of the other references are always (transformed to and) written in an Eulerian formulation, using as much as possible the same symbols and definitions as in our approach, to simplify the comparison. If other symbols and definitions are used as compared to our approach, this is explicitly stated.

4.3.1   Comparison with Boyce et al., Ref. [11]

We start our discussion with considering the work of Boyce et al. [11], where an additional variable is introduced to account for the effects of aging and mechanical rejuvenation. However, [11] does not rely on any thermal (temperature, energy density, or entropy density) variable to describe a configurational subsystem. Rather, a general structural variable is employed, here denoted by $\bar{s}$. For this quantity, used in the yielding kinetics, a

differential equation of the following form is studied (eqn. (28) in [11])

$$D_t \bar{s} = \bar{a}(\bar{s}) + \bar{r}(\bar{s}) \dot{\gamma}^{\mathrm{p}} , \tag{4.56}$$

with the function $\bar{a}(\bar{s})$ describing the physical aging, while $\bar{r}(\bar{s})$ describes how the plastic strain rate $\dot{\gamma}^{\mathrm{p}}$ gives rise to mechanical rejuvenation. Since both of these effects are also present in our modeling approach (as well as in the other models discussed below) one can say that they are in this sense equivalent. We now aim at relating the approach of [11] to ours, by identifying the quantities $Y_{\alpha\beta}$ and $Z_{\alpha\beta}$ in the following way. First, it is noted that in [11] the Cauchy stress tensor is based on the derivative of the Helmholtz free energy with respect to deformation (see their discussion around their eqn. (20) and (21)). This implies in view of our relations (4.45)–(4.48) that

$$Y_{\alpha\beta} = 0 . \tag{4.57}$$

Second, it is concluded from the explanations in [11] that the Helmholtz free energy does not depend on the structural variable $\bar{s}$. In the context of our model with effective temperature, this means that the Helmholtz free energy density (4.44) does not depend on the configurational temperature θ, and hence in the stress tensor expression (4.45)–(4.47) one can set $\sigma_{\alpha\beta}^{\eta} = 0$, since $\eta = a_{,\theta}|_{T,F_{\alpha\beta}^{\mathrm{e}}} = 0$. Third, it is pointed out that in our model, we do not account for strain-hardening. Therefore, we should also not consider the effects of entropic strain-hardening, which are actually included in [11]. While neglecting strain-hardening does in principle not imply that the stress tensor is completely free from (other) entropic contributions, the discussion around eqn. (21) in [11] suggests that one might indeed assume $\sigma_{\alpha\beta}^{s} = 0$, and so it follows

$$\sigma_{\alpha\beta} = \sigma_{\alpha\beta}^{e} + \sigma_{\alpha\beta}^{\epsilon} . \tag{4.58}$$

Using this result in relation with the temperature evolution equation discussed in Sec. 2.5 in [11], and then comparing this with our temperature evolution equation (4.49) with (4.51), one obtains

$$Z_{\alpha\beta} = - \left(\sigma_{\alpha\beta}^{e,\mathrm{d}} + \sigma_{\alpha\beta}^{\epsilon,\mathrm{d}} \right) , \tag{4.59}$$

where we have used that the thermodynamic potential does not depend on the structural variable $\bar{s}$, which in our context implies that the thermodynamic potential does not depend on η, leading to $T_{,\eta} = 0$. Inserting expression (4.59) into our driving force for viscoplastic deformation (4.38) with (4.53), one obtains

$$\Sigma_{\alpha\beta}^{\mathrm{d}} = \frac{1}{T} \left(\sigma_{\alpha\beta}^{e,\mathrm{d}} + \sigma_{\alpha\beta}^{\epsilon,\mathrm{d}} \right) , \tag{4.60}$$

which corresponds to eqn. (7) used in the viscoplastic constitutive relation (11) in [11].

4.3.2   Comparison with Buckley et al., Ref. [75]

The work of Buckley et al. [75] formulates a model in terms of temperature evolution. In that model, the Cauchy stress tensor $\sigma_{\alpha\beta}$ is written as a sum of two contributions, specifically a (traceless) "bond-stretching" contribution $\sigma_{\alpha\beta}^{\mathrm{b}}$ and a "molecular-conformation"

contribution $\sigma_{\alpha\beta}^{\mathsf{c}}$. The thermal evolution equation (eqn. (30) in [75]) can then be written in the form

$$\rho\,\bar{c}\,D_t T + \rho\,\overline{\Delta c}\,D_t\theta = \left(\sigma_{\gamma\mu} - \sigma_{\gamma\mu}^{\mathsf{b}}\right)\nabla_\mu v_\gamma + \sigma_{\gamma\mu}^{\mathsf{b}} D_{\gamma\mu}^{\mathsf{p,d}}\,,\tag{4.61}$$

with $\bar{c}$ the heat capacity and $\overline{\Delta c}$ the heat capacity step across the glass transition. Based on the two temperature equations in our model, (4.49)–(4.50), under the assumptions of no cross-coupling effects, $T_{,\eta} = \theta_{,s} = 0$, and no heat fluxes, one can derive an evolution equation analogous to (4.61). By comparing (4.61) with our counterpart, particularly with respect to the $D_{\alpha\beta}^{\mathsf{p}}$-terms (or conversely the $(\nabla_\beta v_\alpha)$-terms), one finds $\sigma_{\alpha\beta}^{\mathsf{b}} = \sigma_{\alpha\beta}^{e} + \sigma_{\alpha\beta}^{\epsilon}$. This result is valid for any $Y_{\alpha\beta}$ and $Z_{\alpha\beta}$. Both of these quantities describe the exchange between the two thermal subsystems, and therefore they can not be determined from a single evolution equation, as (4.61). However, both of these quantities can actually be determined by considering the constitutive relations for the Cauchy stress as well as for the driving force for viscoplastic flow. As far as the Cauchy stress is concerned, it is explained in [75] that the stress tensor is the sum of a mechanical visco-elastic Maxwell element and of a purely hyperelastic part. Therefore, the entire stress tensor can be derived from a Helmholtz free energy, and one thus concludes that

$$Y_{\alpha\beta} = 0\,.\tag{4.62}$$

Furthermore, let us consider the driving force for viscoplastic flow. By combining eqns. (15) and (26) in [75], one finds that the driving force for viscoplastic deformation is given by the (traceless) stress contribution $\sigma_{\alpha\beta}^{\mathsf{b}} = \sigma_{\alpha\beta}^{e} + \sigma_{\alpha\beta}^{\epsilon}$. Equating this driving force to $\mathfrak{T}\Sigma_{\alpha\beta}^{\mathsf{d}}$ in our approach, with $\mathfrak{T}$ a positive prefactor with units of temperature and $\Sigma_{\alpha\beta}^{\mathsf{d}}$ given by (4.38) with (4.53), one can write

$$Z_{\alpha\beta} = -\frac{1 - \frac{\theta}{\mathfrak{T}}}{1 - \frac{\theta}{T}}\left(\sigma_{\alpha\beta}^{e,\mathsf{d}} + \sigma_{\alpha\beta}^{\epsilon,\mathsf{d}}\right) - \frac{1}{1 - \frac{\theta}{T}}\left(\sigma_{\alpha\beta}^{s,\mathsf{d}} + \sigma_{\alpha\beta}^{\eta,\mathsf{d}}\right)\,.\tag{4.63}$$

Clearly, the second contribution (and for $\mathfrak{T} \neq T$ also the first one) in this expression diverges as $|\theta - T|$ approaches zero. In view of the expression for the driving force for viscoplastic flow, $\Sigma_{\alpha\beta}$, this is not a problem, since $Z_{\alpha\beta}$ is multiplied there by a prefactor that vanishes as $|\theta - T|$ vanishes. However, we note that the split of the viscoplastic contribution between the kinetic and configurational subsystems, see (4.49) and (4.50) with (4.51) and (4.52), does suffer from this divergence in $Z_{\alpha\beta}$ as $|\theta - T|$ tends to zero. This issue deserves further attention in a future study.

4.3.3   Comparison with Kamrin and Bouchbinder, Ref. [79]

In the work of Kamrin and Bouchbinder [79], a two-temperature-based continuum thermo-mechanics model was formulated to describe physical aging and mechanical rejuvenation of deforming amorphous solids. Specifically, by assuming weakly interacting kinetic and configurational subsystems, the evolution equations for corresponding energy densities (their eqns. (9) and (10)) read as follows [79]

$$\rho D_t \hat{e} = -\nabla_\gamma \mathcal{J}_\gamma^{s,\mathsf{h}} + \mathcal{J}^{\Delta,\mathsf{x}} + \sigma_{\gamma\mu}^{\mathsf{dis}} D_{\gamma\mu}^{\mathsf{p,d}}\,,\tag{4.64}$$

$$\rho D_t \hat{\epsilon} = -\nabla_\gamma \mathcal{J}_\gamma^{\eta,\mathsf{h}} - \mathcal{J}^{\Delta,\mathsf{x}} + \sigma_{\gamma\mu}\left(\nabla_\mu v_\gamma - D_{\gamma\mu}^{\mathsf{p,d}}\right) + \sigma_{\gamma\mu}^{\mathsf{store}} D_{\gamma\mu}^{\mathsf{p,d}}\,,\tag{4.65}$$

with the split of the Cauchy stress tensor $\sigma_{\alpha\beta} = \sigma_{\alpha\beta}^{\text{store}} + \sigma_{\alpha\beta}^{\text{dis}}$. The plastic stress-power is split into a contribution that represents the "stored plastic power" and affects the configurational subsystem, while the "plastic dissipation" gives a contribution to the kinetic subsystem [79]. Further, to provide a direct comparison between their and our approach, we neglect in our approach the cross-coupling terms in the energy evolution equations (4.54) and (4.55), i.e. $\hat{e}_{,\hat{\eta}} = \hat{\epsilon}_{,\hat{s}} = 0$, leading to $\hat{e}_{,\hat{s}} = T$ and $\hat{\epsilon}_{,\hat{\eta}} = \theta$. Doing so, the comparison of their (4.64)–(4.65) with our (4.54)–(4.55) is straightforward. Specifically, with the choice

$$TY_{\alpha\beta} = \sigma_{\alpha\beta}^e + \sigma_{\alpha\beta}^s \,, \tag{4.66}$$

one can match the $(\nabla_\beta v_\alpha)$-terms in $D_t\hat{e}$ (or alternatively in $D_t\hat{\epsilon}$). On the other hand, by analyzing the $D_{\alpha\beta}^{\text{p}}$-terms in $D_t\hat{e}$ (or alternatively in $D_t\hat{\epsilon}$), in view of the Cauchy stress tensor together with (4.66), one can establish the connection between $\sigma_{\alpha\beta}^{\text{dis}}$ and $Z_{\alpha\beta}$, explicitly

$$\sigma_{\alpha\beta}^{\text{dis,d}} = -Z_{\alpha\beta} - \left(\sigma_{\alpha\beta}^{e,\text{d}} + \sigma_{\alpha\beta}^{s,\text{d}} \right) \,. \tag{4.67}$$

In [79], the split of $\sigma_{\alpha\beta}$ into $\sigma_{\alpha\beta}^{\text{store}}$ and $\sigma_{\alpha\beta}^{\text{dis}}$ stands for the split of the effect of viscoplastic dissipation into the kinetic and configurational subsystems. In our approach, this corresponds equivalently to the choice of $Z_{\alpha\beta}$, as exemplified by (4.67). However, as we can see from the discussion above, from the evolution equations of the energies one can only determine $Z_{\alpha\beta}$ in relation to $\sigma_{\alpha\beta}^{\text{dis}}$, but not in absolute terms. To make further progress in this direction, one can now proceed by filling this expression for $Z_{\alpha\beta}$ into our driving force for viscoplastic deformation (4.38) with (4.53), leading to

$$\Sigma_{\alpha\beta}^{\text{d}} = \left(\frac{1}{T} - \frac{1}{\theta} \right) \sigma_{\alpha\beta}^{\text{dis,d}} + \frac{1}{T} \left(\sigma_{\alpha\beta}^{e,\text{d}} + \sigma_{\alpha\beta}^{s,\text{d}} \right) + \frac{1}{\theta} \left(\sigma_{\alpha\beta}^{\epsilon,\text{d}} + \sigma_{\alpha\beta}^{\eta,\text{d}} \right) \,. \tag{4.68}$$

For a most general comparison of the driving force for viscoplastic flow used in [79] (eqn.(24) therein), $\sigma_{\alpha\beta}^{\text{dis,d}}$, with our approach, one needs to solve $\sigma_{\alpha\beta}^{\text{dis,d}} = \mathfrak{T}\Sigma_{\alpha\beta}^{\text{d}}$, where $\mathfrak{T}$ is a positive prefactor with units of temperature. Doing so, one obtains the specific relation

$$\sigma_{\alpha\beta}^{\text{dis,d}} = \frac{1}{1 + \theta \left(\frac{1}{\mathfrak{T}} - \frac{1}{T} \right)} \left[\frac{\theta}{T} \left(\sigma_{\alpha\beta}^{e,\text{d}} + \sigma_{\alpha\beta}^{s,\text{d}} \right) + \left(\sigma_{\alpha\beta}^{\epsilon,\text{d}} + \sigma_{\alpha\beta}^{\eta,\text{d}} \right) \right] \,. \tag{4.69}$$

Together with (4.67), this leads to

$$Z_{\alpha\beta} = -\frac{1}{1 + \theta \left(\frac{1}{\mathfrak{T}} - \frac{1}{T} \right)} \left[\left(1 + \frac{\theta}{\mathfrak{T}} \right) \left(\sigma_{\alpha\beta}^{e,\text{d}} + \sigma_{\alpha\beta}^{s,\text{d}} \right) + \left(\sigma_{\alpha\beta}^{\epsilon,\text{d}} + \sigma_{\alpha\beta}^{\eta,\text{d}} \right) \right] \,. \tag{4.70}$$

In other words, [79] uses non-trivial choices for both $Y_{\alpha\beta}$ and $Z_{\alpha\beta}$, in general.

We conclude by noting that for the specific case discussed in Sec. 3 of [79] (see specifically assumptions in eqn.(17) therein), one finds $\sigma_{\alpha\beta}^e = \sigma_{\alpha\beta}^s = \sigma_{\alpha\beta}^\eta = 0$, which implies $Y_{\alpha\beta} = 0$, and $Z_{\alpha\beta}$ becomes proportional to $\sigma_{\alpha\beta}^{\epsilon,\text{d}}$, by virtue of (4.66) and (4.70), respectively.

4.3.4   Comparison with Xiao and Nguyen, Ref. [80]

For the comparison of the work of Xiao and Nguyen [80] with our approach, we start by considering the evolution equations for the temperatures. In [80], it is assumed that the

kinetic (e and s) and configurational (ϵ and η) subsystem quantities do not depend on the temperature of other subsystem (θ and T, respectively). In our context, in view of (4.49)–(4.50), this implies $T_{,\eta} = \theta_{,s} = 0$. Expressing the temperature equations (29) and (30) in [80], one obtains

$$c_g D_t T = -\nabla_\gamma \mathcal{J}^{s,\mathsf{h}}_\gamma + \mathcal{J}^{\Delta,\times} + \sigma^s_{\gamma\varepsilon}\nabla_\varepsilon v_\gamma + \sigma^e_{\gamma\varepsilon} D^{\mathsf{p},\mathsf{d}}_{\gamma\varepsilon} \,, \tag{4.71}$$

$$\Delta c D_t \theta = -\nabla_\gamma \mathcal{J}^{\eta,\mathsf{h}}_\gamma - \mathcal{J}^{\Delta,\times} + \sigma^\eta_{\gamma\varepsilon}\nabla_\varepsilon v_\gamma + \sigma^\epsilon_{\gamma\varepsilon} D^{\mathsf{p},\mathsf{d}}_{\gamma\varepsilon} \,. \tag{4.72}$$

These equations are now discussed from the perspective of our corresponding equations (4.49)–(4.50). One can naturally make the identifications for the subsystem heat capacities $c_g = T\,(T_{,s})^{-1}$ and $\Delta c = \theta\,(\theta_{,\eta})^{-1}$. Furthermore, by comparing the $\nabla_\alpha v_\beta$-terms in the evolution equations for T (or alternatively θ), one finds

$$Y_{\alpha\beta} = 0\,. \tag{4.73}$$

By comparing the $D^{\mathsf{p}}_{\alpha\beta}$-terms in the evolution equations for T (or alternatively θ), one finds

$$Z_{\alpha\beta} = -\left(\sigma^e_{\alpha\beta} + \sigma^s_{\alpha\beta}\right)^{\mathsf{d}}\,. \tag{4.74}$$

It should be noted, that the zero-choice for $Y_{\alpha\beta}$ can also be obtained by comparing the expression for the Cauchy stress in [80] (therein: based on eqn. $(18)_1$ with eqn. (13)) with our form (4.45)–(4.48). Finally, it is interesting to compare the driving force for viscoplastic flow. Using (4.74) in our driving force for viscoplastic deformation (4.38) with (4.53), one obtains

$$\Sigma^{\mathsf{d}}_{\varrho\lambda} = \frac{1}{T}\left(\sigma^{e,\mathsf{d}} + \sigma^{s,\mathsf{d}}\right) + \frac{1}{\theta}\left(\sigma^{\epsilon,\mathsf{d}} + \sigma^{\eta,\mathsf{d}}\right)\,, \tag{4.75}$$

which corresponds to eqn. (25) in [80].

4.3.5   Comparison with Klompen et al., Ref [46]

In the work of Klompen et al. [46], a model has been developed for describing the mechanical response of glassy polymers. Like in all approaches discussed above, also in [46] an additional variable, the so-called state parameter $\bar{S}$, is introduced to describe the effects of physical aging and mechanical rejuvenation, by letting the yielding kinetics depend on this parameter. However, in contrast to all approaches described earlier in this section, the state parameter $\bar{S}$ in [46] is not specified by way of an evolution equation, but rather in an explicit form. Specifically, the state parameter is considered as a product of two explicit state functions, i.e. $\bar{S} = \bar{S}^{\mathsf{a}}\bar{R}^\gamma$, where $\bar{S}^{\mathsf{a}} = \bar{S}^{\mathsf{a}}(t,T)$ represents the aging kinetics dependent on aging time t and temperature T, whereas the mechanical rejuvenation is described by $\bar{R}^\gamma = \bar{R}^\gamma(\gamma^{\mathsf{p}})$, where γ^{p} is an equivalent plastic strain. Specific procedures are developed and explained in [46,90] to determine the explicit functions $\bar{S}^{\mathsf{a}}(\cdot)$ and $\bar{R}^\gamma(\cdot)$. However, in order to establish links with the above discussed thermodynamic approaches to physical aging and mechanical rejuvenation, we briefly comment on how the approach in [46] can be transferred into an evolution equation for the state parameter. Simply differentiating $\bar{S}$ with respect to time results in

$$\dot{\bar{S}} = \left(\frac{\dot{\bar{S}}^{\mathsf{a}}}{\bar{S}^{\mathsf{a}}} + \frac{\left(d\bar{R}^\gamma/d\gamma^{\mathsf{p}}\right)}{\bar{R}^\gamma}\dot{\gamma}^{\mathsf{p}}\right)\bar{S}\,. \tag{4.76}$$

One observes readily that the rate consists of two additive terms, one term representing physical aging and the other representing mechanical rejuvenation. The evolution equation (4.76) for the state parameter $\bar{S}$ strongly resembles that of the state parameter $\bar{s}$, i.e. (4.56). Particularly, the mechanical rejuvenation term is proportional to the rate of the (equivalent) plastic strain. However, while the rate $\dot{\gamma}^{\mathrm{p}}$ can instantaneously be expressed in terms of the plastic strain rate tensor $D_{\alpha\beta}^{\mathrm{p}}$, in the approach of Klompen et al. [46] there is an explicit reference to the plastic strain γ^{p} itself. In practical numerical calculation one can obtain that readily by time-integration of the rate $\dot{\gamma}^{\mathrm{p}}$. However, from a fundamental modeling perspective it implies that γ^{p} is elevated to the level of a dynamic variable. Since our thermodynamic approach does not treat γ^{p} as an independent dynamic variable, we do not go into more detail about comparing our approach with that in [46].

Despite the fact that Klompen et al. [46] do not use an evolution equation for the state parameter, one can still strive to make a more close connection with the dynamic approach in this chapter. As an illustrative example of how to achieve that task, we consider in the following physical aging in the absence of mechanical deformation, i.e., $\bar{R}^{\gamma} = 1$, in which case $\bar{S} = \bar{S}^{\mathrm{a}}$. In agreement with literature, also Klompen et al. [46] use a logarithmic dependence of $\bar{S}^{\mathrm{a}}$ on waiting time t_{w}, i.e., $\bar{S}^{\mathrm{a}} \propto \ln(t_{\mathrm{w}})$. In contrast, in the approach in this chapter, the physical aging in the absence of mechanical deformation is described by the μ^{x}-related contribution in evolution of the configurational temperature (4.50) and (4.52),

$$D_{t_{\mathrm{w}}}\theta \;=\; -\theta^{-1}\theta_{,\eta}\mu^{\mathrm{x}}\left(\frac{1}{T} - \frac{1}{\theta}\right),\tag{4.77}$$

where we have assumed for simplicity $\theta_{,s} = 0$. The goal is to make a certain choice for the kinetic function μ^{x} such that, with the resulting solution $\theta = \theta(t_{\mathrm{w}})$, one obtains $\bar{S}^{\mathrm{a}}(\theta(t_{\mathrm{w}})) \propto \ln(t_{\mathrm{w}})$. If one assumes for illustration purposes that $\bar{S}^{\mathrm{a}}(\theta) = \bar{S}_0 + \bar{S}_1\theta$, one thus looks for a solution $\theta(t_{\mathrm{w}}) \propto \ln(t_{\mathrm{w}})$. As it is shown in the following, this solution is induced by the choice

$$\mu^{\mathrm{x}} = a\,\frac{T\theta}{\theta^{-1}\theta_{,\eta}}\frac{e^{b\,\delta} - 1}{\delta},\tag{4.78}$$

which is always positive as required, $\mu^{\mathrm{x}} > 0$, if $a > 0$, $b > 0$, and the configurational heat capacity $\theta/\theta_{,\eta} > 0$. Considering constant kinetic temperature T, the evolution equation for the temperature difference

$$\delta \equiv \theta - T.\tag{4.79}$$

can be derived from (4.77) and (4.78), leading to

$$D_{t_{\mathrm{w}}}\delta \;=\; -a\left(e^{b\,\delta} - 1\right),\tag{4.80}$$

which is identical to the evolution equation (1) discussed in [99]. Particularly, for constant a and b, the solution is given by [99]

$$\delta(t_{\mathrm{w}}) = -\frac{1}{b}\ln\left(1 - \left(1 - e^{-b\,\delta_0}\right)e^{-a\,b\,t_{\mathrm{w}}}\right),\tag{4.81}$$

with $\delta_0 = \delta(t_{\mathrm{w}} = 0)$. Indeed, for $e^{-b\,\delta_0} \ll 1$ and $a\,b\,t_{\mathrm{w}} \ll 1$, one obtains logarithmic behavior,

$$\delta(t_{\mathrm{w}}) \simeq -\frac{1}{b}\ln\left(a\,b\,t_{\mathrm{w}}\right),\tag{4.82}$$

Table 4.1: Specific forms of the functions $Y_{\alpha\beta}$, $Z_{\alpha\beta}$, and the driving force for viscoplastic deformation, $\Sigma^{\mathrm{d}}_{\alpha\beta}$, for different approaches in the literature. For the cases of Buckley et al. [75] and Kamrin and Bouchbinder [79], the most general forms are given in Sec. 4.3.2 and Sec. 4.3.3, respectively, while in this table the special case $\mathfrak{T} = T$ is considered, inspired by the relation implied by (4.58) and (4.60).

Reference	$TY_{\alpha\beta}$	$-Z_{\alpha\beta}$	$T\Sigma^{\mathrm{d}}_{\alpha\beta}$
Boyce et al. [11] (for this comparison: $\sigma^s_{\alpha\beta} = \sigma^\eta_{\alpha\beta} = 0$)	0	$\sigma^{e,\mathrm{d}}_{\alpha\beta} + \sigma^{\epsilon,\mathrm{d}}_{\alpha\beta}$	$\sigma^{e,\mathrm{d}}_{\alpha\beta} + \sigma^{\epsilon,\mathrm{d}}_{\alpha\beta}$
Buckley et al. [75]	0	$\left(\sigma^{e,\mathrm{d}}_{\alpha\beta} + \sigma^{\epsilon,\mathrm{d}}_{\alpha\beta}\right) + \frac{1}{1-\frac{\theta}{T}}\left(\sigma^{s,\mathrm{d}}_{\alpha\beta} + \sigma^{\eta,\mathrm{d}}_{\alpha\beta}\right)$	$\sigma^{e,\mathrm{d}}_{\alpha\beta} + \sigma^{\epsilon,\mathrm{d}}_{\alpha\beta}$
Kamrin and Bouchbinder [79]	$\sigma^e_{\alpha\beta} + \sigma^s_{\alpha\beta}$	$\left(1+\frac{\theta}{T}\right)\left(\sigma^{e,\mathrm{d}}_{\alpha\beta} + \sigma^{s,\mathrm{d}}_{\alpha\beta}\right) + \left(\sigma^{\epsilon,\mathrm{d}}_{\alpha\beta} + \sigma^{\eta,\mathrm{d}}_{\alpha\beta}\right)$	$\frac{\theta}{T}\left(\sigma^{e,\mathrm{d}}_{\alpha\beta} + \sigma^{s,\mathrm{d}}_{\alpha\beta}\right) + \left(\sigma^{\epsilon,\mathrm{d}}_{\alpha\beta} + \sigma^{\eta,\mathrm{d}}_{\alpha\beta}\right)$
Xiao and Nguyen [80]	0	$\sigma^{e,\mathrm{d}}_{\alpha\beta} + \sigma^{s,\mathrm{d}}_{\alpha\beta}$	$\left(\sigma^{e,\mathrm{d}}_{\alpha\beta} + \sigma^{s,\mathrm{d}}_{\alpha\beta}\right) + \frac{T}{\theta}\left(\sigma^{\epsilon,\mathrm{d}}_{\alpha\beta} + \sigma^{\eta,\mathrm{d}}_{\alpha\beta}\right)$

as desired. In contrast, for sufficiently long waiting times, $a\,b\,t_{\mathrm{w}} \gg 1$, one obtains $\delta \simeq 0$. In view of the system visiting ever deeper energy states in the course of physical aging, it seems more reasonable to have a limiting value for δ for long waiting times, rather than a logarithmic behavior on all time scales.

4.3.6   Discussion of the above comparison, and a further possibility for $Y_{\alpha\beta}$ and $Z_{\alpha\beta}$

In Sec. 4.3, we have compared our model with other models known in the literature [11, 46, 75, 79, 80], in order to identify some choices made in the literature for the coupling tensors $Y_{\alpha\beta}$, $Z_{\alpha\beta}$, and the driving force for viscoplastic deformation, $\Sigma^{\mathrm{d}}_{\alpha\beta}$. The results of that comparison are listed in Table 4.1. Notably, the cases of Buckley et al. [75] and Kamrin and Bouchbinder [79], discussed in Sec. 4.3.2 and Sec. 4.3.3, respectively, contain a yet undetermined positive quantity $\mathfrak{T}$ with the units of temperature. While the general expressions for $Y_{\alpha\beta}$, $Z_{\alpha\beta}$, and $\Sigma^{\mathrm{d}}_{\alpha\beta}$ are given in the respective sections, in Table 4.1 only the special case $\mathfrak{T} = T$ is listed, for illustration purposes. This choice is motivated by the relation implied by (4.58) and (4.60), namely $T\Sigma^{\mathrm{d}}_{\alpha\beta} = \sigma^{\mathrm{d}}_{\alpha\beta}$.

As shown in Table 4.1, only in the work of Kamrin and Bouchbinder [79] there is a nonzero entropy-coupling term $Y_{\alpha\beta}$. Particularly, according to Table 4.1 and with the

help of the stress tensor contributions (4.46) and (4.47), one can write

$$TY_{\alpha\beta} = \sigma^e_{\alpha\beta} + \sigma^s_{\alpha\beta} = 2\rho F^e_{\alpha\gamma}\left(\hat{e}_{,C^e_{\gamma\delta}}\Big|_{T,\theta} - T\,\hat{s}_{,C^e_{\gamma\delta}}\Big|_{T,\theta}\right)F^e_{\beta\delta}\,. \tag{4.83}$$

Since according to [79] the kinetic and configurational subsystems are only weakly coupled, both $\hat{e}$ and $\hat{s}$ can be assumed to be independent of θ, and thus the term in parenthesis in (4.83) can be written in the form $\hat{e}_{,C^e_{\gamma\delta}}|_{\hat{s}}$. Using that $Y_{\alpha\beta}$ is of quasi-potential form as discussed in Sec. 4.2.2, one obtains from (4.83)

$$\frac{1}{y_1}\frac{\partial y_2}{\partial C^e_{\alpha\beta}}\bigg|_{\hat{s}_t,\hat{\eta}} = \frac{2}{T}\hat{e}_{,C^e_{\gamma\delta}}|_{\hat{s}}\,. \tag{4.84}$$

Therefore, a possible choice is $y_1 = T/2$ and $y_2 = \hat{e}$, implying that both y_1 and y_2 depend only on $\hat{s}$ and $\boldsymbol{C}^e$. According to the temperature definition (4.6), one can thus write $\hat{e}_{,\hat{\eta}}|_{\hat{s}_t,\boldsymbol{C}^e} = -\hat{e}_{,\hat{s}}|_{\boldsymbol{C}^e} = -T$ for the case studied in [79], which implies

$$\frac{\partial y_2}{\partial\hat{\eta}}\bigg|_{\hat{s}_t,\boldsymbol{C}^e} = -2y_1\,. \tag{4.85}$$

Inspection of the Jacobi condition (4.26) immediately leads to the conclusion that the Jacobi identity is automatically satisfied, without any restriction on the thermodynamic potential for the kinetic subsystem. Therefore, the choices made in Kamrin and Bouchbinder [79] are fully compatible also with the Hamiltonian structure of the reversible dynamics, which is noteworthy as this criterion, namely the Jacobi identity, has not been used as a guideline in their work [79].

Furthermore, one can infer from Table 4.1 about the relation between the deviatoric part of the total Cauchy stress tensor (4.45), $\sigma^d_{\alpha\beta}$, and the driving force for viscoplastic deformation $\Sigma^d_{\alpha\beta}$, (4.38) with (4.53). It turns out that $T\Sigma^d_{\alpha\beta} = \sigma^d_{\alpha\beta}$ holds for Boyce et al. [11] and Kamrin and Bouchbinder [79], while for the other cases $\sigma^d_{\alpha\beta}$ and $\Sigma^d_{\alpha\beta}$ are not proportional to each other. In general, one might wonder about a condition to actually enforce that $\Sigma^d_{\alpha\beta}$ is proportional to $\sigma^d_{\alpha\beta}$, even if all stress tensor contributions in (4.45–4.48) are non-zero. In the following, we thus consider the case

$$\Sigma^d_{\alpha\beta} = \frac{1}{\mathfrak{T}}\sigma^d_{\alpha\beta}\,, \tag{4.86}$$

where $\mathfrak{T}$ is an arbitrary positive factor with units of temperature, that may depend on the dynamic variables. Enforcing this condition (4.86) with the stress tensor $\sigma_{\alpha\beta}$ (4.45–4.48) and the driving force for viscoplastic flow $\Sigma^d_{\alpha\beta}$, (4.38) with (4.53), one obtains

$$-Z_{\alpha\beta} = \frac{T\theta}{\mathfrak{T}}Y^d_{\alpha\beta} + \frac{T}{\mathfrak{T}}\left(\frac{\theta-\mathfrak{T}}{\theta-T}\right)\left(\sigma^{e,d}_{\alpha\beta} + \sigma^{\epsilon,d}_{\alpha\beta} + \sigma^{s,d}_{\alpha\beta} + \sigma^{\eta,d}_{\alpha\beta}\right)\,. \tag{4.87}$$

Notably, this relation between $Z_{\alpha\beta}$ and $Y^d_{\alpha\beta}$ depends on the factor $\mathfrak{T}$. Two special cases lead to drastic simplifications of (4.87):

$$-Z_{\alpha\beta} = TY^d_{\alpha\beta}\,, \qquad\qquad\qquad\qquad \text{for} \quad \mathfrak{T} = \theta\,, \tag{4.88}$$

$$-Z_{\alpha\beta} = \theta Y^d_{\alpha\beta} + \left(\sigma^{e,d}_{\alpha\beta} + \sigma^{\epsilon,d}_{\alpha\beta} + \sigma^{s,d}_{\alpha\beta} + \sigma^{\eta,d}_{\alpha\beta}\right)\,, \qquad \text{for} \quad \mathfrak{T} = T\,, \tag{4.89}$$

which differ from each other by the deviatoric part of the Cauchy stress tensor, namely $Z_{\alpha\beta}|_{\mathfrak{T}=\theta} - Z_{\alpha\beta}|_{\mathfrak{T}=T} = \sigma^{\mathrm{d}}_{\alpha\beta}$. To complete this section, it should be pointed out that at thermal equilibrium, i.e. $\theta = T$, there seems to be a divergence in the second term on the right-hand side of (4.87). However, since the temperature-like quantity $\mathfrak{T}$ is assumed to be directly related to T and θ, it is reasonable that upon $|\theta - T| \to 0$ also $|\theta - \mathfrak{T}| \to 0$, implying that in the limit the divergence would not exist but rather the entire relation (4.87) would remain well defined.

4.4   Concluding remarks

By applying nonequilibrium thermodynamics in the form of the general equation for the nonequilibrium reversible-irreversible coupling (GENERIC), a model has been formulated for describing the mechanical behavior of amorphous solids (e.g. glassy polymers), in particular physical aging and mechanical rejuvenation. A key ingredient in this approach is the split of the thermal system into a kinetic and a configurational subsystem with corresponding degrees of freedom. Doing so results in evolution equations for the momentum density, kinetic and configurational entropies (or their respective temperatures or energies), and the elastic part of the deformation gradient. Moreover, constitutive expressions have been derived for the Cauchy stress tensor and for the viscoplastic flow rule. The most prominent features of the proposed model are the following:

- The reversible dynamics (see Sec. 4.2.2), induced by the action of the Poisson operator on the energy gradient, couples the evolution equations for kinetic and configurational entropies in a nontrivial manner, quantified by the tensor-valued function $Y_{\alpha\beta}$. Due to the anti-symmetry of the Poisson operator, this coupling in turn leads to additional contributions to the Cauchy stress tensor, the latter being of *hypo*elastic rather than *hyper*elastic nature in general. The reversible entropy-coupling, and thus also the additional stress tensor contributions, are subject to conditions implied by the Jacobi identity.

- In the irreversible dynamics (see Sec. 4.2.3), the split of dissipation due to viscoplastic deformation onto the two thermal subsystems (kinetic and configurational) is controlled by another tensor-valued function $Z_{\alpha\beta}$. This latter quantity occurs not only in the irreversible dynamics of the specific subsystem entropies, but also in the constitutive relation for the viscoplastic flow.

The tensor-valued functions, $Y_{\alpha\beta}$ and $Z_{\alpha\beta}$, that couple the two thermal subsystems in the reversible and irreversible dynamics, respectively, are still quite general. Specifying their form, one can represent many other models known in the literature, as elaborated in detail in Sec. 4.3.

An essential part of this chapter is devoted to devise appropriate coupling of the two thermal subsystems in the reversible dynamics. In this respect, using GENERIC proves beneficial, since this framework respects the Hamiltonian structure, and therefore imposes severe constraints for the model formulation. Particularly, the importance of the Jacobi identity is highlighted, which represents the time-structure invariance of the reversible dynamics [29]. In this chapter, the implications of the Jacobi identity on the reversible

coupling (quantity $Y_{\alpha\beta}$ or $\hat{Y}_{\alpha\beta}$, respectively) of the kinetic and configurational entropies has been examined. It seems that this is a research direction that to date has received only limited attention. To foster further research activities in this direction, some comments in relation to the developments in Sec. 4.2.2 are added. While the condition (4.24) for $\hat{Y}_{\alpha\beta}$ is fully general, we believe that a large fraction of physically reasonable models are of quasi-potential type $\hat{Y}_{\alpha\beta} = (1/y_1)(\partial y_2/\partial C^{\mathrm{e}}_{\alpha\beta})|_{\hat{s}_{\mathrm{t}},\hat{\eta}}$ as discussed in Sec. 4.2.2, in which case the relevant condition on the two scalar-valued functions y_1 and y_2 is given by (4.26), or (4.27), respectively. It is noteworthy that a possible solution to comply with the Jacobi identity, (4.26) or (4.27), is given by

$$\left.\frac{\partial y_2}{\partial \hat{\eta}}\right|_{\hat{s}_{\mathrm{t}},\boldsymbol{C}^{\mathrm{e}}} + 2y_1 = 0\,. \tag{4.90}$$

As a matter of fact, it can be shown that (4.90) results in a vanishing material time-derivative of y_2,

$$D_t\,y_2 = 0\,, \tag{4.91}$$

completely analogous to the evolution of $\hat{s}_{\mathrm{t}}$, $D_t\,\hat{s}_{\mathrm{t}} = 0$. Therefore, instead of working with the set of variables $\boldsymbol{\mathcal{X}} = (\boldsymbol{m}, s, \eta, \boldsymbol{F}^{\mathrm{e}})$ with reversible entropy-coupling described by (4.90), one could perform a transformation of variables to $\boldsymbol{\mathcal{X}}' = (\boldsymbol{m}, \hat{s}_{\mathrm{t}}, y_2, \boldsymbol{F}^{\mathrm{e}})$. The latter set is technically more convenient, since the Jacobi identity is known to be fulfilled for $(\boldsymbol{m}, \hat{s}_{\mathrm{t}}, \boldsymbol{F}^{\mathrm{e}})$ [32]. Viewing this in a Lagrangian setting [100], it is immediately clear that including an additional variable (namely y_2) with dynamics given by (4.91) does not disturb the compatibility with the Jacobi identity. Since the Jacobi identity is invariant with respect to a transformation of variables $\boldsymbol{\mathcal{X}} \leftrightarrow \boldsymbol{\mathcal{X}}'$, there is thus a clear understanding why the class of models described by (4.90) respects the Jacobi identity, namely by viewing y_2 as a fundamental dynamic variable. However, it is emphasized that from a physical, modeling perspective, it may be beneficial to keep the configurational entropy (η or $\hat{\eta}$, respectively) as a fundamental variable instead. In any case, when formulating the thermomechanics of amorphous solids with two thermal subsystems, the condition (4.90) makes it possible to include a reversible entropy-coupling of quasi-potential form in a straightforward way. While the case of Kamrin and Bouchbinder [79] discussed above is an example thereof, the class of models covered by (4.90) is even richer.

Chapter 5

Two-scale model for the Mullins effect in elastomers filled with hard nanoparticles

Abstract

A two-scale model is developed, and solved numerically, to describe the mechanical behavior of elastomers filled with hard nanoparticles. Of particular interest is the Mullins effect, i.e. the slow increase of the elastic modulus after large-amplitude oscillatory deformation. To account for the Mullins effect, the physical aging of the glassy bridges between the filler particles is captured with two thermal degrees of freedom for the matrix material, namely a kinetic and a configurational one. Formulating the two-scale model enriched with aging in a nonequilibrium thermodynamics context, first results in a constitutive relation for the Cauchy stress tensor. Second, the dynamics of physical aging is described, which eventually gives rise to the Mullins effect. The proposed model is investigated numerically under large amplitude oscillatory shear deformation. Of particular interest in this respect is the coupling of the micro-scale dynamics with the physical aging on the macroscopic scale. This coupling is examined in detail, both in an approximate way using a Gaussian approximation, as well as numerically, under specific conditions. It turns out that the CONNFFESSIT approach (M. Laso, H. C. Öttinger, J. Non-Newtonian Fluid Mech., 47:1–20, 1993) can not be employed for the numerical solution of the model under arbitrary loading conditions because of the novel structure of the two-level coupling term. While a procedure for solving the model numerically for the case of strong applied deformation is presented in this chapter, other solution methodologies need to be sought for the cases of weak and no applied deformation.

5.1   Introduction

Composite materials, being widely used in different practical applications due to their remarkable properties, are of great interest to researchers concerned with fundamental modeling. This is because the behavior of entire system is the result of an intricate combination and coupling of dynamics on different length- as well as time-scales. The particular interest of this work is the analytical modeling and numerical simulation of the mechanical behavior of composites that consist of an elastomer matrix filled with hard particles of nanometers size.

Filling an elastomer with nanoparticles adds significant rate-dependence to its mechanical behavior, and thus results in increased dissipation, as compared to the unfilled elastomer [1]. A possible explanation, that is used in this chapter as a basis for the model formulation, for these significant changes in the material behavior is the following. If the matrix material adheres well to the filler particle surface, the mobility in the matrix is slowed down close to these surfaces. More specifically, the mobility in a matrix material element is decreased gradually the closer this element is located to the filler particle surface. Effectively, this can be captured by an increase in the local glass transition temperature of matrix material as the distance to the filler particle surface decreases. If, in close enough vicinity to the particle surface, the local glass transition temperature is higher than the actual (laboratory) temperature, an effective glassy layer is present around the filler particle. At high enough volume fraction of filler particles and in a certain temperature regime, these glassy layers may then overlap, thereby creating so-called glassy bridges between the filler particles. Therefore, such composites consist essentially of a rubbery-state elastomer matrix that is permeated by a glassy network with filler particles, leading in mechanical reinforcements of up to about 100 times. The existence of glassy layers around filler particles is supported by the literature, e.g. by NMR studies [8] or more recently by a mechanical analysis of model systems [9, 10]. For more details on this issue, the reader is referred to, e.g., [7] and references therein.

Once the glassy bridges are formed between the particles, the interparticle dynamics can be analyzed in terms of the knowledge about the thermo-mechanics of bulk polymer glasses [11, 13]. Specific features of bulk polymer glasses that are relevant also for the glassy-bridge induced effects are the viscoplastic yielding behavior and strain softening, as well as the effect of physical aging on the mechanical behavior. For example, when making use of bulk yielding kinetics in the nanocomposite context, one can rationalize the highly nonlinear rate-dependent mechanical response of such nanocomposites, including the prominent Payne effect [7, 17–19].

In an earlier publication, a thermodynamically-inspired concurrent two-scale model has been developed to describe the mechanical behavior of elastomers filled with hard nanoparticles [7]. While that model takes the yielding kinetics of the glassy bridges into account, the physical aging of the glassy bridges is neglected. However, it is assumed that the physical aging of the glassy bridges may be related to the so-called Mullins effect in cyclic deformation [3–5]. This effect consists in a softening due to mechanical deformation, however, that softening is only present at strains smaller than the maximal previously applied strain. If the material is loaded beyond the maximal previously applied strain, initially no softening is present at these previously unvisited strains, while after repeated loading to these higher strains there is again softening. It has been found that

the softening is not permanent, but that e.g. the permanent set or the complete stress-strain response can recover (partly) at a rate that is temperature-dependent, which is also sometimes called 'healing' [3–5, 101]. In this chapter, the Mullins effect is examined using the deformation protocol of [17, 18], that consists of a specific combination of mechanical rejuvenation (softening) and physical aging. Since the proper description of physical aging is rather involved and a topic of current research activities in the literature, the modeling of the Mullins effect in nanocomposites can be split into two steps. First, the physical aging and mechanical rejuvenation can be studied from a thermodynamic perspective for bulk glassy polymers, e.g. as done in [79, 80, 97, 102]. Second, the lessons learned from that latter work can be built into the two-scale nanocomposite model developed in [7], which is the topic of this chapter.

The manuscript is organized as follows. In Sec. 5.2 is presented the model development for nanoparticle-filled elastomers. The general concurrent two-scale model is summarized in Sec. 5.2.5. In Sec. 5.3, this model is made material-specific, whereafter it is analyzed numerically for illustration purposes by means of CONNFFESSIT-type simulations in Sec. 5.4. Finally, conclusions are drawn in Sec. 5.5.

Before we start, let us comment about the notation used throughout the entire chapter. Greek indices α, β, γ, ... are used for the Cartesian components of vectors and tensors, and Einstein's summation convention is used for indices that occur twice. Furthermore, with respect to operators, subscripts α and (α, β) imply contraction with any vector A_α and any tensor $A_{\alpha\beta}$ multiplied from the left, respectively, while subscripts γ and (γ, ε) imply contraction with the vector A_γ and tensor $A_{\gamma\varepsilon}$ multiplied from the right, respectively. An analogous notation is used for continuous indices. Specifically, let $\boldsymbol{\xi}$ denote the position in the space of (micro-)states. If a generalized field depends on $\boldsymbol{\xi}$, this implies continuous contraction (i.e. integration) over $\boldsymbol{\xi}$ with what is multiplied from the left, while a dependence on $\boldsymbol{\xi}'$ implies continuous contraction (i.e. integration) over $\boldsymbol{\xi}'$ with what is multiplied from the right. Finally, it is mentioned that boundary terms are neglected entirely, because the main goal of this chapter is the modeling of bulk material behavior. In contrast, the case where boundaries and interaction with the surrounding are of interest has been studied, e.g. in [35, 36].

5.2 Model development

5.2.1 Dynamic variables and generating functionals

The state of deformation of a purely elastic material can be quantified by the deformation gradient $\boldsymbol{F}$. This quantity contains also the mass density, $\rho = \rho_0 / \det \boldsymbol{F}$ with ρ_0 the mass density in the undeformed state. To describe the evolution of the material deformation, the velocity field $\boldsymbol{v}$ or the momentum density $\boldsymbol{m} = \rho \boldsymbol{v}$ are suitable candidates. While all these quantities are macroscopic, the microstructure in terms of the arrangement of the filler particles in the elastomer matrix is of interest as well, as discussed in the Introduction, Sec. 5.1. It has been discussed in detail in [7] that, in order to strike a balance between detail and model efficiency, it is useful to consider a single representative filler-particle pair only, instead of a large number of filler particles. Particularly, if $\boldsymbol{R}$ denotes the actual particle separation vector of the representative particle pair, and $\boldsymbol{Q}$ is the particle separation vector in the corresponding mechanically unloaded state, then the

distribution function $p(\boldsymbol{r}, \boldsymbol{R}, \boldsymbol{Q})$ is a useful microstructural quantity, which also depends on macroscopic position $\boldsymbol{r}$. The normalization of $p(\boldsymbol{r}, \boldsymbol{R}, \boldsymbol{Q})$ is such that integration over $\boldsymbol{R}$ and $\boldsymbol{Q}$ leads to the number density of (representative) particle pairs per unit volume [7].

In [7], this just discussed set of variables is augmented by the absolute temperature T in order to account for the thermal state and to be able to model nonisothermal processes. However, it turns out that for the extension sought in this chapter, namely the extension of [7] to account for the physical aging of the glassy bridges, the model formulation simplifies drastically when using the total entropy density per unit volume s_{t}, including all entropy contributions of the elastomer matrix as well as of the filler-particle arrangement.

To describe the physical aging of the glassy bridges, one needs to be able to model the physical aging of the glassy matrix material. As discussed in detail in [97, 102] and references therein, a practical way to achieve that is by accounting for an additional thermal variable. This is needed in order to mimic the fact that, in the glassy state, there is a substantial difference between the (rapid) relaxation and equilibration of vibrations around energy minima on the one hand, and on the other hand the population of different low-energy states by way of transitions across high energy barriers (by rare events). This discrepancy in dynamics can be captured by splitting the total entropy of the glassy material into its so-called kinetic (s) and configurational (η) parts, where the former describes the local intra-basin dynamics in the energy landscape, while the latter describes the much slower inter-basin dynamics [97, 102]. For the current study, however, one notices that only η needs to be included in the set of variables, while s can be obtained by subtracting η and the filler particle entropy from s_{t}.

In summary, the complete set of independent dynamic variables in an Eulerian (i.e. spatial) setting for the model formulation in this chapter is chosen as

$$\boldsymbol{\mathcal{X}} = \big(\boldsymbol{m}(\boldsymbol{r}),\, s_{\mathrm{t}}(\boldsymbol{r}),\, \eta(\boldsymbol{r}),\, \boldsymbol{F}(\boldsymbol{r}),\, p(\boldsymbol{r}, \boldsymbol{\xi})\big), \tag{5.1}$$

with macroscopic position $\boldsymbol{r}$, momentum density $\boldsymbol{m}$, total entropy density of elastomer matrix plus filler particles s_{t}, configurational entropy density of the elastomer matrix η, deformation gradient $\boldsymbol{F}$, and the filler particle arrangement described by p with $\boldsymbol{\xi} = (\boldsymbol{R}, \boldsymbol{Q})$. Note that also previously entropies have been used to model the effect of physical aging in glassy systems [80, 81, 85].

The total energy and the total entropy of the system in terms of the complete set of variables $\boldsymbol{\mathcal{X}}$ can be written in the form

$$E = \int \frac{m_\gamma m_\gamma}{2\rho}\, d^3\boldsymbol{r} + U\left[s_{\mathrm{t}}, \eta, \boldsymbol{F}, p\right], \tag{5.2}$$

$$S = \int s_{\mathrm{t}}\, d^3\boldsymbol{r}, \tag{5.3}$$

with U the non-kinetic, i.e. internal, energy contribution that is a yet unspecified functional of its arguments. The gradients of energy and entropy with respect to $\boldsymbol{\mathcal{X}}$ are then given by

$$\frac{\delta E}{\delta \boldsymbol{\mathcal{X}}} = \left(\boldsymbol{v},\, \left.\frac{\delta U}{\delta s_{\mathrm{t}}}\right|_{\eta,\boldsymbol{F},p},\, \left.\frac{\delta U}{\delta \eta}\right|_{s_{\mathrm{t}},\boldsymbol{F},p},\, \left.\frac{\delta U}{\delta \boldsymbol{F}}\right|_{s_{\mathrm{t}},\eta,p} - \frac{\boldsymbol{v}^2}{2}\rho_{,\boldsymbol{F}},\, \left.\frac{\delta U}{\delta p}\right|_{s_{\mathrm{t}},\eta,\boldsymbol{F}}\right), \tag{5.4}$$

$$\frac{\delta S}{\delta \boldsymbol{\mathcal{X}}} = (\boldsymbol{0}, 1, 0, \boldsymbol{0}, 0). \tag{5.5}$$

For the sake of simplifying the notation, the following abbreviations for the derivatives of the energy with respect to the entropies are introduced,

$$T_1 = \left.\frac{\delta U}{\delta s_{\mathrm{t}}}\right|_{\eta,\boldsymbol{F},p}, \tag{5.6}$$

$$T_2 = \left.\frac{\delta U}{\delta \eta}\right|_{s_{\mathrm{t}},\boldsymbol{F},p}. \tag{5.7}$$

At this point, the quantities T_1 and T_2 are no more than mere abbreviations for the functional derivatives. Their physical meaning will be explained in the following.

5.2.2 Physical meaning of the temperatures T_1 and T_2

In order to give a physical interpretation of the temperatures T_1 and T_2, first of all we recall that two temperatures, namely kinetic (T) and configurational (θ), have been used previously in the literature [74, 77, 79, 80, 82, 84, 87, 97] to describe aging and mechanical rejuvenation of amorphous solids, specifically [97]

$$T = \left.\frac{\delta U_{\mathrm{em}}}{\delta s}\right|_{\eta,\boldsymbol{F}}, \tag{5.8}$$

$$\theta = \left.\frac{\delta U_{\mathrm{em}}}{\delta \eta}\right|_{s,\boldsymbol{F}}, \tag{5.9}$$

with $U_{\mathrm{em}} = U_{\mathrm{em}}[s, \eta, \boldsymbol{F}]$ the internal energy of the elastomer matrix, and the kinetic (s) and configurational (η) entropy densities of the elastomer matrix, which add up to the total entropy density of the elastomer matrix $s_{\mathrm{em}} = s + \eta$. In the following, the relation between the temperature pairs (T, θ) and (T_1, T_2) is elaborated.

In the present study, in contrast to [97], the internal energy U and the entropy S depend on the filler-particle arrangement p. To proceed, we assume that

$$U = U_{\mathrm{em}}[s, \eta, \boldsymbol{F}] + U_{\mathrm{p}}[p], \tag{5.10}$$

in other words, there is an additive filler-particle contribution to the energy that is independent of the partial elastomer entropies s and η. Hence, the entropy-derivatives of U become

$$\left.\frac{\delta U}{\delta s}\right|_{\eta,\boldsymbol{F},p} = \left.\frac{\delta U_{\mathrm{em}}}{\delta s}\right|_{\eta,\boldsymbol{F}} = T, \tag{5.11}$$

$$\left.\frac{\delta U}{\delta \eta}\right|_{s,\boldsymbol{F},p} = \left.\frac{\delta U_{\mathrm{em}}}{\delta \eta}\right|_{s,\boldsymbol{F}} = \theta, \tag{5.12}$$

according to (5.8) and (5.9). Consideration of the change of variables $s \rightarrow s_{\mathrm{t}}$ implies that the internal energy U can be written in the form $U = U_{\mathrm{em}}[s(s_{\mathrm{t}}, \eta, s_{\mathrm{p}}), \eta, \boldsymbol{F}] + U_{\mathrm{p}}[p]$, with derivatives

$$T_1 = \left.\frac{\delta U}{\delta s_{\mathrm{t}}}\right|_{\eta,\boldsymbol{F},p} = \left.\frac{\delta U_{\mathrm{em}}[s, \eta, \boldsymbol{F}]}{\delta s}\right|_{\eta,\boldsymbol{F}} \left.\frac{\partial s}{\partial s_{\mathrm{t}}}\right|_{\eta,s_{\mathrm{p}}} = T, \tag{5.13}$$

$$T_2 = \left.\frac{\delta U}{\delta \eta}\right|_{s_{\mathrm{t}},\boldsymbol{F},p} = \left.\frac{\delta U_{\mathrm{em}}[s, \eta, \boldsymbol{F}]}{\delta s}\right|_{\eta,\boldsymbol{F}} \left.\frac{\partial s}{\partial \eta}\right|_{s_{\mathrm{t}},s_{\mathrm{p}}} + \left.\frac{\delta U_{\mathrm{em}}}{\delta \eta}\right|_{s,\boldsymbol{F}} = -T + \theta, \tag{5.14}$$

where we have again used the definitions (5.8) and (5.9) as well as the split, in complete analogy to (5.10),

$$s_{\mathrm{t}} = s + \eta + s_{\mathrm{p}}[p] \,, \tag{5.15}$$

where the filler-particle entropy s_{p} does not depend on s and η. It should be noted, that in the expressions (5.13) and (5.14), constant p implies that s_{p} is constant, by virtue of (5.15). Equations (5.13) and (5.14) provide the desired physical interpretation of T_1 and T_2 defined in (5.6) and (5.7) by relating them to the kinetic and configurational temperatures, (5.8) and (5.9), respectively.

The assumptions (5.10) and (5.15) state that the filler-particle contributions to the internal energy and to the entropy do not depend on the thermodynamic state of the elastomer matrix. To support these assumptions, one can argue as follows. Using the assumptions (5.10) and (5.15), the temperatures T and θ, derived from (5.13) and (5.14), are functions $T = T(s, \eta, \boldsymbol{F})$, $\theta = \theta(s, \eta, \boldsymbol{F})$, from which one can obtain the inverse functions $s = s(T, \theta, \boldsymbol{F})$, $\eta = \eta(T, \theta, \boldsymbol{F})$. Substituting these into (5.10) and (5.15), one obtains

$$
\begin{aligned}
U &= U_{\mathrm{em}}[T, \theta, \boldsymbol{F}] + U_{\mathrm{p}}[p] \,, & (5.16) \\
S &= S_{\mathrm{em}}[T, \theta, \boldsymbol{F}] + S_{\mathrm{p}}[p] \,, & (5.17)
\end{aligned}
$$

in terms of temperatures.

In the sequel, it is discussed under what circumstances the forms (5.16) and (5.17) for the energy U and the entropy S are the natural ones. In the most general case, the internal energy U and the entropy S are functionals of all dynamic variables. In practical applications, however, it is convenient to split these functionals additively into their elastomer-matrix and filler-particle contributions. Let us consider the potential Φ describing the energy stored in the system because of the current state $\boldsymbol{R}$ being different from the load-free state $\boldsymbol{Q}$. Since Φ plays the role of a Helmholtz free energy, it decomposes into energetic and entropic parts, $\Phi = \Phi^{\mathsf{E}} + \Phi^{\mathsf{S}}$ [7, 29] by way of

$$
\begin{aligned}
\Phi^{\mathsf{E}} &= \Phi - T\frac{\partial \Phi}{\partial T} \,, & (5.18) \\
\Phi^{\mathsf{S}} &= T\frac{\partial \Phi}{\partial T} \,. & (5.19)
\end{aligned}
$$

For the case that the potential Φ depends linearly on temperature T, namely $\Phi = \Phi_0 + T\Phi_1$ with T-independent Φ_0 and Φ_1, one can readily see that $\Phi^{\mathsf{S}} = T\Phi_1$ and $\Phi^{\mathsf{E}} = \Phi_0$. For the p-dependent contribution U_{p} to the internal energy $U = U_{\mathrm{em}}[T, \theta, \boldsymbol{F}] + U_{\mathrm{p}}[p]$ and the p-dependent contribution S_{p} to the entropy $S = S_{\mathrm{em}}[T, \theta, \boldsymbol{F}] + S_{\mathrm{p}}[p]$, one thus finds

$$
\begin{aligned}
U_{\mathrm{p}}[p] &= \iint p\Phi_0 d^6\boldsymbol{\xi}d^3\boldsymbol{r} \,, & (5.20) \\
S_{\mathrm{p}}[p] &= -\iint p\Big(\Phi_1 + k_{\mathrm{B}}\ln p\Big)d^6\boldsymbol{\xi}d^3\boldsymbol{r} \,, & (5.21)
\end{aligned}
$$

in agreement with (5.16) and (5.17), i.e. the filler-particle contributions U_{p} and S_{p} do not depend on the thermodynamic state of the elastomer matrix. This argument cannot only be used if $\Phi = \Phi_0 + T\Phi_1$ holds for the entire range of temperature, but also if this holds over a finite temperature range of interest.

In summary, the temperature-pairs (T, θ) and (T_1, T_2) have been related through (5.13) and (5.14). In what follows in this chapter, we will work with T, θ rather than T_1, T_2, since the first set is more intuitive and relates to the previous studies [7] and [97].

5.2.3   Reversible dynamics

The reversible part of the dynamics of $\mathcal{X}$, according to $(2.2)_1$, is related to the gradient of energy $\delta E/\delta \mathcal{X}$ (5.4) through the Poisson operator $\mathcal{L}$. The reversible dynamics considered in this chapter is all related to the deformation field, $\boldsymbol{v}(\boldsymbol{r})$. Inspection of the energy gradient (5.4) thus suggests that the determination of the Poisson operator should focus on the first column, and due to the anti-symmetry (2.5a), the first row of $\mathcal{L}$. To that end, one can depart from the model developed in [7] where the physical aging has not been included, and then add the configurational entropy η to that description in order to account for the physical aging. This leads to (see also [7, 97])

$$
\mathcal{L} = \begin{pmatrix}
\mathcal{L}_{\alpha\gamma}^{(mm)} & \mathcal{L}_{\alpha}^{(ms_t)} & \mathcal{L}_{\alpha}^{(m\eta)} & \mathcal{L}_{\alpha\gamma\varepsilon}^{(mF)} & \mathcal{L}_{\alpha}^{(mp)} \\
\mathcal{L}_{\gamma}^{(s_t m)} & 0 & 0 & 0 & 0 \\
\mathcal{L}_{\gamma}^{(\eta m)} & 0 & 0 & 0 & 0 \\
\mathcal{L}_{\alpha\beta\gamma}^{(Fm)} & 0 & 0 & 0 & 0 \\
\mathcal{L}_{\gamma}^{(pm)} & 0 & 0 & 0 & 0
\end{pmatrix},
\tag{5.22}
$$

with the operators

$$
\begin{align}
\mathcal{L}_{\alpha\gamma}^{(mm)} &= -\nabla_{\gamma}^r \, m_\alpha - m_\gamma \nabla_\alpha^r, \tag{5.23} \\
\mathcal{L}_{\alpha}^{(ms_t)} &= -s_t \nabla_\alpha^r, \tag{5.24} \\
\mathcal{L}_{\alpha}^{(m\eta)} &= -\eta \nabla_\alpha^r, \tag{5.25} \\
\mathcal{L}_{\gamma}^{(s_t m)} &= -\nabla_\gamma^r \, s_t, \tag{5.26} \\
\mathcal{L}_{\gamma}^{(\eta m)} &= -\nabla_\gamma^r \, \eta, \tag{5.27} \\
\mathcal{L}_{\alpha\gamma\varepsilon}^{(mF)} &= \left(\nabla_\alpha^r \, F_{\gamma\varepsilon} \right) + \nabla_\mu^r \, F_{\mu\varepsilon} \delta_{\alpha\gamma}, \tag{5.28} \\
\mathcal{L}_{\alpha\beta\gamma}^{(Fm)} &= -\left(\nabla_\gamma^r \, F_{\alpha\beta} \right) + F_{\mu\beta} \nabla_\mu^r \delta_{\alpha\gamma}, \tag{5.29} \\
\mathcal{L}_{\alpha}^{(mp)} &= -p' \nabla_\alpha^r + \nabla_\mu^r R_\mu' p' \nabla_\alpha^{R'}, \tag{5.30} \\
\mathcal{L}_{\gamma}^{(pm)} &= -\nabla_\gamma^r \, p - \nabla_\gamma^R R_\mu p \nabla_\mu^r. \tag{5.31}
\end{align}
$$

where f' stands for $f(\boldsymbol{\xi}')$ for any quantity f. It is emphasized that all differential operators, specifically ∇^r, ∇^R, and $\nabla^{R'}$ in (5.23)–(5.31), act on everything to their right, also on what will be multiplied to the right of $\mathcal{L}$. The only exception to this rule is if the differential operator together with its object of action is enclosed in parenthesis. The same convention will be used in the remained of this chapter, i.e. also in Sec. 5.2.4.

It should be pointed out that for the Poisson operator (5.22)–(5.31) both the degeneracy condition (2.4a) and the anti-symmetry property (2.5a) are satisfied. Moreover, the Jacobi identity (2.6) is satisfied as well, which can be proven as follows. In general, the Poisson operator in the Eulerian setting is induced by a Poisson operator in the Lagrangian setting [100]. Furthermore, it can be shown that the Jacobi identity in the Eulerian setting is guaranteed by the Jacobi identity in the Lagrangian setting. This result is useful

here, since it is much easier to check the Jacobi identity in the Lagrangian setting, where the Poisson operator is almost trivial. Note that, with (5.27), it can be shown that the material time derivative (D_t) of the specific configurational entropy density, $\hat{\eta} = \eta/\rho$, is $D_t \hat{\eta} = 0$. Therefore, from a Lagrangian viewpoint, η does not participate in the reversible dynamics. With respect to the verification of the Jacobi identity, the case with variables (5.1) is thus identical with the one studied in [7], where the Jacobi identity has been found to be satisfied.

Having an explicit form for the Poisson operator, and multiplying it with the gradient of energy (5.4), one can write the reversible part $(2.2)_1$ of the $\mathcal{X}$-evolution equation in the form

$$
\begin{aligned}
\partial_t m_\alpha |_{\text{rev}} &= -\nabla_\gamma^r (m_\alpha v_\gamma) + \nabla_\gamma^r \hat{\sigma}_{\alpha\gamma} \,, & (5.32) \\
\partial_t s_{\text{t}} |_{\text{rev}} &= -\nabla_\gamma^r (s_{\text{t}} v_\gamma) \,, & (5.33) \\
\partial_t \eta |_{\text{rev}} &= -\nabla_\gamma^r (\eta v_\gamma) \,, & (5.34) \\
\partial_t F_{\alpha\beta} |_{\text{rev}} &= -v_\mu (\nabla_\mu^r F_{\alpha\beta}) + F_{\mu\beta} (\nabla_\mu^r v_\alpha) \,, & (5.35) \\
\partial_t p |_{\text{rev}} &= -\nabla_\gamma^r (p v_\gamma) - \nabla_\gamma^R (R_\mu p (\nabla_\mu^r v_\gamma)) \,, & (5.36)
\end{aligned}
$$

with the stress-like quantity

$$
\begin{aligned}
\hat{\sigma}_{\alpha\gamma} &= \left(u - T s_{\text{t}} - (\theta - T)\eta - \int p \left. \frac{\delta U}{\delta p} \right|_{s_{\text{t}}, \eta, \boldsymbol{F}} d^6 \boldsymbol{\xi} \right) \delta_{\alpha\gamma} \\
&+ \left. \frac{\delta U}{\delta F_{\alpha\varepsilon}} \right|_{s_{\text{t}}, \eta, p} F_{\gamma\varepsilon} + \int p R_\gamma \left(\nabla_\alpha^R \left. \frac{\delta U}{\delta p} \right|_{s_{\text{t}}, \eta, \boldsymbol{F}} \right) d^6 \boldsymbol{\xi} \,, & (5.37)
\end{aligned}
$$

as an extension of [7] with respect to the additional variable η. Here, u denotes the density of internal energy per unit volume, containing contributions of both the elastomer matrix and the filler particles. In view of (5.2), one therefore has $U = \int u \, d^3 \boldsymbol{r}$. As will be discussed further below, the relation (5.37) is not yet the complete Cauchy stress tensor, particularly because the last particle-based contribution is not symmetric.

5.2.4   Irreversible dynamics

In this section, the irreversible contributions $(2.2)_2$ to the $\mathcal{X}$-evolution equations will be discussed. In view of [7, 97], the irreversible dynamics can be split into dissipative and non-dissipative parts. Specifically the viscoplastic deformation of glassy bridges [7] and physical aging of glassy material [97] enter as dissipative contributions to the dynamics, while non-affine deformation of the glassy network is represented by non-dissipative, but still irreversible, dynamics (see [7] for a detailed discussion on this latter point).

5.2.4.1   Dissipative part: Viscoplastic deformation and physical aging

In order to formulate the dissipative dynamics within the GENERIC framework, one starts from a factorization of the friction matrix [41]

$$
\mathcal{M} = \mathcal{C}\mathcal{R}\mathcal{C}^* \,, \tag{5.38}
$$

with a symmetric and positive semi-definite matrix $\mathcal{R}$, the operator $\mathcal{C}$ that represents the so-called mechanical part, and its adjoint operator $\mathcal{C}^*$. Here and in what follows, the symbol $*$ stands for the adjoint operator. It is essential to note that the symmetry and positive semi-definiteness of $\mathcal{R}$ automatically imply the corresponding conditions (2.5b) and (2.5c) for the friction matrix $\mathcal{M}$. By requiring

$$\mathcal{C}^* \frac{\delta E}{\delta \mathcal{X}} = 0\,, \tag{5.39}$$

the degeneracy condition (2.4b) can be satisfied. It is emphasized that for these dissipative contributions to the dynamics, the Onsager-symmetry is relevant, i.e. (2.5b) applies to $\mathcal{M}$, and an analogous condition follows for $\mathcal{R}$.

Since two different dissipative processes, i.e. viscoplastic deformation and physical aging of the glassy bridges, are to be modeled, one considers a matrix $\mathcal{R}$ of rank two, and consequently $\mathcal{C}$ and $\mathcal{C}^*$ are 2×5 and 5×2 (generalized) matrices, respectively. The focus on these two dissipative processes implies that there will be two thermodynamic forces, denoted by $\mathcal{F} = \left(\mathcal{F}^\Delta, \mathcal{F}^p\right)$, and two corresponding thermodynamic fluxes, denoted by $\mathcal{J} = \left(\mathcal{J}^\Delta, \mathcal{J}^p\right)$ [29, 42].

If Newtonian viscous stresses are neglected, in analogy to [13], and since the total deformation gradient describes purely affine kinematics, the evolution equations of both m and F do not have any dissipative contributions. Therefore, it is reasonable to assume that the first and fourth rows of $\mathcal{C}$, and therefore the first and fourth columns of $\mathcal{C}^*$, must be zero. Hence, a reasonable ansatz for the operators $\mathcal{C}$ and $\mathcal{C}^*$ is given by

$$\mathcal{C} = \begin{pmatrix} 0 & 0 \\ \left(\frac{1}{T} - \frac{1}{\theta}\right) & \mathcal{C}_\gamma^{(s_t)} \\ -\frac{1}{\theta} & \mathcal{C}_\gamma^{(\eta)} \\ 0 & 0 \\ 0 & \mathcal{C}_\gamma^{(p)} \end{pmatrix}\,, \quad \mathcal{C}^* = \begin{pmatrix} 0 & \left(\frac{1}{T} - \frac{1}{\theta}\right) & -\frac{1}{\theta} & 0 & 0 \\ 0 & \mathcal{C}_\alpha^{*(s_t)} & \mathcal{C}_\alpha^{*(\eta)} & 0 & \mathcal{C}_\alpha^{*(p)} \end{pmatrix}\,. \tag{5.40}$$

The explicit form of the first row of $\mathcal{C}^*$, and as consequence the first column of $\mathcal{C}$, is motivated by [97] in order to obtain the thermodynamic driving force for physical aging, i.e. $\mathcal{F}^\Delta = (1/T - 1/\theta)$. More explicitly, the process of physical aging goes on until the configurational temperature θ approaches the kinetic temperature T, in which case the thermodynamic driving force $\mathcal{F}^\Delta$ vanishes. Moreover, the given form of the first row of $\mathcal{C}^*$ satisfies the degeneracy condition (5.39).

In order to determine all other unknown elements of the operators $\mathcal{C}$ and $\mathcal{C}^*$, one starts with considering the evolution equation of the filler-particle arrangement p. While this has been studied in [7] in the absence of aging, that procedure is adapted in this chapter to account for physical aging. In view of the Liouville theorem [103], the (irreversible part of the) evolution of p must have the form of the divergence of the thermodynamic flux, namely

$$\partial_t p(\boldsymbol{r}, \boldsymbol{\xi})|_{\text{diss}} = \int \delta(\boldsymbol{R} - \boldsymbol{R}') \left(\nabla_\gamma^{Q'} \delta(\boldsymbol{Q} - \boldsymbol{Q}')\right) \mathcal{J}_\gamma^p(\boldsymbol{\xi}')\, d^6\boldsymbol{\xi}'\,, \tag{5.41}$$

with the thermodynamic flux $\mathcal{J}_\gamma^p$ for viscoplastic deformation. In view of the last row of

$\mathcal{C}$ and the equation (5.41), one can explicitly determine $\mathcal{C}_\gamma^{(p)}$ and its adjoint $\mathcal{C}_\alpha^{*(p)}$ [7],

$$\mathcal{C}_\gamma^{(p)} = \delta\left(\boldsymbol{R} - \boldsymbol{R}'\right)\left(\nabla_\gamma^{Q'}\delta\left(\boldsymbol{Q} - \boldsymbol{Q}'\right)\right), \tag{5.42}$$

$$\mathcal{C}_\alpha^{*(p)} = \delta\left(\boldsymbol{R}' - \boldsymbol{R}\right)\left(\nabla_\alpha^{Q}\delta\left(\boldsymbol{Q}' - \boldsymbol{Q}\right)\right). \tag{5.43}$$

Consequently, the degeneracy condition (5.39) applied to the second row of $\mathcal{C}^*$ reads

$$\mathcal{C}_\alpha^{*(s_\mathrm{t})}T + \mathcal{C}_\alpha^{*(\eta)}(\theta - T) = -\left(\nabla_\alpha^{Q}\left.\frac{\delta U}{\delta p}\right|_{s_\mathrm{t},\eta,\boldsymbol{F}}\right). \tag{5.44}$$

This condition, however, does not give a unique solution for the operators $\mathcal{C}_\alpha^{*(s_\mathrm{t})}$ and $\mathcal{C}_\alpha^{*(\eta)}$, but rather needs to be supplemented by an extra assumption. An intuitive assumption is to adopt the case where both $\mathcal{C}_\alpha^{*(s_\mathrm{t})}$ and $\mathcal{C}_\alpha^{*(\eta)}$ are proportional to the right-hand side expression. Motivated by [97], where instead of the total entropy density as a dynamic variable the entropy density of the kinetic subsystem is used (rendering the description more "symmetric"), we choose the operators $\mathcal{C}_\alpha^{*(s_\mathrm{t})}$ and $\mathcal{C}_\alpha^{*(\eta)}$ to be of the form

$$\mathcal{C}_\alpha^{*(s_\mathrm{t})} = -\left(\frac{\varphi}{T} + \frac{(1-\varphi)}{\theta}\right)\left(\nabla_\alpha^{Q}\left.\frac{\delta U}{\delta p}\right|_{s_\mathrm{t},\eta,\boldsymbol{F}}\right), \tag{5.45}$$

$$\mathcal{C}_\alpha^{*(\eta)} = -\frac{(1-\varphi)}{\theta}\left(\nabla_\alpha^{Q}\left.\frac{\delta U}{\delta p}\right|_{s_\mathrm{t},\eta,\boldsymbol{F}}\right), \tag{5.46}$$

with an arbitrary function $\varphi(\boldsymbol{\mathcal{X}})$. This specific choice satisfies the degeneracy condition (5.44), and it switches off either the T- or the θ-contributions to $\mathcal{C}_\alpha^{*(s_\mathrm{t})}$ and $\mathcal{C}_\alpha^{*(\eta)}$ for $\varphi = 0$ or $\varphi = 1$, respectively, in analogy to [97]. Making use of the symmetry-condition of $\mathcal{M}$ leads to

$$\mathcal{C}_\gamma^{(s_\mathrm{t})} = -\left(\frac{\varphi'}{T} + \frac{(1-\varphi')}{\theta}\right)\left(\nabla_\gamma^{Q'}\left.\frac{\delta U}{\delta p'}\right|_{s_\mathrm{t},\eta,\boldsymbol{F}}\right), \tag{5.47}$$

$$\mathcal{C}_\gamma^{(\eta)} = -\frac{(1-\varphi')}{\theta}\left(\nabla_\gamma^{Q'}\left.\frac{\delta U}{\delta p'}\right|_{s_\mathrm{t},\eta,\boldsymbol{F}}\right). \tag{5.48}$$

At this point, we have determined the operators $\mathcal{C}$ and $\mathcal{C}^*$, and therefore one can calculate the thermodynamic driving forces for physical aging ($\mathcal{F}^\Delta$) and viscoplastic deformation of the glassy bridges ($\mathcal{F}^p$), namely

$$\mathcal{F}^\Delta = \frac{1}{T} - \frac{1}{\theta} \tag{5.49}$$

$$\boldsymbol{\mathcal{F}}^p = -\left(\frac{\varphi}{T} + \frac{(1-\varphi)}{\theta}\right)\left(\nabla_\alpha^{Q}\left.\frac{\delta U}{\delta p}\right|_{s_\mathrm{t},\eta,\boldsymbol{F}}\right). \tag{5.50}$$

To obtain the thermodynamic flux $\boldsymbol{\mathcal{J}}$, first of all we use the decomposition $\mathcal{R} = \mathcal{R}^\times + \mathcal{R}^p$, with contributions representative of the exchange between the kinetic and

configurational subsystems ("x") for the process of physical aging, and of viscoplastic deformation ("p") of the glassy bridges. Motivated by [97], one can express the operator $\mathcal{R}^{\mathsf{x}}$ in the following form

$$\mathcal{R}^{\mathsf{x}} = \begin{pmatrix} \mu^{\mathsf{x}} & 0 \\ 0 & 0 \end{pmatrix} , \tag{5.51}$$

with $\mu^{\mathsf{x}} \geq 0$, which leads to the flux $\boldsymbol{\mathcal{J}}^{\mathsf{x}} = \mathcal{R}^{\mathsf{x}}\boldsymbol{\mathcal{F}} = (\mathcal{J}^{\Delta,\mathsf{x}}, 0)$ with

$$\mathcal{J}^{\Delta,\mathsf{x}} = \mu^{\mathsf{x}}\mathcal{F}^{\Delta} = \mu^{\mathsf{x}} \left(\frac{1}{T} - \frac{1}{\theta} \right) . \tag{5.52}$$

Next, the formulation of viscoplastic deformation of the glassy bridges is considered. Since the driving force $\boldsymbol{\mathcal{F}}^{p}$ in (5.50) contains a term proportional to $(1/T - 1/\theta)$ as does $\mathcal{F}^{\Delta}$ in (5.49), one needs to allow in principle for a combination of both $\mathcal{F}^{\Delta}$ and $\boldsymbol{\mathcal{F}}^{p}$ to obtain the effective driving force for viscoplastic deformation, similarly to [97], which can be represented by

$$\mathcal{R}^{\mathsf{p}} = \begin{pmatrix} \omega_{\mu}(\boldsymbol{\xi}) \\ \delta_{\alpha\mu} \end{pmatrix} \lambda_{\mu\nu}(\boldsymbol{\xi}, \boldsymbol{\xi}') \begin{pmatrix} \omega_{\nu}(\boldsymbol{\xi}') & \delta_{\nu\gamma} \end{pmatrix} , \tag{5.53}$$

where the symmetry and positive semi-definiteness of $\mathcal{R}^{\mathsf{p}}$ requires the same for $\lambda_{\mu\nu}$. With the ansatz (5.53), one can determine the fluxes, related to viscoplastic deformation, namely $\boldsymbol{\mathcal{J}}^{\mathsf{p}} = \mathcal{R}^{\mathsf{p}}\boldsymbol{\mathcal{F}} = (\mathcal{J}^{\Delta,\mathsf{p}}, \mathcal{J}^{p,\mathsf{p}})$ with

$$\mathcal{J}^{\Delta,\mathsf{p}} = \omega_{\mu}\mathcal{J}^{p,\mathsf{p}}_{\mu} , \tag{5.54}$$

$$\mathcal{J}^{p,\mathsf{p}}_{\alpha}(\boldsymbol{\xi}) = \int \lambda_{\alpha\nu}(\boldsymbol{\xi}, \boldsymbol{\xi}')\mathcal{F}^{p,\mathrm{eff}}_{\nu}(\boldsymbol{\xi}')\, d^{6}\boldsymbol{\xi}' , \tag{5.55}$$

with the effective driving force

$$\mathcal{F}^{p,\mathrm{eff}}_{\alpha} = \omega_{\alpha}\mathcal{F}^{\Delta} + \mathcal{F}^{p}_{\alpha} . \tag{5.56}$$

Equation (5.54) relates the effective driving force to the current density in the filler-particle arrangement space. Furthermore, relations (5.54) and (5.55) show that ω_{α} plays a twofold role. On the one hand it enters the effective driving force (5.56). On the other hand, it leads to a non-zero contribution to the exchange between the kinetic and configurational subsystems, (5.54), due to viscoplastic deformation. As will be discussed below, the quantity ω_{α} will become essential for modeling the so-called mechanical rejuvenation of the glassy bridges, i.e., the fluidization of the glassy bridges due to the applied load, thereby affecting the macroscopic mechanical response of the entire nanocomposite. The mechanical rejuvenation of bulk glassy polymers has been studied in detail, both experimentally [69,72] as well as in modeling and simulation [79,80], and it has also been incorporated previously in nanocomposite models in a non-thermodynamic manner [17,18].

Finally, collecting all dissipative contributions discussed above, the corresponding con-

tributions to the evolution equations of $\boldsymbol{\mathcal{X}}$ become

$$\partial_t m_\alpha|_{\text{diss}} = 0, \tag{5.57}$$

$$\begin{aligned}\partial_t s_t|_{\text{diss}} = {}& \left(\frac{1}{T} - \frac{1}{\theta}\right) \mathcal{J}^{\Delta,\times} + \left(\frac{1}{T} - \frac{1}{\theta}\right) \int \mathcal{J}^{\Delta,\text{p}}\, d^6\boldsymbol{\xi} \\ & - \int \left(\frac{\varphi}{T} + \frac{(1-\varphi)}{\theta}\right) \left(\nabla_\gamma^Q \left.\frac{\delta U}{\delta p}\right|_{s_t,\eta,\boldsymbol{F}}\right) \mathcal{J}_\gamma^{\text{p,p}}\, d^6\boldsymbol{\xi}, \end{aligned}$$

$$\begin{aligned}\partial_t \eta|_{\text{diss}} = {}& -\frac{1}{\theta} \mathcal{J}^{\Delta,\times} - \frac{1}{\theta} \int \mathcal{J}^{\Delta,\text{p}} d^6\boldsymbol{\xi} \\ & - \int \frac{(1-\varphi)}{\theta} \left(\nabla_\gamma^Q \left.\frac{\delta U}{\delta p}\right|_{s_t,\eta,\boldsymbol{F}}\right) \mathcal{J}_\gamma^{\text{p,p}}\, d^6\boldsymbol{\xi}, \end{aligned} \tag{5.58}$$

$$\partial_t F_{\alpha\beta}|_{\text{diss}} = 0, \tag{5.59}$$

$$\partial_t p|_{\text{diss}} = -\nabla_\gamma^Q \mathcal{J}_\gamma^{\text{p,p}}, \tag{5.60}$$

with the thermodynamic fluxes $\mathcal{J}^{\Delta,\times}$, $\mathcal{J}^{\Delta,\text{p}}$ and $\mathcal{J}_\gamma^{\text{p,p}}$, given by the expressions (5.52) and (5.54)–(5.55), respectively. The set of equations (5.57)–(5.60) clearly shows the effects of heat exchange between the two thermal subsystems ("x") representative of physical aging, and of viscoplastic deformation ("p").

5.2.4.2   Non-dissipative part: Non-affine deformation

Finally, let us discuss the irreversible but non-dissipative contributions to the evolution of $\boldsymbol{\xi}$. In complete analogy to [7], the only reason to include such contributions is the observation that the stress-like quantity (5.37) is not symmetric in general, e.g. if $\nabla^R(\delta U/\delta p)$ is proportional to $\boldsymbol{R} - \boldsymbol{Q}$ (see below). However, it was argued in [7] that the symmetry of the stress tensor can indeed be restored by excluding the anti-symmetric part of the imposed velocity gradient from the last contribution to the p-evolution equation (5.36). It is pointed out that, in contrast to the dissipative dynamics discussed in Sec. 5.2.4.1, in this section the Onsager-symmetry (2.5b) must be replaced by the Casimir-symmetry, namely $\boldsymbol{\mathcal{M}}^{\text{T}} = -\boldsymbol{\mathcal{M}}$, leading to the absence of dissipation. The reader is referred to [29] for the conceptual details on this issue, and for an example in complex fluids modeling.

To exclude the anti-symmetric part of the imposed velocity gradient from the last contribution to the p-evolution equation (5.36), the following contribution to its evolution needs to be added [7],

$$\partial_t p|_{\text{non-a}} = -\nabla_\nu^R \left(\frac{1}{2}\left[(\nabla_\nu^r v_\mu) - (\nabla_\mu^r v_\nu)\right] R_\mu p\right). \tag{5.61}$$

As an extension to the case studied in [7], we consider the irreversible but non-dissipative operator $\tilde{\boldsymbol{\mathcal{M}}}$ of the form

$$\tilde{\boldsymbol{\mathcal{M}}} = \begin{pmatrix} 0 & \tilde{\mathcal{M}}_\alpha^{(ms_t)} & \tilde{\mathcal{M}}_\alpha^{(m\eta)} & 0 & \tilde{\mathcal{M}}_\alpha^{(mp)} \\ \tilde{\mathcal{M}}_\gamma^{(s_t m)} & 0 & 0 & 0 & \tilde{\mathcal{M}}^{(s_t p)} \\ \tilde{\mathcal{M}}_\gamma^{(\eta m)} & 0 & 0 & 0 & \tilde{\mathcal{M}}^{(\eta p)} \\ 0 & 0 & 0 & 0 & 0 \\ \tilde{\mathcal{M}}_\gamma^{(pm)} & \tilde{\mathcal{M}}^{(ps_t)} & \tilde{\mathcal{M}}^{(p\eta)} & 0 & 0 \end{pmatrix}, \tag{5.62}$$

where the structure of the third row is such, that the configurational entropy density of the elastomer, η, is not altered, similarly to s_t. In view of the specific form of $\tilde{\mathcal{M}}$ and the entropy gradient (5.5), one can uniquely determine $\tilde{\mathcal{M}}^{(ps_t)}$,

$$\tilde{\mathcal{M}}^{(ps_t)} = -\frac{1}{2} \left(\nabla_\nu^R R_\mu p \right) \left[\left(\nabla_\nu^r v_\mu \right) - \left(\nabla_\mu^r v_\nu \right) \right] ,\tag{5.63}$$

in order to reproduce (5.61) [7]. Subsequently applying the degeneracy condition (2.4b) to the last row of $\tilde{\mathcal{M}}$ leads to

$$\tilde{\mathcal{M}}_\gamma^{(pm)} v_\gamma + \tilde{\mathcal{M}}^{(ps_t)} T + \tilde{\mathcal{M}}^{(p\eta)}(\theta - T) = 0 .\tag{5.64}$$

Requiring the same structure for $\tilde{\mathcal{M}}^{(ps_t)}$ and $\tilde{\mathcal{M}}^{(p\eta)}$, and consequently for $\tilde{\mathcal{M}}_\gamma^{(pm)} v_\gamma$, one finds

$$\tilde{\mathcal{M}}_\gamma^{(pm)} = \frac{1}{2} \left(\nabla_\nu^R R_\mu p \right) (T + (\theta - T)\zeta) \left[\delta_{\gamma\mu} \nabla_\nu^r - \delta_{\gamma\nu} \nabla_\mu^r \right] ,\tag{5.65}$$

$$\tilde{\mathcal{M}}^{(p\eta)} = -\frac{1}{2} \left(\nabla_\nu^R R_\mu p \right) \zeta \left[\left(\nabla_\nu^r v_\mu \right) - \left(\nabla_\mu^r v_\nu \right) \right] ,\tag{5.66}$$

with an arbitrary function ζ of the variables $\boldsymbol{\mathcal{X}}$, $\zeta(\boldsymbol{\mathcal{X}})$. In order to obtain the operator $\tilde{\mathcal{M}}^{(s_t p)}$, we make use of the Casimir-symmetry condition, applied to (5.63), which results in

$$\tilde{\mathcal{M}}^{(s_t p)} = \frac{1}{2} \left(\nabla_\nu^{R'} R_\mu' p' \right) \left[\left(\nabla_\nu^r v_\mu \right) - \left(\nabla_\mu^r v_\nu \right) \right] ,\tag{5.67}$$

$$\tilde{\mathcal{M}}_\gamma^{(s_t m)} = -\frac{1}{2} \int \left. \frac{\delta U}{\delta p} \right|_{s_t, \eta, \boldsymbol{F}} \left(\nabla_\nu^R R_\mu p \right) d^6\boldsymbol{\xi} \left[\delta_{\gamma\mu} \nabla_\nu^r - \delta_{\gamma\nu} \nabla_\mu^r \right] ,\tag{5.68}$$

where (5.68) was obtained by using the degeneracy condition (2.4b). Further, using again the Casimir-symmetry for (5.66) followed by the the degeneracy condition (2.4b), one obtains

$$\tilde{\mathcal{M}}^{(\eta p)} = \frac{1}{2} \left(\nabla_\nu^{R'} R_\mu' p' \right) \zeta' \left[\left(\nabla_\nu^r v_\mu \right) - \left(\nabla_\mu^r v_\nu \right) \right] ,\tag{5.69}$$

$$\tilde{\mathcal{M}}_\gamma^{(\eta m)} = -\frac{1}{2} \int \left. \frac{\delta U}{\delta p} \right|_{s_t, \eta, \boldsymbol{F}} \left(\nabla_\nu^R R_\mu p \right) \zeta \, d^6\boldsymbol{\xi} \left[\delta_{\gamma\mu} \nabla_\nu^r - \delta_{\gamma\nu} \nabla_\mu^r \right] .\tag{5.70}$$

Finally, applying the Casimir-symmetry condition to (5.68), (5.70) and (5.65), the remaining elements of $\mathcal{M}$ can be determined,

$$\tilde{\mathcal{M}}_\alpha^{(ms_t)} = -\frac{1}{2} \left[\delta_{\alpha\mu} \nabla_\nu^r - \delta_{\alpha\nu} \nabla_\mu^r \right] \int \left. \frac{\delta U}{\delta p} \right|_{s_t, \eta, \boldsymbol{F}} \left(\nabla_\nu^R R_\mu p \right) d^6\boldsymbol{\xi} ,\tag{5.71}$$

$$\tilde{\mathcal{M}}_\alpha^{(m\eta)} = -\frac{1}{2} \left[\delta_{\alpha\mu} \nabla_\nu^r - \delta_{\alpha\nu} \nabla_\mu^r \right] \int \zeta \left. \frac{\delta U}{\delta p} \right|_{s_t, \eta, \boldsymbol{F}} \left(\nabla_\nu^R R_\mu p \right) d^6\boldsymbol{\xi} ,\tag{5.72}$$

$$\tilde{\mathcal{M}}_\alpha^{(mp)} = \frac{1}{2} \left[\delta_{\alpha\mu} \nabla_\nu^r - \delta_{\alpha\nu} \nabla_\mu^r \right] (T + (\theta - T)\zeta') \left(\nabla_\nu^{R'} R_\mu' p' \right) .\tag{5.73}$$

It can be shown that the first row of the matrix $\tilde{\mathcal{M}}$ complies with the degeneracy condition (2.4b), which completes the procedure of determining $\tilde{\mathcal{M}}$.

Summarizing the above, the contribution of non-affine dynamics to the evolution equations of $\mathcal{X}$ can be written in the form

$$\partial_t m_\alpha|_{\text{non-a}} = \frac{1}{2} \nabla_\gamma^r \left[\int pR_\alpha \left(\nabla_\gamma^R \frac{\delta U}{\delta p} \bigg|_{s_t,\eta,\boldsymbol{F}} \right) d^6\boldsymbol{\xi} \right.$$

$$\left. - \int pR_\gamma \left(\nabla_\alpha^R \frac{\delta U}{\delta p} \bigg|_{s_t,\eta,\boldsymbol{F}} \right) d^6\boldsymbol{\xi} \right], \tag{5.74}$$

$$\partial_t s_t|_{\text{non-a}} = 0, \tag{5.75}$$

$$\partial_t \eta|_{\text{non-a}} = 0, \tag{5.76}$$

$$\partial_t F_{\alpha\beta}|_{\text{non-a}} = 0, \tag{5.77}$$

$$\partial_t p|_{\text{non-a}} = -\frac{1}{2} \left(\nabla_\nu^R R_\mu p \right) \left[\left(\nabla_\nu^r v_\mu \right) - \left(\nabla_\mu^r v_\nu \right) \right]. \tag{5.78}$$

It can be seen from (5.75) that the total entropy of the system is not affected by these irreversible contributions, i.e. that the non-affine deformation implemented above is indeed free of dissipation.

5.2.5 Final set of evolution equations

5.2.5.1 Entropy-based formulation

The complete set of evolution equations for $\mathcal{X}$, (2.1), is obtained by adding the reversible contributions discussed in Sec. 5.2.3 and the irreversible contributions discussed in Sec. 5.2.4.1 and Sec. 5.2.4.2, which leads to

$$\partial_t m_\alpha = -\nabla_\gamma^r \left(m_\alpha v_\gamma \right) + \nabla_\gamma^r \sigma_{\alpha\gamma}, \tag{5.79}$$

$$\partial_t s_t = -\nabla_\gamma^r \left(s_t v_\gamma \right) + \left(\frac{1}{T} - \frac{1}{\theta} \right) \mathcal{J}^{\Delta,\times} + \left(\frac{1}{T} - \frac{1}{\theta} \right) \int \mathcal{J}^{\Delta,\text{p}} \, d^6\boldsymbol{\xi}$$

$$- \int \left(\frac{\varphi}{T} + \frac{(1-\varphi)}{\theta} \right) \left(\nabla_\gamma^Q \frac{\delta U}{\delta p} \bigg|_{s_t,\eta,\boldsymbol{F}} \right) \mathcal{J}_\gamma^{\text{p,p}} \, d^6\boldsymbol{\xi}, \tag{5.80}$$

$$\partial_t \eta = -\nabla_\gamma^r \left(\eta v_\gamma \right) - \frac{1}{\theta} \mathcal{J}^{\Delta,\times} - \frac{1}{\theta} \int \mathcal{J}^{\Delta,\text{p}} \, d^6\boldsymbol{\xi}$$

$$- \int \frac{(1-\varphi)}{\theta} \left(\nabla_\gamma^Q \frac{\delta U}{\delta p} \bigg|_{s_t,\eta,\boldsymbol{F}} \right) \mathcal{J}_\gamma^{\text{p,p}} \, d^6\boldsymbol{\xi}, \tag{5.81}$$

$$\partial_t F_{\alpha\beta} = -v_\mu \left(\nabla_\mu^r F_{\alpha\beta} \right) + F_{\mu\beta} \left(\nabla_\mu^r v_\alpha \right), \tag{5.82}$$

$$\partial_t p = -\nabla_\gamma^r \left(p v_\gamma \right) - \nabla_\gamma^R \left(pR_\mu \left[\nabla_\mu^r v_\gamma \right]^{\text{sym}} \right) - \nabla_\gamma^Q \mathcal{J}_\gamma^{\text{p,p}}, \tag{5.83}$$

with the stress tensor

$$\sigma_{\alpha\gamma} = \left(u - Ts_t - (\theta - T)\eta - \int p \frac{\delta U}{\delta p} \bigg|_{s_t,\eta,\boldsymbol{F}} d^6\boldsymbol{\xi} \right) \delta_{\alpha\gamma}$$

$$+ \frac{\delta U}{\delta F_{\alpha\varepsilon}} \bigg|_{s_t,\eta,p} F_{\gamma\varepsilon} + \int \left[pR_\gamma \left(\nabla_\alpha^R \frac{\delta U}{\delta p} \bigg|_{s_t,\eta,\boldsymbol{F}} \right) \right]^{\text{sym}} d^6\boldsymbol{\xi}, \tag{5.84}$$

and thermodynamic fluxes $\mathcal{J}^{\Delta,\times}$, $\mathcal{J}^{\Delta,\mathrm{p}}$ and $\mathcal{J}_\gamma^{\mathrm{p},\mathrm{p}}$, given by (5.52), (5.54) and (5.55), respectively.

The Cauchy stress tensor (5.84) consists of (i) an isotropic pressure contribution due to both the elastomer matrix and the glassy network (first term on the right-hand side (r.h.s.)), (ii) a conventional anisotropic contribution of the elastomer matrix (second term), and (iii) an anisotropic contribution of the glassy network (third term). The latter is in agreement with statistical mechanics results [54, 104, 105] and formally corresponds to what is used in polymer kinetic theory [29, 38, 39]. For the case of thermal equilibrium, i.e. $\theta = T$ after long aging, this expression reduces to the one in [7]. Finally, it is noted that the Cauchy stress tensor (5.84) is manifestly symmetric.

5.2.5.2   Temperature-based formulation

The choice of the total entropy density s_t and the elastomer configurational entropy density η as dynamic variables is convenient from a fundamental model-development viewpoint. In practical applications, however, it is more convenient to work with temperatures. To that end, one must re-express the expressions for the $\boldsymbol{F}$- and p-derivatives of U, as well as the time-evolution of the entropies s_t and η when using other dynamic variables than (s_t, η). Under a transformation of variables $(\boldsymbol{m}, s_\mathrm{t}, \eta, \boldsymbol{F}, p) \to (\boldsymbol{m}, T, \theta, \boldsymbol{F}, p)$, the internal energy becomes a functional of the form $U = U[s_\mathrm{t}[T, \theta, \boldsymbol{F}, p], \eta(T, \theta, \boldsymbol{F}), \boldsymbol{F}, p]$. For thermodynamic functions of the form (5.10) and (5.15), or (5.16) and (5.17), respectively, one can show that derivatives of U with respect to $\boldsymbol{F}$ and p become

$$\left.\frac{\delta U}{\delta F_{\gamma\varepsilon}}\right|_{s_\mathrm{t},\eta,p} = \left.\frac{\delta U}{\delta F_{\gamma\varepsilon}}\right|_{T,\theta,p} - T\left.\frac{\delta(S_\mathrm{em} - H)}{\delta F_{\gamma\varepsilon}}\right|_{T,\theta} - \theta\left.\frac{\delta H}{\delta F_{\gamma\varepsilon}}\right|_{T,\theta}, \qquad (5.85)$$

$$\left.\frac{\delta U}{\delta p}\right|_{s_\mathrm{t},\eta,\boldsymbol{F}} = \left.\frac{\delta U}{\delta p}\right|_{T,\theta,\boldsymbol{F}} - T\left.\frac{\delta S}{\delta p}\right|_{T,\theta,\boldsymbol{F}}, \qquad (5.86)$$

with $H = \int \eta \, d^3\boldsymbol{r}$. Therefore, when translating the dynamic model from an entropy-based formulation to a temperature-based formulation, all occurrences of the derivatives on the left-hand side (l.h.s.) of (5.85) and (5.86) need to be replaced by their corresponding counter-parts on the r.h.s. of (5.85) and (5.86), respectively.

The expression (5.85) can be rationalized as follows: In terms of $(T, \theta, \boldsymbol{F}, p)$, both the internal energy U as well as the two partial entropies (kinetic and configurational) of the elastomer matrix, $S_\mathrm{em} - H$ and H, depend on $\boldsymbol{F}$. These entropy contributions are combined with the internal energy by pre-multiplying them with the respective (kinetic and configurational) temperature, similar to the expression for a Helmholtz free energy. In contrast, in (5.86), the p-dependent contributions of both the internal energy and the entropy are linked to neither the kinetic nor the configurational subsystems of the elastomer matrix, and one might hence wonder how to combine the p-derivatives of the energy and the entropy with each other. To that end, as the derivation of (5.86) also shows, the relevant factor is the functional derivative of the internal energy U with respect to s_t, which is in the first place equal to T_1. For the special form of thermodynamic potentials considered in this chapter, Sec. 5.2.2, T_1 is equal to the kinetic temperature of the elastomer matrix, T. In this sense, the expression (5.86) is not as asymmetric with respect to the kinetic/configurational subsystems as it might seem on first sight.

The time-evolution of s_t and η can be reformulated by remembering that $S = S_\text{em}[T, \theta, \boldsymbol{F}] + S_\text{p}[p]$ and $H = H[T, \theta, \boldsymbol{F}]$, leading to

$$
\begin{aligned}
\partial_t s_\text{t} &= \left.\frac{\partial s_\text{em}}{\partial T}\right|_{\theta,\boldsymbol{F}} \partial_t T + \left.\frac{\partial s_\text{em}}{\partial \theta}\right|_{T,\boldsymbol{F}} \partial_t \theta + \left.\frac{\partial s_\text{em}}{\partial F_{\gamma\varepsilon}}\right|_{T,\theta} \partial_t F_{\gamma\varepsilon} \\
&\quad + \int \frac{\delta S_\text{p}}{\delta p} \, \partial_t p \, d^6\boldsymbol{\xi} ,
\end{aligned}
\tag{5.87}
$$

$$
\partial_t \eta = \left.\frac{\partial \eta}{\partial T}\right|_{\theta,\boldsymbol{F}} \partial_t T + \left.\frac{\partial \eta}{\partial \theta}\right|_{T,\boldsymbol{F}} \partial_t \theta + \left.\frac{\partial \eta}{\partial F_{\gamma\varepsilon}}\right|_{T,\theta} \partial_t F_{\gamma\varepsilon} .
\tag{5.88}
$$

Substituting all the ingredients above, namely (5.85), (5.86), (5.87) and (5.88), into the evolution equations for s_t and η, results in

$$
\begin{aligned}
s_{\text{em},T} D_t T \;+\; s_{\text{em},\theta} D_t \theta &= \left[\left(-s_\text{t} + \int \frac{\delta S_\text{p}}{\delta p} p \, d^6\boldsymbol{\xi}\right)\delta_{\gamma\mu} - \left.\frac{\partial s_\text{em}}{\partial F_{\gamma\varepsilon}}\right|_{T,\theta} F_{\mu\varepsilon}\right. \\
&\quad - \left.\int p \left[R_\mu \left(\nabla_\gamma^R \frac{\delta S_\text{p}}{\delta p}\right)\right]^{\text{sym}} d^6\boldsymbol{\xi}\right] (\nabla_\mu^r v_\gamma) \\
&\quad + \int \frac{\delta S_\text{p}}{\delta p} (\nabla_\gamma^Q \mathcal{J}_\gamma^{\text{p,p}}) \, d^6\boldsymbol{\xi} + \left(\frac{1}{T} - \frac{1}{\theta}\right) \mathcal{J}^{\Delta,\text{x}} \\
&\quad + \left(\frac{1}{T} - \frac{1}{\theta}\right)\int \mathcal{J}^{\Delta,\text{p}} \, d^6\boldsymbol{\xi} \\
&\quad - \int \left(\frac{\varphi}{T} + \frac{(1-\varphi)}{\theta}\right)\left[\nabla_\gamma^Q \left(\left.\frac{\delta U}{\delta p}\right|_{T,\theta,\boldsymbol{F}} - T\left.\frac{\delta S}{\delta p}\right|_{T,\theta,\boldsymbol{F}}\right)\right] \mathcal{J}_\gamma^{\text{p,p}} d^6\boldsymbol{\xi} ,
\end{aligned}
\tag{5.89}
$$

$$
\begin{aligned}
\eta_{,T} D_t T \;+\; \eta_{,\theta} D_t \theta &= \left(-\eta\delta_{\gamma\mu} - \left.\frac{\partial \eta}{\partial F_{\gamma\varepsilon}}\right|_{T,\theta} F_{\mu\varepsilon}\right)(\nabla_\mu^r v_\gamma) \\
&\quad - \frac{1}{\theta}\mathcal{J}^{\Delta,\text{x}} - \frac{1}{\theta}\int \mathcal{J}^{\Delta,\text{p}} \, d^6\boldsymbol{\xi} \\
&\quad - \int \frac{(1-\varphi)}{\theta}\left[\nabla_\gamma^Q \left(\left.\frac{\delta U}{\delta p}\right|_{T,\theta,\boldsymbol{F}} - T\left.\frac{\delta S}{\delta p}\right|_{T,\theta,\boldsymbol{F}}\right)\right] \mathcal{J}_\gamma^{\text{p,p}} d^6\boldsymbol{\xi} ,
\end{aligned}
\tag{5.90}
$$

with $D_t = \partial_t + v_\gamma \nabla_\gamma^r$ the substantial (material) time-derivative, and with the abbreviations

$$
s_{\text{em},T} = \left.\frac{\partial s_\text{em}}{\partial T}\right|_{\theta,\boldsymbol{F}}, \quad s_{\text{em},\theta} = \left.\frac{\partial s_\text{em}}{\partial \theta}\right|_{T,\boldsymbol{F}}, \quad \eta_{,T} = \left.\frac{\partial \eta}{\partial T}\right|_{\theta,\boldsymbol{F}}, \quad \eta_{,\theta} = \left.\frac{\partial \eta}{\partial \theta}\right|_{T,\boldsymbol{F}}.
\tag{5.91}
$$

In summary, the entropy-based model formulated in Sec. 5.2.5.1 takes the following form when formulated in terms of temperatures. The momentum balance (5.79) remains valid. The entropy evolution equations (5.80) and (5.81) are replaced by (5.89) and (5.90), while the evolution equations for the deformation gradient (5.82) and for the filler-particle arrangement (5.83) remain unchanged. In all of this, specifically in the stress tensor $\sigma_{\alpha\gamma}$ (5.84) and the thermodynamic flux contributions $\mathcal{J}^{\Delta,\text{x}}$, $\mathcal{J}^{\Delta,\text{p}}$, $\mathcal{J}_\gamma^{\text{p,p}}$ given by (5.52),

(5.54), (5.55), respectively, the functional derivatives with respect to $\boldsymbol{F}$ and p are subject to the replacements (5.85) and (5.86).

5.3   Specific system realization

5.3.1   Reduction on the level of evolution equations

In the procedure above, the model is formulated in terms of (i) evolution equations (5.79)–(5.83) or its equivalent temperature-formulation, (ii) the constitutive expression for the Cauchy stress tensor (5.84), and (iii) the thermodynamic fluxes (5.52), (5.54), (5.55). To make this model material specific, choices need to be made for the internal energy U and entropy S, the kinetic functions $\lambda_{\alpha\beta}$ and $\mu^{\times}$, and the functions φ and ω_{α}.

For illustration purposes, several assumptions will be made to simplify the model. Particularly, it is assumed that the interaction of the two thermal subsystems, kinetic and configurational, of the glassy elastomer material is negligibly small. This implies that each subsystem entropy does not depend on the temperature of the other subsystem [79, 80]. Based on this, one can show that the temperature evolution equations (5.89) and (5.90) can be written in the form

$$
\begin{aligned}
s_{,T}\, D_t T \;=\;& \left[\left(-s - s_{\mathrm{p}}[p] + \int \frac{\delta S_{\mathrm{p}}}{\delta p}\, p\, d^6\boldsymbol{\xi}\right)\delta_{\gamma\mu} - \left.\frac{\partial s}{\partial F_{\gamma\varepsilon}}\right|_{T,\theta} F_{\mu\varepsilon}\right. \\
& \left. - \int p\left[R_\mu\left(\nabla_\gamma^R \frac{\delta S_{\mathrm{p}}}{\delta p}\right)\right]^{\mathrm{sym}} d^6\boldsymbol{\xi}\right](\nabla_\mu^r v_\gamma) \\
& + \frac{1}{T}\mu^{\times}\left(\frac{1}{T} - \frac{1}{\theta}\right) + \frac{1}{T}\int\left(\breve{\omega}_\gamma - \left(\nabla_\gamma^Q \frac{\delta U_{\mathrm{p}}}{\delta p}\right)\right)\mathcal{J}_\gamma^{p,\mathrm{p}} d^6\boldsymbol{\xi}\,, \quad (5.92)
\end{aligned}
$$

$$
\begin{aligned}
\eta_{,\theta}\, D_t\theta \;=\;& \left(-\eta\delta_{\gamma\mu} - \left.\frac{\partial \eta}{\partial F_{\gamma\varepsilon}}\right|_{T,\theta} F_{\mu\varepsilon}\right)(\nabla_\mu^r v_\gamma) \\
& - \frac{1}{\theta}\mu^{\times}\left(\frac{1}{T} - \frac{1}{\theta}\right) - \frac{1}{\theta}\int \breve{\omega}_\gamma \mathcal{J}_\gamma^{p,\mathrm{p}} d^6\boldsymbol{\xi}\,, \quad (5.93)
\end{aligned}
$$

with the thermodynamic flux representative of viscoplastic deformation given by

$$
\mathcal{J}_\alpha^{p,\mathrm{p}}(\boldsymbol{\xi}) = \int \lambda_{\alpha\gamma}(\boldsymbol{\xi},\boldsymbol{\xi}')\left(\left(\frac{1}{T} - \frac{1}{\theta}\right)\breve{\omega}_\gamma(\boldsymbol{\xi}') - \frac{1}{T}\nabla_\gamma^{Q'}\left[\frac{\delta U_{\mathrm{p}}}{\delta p'} - T\frac{\delta S_{\mathrm{p}}}{\delta p'}\right]\right) d^6\boldsymbol{\xi}'\,, \quad (5.94)
$$

and the abbreviation

$$
\breve{\omega}_\gamma \;=\; \omega_\gamma + (1 - \varphi)\nabla_\gamma^Q\left(\frac{\delta U_{\mathrm{p}}}{\delta p} - T\frac{\delta S_{\mathrm{p}}}{\delta p}\right)\,. \quad (5.95)
$$

It should be noted that at thermal equilibrium, $\theta = T$, and for $\breve{\omega}_\gamma = 0$, the evolution equation (5.92) for T is the same as the temperature equation in the earlier two-scale model [7], where aging and mechanical rejuvenation has not been considered.

A physically meaningful choice for $\breve{\omega}_\alpha$ can be made by considering the consequences of mechanical rejuvenation in more detail [72]. For the modeling of the mechanical

rejuvenation of bulk polymer glasses, it has been suggested that mechanical rejuvenation leads to an increase of the configurational temperature [79, 80]. Transferring this to the case of glassy bridges modeling in this chapter, implies that the last term on the right-hand side of (5.93) must be positive semi-definite always. This can be achieved by specifying $\breve{\omega}_\alpha$ in such a way that the product $\breve{\omega}_\alpha \mathcal{J}_\alpha^{p,p}$ is a quadratic form, specifically by

$$\breve{\omega}_\gamma = \frac{\mathfrak{T}}{T + \mathfrak{T}(1 - \frac{T}{\theta})} \nabla_\gamma^Q \left(\frac{\delta U_{\mathrm{p}}}{\delta p} - T \frac{\delta S_{\mathrm{p}}}{\delta p} \right) , \tag{5.96}$$

with a positive prefactor $\mathfrak{T}$. For simplicity, we choose $\mathfrak{T} = \theta$, which in turn simplifies the thermodynamic flux as well as the evolution equations significantly.

5.3.2   Specification of energy E and entropy S, and dissipative matrix λ

For filler-particle contribution to the energy and entropy, we use the assumptions (5.16)–(5.21) made in Sec. 5.2.2, specifically (see also [7])

$$U_{\mathrm{p}}[p] = \iint p\, \Phi^{\mathsf{E}} d^6\boldsymbol{\xi} d^3\boldsymbol{r} , \tag{5.97}$$

$$S_{\mathrm{p}}[p] = -\iint p \left(\frac{\Phi^{\mathsf{S}}}{T} + k_{\mathrm{B}} \ln p \right) d^6\boldsymbol{\xi} d^3\boldsymbol{r} . \tag{5.98}$$

These expressions imply

$$\nabla_\gamma^Q \left(\frac{\delta U_{\mathrm{p}}}{\delta p} - T \frac{\delta S_{\mathrm{p}}}{\delta p} \right) = \nabla_\gamma^Q \Phi + k_{\mathrm{B}} T \frac{\nabla_\gamma^Q p}{p} , \tag{5.99}$$

which enters at several spots in the complete dynamic model, most prominently in the stress tensor (5.84) and the viscoplastic deformation of the glassy bridges (5.94). The first term on the r.h.s. of (5.99) is a deterministic force, while the second term is a statistical contribution.

In the remainder of this chapter, a Hookean spring potential is used for the energy $\Phi(\boldsymbol{\xi})$ associated with the mismatch between the current ($\boldsymbol{R}$) and the load-free ($\boldsymbol{Q}$) state [7],

$$\Phi(\boldsymbol{\xi}) = \Phi^{\mathsf{E}}(\boldsymbol{\xi}) + \Phi^{\mathsf{S}}(\boldsymbol{\xi}) = \frac{1}{2}k(\boldsymbol{R} - \boldsymbol{Q})^2 , \tag{5.100}$$

with spring constant k. In this case, $\nabla_\gamma^Q \Phi = k(Q_\gamma - R_\gamma)$. Therefore, with the aid of (5.99), one concludes that the deterministic contributions to both the filler-particle related contribution to the stress tensor (5.84) as well as to the viscoplastic deformation (5.94) vanish as the current state $\boldsymbol{R}$ becomes equal to the load-free state $\boldsymbol{Q}$, as expected. This leaves only the statistical contributions, related to the second term on the r.h.s. of (5.99), in the stress tensor and the viscoplastic deformation.

The elastomer-matrix contribution to the energy and entropy,

$$U_{\mathrm{em}} = \int u_{\mathrm{em}}(T, \theta, \boldsymbol{F}) d^3\boldsymbol{r} , \tag{5.101}$$

$$S_{\mathrm{em}} = \int s_{\mathrm{em}}(T, \theta, \boldsymbol{F}) d^3\boldsymbol{r} , \tag{5.102}$$

can be derived from the Helmholtz free energy a_{em} by way of

$$u_{em} = a_{em} - T\frac{\partial a_{em}}{\partial T}, \quad s_{em} = -\frac{\partial a_{em}}{\partial T}. \tag{5.103}$$

As a slight extension of [7] with respect to a dependence on the configurational temperature θ, we use for illustration purposes

$$a_{em} = \frac{G_{em}(T)}{2}(J_1 - 3 - 2\ln J) + \frac{\kappa_{em}(T)}{2}(\ln J)^2 + \rho\, a_\theta(\theta), \tag{5.104}$$

where G_{em} and κ_{em} denote the T-dependent shear and bulk moduli, respectively, $J_1 = \text{tr}(\boldsymbol{F}^\top \cdot \boldsymbol{F})$, and $J = \det \boldsymbol{F}$. It should be noted that the only θ-dependent contribution is the last one on the r.h.s. of (5.104).

To specify the viscoplastic deformation of the glassy bridges, the dissipative matrix $\lambda_{\alpha\beta}$ in (5.94) needs to be specified. In complete analogy to [7], the following form is adopted,

$$\lambda_{\alpha\beta}(\boldsymbol{\xi}, \boldsymbol{\xi}') = \delta(\boldsymbol{R} - \boldsymbol{R}')\delta(\boldsymbol{Q} - \boldsymbol{Q}')\frac{\theta p}{\zeta}\delta_{\alpha\beta}, \tag{5.105}$$

with a friction coefficient ζ, with $\zeta > 0$. The ansatz (5.105) implies that there is no inherent material anisotropy, and the viscoplastic flux $\mathcal{J}_\alpha^{p,p}(\boldsymbol{\xi})$ depends on the driving force only for $\boldsymbol{\xi}' = \boldsymbol{\xi}$.

5.3.3   Resulting simplified model

Compilation of all of the model specifications discussed in Sec. 5.3.1 and Sec. 5.3.2, and further assuming that one is interested in situations of constant kinetic temperature, $D_t T = 0$, the model reduces to

$$
\begin{aligned}
D_t\theta &= -\frac{1}{\tau_R}(\theta - T) + \frac{1}{\theta\eta,\theta}\int \frac{p}{k\tau_\alpha}\left(k(Q_\gamma - R_\gamma) + k_B T\frac{\nabla_\gamma^Q p}{p}\right)^2 d^6\boldsymbol{\xi}, & \text{(5.106)}\\
\partial_t p &= -\nabla_\gamma^r (p v_\gamma) - \nabla_\gamma^R \left([\nabla_\mu^r v_\gamma]^{\text{sym}} R_\mu p\right)\\
&\quad - \nabla_\gamma^Q \left[\left(-\frac{1}{\tau_\alpha}(Q_\gamma - R_\gamma) + \frac{k_B T}{k}\left(\nabla_\gamma^Q \frac{1}{\tau_\alpha}\right)\right)p\right]\\
&\quad + \nabla_\gamma^Q \nabla_\gamma^Q \left(\frac{k_B T}{k\tau_\alpha}p\right), & \text{(5.107)}
\end{aligned}
$$

together with the evolution of the deformation gradient (5.82) and the momentum balance (5.79). With the ansatz (5.104), the Cauchy stress tensor (5.84) takes the specific form

$$
\begin{aligned}
\sigma_{\alpha\gamma} &= (a_{em} + \kappa_{em}\ln J - 2nk_B T)\delta_{\alpha\gamma} + G_{em}(B_{\alpha\gamma} - \delta_{\alpha\gamma})\\
&\quad + \int p\left[R_\gamma(\nabla_\alpha^R\Phi)\right]^{\text{sym}} d^6\boldsymbol{\xi}, & \text{(5.108)}
\end{aligned}
$$

with $n = \int p\, d^6\boldsymbol{\xi}$ the number density of representative pairs, and the left Cauchy-Green strain tensor $B_{\alpha\gamma} = F_{\alpha\mu}F_{\gamma\mu}$. To obtain (5.108), the relations (5.85), (5.86), and (5.97)–(5.99) have been employed. In the above, it has been used that, by virtue of the ansatz

(5.104), the configurational entropy density per unit mass, η/ρ with $\eta = -\partial a_{\mathsf{em}}/\partial\theta|_{\boldsymbol{F},T} = -\rho(\mathrm{d}a_\theta/\mathrm{d}\theta)$, is independent of $\boldsymbol{F}$, which eventually results in the absence of $(\nabla_\mu^r v_\gamma)$-related contributions to (5.106). Furthermore, two relaxation times have been defined, namely the time scale τ_{R} for the relaxation of the configurational temperature θ towards T, and the time scale τ_α for the relaxation of the load-free state $\boldsymbol{Q}$ towards $\boldsymbol{R}$,

$$\tau_{\mathsf{R}} = \frac{T\theta^2\eta_{,\theta}}{\mu^\times}\,, \tag{5.109}$$

$$\tau_\alpha = \frac{\zeta}{k}\,. \tag{5.110}$$

In all equations, the friction coefficient ζ is eliminated in favor of τ_α, and $\mu^\times$ in favor of τ_{R}.

For computational purposes, it is convenient to realize that the above Fokker-Planck equation (5.107) can be translated into an equivalent system of stochastic differential equations [39], specifically

$$\mathrm{d}R_\gamma = \left[\nabla_\mu^r v_\gamma\right]^{\mathsf{sym}} R_\mu \mathrm{d}t\,, \tag{5.111}$$

$$\mathrm{d}Q_\gamma = -\frac{1}{\tau_\alpha}(Q_\gamma - R_\gamma)\mathrm{d}t + \frac{k_{\mathsf{B}}T}{k}\left(\nabla_\gamma^Q \frac{1}{\tau_\alpha}\right)\mathrm{d}t + \sqrt{\frac{2k_{\mathsf{B}}T}{k\tau_\alpha}}\mathrm{d}W_{\mathsf{t}\gamma}\,, \tag{5.112}$$

which will be used for the numerical simulations in Sec. 5.4. The last term in (5.112) represents the fluctuating Brownian contributions, that add stochasticity to the $\boldsymbol{Q}$-dynamics. The symbol $\mathrm{d}\mathbf{W}_t$ stands for increments of Wiener processes [39], with average and variance

$$\langle \mathrm{d}\,W_{t\alpha}\rangle = 0\,, \tag{5.113}$$
$$\langle \mathrm{d}\,W_{t\alpha}\mathrm{d}W_{t'\beta}\rangle = \delta_{\alpha\beta}\,\delta_{tt'}\,\mathrm{d}t\,, \tag{5.114}$$

respectively. In other words $\mathrm{d}\mathbf{W}_t$ represents white noise, being uncorrelated in time. It is pointed out that the stochastic differential equations (5.112) are to be interpreted in the Itô-sense [39], which is convenient for an explicit forward Euler integration of the system of equations (5.111) and (5.112) in Sec. 5.4.

5.3.4   Relaxation processes

In the system of evolution equations presented in Sec. 5.3.3, the relaxation times τ_{R} and τ_α require further specification, which is discussed in this section.

The relaxation time τ_α for the vector $\boldsymbol{Q}$ contains all the information about temperature- and load-dependence of the thermo-mechanics of the glassy bridges. To specify this dependence, the procedures outlined in [17–19] are followed, as done in our earlier work [7], and the reader is referred to those publications for further detail. At this point, the main physical features encoded in τ_α are briefly summarized. If the elastomer matrix material adheres well to the particle surface, the mobility of the elastomer chain segments decreases as the filler-particle surface is approached, which can be captured phenomenologically by an increase in the local glass-transition temperature. At a certain distance this increase is such that even at room temperature there exists a glassy layer around the particles.

Formally, the shift of glass transition temperature due to the fillers can be described by $T_g(z) = T_{g,b}(1 + \beta/z)$, where $T_{g,b}$ stands for bulk glass transition temperature, β accounts for the strength of the particle-matrix interaction, and z is the distance from the particle surface [9, 10]. On the other hand, an applied dynamic load increases the mobility of matrix material around filler particles, i.e., effectively resulting in a decrease of the local glass transition temperature. Considering two particles with a local interparticle mechanical load Σ_{loc} and separated by a surface-to-surface distance $|\boldsymbol{R}| - d = 2z$ with filler-particle diameter d, the glass transition temperature relevant for that respective glassy bridge is given by [17, 18]

$$T_g(z, \Sigma_{loc}) = T_{g,b}\left(1 + \frac{\beta}{z}\right) - \frac{\Sigma_{loc}}{K}, \tag{5.115}$$

where K relates the yield stress σ_y to the glass transition temperature T_g by way of the relation $\sigma_y = K(T_g - T)$. Both K and β are material parameters that can be experimentally measured.

In [7, 17, 18], a relation between the relaxation time τ_α and the local glass transition temperature (5.115) has been employed. In this chapter, this relation is extended in order to account for the configurational temperature θ, i.e., to account for the effects of physical aging and mechanical rejuvenation. This is achieved by employing the Hodge-Scherer equation [76, 106, 107]

$$\tau_\alpha = \tau_g \exp\left[-c_1 \frac{c_2(T - \theta) + T(\theta - T_g(z, \Sigma_{loc}))}{T(c_2 + \theta - T_g(z, \Sigma_{loc}))}\right], \tag{5.116}$$

with c_1 and c_2 the polymer-specific WLF parameters, and τ_g the relaxation time at $T = \theta = T_g$. It should be noted that the expression above for the relaxation time τ_α converges to the conventional WLF law [108] at $\theta = T$, in other words for a completely aged sample the relaxation time is governed by the usual WLF law. As explained in [7], the scalar measure Σ_{loc} for the local interparticle stress can be approximated by

$$\Sigma_{loc} = \sqrt{|I_2|}, \tag{5.117}$$

where I_2 is the second invariant, namely $I_2 = (1/2)[(\mathrm{tr}\boldsymbol{\Sigma})^2 - \mathrm{tr}(\boldsymbol{\Sigma} \cdot \boldsymbol{\Sigma})]$, of the local interparticle stress tensor

$$\boldsymbol{\Sigma}_{loc} = \left[\boldsymbol{R}\nabla^R\Phi_t\right]. \tag{5.118}$$

For completeness, it is mentioned that Φ_t in (5.118) does not only contain the glassy-bridge contribution specified in (5.100), but also a second contribution that represents the elastomer matrix stress on the particle level; the reader is referred to Sec. 4.2 in [7] for further details.

As far as the specification of the relaxation time τ_R is concerned, i.e., the approach of the configurational (θ) to the kinetic (T) temperature during physical aging, we refer to [76]. In particular, there it was argued that τ_R shares the same type of relaxation as that specified for τ_α in (5.116), with the only exception that the local interparticle load is not included. Therefore,

$$\tau_R = \tau_R^0 \exp\left[-c_1 \frac{c_2(T - \theta) + T(\theta - T_g(z, 0))}{T(c_2 + \theta - T_g(z, 0))}\right], \tag{5.119}$$

with τ_R^0 a constant, positive prefactor.

5.4   Numerical solution

5.4.1   Coupling of micro-scale to macro-scale components

The numerical solution of the model summarized in Sec 5.3.3 is cumbersome. On the one hand, there is an influence of the macroscopic state of the system, e.g. through the temperature T and the imposed velocity field v on the microscopic dynamics (5.107), or (5.111)–(5.112), respectively. On the other hand, the microscopic state enters the evolution of the configurational temperature of the elastomer θ on the macroscopic scale by way of the second term on the r.h.s. of (5.106). This is exactly the source of complications when attempting to solve this coupled system of equations numerically, as explained in the following.

    As mentioned earlier, it is convenient to solve the configurational temperature evolution (5.106) in combination with the stochastic differential equations (5.111)–(5.112), rather than in combination with the Fokker-Planck equation (5.107). Specifically, (5.111) is an ordinary differential equation, which in many cases might be solved analytically, to determine the motion of vector R due to the imposed deformation. The vector Q, that stands for a load-free particle configuration, is described by the stochastic differential equation (5.112). Inspecting the structure of both of these evolution equations together with the fact that the Itô-calculus applies for their stochastic interpretation [39], as mentioned in Sec. 5.3.3, one concludes that conventional numerical techniques can be employed for solving (5.111)–(5.112) (see e.g. [39]). The situation, however, looks more involved if one attempts to solve (5.111)–(5.112) simultaneously with (5.106), for the following reason. The integral on the r.h.s. of (5.106) can be expressed as a series of terms in powers of $k_\mathrm{B}T$, namely

$$I = \int \frac{p}{k\tau_\alpha} \left(k(Q_\gamma - R_\gamma) + k_\mathrm{B}T \frac{\nabla_\gamma^Q p}{p} \right)^2 d^6\boldsymbol{\xi} = I_1 + I_2 + I_3 \geq 0 \,, \qquad (5.120)$$

with the definitions

$$I_1 = k \int \frac{1}{\tau_\alpha} (R_\gamma - Q_\gamma)^2 \, p \, d^6\boldsymbol{\xi} \,, \qquad\qquad (5.121)$$

$$I_2 = 2k_\mathrm{B}T \int \left[(R_\gamma - Q_\gamma) \left(\nabla_\gamma^Q \frac{1}{\tau_\alpha} \right) - \frac{3}{\tau_\alpha} \right] p \, d^6\boldsymbol{\xi} \,, \qquad (5.122)$$

$$I_3 = -\frac{(k_\mathrm{B}T)^2}{k} \int \left[\nabla^Q \left(\frac{1}{\tau_\alpha} \nabla^Q \ln p \right) \right] p \, d^6\boldsymbol{\xi} \,. \qquad (5.123)$$

In the first two integrals, I_1 and I_2, the function p as such occurs as a multiplicative factor in the integral. Denoting the respective integrand divided by p as as i_k, i.e. $I_k = \int i_k \, p \, d^6\boldsymbol{\xi}$ for $k = 1, 2$, these integrals can be interpreted in terms of averages of i_k with respect to the microscopic filler-particle arrangement. From a simulation perspective, this means that one could simulate a large number of realizations of R- and Q-dynamics, measure for each of the realizations the quantity i_k, and then averaging that over all realizations. This is exactly the procedure used in the CONNFFESSIT (Calculation of Non-Newtonian Flow: Finite Elements and Stochastic Simulation Techniques) approach [39, 109]. However,

inspection of (5.123) makes clear that such a procedure can not be applied to I_3, because in this case one obtains $i_3 = -(k_B^2 T^2 / k) \nabla^Q \left(\tau_\alpha^{-1} \nabla^Q \ln p \right)$, which can not be measured for each realization individually but rather depends on the distribution of all realizations. Therefore, the possibilities are to either search for a new technique that can deal with the type of coupling represented in I_3 or, alternatively, one tries to assess how significant the contribution I_3 to the entire integral I actually is.

5.4.2 Gaussian approximation

As it was mentioned in the previous section, the CONNFFESSIT approach can in general not be applied to the model developed in this chapter due to the specific form of the contribution I_3, given in (5.123). However, one can attempt to estimate the relative magnitude of the three contributions (5.121)–(5.123) to the total integral I (5.120), under certain circumstances, which is the purpose of this section.

   The specific case, for which a concrete calculation of the three contributions to (5.120) can be performed is when the relaxation time τ_α does not depend on Q (and R). In this case, the distribution corresponding to the Fokker-Planck equation (5.107), or the corresponding stochastic differential equations (5.111)–(5.112), respectively, is Gaussian [39]. Specifically, the Gaussian distribution can be written in the form

$$p(\boldsymbol{r}, \boldsymbol{\xi}) = N \exp \left\{ -\frac{1}{2} \xi_\alpha \, \Theta_{\alpha\beta}^{-1} \, \xi_\beta \right\} , \qquad (5.124)$$

with normalization constant $N = (2\pi)^{-3} (\det \boldsymbol{\Theta})^{-1/2}$, and the symmetric positive semi-definite matrix $\boldsymbol{\Theta}$, defined by

$$\boldsymbol{\Theta} = \left\langle \boldsymbol{\xi} \, \boldsymbol{\xi} \right\rangle = \begin{pmatrix} \langle \boldsymbol{R} \, \boldsymbol{R} \rangle & \langle \boldsymbol{R} \, \boldsymbol{Q} \rangle \\ \langle \boldsymbol{Q} \, \boldsymbol{R} \rangle & \langle \boldsymbol{Q} \, \boldsymbol{Q} \rangle \end{pmatrix} , \quad \text{with} \quad \langle \boldsymbol{R} \, \boldsymbol{Q} \rangle = \langle \boldsymbol{Q} \, \boldsymbol{R} \rangle^\top . \qquad (5.125)$$

After straight-forward calculation one can show that

$$\nabla_\alpha^Q \ln p \;=\; \lambda_{\alpha\varepsilon} \left(\mu_{\varepsilon\gamma} R_\gamma - Q_\varepsilon \right) , \qquad (5.126)$$

with

$$\lambda_{\alpha\varepsilon} \;\equiv\; \left[\langle \boldsymbol{Q} \, \boldsymbol{Q} \rangle - \langle \boldsymbol{Q} \, \boldsymbol{R} \rangle \cdot \langle \boldsymbol{R} \, \boldsymbol{R} \rangle^{-1} \cdot \langle \boldsymbol{R} \, \boldsymbol{Q} \rangle \right]_{\alpha\varepsilon}^{-1} , \qquad (5.127)$$

$$\mu_{\varepsilon\gamma} \;\equiv\; \left[\langle \boldsymbol{Q} \, \boldsymbol{R} \rangle \cdot \langle \boldsymbol{R} \, \boldsymbol{R} \rangle^{-1} \right]_{\varepsilon\gamma} . \qquad (5.128)$$

With the representation (5.126), all integrals I_k specified in (5.121)–(5.123) can be expressed in terms of the second moments (5.125),

$$I_1 \;=\; \frac{k}{\tau_\alpha} \left(\langle R_\gamma R_\gamma \rangle - 2 \langle R_\gamma Q_\gamma \rangle + \langle Q_\gamma Q_\gamma \rangle \right) , \qquad (5.129)$$

$$I_2 \;=\; -\frac{6 k_B T}{\tau_\alpha} , \qquad (5.130)$$

$$I_3 \;=\; \frac{k_B^2 T^2}{k \tau_\alpha} \lambda_{\gamma\gamma} , \qquad (5.131)$$

where $\lambda_{\alpha\varepsilon}$ is given by (5.127).

For the simulations performed in Sec. 5.4.4, the relative importance of the three contributions will be examined, with the goal to identify those conditions under which I_3 can be neglected, and thus the CONNFFESSIT approach could be employed for solving the dynamics of the model specified in Sec. 5.3.3 and Sec. 5.3.4.

5.4.3   Simulation setup and model parameters

Table 5.1: Parameters of the model. The values of the parameters correspond to particle volume fraction $\phi = 0.4$.

parameter	symbol	physical value
particle diameter	d	$2 \cdot 10^{-8}$ m
number density of pairs	n	$1.05 \cdot 10^{23}$ m^{-3}
bulk glass transition temperature	$T_{\text{g,b}}$	213 K
relaxation time	τ_{g}	100 s
relaxation time of heat exchange	τ_{R}^0	74 s
temperature of the experiment	T	263 K
distance-sensitivity parameter	β	$9 \cdot 10^{-10}$ m
stress-sensitivity parameter	K	$2 \cdot 10^{-20}$ J K^{-1}
glassy spring constant	k	1.94 N/m
elastomer spring constant	k_{em}	$k/50$ (see [19])
WLF-constants	C_1, C_2	12.8, 34 K
shear modulus elastomer	G_{em}	10^6 Pa
heat capacity of configurational subsystem of elastomer matrix	$c_\theta = \theta \eta_{,\theta}$	$2.5 \cdot 10^5$ J m^{-3}

In Sec. 5.3, we have made assumptions on the energy and entropy, as well as on the dynamics of the glassy bridges and the heat exchange between the two thermal subsystems of the elastomer matrix. To solve the model presented in Sec. 5.3.3 and Sec. 5.3.4 numerically, the CONNFFESSIT approach [39] is used, in order to obtain the stress-strain response for isothermal conditions, i.e. $D_t T = 0$, with physical aging and mechanical rejuvenation. The CONNFFESSIT approach is chosen in anticipation of the outcome that (see Sec. 5.4.4), for the conditions studied numerically in this chapter, I_3 defined in (5.123) can be neglected in comparison to the other contributions to (5.120).

The particle configuration used for the initial state is the same as was used in our earlier publication [7], specifically the initial configuration corresponds to the unloaded state, $\boldsymbol{R} = \boldsymbol{Q}$. In addition, the vector $\boldsymbol{R}$ is isotropically distributed, i.e. the length $R = |\boldsymbol{R}|$ was sampled from a narrow distribution of the form $w(R) \propto (d - \langle R \rangle)^2 - (R - \langle R \rangle)^2$ for $R \in [d, 2\langle R \rangle - d]$. This distribution has mean $\langle R \rangle = d/\sqrt[3]{\phi} = 2.71 \cdot 10^{-8}$m and standard deviation $\sqrt{\langle R^2 \rangle - \langle R \rangle^2} = (\langle R \rangle - d)/\sqrt{5} = 3.2 \cdot 10^{-9}$m for volume fraction $\phi = 0.4$. To this initial particle configuration, an oscillatory shear deformation is applied with a velocity field of the form $\boldsymbol{v} = (v_1, v_2, v_3)$ with components $v_1(r_2, t) = \dot{\gamma}(t)r_2$ and $v_2 \equiv v_3 \equiv 0$.

The time-dependent imposed deformation is sinusoidal,

$$\gamma(t) = \gamma_0 \sin(\omega t), \qquad (5.132)$$

with amplitude γ_0 and angular frequency ω.

The parameters used for the numerical study are listed in Table 5.1, and are closely related to those considered in [7] for particle volume fraction $\phi = 0.4$. The matrix material, in which the silica nanoparticles are uniformly dispersed, is a poly(ethyl acrylate) matrix. All these parameters can be related to physical parameters, as explained in [17]. In particular, the value we chose for the parameter $\beta = 0.9$ nm, which sets the amplitude of the T_g-shift in the vicinity of the filler particles, corresponds to that measured experimentally in [9, 10]. In the simulations, the stress-induced shift in the glass transition temperature (5.115) has been limited to ≤ 200 K, since above that value the system is already plasticized (see also [18]). For numerical reasons, the range of the relaxation time (5.116) has been limited to 0.01 s $\leq \tau_\alpha \leq 100$ s [19]. For the simulation presented below, the initial relaxation time is equal to $\langle \tau_\alpha^{\text{init}} \rangle = \tau_g$.

The specific choice for the heat capacity of the configurational subsystem of the elastomer matrix $c_\theta = \theta \eta_{,\theta}$ needs to be explained, since this is an aspect of the model that was absent in [7]. To determine its value, we have taken the corresponding value, i.e. the heat capacity per unit mass $\Delta c = 0.25$ Jg^{-1}K^{-1}, used in [80]. In contrast, in this chapter, η is expressed per unit volume of the entire nanocomposite, and therefore $c_\theta = \rho_g \Delta c$, with ρ_g the mass density of glassy network per unit volume of the entire nanocomposite. One can show that $\rho_g = \rho_{\text{em}} \phi [(1 + 2\delta/d)^3 - 1]$, where ρ_{em} represents the mass density of elastomer matrix per unit volume of elastomer matrix, and δ is the thickness of the glassy layer around the filler particle, that depends of temperature and particle-matrix interaction. The value for c_θ, listed in Table 5.1 corresponds to $\phi = 0.4$, $d = 2 \cdot 10^{-8}$m, $\delta = 3.834 \cdot 10^{-9}$m and $\rho_{\text{em}} = 1.52 \cdot 10^6$g m^{-3}.

5.4.4 Assessment of the Gaussian approximation

Simulations have been performed in order to judge the relative importance of the three contributions to the integral (5.120), which stands for the effect of mechanical rejuvenation on the configurational temperature, see (5.106). To that end, simulations have been performed, using the above specifications and for $\theta = T$. Three simulations have been conducted under oscillatory shear deformation with deformation amplitudes $\gamma_0 = 0.1$, $\gamma_0 = 0.2$, and $\gamma_0 = 0.3$. For each deformation amplitude, an intermediate frequency has been chosen such that the material response shows both elastic as well as viscoplastic contributions. At $\gamma_0 = 0.1$, one finds $|I_1/I_2| > 20$ and $|I_2/I_3| \simeq 11$. When increasing the amplitude to $\gamma_0 = 0.2$, $|I_1/I_2| > 65$ and $|I_2/I_3| \simeq 25$. Finally, at the largest deformation amplitude $\gamma_0 = 0.3$, $|I_1/I_2| > 63$ and $|I_2/I_3| \simeq 40$. The conclusion is that, under the conditions studied, the Gaussian approximation predicts $I_1 > I_2 > I_3$, with factors of order ten or more in between. This suggests that one might neglect the I_3-contribution to I. It should be emphasized, however, that this conclusion can only hold if the deformation is sufficiently strong. Or, conversely, at equilibrium I_3 must be of similar order of magnitude like the other terms. This originates from the fact that the term in parenthesis in (5.120) vanishes for the equilibrium distribution, according to (5.107). Therefore, $I = 0$
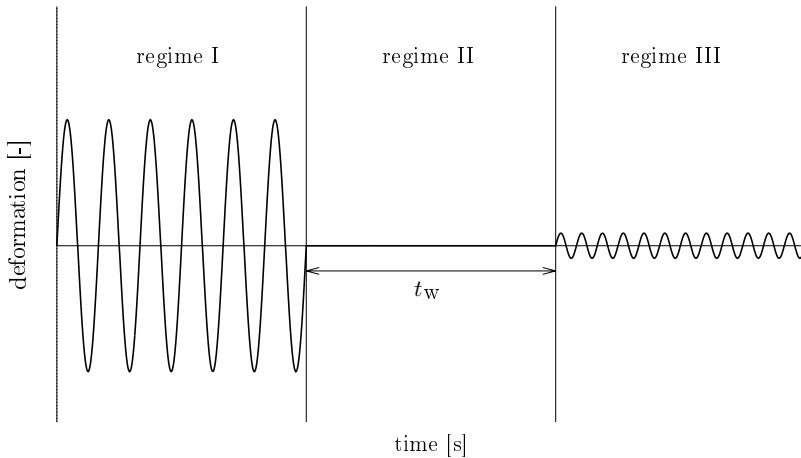
Figure 5.1: Deformation protocol: To an initially aged sample, large amplitude oscillatory deformation is applied (region I), followed by a deformation-free period of duration t_{w} (region II). Finally, after the waiting time t_{w}, the mechanics of the sample is probed under small amplitude oscillatory deformation (region III).

at equilibrium implies that I can not be dominated simply by I_1, but rather that also I_2 and I_3 contribute significantly.

According to the Gaussian approximation, one may thus neglect the third contribution I_3 to the integral (5.120) when performing simulations at strong enough deformation. In the following section, simulations are performed for $\gamma_0 = 0.3$, for which the third integral I_3 is much smaller than the other two if the Gaussian approximation is used. To what extent this implies that the third contribution I_3 can be neglected also in the absence of the Gaussian approximation, i.e. when performing CONNFFESSIT-type simulations, this is discussed below.

5.4.5   Simulation of the Mullins effect

The main goal of this section is to perform a deformation protocol on the dynamic model described in Sec. 5.3.3 and Sec. 5.3.4 that is typical to assess the Mullins effect. These specific measurements are of interest because both physical aging and mechanical rejuvenation of the glassy bridges, as implemented in the configurational temperature evolution (5.106), are relevant for the Mullins effect according to the protocol described in [17, 18]. The deformation protocol contains the following components, also shown in Figure 5.1. Starting with a state of mechanical equilibrium and with an aged state with $\theta \geq T$, large amplitude oscillatory shear deformation is applied. It is anticipated that this results in the mechanical rejuvenation of the nanocomposite (region I). This is followed by letting the system at rest for a certain waiting period t_{w} (region II). Finally, the linear viscoelastic properties are measured (region III), and the effect of the waiting time t_{w} is studied.

5.4.5.1 Mechanical rejuvenation (regime I)

Mechanical rejuvenation is represented by the second term on the r.h.s. of the configurational temperature evolution (5.106), namely in terms of I given by (5.120). It can thus be anticipated that, upon the application of substantial deformation, the configurational temperature θ will increase with increasing time of deformation, by virtue of $I \geq 0$ (see (5.120)). More specifically, the rate of change of θ in (5.106) consists of two contributions with different signs. On the one hand, according to the first term on the r.h.s. of (5.106), the difference of temperatures always leads to decrease of θ to T, for $\theta \geq T$. On the other hand, according to the second term on the r.h.s. of (5.106), the deformation always leads to an increase of θ, due to the mechanical rejuvenation, $I \geq 0$. Therefore, there is a competition between physical aging and mechanical rejuvenation. This fact one can use to determine the yet undetermined prefactor τ_R^0 in (5.119), such that under certain loading conditions, θ approaches the local glass transition temperature from below, but does not surpass it as the deformation is continued for a prolonged period of time, i.e. a steady state is reached. By performing several simulations, we have determined the parameter τ_R^0 such that the θ asymptotically approaches the statistical average of the initial (in the undeformed configuration) local glass transition temperature, $\langle T_g^{\text{init}}(z,0) \rangle$, for $\gamma_0 = 0.3$ and $\omega = 20\,\text{s}^{-1}$. For this deformation protocol, the corresponding shear stress, the configurational temperature, and the first and second integrals (I_1 and I_2) are shown in Fig. 5.2.

With respect to these simulations in regime I of Fig. 5.1, the reader is reminded of the Gaussian approximation considerations in Sec. 5.4.4 that lead us to conclude that the contribution I_3 to I in (5.120) can be neglected, specifically also for the conditions studied above, $\gamma_0 = 0.3$ and $\omega = 20\,\text{s}^{-1}$. In the absence of the Gaussian approximation, the error introduced by neglecting I_3 can not be assessed easily. However, one can instead study the relative importance of the first two contributions, I_1 and I_2, and compare that to the prediction for the Gaussian approximation. This would serve, partly, as an *a posteriori* justification for using the CONNFFESSIT approach. As we can see from Fig. 5.2(c), even at the early stages of deformation, I_1 dominates over I_2, while as we will see later on, this statement does not hold for smaller deformation rates. When the system goes towards the regime of an oscillatory steady-state, the value of I_1 is significantly larger than I_2. This can be quantified in terms of the time averages of these two integrals, $\langle I_1 \rangle$ and $\langle I_2 \rangle$, and specifically their ratio $\langle I_2 \rangle / \langle I_1 \rangle$ can be used as a measure of the applicability of our numerical approach. In short, the numerical approach gets more trustworthy the smaller the ratio $\langle I_2 \rangle / \langle I_1 \rangle$, while the numerical approach is erroneous if $I_1 + I_2$ is negative, since I in (5.120) is based on a quadratic form and should thus be positive semi-definite. For the particular case simulated for the mechanical rejuvenation in region I with $\gamma_0 = 0.3$ and $\omega = 20\,\text{s}^{-1}$, one obtains $\langle I_1 \rangle = 4.1 \cdot 10^6 \text{N m s}^{-1}$ and $\langle I_2 \rangle = 9.7 \cdot 10^4 \text{N m s}^{-1}$, resulting in $\langle I_2 \rangle / \langle I_1 \rangle = 0.024$, which, in combination with the finding $I_1 + I_2 > 0$, suggests that the CONNFFESSIT approach may be used, because it seems admissible to neglect I_3.

Varying the frequency ω of the applied load, one can also see its influence on the evolution of θ. Specifically, one finds $\langle I_2 \rangle / \langle I_1 \rangle = 0.022$ and $I_1 + I_2 > 0$ for $\omega = 15\,\text{s}^{-1}$ (Fig. 5.3), and $\langle I_2 \rangle / \langle I_1 \rangle = 0.014$ and $I_1 + I_2 > 0$ for $\omega = 10\,\text{s}^{-1}$ (Fig. 5.4). However, for the lowest frequency studied, $\omega = 5\,\text{s}^{-1}$ (Fig. 5.5), one observes that $I_1 + I_2$ becomes temporarily negative, which is inadmissible. This clearly indicates that the CONNFFESSIT

approach must not be used under these loading conditions.

From these simulation results, one concludes in general that the configurational temperature of the glassy bridges is increased due to mechanical rejuvenation, as expected. In other words, to some extent, the thermal history is erased. This effect is more significant the stronger the applied deformation.

5.4.5.2   Aging (regime II)

In order to discuss the physical aging in the undeformed state, one can not employ the CONNFFESSIT approach, because in this regime it is not appropriate to neglect the contribution I_3 to (5.120), as discussed earlier. Instead, the evolution equations for the configurational temperature (5.106) and for the filler-particle arrangement (5.107) are studied in a qualitative manner.

At the beginning of region II, p is in a non-equilibrium state, however, it will relax towards the equilibrium state over a period of the order of τ_α. As this relaxation takes place, the mechanical rejuvenation contribution, i.e. the second contribution on the r.h.s. of (5.106), continuously decreases in magnitude until it vanishes at thermal equilibrium. Simultaneously, the configurational temperature decays from its value $\theta > T$ at the beginning of region II towards T with increasing waiting time t_w, i.e. $\partial\theta/\partial t_\mathsf{w} < 0$. In view of the concrete form of relaxation time τ_α in (5.116), one can show that a decrease of θ results in an increase of τ_α. In turn, this implies that τ_α increases with increasing waiting time, i.e. with increasing age, $\partial\tau_\alpha/\partial t_\mathsf{w} > 0$.

5.4.5.3   Probing the linear response (regime III)

In this regime, the linear response of the material is probed, particularly in terms of the storage modulus G' [110]. The Mullins effect then means that, at a fixed frequency, the storage modulus G' increases with waiting time t_w [17, 18]. The goal is to examine whether the model in this chapter shows such behavior. Similarly to Sec. 5.4.5.2, also in this case of linear oscillatory deformation it is not appropriate to use the CONNFFESSIT approach for a numerical study of the Mullins effect. Therefore, we seek a qualitative understanding of the Mullins effect for the model in this chapter.

As discussed in Sec. 5.4.5.2, the relaxation time τ_α increases with increasing waiting time t_w, and a similar statement also holds for the relaxation time τ_R. This can be used in an argument about the Mullins effect as follows. In general, the storage modulus is an increasing function of frequency. If one assumes for illustration purposes that the storage modulus depends just on a single relaxation time, denoted by τ in the sequel, the storage modulus can be written in the form $G'(\omega, \tau) = G'_0 f(\omega\tau)$ with $\mathrm{d}f(x)/\mathrm{d}x > 0$ and $G'_0 > 0$. One then finds

$$\mathrm{sign}\left(\left.\frac{\partial G'}{\partial t_\mathsf{w}}\right|_\omega\right) = \mathrm{sign}\left(\left.\frac{\partial G'}{\partial \tau}\right|_\omega\right) = \mathrm{sign}\left(\frac{\partial G'}{\partial(\omega\tau)}\right) = \mathrm{sign}\left(\frac{\mathrm{d}f}{\mathrm{d}x}\right) = 1\,, \qquad (5.133)$$

where in the first equality we have used $\partial\tau/\partial t_\mathsf{w} > 0$. Therefore, one has proven that the storage modulus G' at a fixed frequency increases with waiting time t_w, i.e., as the systems ages physically.
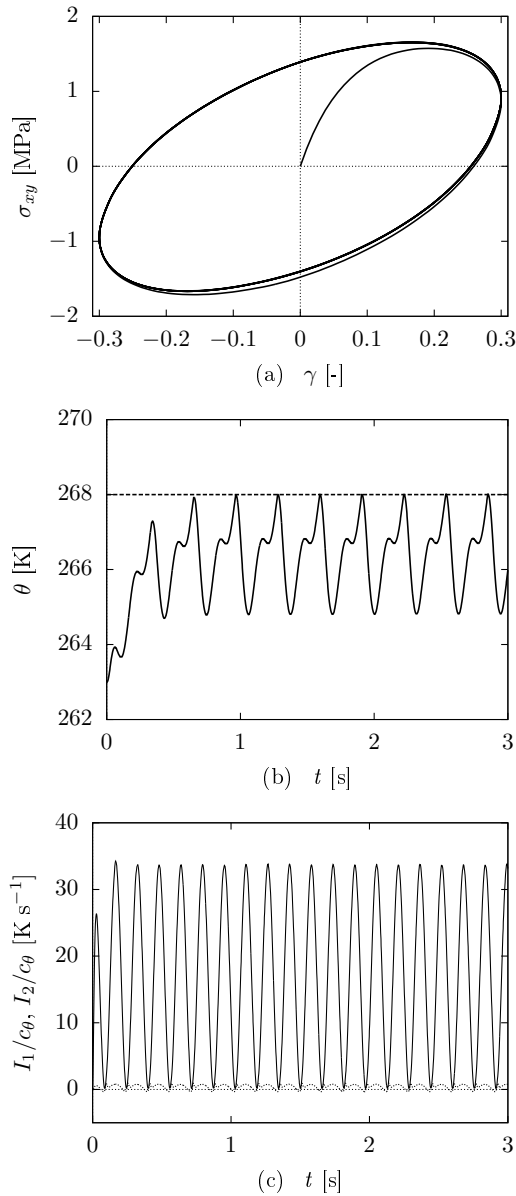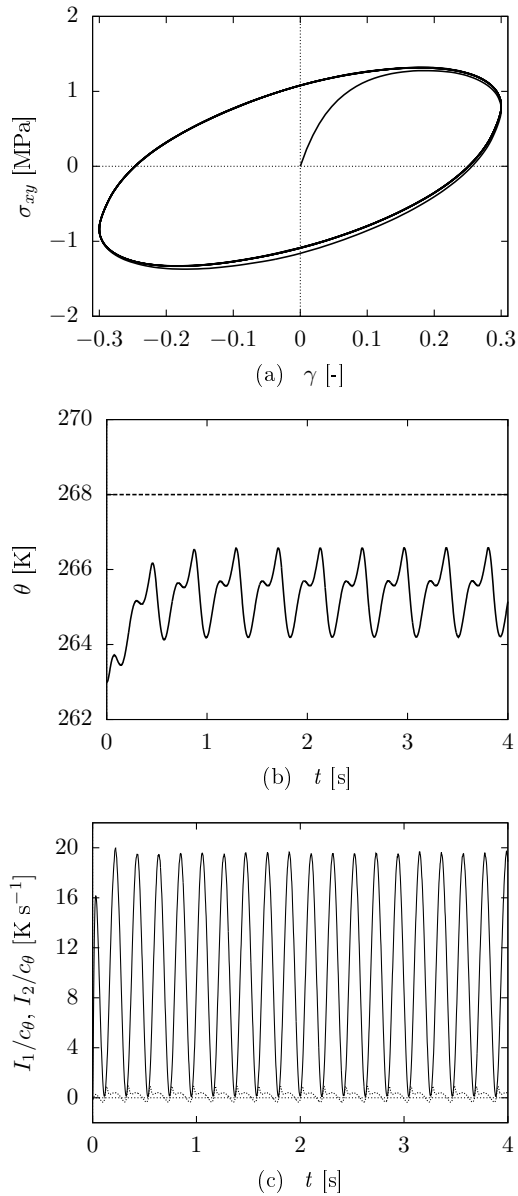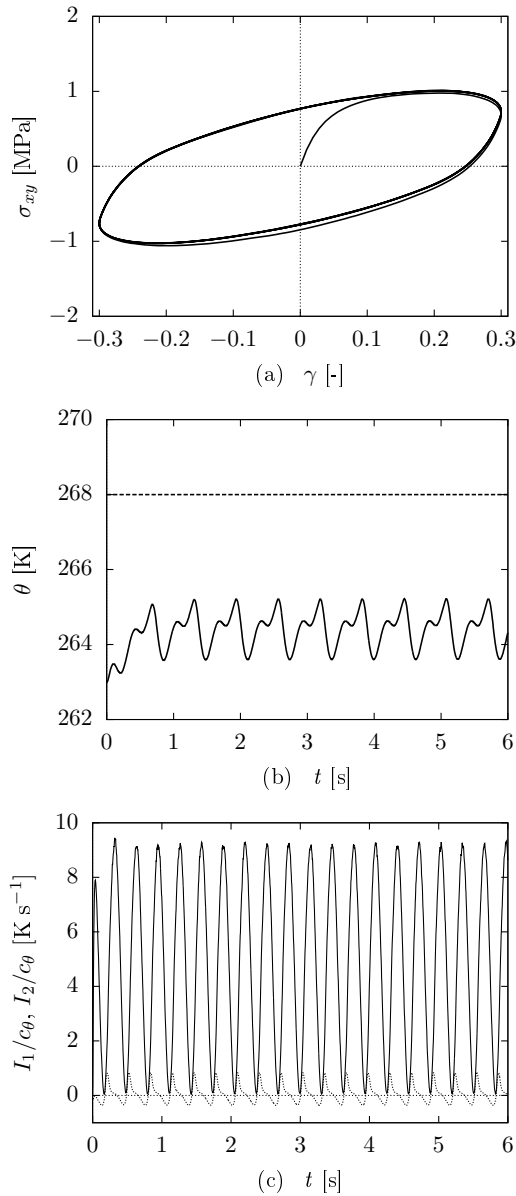
Figure 5.2: Oscillatory deformation for ten cycles, for deformation amplitude $\gamma_0 = 0.3$ and frequency $\omega = 20\,\mathrm{s}^{-1}$. Shear stress σ_{xy} as a function of the applied shear strain (a). Configurational temperature θ (b), and the quantities I_1/c_θ and I_2/c_θ (see (5.121) and (5.122)) (c), as functions of time. The dashed line in (b) denotes the statistical average of the initial local glass transition temperature, $\langle T_{\mathrm{g}}^{\mathrm{init}}(z,0) \rangle$.
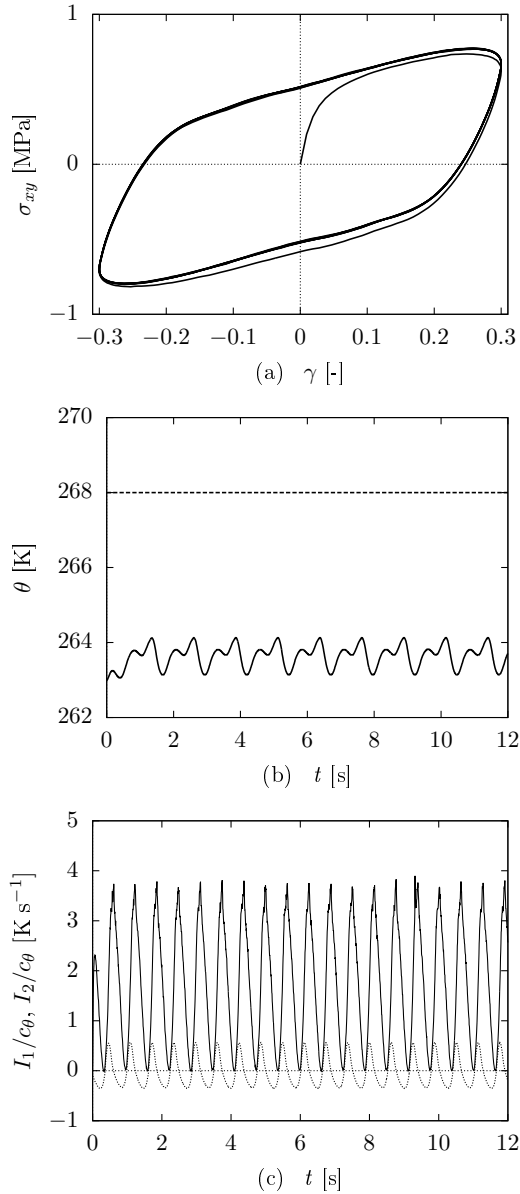
Figure 5.3: Oscillatory deformation for ten cycles, for deformation amplitude $\gamma_0 = 0.3$ and frequency $\omega = 15\,\mathrm{s}^{-1}$. Shear stress σ_{xy} as a function of the applied shear strain (a). Configurational temperature θ (b), and the quantities I_1/c_θ and I_2/c_θ (see (5.121) and (5.122)) (c), as functions of time. The dashed line in (b) denotes the statistical average of the initial local glass transition temperature, $\langle T_\mathrm{g}^\mathrm{init}(z,0) \rangle$.

Figure 5.4: Oscillatory deformation for ten cycles, for deformation amplitude $\gamma_0 = 0.3$ and frequency $\omega = 10\,\mathrm{s}^{-1}$. Shear stress σ_{xy} as a function of the applied shear strain (a). Configurational temperature θ (b), and the quantities I_1/c_θ and I_2/c_θ (see (5.121) and (5.122)) (c), as functions of time. The dashed line in (b) denotes the statistical average of the initial local glass transition temperature, $\langle T_\mathrm{g}^\mathrm{init}(z,0)\rangle$.

Figure 5.5: Oscillatory deformation for ten cycles, for deformation amplitude $\gamma_0 = 0.3$ and frequency $\omega = 5\,\mathrm{s}^{-1}$. Shear stress σ_{xy} as a function of the applied shear strain (a). Configurational temperature θ (b), and the quantities I_1/c_θ and I_2/c_θ (see (5.121) and (5.122)) (c), as functions of time. The dashed line in (b) denotes the statistical average of the initial local glass transition temperature, $\langle T_\mathrm{g}^\mathrm{init}(z, 0)\rangle$.

In summary, it can be said that the model presented in this chapter carries the features necessary to describe the Mullins effect according to the protocol described in [17, 18], for hard-particle filled elastomer nanocomposites. However, due to the numerical limitations discussed above, only the regime I with the large-amplitude deformation could be assessed numerically, while regime II and III have been studied in a qualitative manner. It is clearly desirable to extend the numerical studies also to these two regimes in the future.

5.5   Conclusions

By applying nonequilibrium thermodynamics in the form of the General Equation for the Non-Equilibrium Reversible-Irreversible Coupling (GENERIC), a concurrent two-scale model was developed to describe the nonlinear elasto-viscoplastic mechanical behavior of elastomers filled with hard nanoparticles. In particular, the major part of the work was devoted to incorporating the physical aging of the interparticle glassy material, which leads to the Mullins effect. Doing so, the nanocomposite model developed in [7] is naturally extended by the thermodynamic modeling of physical aging and mechanical rejuvenation, that was studied for bulk glassy materials in [97, 102]. The extension is based on the idea that the glassy interparticle amorphous system is considered as a sum of kinetic and configurational subsystems, and characterized by their specific entropies or equivalent temperatures, for which the evolution equations are formulated. Specifically, the evolution equation for the configurational temperature consists of two parts, representative of physical aging and mechanical rejuvenation, respectively.

The developed model has been studied numerically under oscillatory deformation. A deformation protocol [17, 18] has been used to examine the Mullins effect, and it was found that the model presented in this chapter carries the features necessary to describe the Mullins effect.

With respect to the aging dynamics implemented in the above model, it must be pointed out that the evolution for the configurational temperature has its limitations. Considering a sample with $\theta > T$ (e.g. after a rapid quench to a low temperature), the contributions to the θ-evolution representative of physical aging and mechanical rejuvenation have opposite sign. By choosing the prefactor in the expression of τ_R, one can actually tune the limit to which θ can possibly increase due to mechanical rejuvenation, under certain loading conditions. In this sense, there is a coupling between this prefactor to τ_R and the loading condition, which seems unphysical. It is left as a task for future research to address this issue.

It was discussed that the numerical solution of the mutually coupled two-scale model is cumbersome. Specifically, the effect of mechanical rejuvenation on the configurational temperature of the matrix material contribution depends in an intricate way on the filler-particle arrangement. This dependence is of a type that makes it impossible, in general, to use the CONNFFESSIT approach for the numerical solution. In order to estimate the significance of the problematic contribution in comparison to other contributions, a Gaussian approximation was used. It turned out that under strong deformation, the problematic term can actually be neglected, and the quality of this approximation has been assessed in an accurate way. However, the limits of this numerical approximation are evident; particularly at small deformations and at equilibrium it is inappropriate. Therefore, this

poses a task for the community of computational physics for the near future. Solving this issue is not only relevant for the specific work presented in this chapter. More importantly, it can be envisioned that, as part of the ever increasing research activity in the field of multiscale materials modeling, other models of a similar kind will be developed that await to be solved with adequate numerical tools.

Chapter 6

Conclusions and outlook

6.1 Conclusions

In this thesis, the mechanics of elastomers filled with hard nanoparticles was considered from a fundamental thermodynamic point of view. By applying the general equation for the non-equilibrium reversible-irreversible coupling (GENERIC) of nonequilibrium thermodynamics [27–29], a concurrent dynamic two-scale model was formulated to describe the nonlinear amplitude- and rate-dependent mechanical behavior of this class of nanocomposites, including the prominent Payne effect [2, 17–19] and Mullins effect [3–5]. The analytical model was translated into a numerical scheme, in order to perform a quantitative analysis, as well as to validate the proposed approach in comparison to others in the literature. To be specific:

In Chapter 2, the two scales, namely the macroscopic continuum scale where the mechanical deformation is applied was coupled with the level of the filler particles. This resulted in (i) a closed system of evolution equations for the momentum density, the temperature, the total macroscopic deformation gradient, and the particle-pair distribution function, all formulated in an Eulerian setting, and (ii) constitutive relations for the Cauchy stress tensor and for the viscoplastic flow rule on the level of the filler particles. The filler particle structure is represented by a representative particle-pair only, since one of the main goals of this thesis is the formulation of a compact and thus highly efficient model. Particularly, the particle pair is described by the current particle separation vector that deforms (pseudo-) affinely due to the imposed macroscopic deformation. This is supplemented by the separation vector of the corresponding force-free state that continuously relaxes towards the current state. While the form of the macroscopic evolution equations is commonly known to the general theories of elasticity and hydrodynamics, the evolution equation for the particle-pair distribution function and the constitutive relations are essential results of the GENERIC framework for coupling the two levels of description. The macroscopic deformation, particularly the gradient of the macroscopic velocity field, enters the evolution equation for the particle-pair distribution function on the microscopic scale, thereby achieving the macro→micro coupling. This deformation will result in unbalanced forces between the particles which in turn has two ramifications.

On the one hand, the particle arrangement relaxes towards a force-free state, which is incorporated in the microscopic dynamics of the model. On the other hand, the forces on the microscopic particle level enter the Cauchy-stress tensor on the macroscopic scale, in terms of a Kramers-Kirkwood type expression [54], which constitutes the micro→macro coupling. The formulated model can be applied to systems with relatively high particle volume fraction ($0.2 \lesssim \phi \lesssim 0.4$), since the modeling approach essentially builds on the overlap of the glassy layers around the filler particles, i.e. on the existence of glassy bridges between filler particles. The two-scale model was translated into a numerical Brownian dynamics scheme to examine its response for large amplitude oscillatory shear deformation. It was observed that the non-linear storage modulus decreases significantly when increasing the deformation amplitude, which is known as the Payne effect. This result can be rationalized by noticing that the imposed deformation leads to interparticle stresses that in turn decrease the local glass transition temperature and thereby the glassy bridges weaken. To validate the proposed model, it was compared with the many-particle model published in [17,18]. While the stress-strain response of these two approaches agree quite well for a wide regime of applied deformation, a marked difference is observed for very large deformation amplitudes. This difference is a result of heterogeneity (local crowding) on the particle level, which can be captured in a many-particle approach, however which is absent in the representative particle-pair approach developed in this thesis.

In Chapter 3, the elasto-viscoplasticity of amorphous solids was modeled with a focus on the effect of physical aging on the mechanical response. This research line was initiated for the following reason. After the strain-softening of a hard-particle filled elastomer nanocomposite due to large amplitude oscillatory deformation (Payne effect), the subsequent recovery of the storage modulus is related to the physical aging of the interparticle glassy material. In order to include this effect in an appropriate way in the model developed in Chapter 2, the research in Chapter 3 was undertaken to model the physical aging of bulk glassy materials. The approach adopted for the corresponding modeling was based on the concept of two-subsystem thermodynamics [74, 79, 80]. Due to this concept the entire amorphous system can be considered as a sum of two subsystems, i.e. the kinetic (vibrational) one with fast dynamics around local energy minima, and a configurational one with relatively slow dynamics representative of the transitions between different minima across energy barriers. Introducing the kinetic and configurational entropy densities of each subsystem, their evolution equations as well as those of the momentum density and of the elastic part of a deformation gradient have been derived by applying the GENERIC framework. It was found that the way in which the dissipated energy due to viscoplastic deformation is distributed between the two thermal subsystems is controlled by some tensor-valued function, which couples the kinetic and configurational subsystems in the irreversible dynamics. Specifically, it was found that this tensor-valued coupling function dictates the form of mechanical rejuvenation in amorphous solids.

In Chapter 4, the model developed in Chapter 3 was extended to allow for a most general coupling of the two thermal subsystems of bulk glassy solids also in the reversible dynamics. In particular, the nonzero coupling in the reversible parts of the subsystem entropy evolution equations was formulated using the GENERIC framework. Similar to Chapter 3, also in the case of reversible dynamics the coupling of the two thermal subsystems is achieved by a tensor-valued function. Two main conclusions about this coupling emerged. First, the tensor-valued coupling function resulted in an extra contribution to

the Cauchy stress tensor, rendering the stress tensor *hypo*elastic rather than *hyper*elastic. Second, the Hamiltonian structure of the reversible dynamics in GENERIC in the form of the Jacobi identity [27, 29] imposes severe constraints on the possible choice of the tensor-valued coupling function. Finally, having available the model with two general tensor-valued functions for the subsystem coupling in the reversible and irreversible dynamics, respectively, a detailed comparison with other approaches known in the literature was made. It was found that there is to date no consensus on the proper choice of the two tensor-valued coupling functions.

Finally, in Chapter 5, the two-scale model formulated in Chapter 2, has been extended in order to account for the Mullins effect. This extension is achieved by combining the two-scale model developed in Chapter 2 with the two-subsystem thermodynamics for aging amorphous solids studied in Chapters 3 and 4, using the GENERIC framework. The resulting model consists of a closed set of evolution equations for the momentum density, the entropy densities of the two thermal subsystems, the total deformation gradient, and the particle-pair distribution function. Furthermore, the constitutive relation for the Cauchy stress tensor was derived. Since the entropy densities are not convenient to work with in practical applications of the model, the dynamic model was reformulated in terms of kinetic and configurational temperatures, specific to each of the thermal subsystems. The proposed set of evolution equations together with the constitutive relations have been translated to a numerical scheme. However, due to the coupling of the microscopic and macroscopic dynamics in the presence of physical aging and mechanical rejuvenation, it is not possible to use Brownian dynamics simulations in combination with the CON-NFFESSIT approach [39, 109] in general for arbitrary deformations. The complication arises from how the dissipative filler-particle dynamics gives rise to an increase in the configurational temperature, representative of mechanical rejuvenation. However, it was shown that under conditions of strong imposed deformation, this two-scale coupling can be approximated in a way that makes it manageable for the CONNFFESSIT approach. Performing numerical simulations for large amplitude oscillatory shear deformation, the Mullins effect was investigated. It was found the the model contains the features necessary to describe both the Payne effect and the Mullins effect.

6.2   Outlook

The work presented in this thesis can in principle be divided into two parts. The first part concerns the two-scale modeling of hard-particle filled elastomer nanocomposites where an important aspect is the proper thermodynamic coupling of the macroscopic and microscopic scales. The second part discusses the modeling of the physical aging and mechanical rejuvenation of bulk amorphous solids. Correspondingly, one can think of two different groups of research questions for further investigation.

Two-scale modeling of hard-particle filled elastomer nanocomposites

- As it was already mentioned in Sec. 2, one of main ingredients of the two-scale model is the total entropy, that includes also the contribution due to the filler particle distribution. The expression related to the filler particle distribution can be formulated in a standard form if one considers the distribution function of either

only one or all particles, respectively, however for any particle number in between it is not straight forward, which is relevant for the case of a representative particle pair. The situation in this thesis is even more complicated, since the representative particle pair is characterized by two vectors describing the current and the force-free states, respectively. In Sec. 2, it was discussed in what sense the entropy of such a particle pair can be interpret similarly to a dumbbell model. It is, however, desirable to further investigate the entropy expression in more detail, because it will eventually affect the entire two-scale model.

- In the developed two-scale model, the interparticle relaxation mechanism has a significant influence on the macroscopic response. The corresponding relaxation time depends strongly on the surface-to-surface distance and the local stress between two neighboring particles. In the current formulation of the model, only a single particle-pair is considered. Doing so, one disregards the fact that each particle has in principle several neighbors, which leads to a distribution of relaxation times relevant for that one center particle. It would be interesting to study how this distribution in the particle-pair relaxation time can be taken into account, possibly by a modification of the existing two-scale model.

- The two-scale model developed in this thesis (Sec. 2 and Sec. 5) is built on the assumption that the desired microscopic physics can be captured by considering just a single representative particle pair. This implies that only systems with a relatively homogeneous particle distribution can be described. However, often nanometer-sized filler particles are far from homogeneously dispersed but rather they are clustered in agglomerates, and furthermore local crowding may occur at strong deformation. Both of these aspects are supposed to have a significant effect on the mechanical response of the nanocomposite. Therefore, as for future research one might consider inhomogeneous filler-particle arrangements.

- The evolution equation for the configurational temperature θ contains two contributions representative of physical aging and mechanical rejuvenation. While the first contribution represents the relaxation of θ towards the kinetic temperature T, the mechanical rejuvenation works to permanently increase θ. It is by the balance of these two contributions that a stationary θ is obtained during ongoing mechanical deformation. This implies that the stronger the mechanical deformation the higher is the stationary value for θ. It seems that this is unphysical, specifically if θ reaches temperatures significantly above the glass transition temperature, and therefore the proposed model should be revised in this respect.

- In Sec. 5, the numerical solution of the two-scale model was discussed, with the aging dynamics included. It was found that the CONNFFESSIT technique can be applied only for relatively strong deformations, since in this case the problematic term in the micro-macro coupling, i.e. in the evolution equation for the configurational temperature, can be omitted. However, this significantly limits the applicability of this numerical technique. Therefore, there is a need for an extension of the CONNFFESSIT approach or for the development of an even different technique, to be able to study the model for a wider range of applied deformations, in particular

with small deformation amplitudes. It is anticipated that such extension of the numerical techniques is not only useful for the model in this thesis, but also for other models with a comparable structure of the micro-macro coupling.

- In the developed two-scale model, the dynamics of the microstructure is represented by the Fokker-Planck equation for the particle distribution function p, or equivalently by the system of stochastic differential equations for structural variables. Since the numerical solution of this model is challenging particularly in macroscopically inhomogeneous situations, one can think of model reduction. For example, the presented model could be reduced to a coupled set of evolution equations for the moments of the distribution function. Such a mean-field approximation might be more convenient for practical purposes.

Two-subsystem thermo-mechanics for the aging and mechanical rejuvenation of bulk amorphous solids

- In Sec. 3 and Sec. 4, a general model to account for the effects of physical aging and mechanical rejuvenation in amorphous solids was developed. In particular, the nontrivial coupling between two thermal subsystems, i.e. kinetic and configurational, in the reversible and irreversible dynamics was considered. These couplings are represented in the form of two tensor-valued functions that must comply with thermodynamic criteria encoded into the GENERIC framework, e.g. with the Jacobi identity of reversible dynamics. While these criteria help to assess the admissibility of the tensor-valued coupling functions, there is only limited physical intuition on how they should be chosen concretely. It is interesting to attempt to get a deeper understanding about the physical meaning and concrete forms of the two tensor-valued coupling functions by microscopic considerations, i.e. in terms of characteristic features on the level of the constituent microscopic particles.

Details about calculations in Chapter 2

A.1 Calculation of the Poisson operator $\mathcal{L}$

Given the set of state variables $\mathcal{X}$, one can specify the meaning of the sign $\odot$, used in Sec. 2.2, that in general implies integrations. The state variables $\mathcal{X}$ in (2.11) depend on spatial position r and internal configuration ξ. On the one hand, the Poisson operator and friction matrix depend in general on both r and r' (r' is different from r), i.e. $\mathcal{L}(r, r')$, $\mathcal{M}(r, r')$. The evolution equation (2.1) thus implies that $\partial_t \mathcal{X}(r)$ is affected not only by the driving forces at the same space point r, but also by the driving forces at any other points r'. However, for local field theories, there are only contributions for $r = r'$, and therefore no integration is needed, i.e., both the Poisson operator and the friction matrix vanish for any $r' \neq r$. The situation is different for the variable ξ in (2.12) describing the internal configuration, as can be seen by the following argument. The momentum balance equation has the form $\partial_t m(r) = -\nabla^r \cdot [m(r) v(r)] + \nabla^r \cdot \sigma(r)$. Here the stress tensor σ depends implicitly on the variable ξ through the distribution function $p(r, \xi)$, which implies that an integration over the variable ξ occurs, in the sense of an averaging operation. One thus concludes that $\odot$ implies an integration over internal configurations, and therefore the Poisson operator and the friction matrix depend in general on both ξ and ξ', $\mathcal{L} = \mathcal{L}(r, \xi, \xi')$ and $\mathcal{M} = \mathcal{M}(r, \xi, \xi')$. Therefore, the time evolution equation (2.1) can be written in the more explicit form

$$\partial_t \mathcal{X}_i(r, \xi) = \int \mathcal{L}_{ij}(r, \xi, \xi') \frac{\delta E}{\delta \mathcal{X}_j(r, \xi')} \mathrm{d}^6\xi' + \int \mathcal{M}_{ij}(r, \xi, \xi') \frac{\delta S}{\delta \mathcal{X}_j(r, \xi')} \mathrm{d}^6\xi', \quad \text{(A.1)}$$

where the indices i and j refer to state variables in the set $\mathcal{X}$. We are thus dealing with a field theory that is local with respect to the macroscopic position r, but non-local with respect to the internal configuration ξ.

   To simplify notation in this work, we are going to use the following notation. Since the general evolution equation (A.1) is local in terms of r, the argument r is omitted, except in special cases. As for the dependence of a function f on the internal configuration ξ, we use the shorthand notation $f = f(\xi)$, $f' = f(\xi')$, $f'' = f(\xi'')$, and $f''' = f(\xi''')$, respectively, unless the explicit notation with arguments is required for clarity.

Following the arguments given in Sec 2.3.3, and using the result obtained in [29, 32], one can show that the Poisson operator takes the form

$$\mathcal{L}[\mathcal{X}] = \begin{pmatrix} \mathcal{L}^{(mm)}(\boldsymbol{r}) & \mathcal{L}^{(mT)}(\boldsymbol{r}) & \mathcal{L}^{(mF)}(\boldsymbol{r}) & \mathcal{L}^{(mp)}(\boldsymbol{r}, \boldsymbol{\xi}') \\ \mathcal{L}^{(Tm)}(\boldsymbol{r}) & 0 & 0 & 0 \\ \mathcal{L}^{(Fm)}(\boldsymbol{r}) & 0 & 0 & 0 \\ \mathcal{L}^{(pm)}(\boldsymbol{r}, \boldsymbol{\xi}) & 0 & 0 & 0 \end{pmatrix}, \qquad (A.2)$$

with

$$\mathcal{L}_{\alpha\gamma}^{(mm)} \equiv -\nabla_\gamma^r \, m_\alpha - m_\gamma \nabla_\alpha^r \,, \qquad (A.3a)$$

$$\mathcal{L}_{\alpha\gamma\varepsilon}^{(mF)} \equiv (\nabla_\alpha^r \, F_{\gamma\varepsilon}) + \nabla_\mu^r \, F_{\mu\varepsilon} \, \delta_{\alpha\gamma} \,, \qquad (A.3b)$$

$$\mathcal{L}_{\alpha\beta\gamma}^{(Fm)} \equiv - (\nabla_\gamma^r \, F_{\alpha\beta}) + F_{\mu\beta} \, \nabla_\mu^r \delta_{\alpha\gamma} \,, \qquad (A.3c)$$

$$\mathcal{L}_\alpha^{(mp)} \equiv -p' \, \nabla_\alpha^r + \nabla_\mu^r \, R'_\mu \, p' \, \nabla_\alpha^{R'} \,, \qquad (A.3d)$$

$$\mathcal{L}_\gamma^{(pm)} \equiv -\nabla_\gamma^r \, p - \nabla_\gamma^R \, R_\mu \, p \, \nabla_\mu^r \,. \qquad (A.3e)$$

Here, it should be pointed out that all ∇-operators occurring in (A.3) act also on functions multiplied to $\mathcal{L}$ from the right (e.g. $\delta E/\delta\mathcal{X}$), except when enclosed in parentheses like $(\nabla^r f(\boldsymbol{r}))$, where ∇^r acts only on the function $f(\boldsymbol{r})$ enclosed in the parentheses.

The two yet unspecified elements $\mathcal{L}^{(mT)}$ and $\mathcal{L}^{(Tm)}$ can be determined by using the degeneracy condition (2.4a) and the antisymmetry condition (2.5a). From the degeneracy condition (2.4a) it follows

$$\mathcal{L}_\alpha^{(mT)} \frac{\delta S}{\delta T} + \mathcal{L}_{\alpha\gamma\varepsilon}^{(mF)} \frac{\delta S}{\delta F_{\gamma\varepsilon}} + \int_{\mathcal{Q}^2} \mathcal{L}_\alpha^{(mp)} \frac{\delta S}{\delta p'} \mathrm{d}^6\boldsymbol{\xi}' = 0 \,, \qquad (A.4)$$

where we have used $\delta S/\delta\boldsymbol{m} = \boldsymbol{0}$. Note, that without violating the degeneracy condition, we can add a term of the form $f(\mathcal{X})\nabla_\alpha^r 1$ to (2.4a), with any arbitrary function f (since $\nabla_\alpha^r 1 = 0$). This implies that $\mathcal{L}_\alpha^{(mT)}$ can only be determined up to an additive operator of the form $f(\mathcal{X})\nabla_\alpha^r (\delta S/\delta T)^{-1}$. However, requiring that the entropy evolution equation assumes the form

$$\partial_t s = -\nabla_\gamma^r (s \, v_\gamma) \,, \qquad (A.5)$$

renders the element $\mathcal{L}_\alpha^{(mT)}$ unique, namely

$$\mathcal{L}_\alpha^{(mT)} \equiv [\nabla_\alpha^r T] - \nabla_\alpha^r \left(\frac{\delta S}{\delta T}\right)^{-1} s - \nabla_\mu^r F_{\mu\varepsilon} \frac{\delta S}{\delta F_{\alpha\varepsilon}} \left(\frac{\delta S}{\delta T}\right)^{-1}$$

$$+ \quad \nabla_\alpha^r \int_{\mathcal{Q}^2} p' \frac{\delta S}{\delta p'} \left(\frac{\delta S}{\delta T}\right)^{-1} \mathrm{d}^6\boldsymbol{\xi}'$$

$$- \quad \nabla_\mu^r \int_{\mathcal{Q}^2} p' \, R'_\mu \left(\nabla_\alpha^{R'} \frac{\delta S}{\delta p'}\right) \left(\frac{\delta S}{\delta T}\right)^{-1} \mathrm{d}^6\boldsymbol{\xi}' \,. \qquad (A.7)$$

Use has been made of the relation (in analogy to Eq. (14) in [111])

$$\nabla^r a = \frac{\delta A}{\delta T} (\nabla^r T) + \frac{\delta A}{\delta \boldsymbol{F}} : (\nabla^r \boldsymbol{F}) + \int_{\mathcal{Q}^2} \frac{\delta A}{\delta p} (\nabla^r p) \mathrm{d}^6\boldsymbol{\xi} \,, \qquad (A.6)$$

for a functional $A[T, \boldsymbol{F}, p]$ with spatial density a, $A = \int a \, \mathrm{d}^3\boldsymbol{r}$.

The $\mathcal{L}^{(Tm)}$-entry can be determined by way of the antisymmetry of Poisson operator, leading to

$$
\begin{aligned}
\mathcal{L}_\gamma^{(Tm)} \quad \equiv \quad & - \left[\nabla_\gamma^r T \right] - \left(\frac{\delta S}{\delta T} \right)^{-1} s \, \nabla_\gamma^r - \frac{\delta S}{\delta F_{\gamma \nu}} \left(\frac{\delta S}{\delta T} \right)^{-1} F_{\varkappa \nu} \nabla_\varkappa^r \\
& + \int_{\mathcal{Q}^2} \frac{\delta S}{\delta p'} \left(\frac{\delta S}{\delta T} \right)^{-1} p' \mathrm{d}^6 \boldsymbol{\xi}' \nabla_\gamma^r \\
& - \int_{\mathcal{Q}^2} p' \, R_\mu' \left(\nabla_\gamma^{R'} \frac{\delta S}{\delta p'} \right) \left(\frac{\delta S}{\delta T} \right)^{-1} \mathrm{d}^6 \boldsymbol{\xi}' \, \nabla_\mu^r .
\end{aligned}
\tag{A.8}
$$

So far we have respected all GENERIC conditions when specifying the Poisson operator, except the Jacobi identity (2.6). To check the Jacobi identity, it is useful to note that a transformation of dynamical variables does not affect the Jacobi identity. Particularly, it can be shown that the Poisson operator is considerably simplified when using $\boldsymbol{\mathcal{X}}' = \{\boldsymbol{m}, s, \boldsymbol{F}, p\}$ instead of $\boldsymbol{\mathcal{X}} = \{\boldsymbol{m}, T, \boldsymbol{F}, p\}$. Using the $\boldsymbol{\mathcal{X}}'$-formulation, the Jacobi identity can be checked and verified analytically, by a lengthy but straightforward calculation. For a computer-code to symbolically calculate the Jacobi identity, the reader is referred to [112].

A.2 Calculation of the friction matrix $\mathcal{M}$

A.2.1 Dissipative matrix $\bar{\mathcal{M}}$

In this appendix, the elements of $\mathcal{C}$ in the decomposition (2.23) are determined. To that end, the reader is reminded (as in (A.1)) that the symbol $\odot$ in (2.23) also implies integrations, and therefore the explicit form of (2.23) is given by

$$
\bar{\mathcal{M}}_{ij}(\boldsymbol{r}, \boldsymbol{\xi}, \boldsymbol{\xi}') = \iint_{\mathcal{Q}^2} \mathcal{C}_{ik}(\boldsymbol{r}, \boldsymbol{\xi}, \boldsymbol{\xi}'') \, \mathcal{D}_{kn}(\boldsymbol{r}, \boldsymbol{\xi}'', \boldsymbol{\xi}''') \, \mathcal{C}_{nj}^*(\boldsymbol{r}, \boldsymbol{\xi}''', \boldsymbol{\xi}') \, \mathrm{d}^6 \boldsymbol{\xi}'' \mathrm{d}^6 \boldsymbol{\xi}''' . \tag{A.9}
$$

Since the relaxation dynamics, $\mathcal{J}$, of the unloaded state $\boldsymbol{Q}$ toward the current state $\boldsymbol{R}$ originates from the viscoplastic deformation of glassy material and hence involves friction-related, dissipative effects, the temperature of the system will be affected by $\mathcal{J}$. In view of the complete set of variables $\boldsymbol{\mathcal{X}} = \{\boldsymbol{m}, T, \boldsymbol{F}, p\}$, the general operator $\mathcal{C}$ in (2.27) thus assumes the form

$$
\mathcal{C} = \begin{pmatrix} 0 & \bullet & 0 & \bullet \end{pmatrix}^\top , \qquad \mathcal{C}^* = \begin{pmatrix} 0 & \bullet^* & 0 & \bullet^* \end{pmatrix} , \tag{A.10}
$$

with adjoint operator $\mathcal{C}^*$. The symbol $\bullet$ denotes yet unknown elements, that are determined as follows. The p-evolution equation (2.29) can be re-written in the form

$$
\partial_t \, p(\boldsymbol{r}, \boldsymbol{\xi})|_{\mathrm{relax}} = \int_{\mathcal{Q}^2} \delta(\boldsymbol{R} - \boldsymbol{R}'') \left[\nabla_\gamma^{Q''} \delta(\boldsymbol{Q} - \boldsymbol{Q}'') \right] \mathcal{J}_\gamma'' \mathrm{d}^6 \boldsymbol{\xi}'' , \tag{A.11}
$$

which, in view of (2.27) and the ansatz (A.10), leads to

$$
\mathcal{C}_\gamma^{(p)} = \delta(\boldsymbol{R} - \boldsymbol{R}'') \left[\nabla_\gamma^{Q''} \delta(\boldsymbol{Q} - \boldsymbol{Q}'') \right] , \tag{A.12a}
$$

$$
\mathcal{C}_\alpha^{*(p)} = \delta(\boldsymbol{R}' - \boldsymbol{R}''') \left[\nabla_\alpha^{\boldsymbol{Q}'''} \delta(\boldsymbol{Q}' - \boldsymbol{Q}''') \right] , \tag{A.12b}
$$

with $\mathcal{C}_\alpha^{*(p)}$ the operator-adjoint of $\mathcal{C}_\gamma^{(p)}$. Then, the degeneracy condition (2.24) can be used to specify $\mathcal{C}_\alpha^{(T)*}$,

$$\mathcal{C}_\alpha^{*(T)} = -\left[\nabla_\alpha^{Q'''}\frac{\delta U}{\delta p'''}\right]\left(\frac{\delta U}{\delta T}\right)^{-1}, \tag{A.13a}$$

$$\mathcal{C}_\gamma^{(T)} = -\left[\nabla_\gamma^{Q''}\frac{\delta U}{\delta p''}\right]\left(\frac{\delta U}{\delta T}\right)^{-1}, \tag{A.13b}$$

with $\mathcal{C}_\gamma^{(T)}$ the operator-adjoint of $\mathcal{C}_\alpha^{*(T)}$. It should be mentioned that, similarly to the discussion in relation to (A.4), a term of the form $f(\boldsymbol{\mathcal{X}})\nabla_\alpha^r\left(\delta U/\delta T\right)^{-1}$ could be added to $\mathcal{C}_\alpha^{*(T)}$ without violating the degeneracy condition, with an arbitrary function $f(\boldsymbol{\mathcal{X}})$. However, it can be shown that such a contribution leads to heat conduction [34], in which we are not interested in this work, as stated earlier. Finally, the explicit form of $\boldsymbol{\mathcal{C}}$ and $\boldsymbol{\mathcal{C}}^*$ is given by

$$\mathcal{C} = \begin{pmatrix} 0 \\ -\left[\nabla_\gamma^{Q''}\frac{\delta U}{\delta p''}\right]\left(\frac{\delta U}{\delta T}\right)^{-1} \\ 0 \\ \delta(\boldsymbol{R}-\boldsymbol{R}'')\left[\nabla_\gamma^{Q''}\delta(\boldsymbol{Q}-\boldsymbol{Q}'')\right] \end{pmatrix}, \tag{A.14a}$$

$$\mathcal{C}^* = \left(0, -\left[\nabla_\alpha^{Q'''}\frac{\delta U}{\delta p'''}\right]\left(\frac{\delta U}{\delta T}\right)^{-1}, 0, \delta(\boldsymbol{R}'-\boldsymbol{R}''')\left[\nabla_\alpha^{Q'''}\delta(\boldsymbol{Q}'-\boldsymbol{Q}''')\right]\right). \tag{A.14b}$$

In turn, the thermodynamic driving force (2.25) assumes the form

$$\mathcal{F}_\alpha''' = -\frac{1}{\Theta}\left[\nabla_\alpha^{Q'''}\frac{\delta A}{\delta p'''}\right], \tag{A.15}$$

where the abbreviation (2.20b) has been used. Once a relation for a symmetric and positive semi-definite $\boldsymbol{\mathcal{D}}$ is specified, the expression for the thermodynamic flux (2.26) is known.

A.2.2 Antisymmetric contribution $\tilde{\mathcal{M}}$

Following the discussion in Sec.2.3.4.2 and in analogy to pp. 119 - 120 in [29], one can show that the non-affine contribution $\tilde{\mathcal{M}}$ can be written in the form

$$\tilde{\mathcal{M}}[\boldsymbol{\mathcal{X}}] = \begin{pmatrix} 0 & \tilde{\mathcal{M}}^{(mT)}(\boldsymbol{r}) & 0 & \tilde{\mathcal{M}}^{(mp)}(\boldsymbol{r},\boldsymbol{\xi}') \\ \tilde{\mathcal{M}}^{(Tm)}(\boldsymbol{r}) & 0 & 0 & \tilde{\mathcal{M}}^{(Tp)}(\boldsymbol{r},\boldsymbol{\xi}') \\ 0 & 0 & 0 & 0 \\ \tilde{\mathcal{M}}^{(pm)}(\boldsymbol{r},\boldsymbol{\xi}) & \tilde{\mathcal{M}}^{(pT)}(\boldsymbol{r},\boldsymbol{\xi}) & 0 & 0 \end{pmatrix}. \tag{A.16}$$

For the construction of all components, we start by assuming that the antisymmetry of the stress tensor is related to the rotational component in the applied flow field, i.e. to

---

This assumption is not only plausible, but it can also be verified to hold true in hindsight, based on the complete model.

the antisymmetric contribution to the velocity gradient, $\nabla^r \boldsymbol{v}$. In order to eliminate the rotational effects of the flow field, we strive to replace the velocity gradient in (2.18d) by its symmetric part. This is achieved by adding to the dynamics of the structural variable p (2.18d) an additional contribution in the irreversible part, specifically accounting for the non-affinity with

$$\partial_t \, p|_{\text{non-a}} = -\nabla_\nu^R \left(\frac{1}{2} \Big[(\nabla_\nu^r v_\mu) - (\nabla_\mu^r v_\nu) \Big] R_\mu p \right) . \tag{A.17}$$

The identification of the elements in $\tilde{\boldsymbol{\mathcal{M}}}$ is done as follows. Since $\delta S / \delta \boldsymbol{m} = 0$, one can use (A.17) to determine $\tilde{\mathcal{M}}^{(pT)}$ by virtue of $\partial_t p|_{\text{non-a}} = \tilde{\mathcal{M}}^{(pT)}(\delta S / \delta T)$, from which $\tilde{\mathcal{M}}^{(pm)}$ follows by using the degeneracy condition (2.4b). Consecutively, $\tilde{\mathcal{M}}^{(Tp)}$ and $\tilde{\mathcal{M}}^{(mp)}$ follow from the condition of antisymmetry of $\tilde{\boldsymbol{\mathcal{M}}}$. Again using the degeneracy condition (2.4b) leads to $\tilde{\mathcal{M}}^{(Tm)}$ and $\tilde{\mathcal{M}}^{(mT)}$. It must be mentioned that at two points of this procedure a non-uniqueness of the elements of $\tilde{\boldsymbol{\mathcal{M}}}$ arises, leading to four possible solutions. However, when requiring that $\tilde{\mathcal{M}}^{(Tm)}$ and $\tilde{\mathcal{M}}^{(mT)}$ are such that the entire $\tilde{\boldsymbol{\mathcal{M}}}$ is antisymmetric (which has not yet been enforced), only one of the four solutions remains, and is hence unique, namely

$$\tilde{\mathcal{M}}_\alpha^{(mT)} = -\frac{1}{2} \left[\delta_{\alpha\mu} \nabla_\nu^r - \delta_{\alpha\nu} \nabla_\mu^r \right] \left(\frac{\delta S}{\delta T} \right)^{-1} \int_{\mathcal{Q}^2} \frac{\delta U}{\delta p'} \left(\nabla_\nu^{R'} R_\mu' \, p' \right) \mathrm{d}^6 \boldsymbol{\xi}' , \tag{A.18a}$$

$$\tilde{\mathcal{M}}_\alpha^{(mp)} = \frac{1}{2} \left[\delta_{\alpha\mu} \nabla_\nu^r - \delta_{\alpha\nu} \nabla_\mu^r \right] \Theta \left(\nabla_\nu^{R'} R_\mu' \, p' \right) , \tag{A.18b}$$

$$\tilde{\mathcal{M}}_\gamma^{(Tm)} = -\frac{1}{2} \left(\frac{\delta S}{\delta T} \right)^{-1} \int_{\mathcal{Q}^2} \frac{\delta U}{\delta p'} \left(\nabla_\nu^{R'} R_\mu' \, p' \right) \mathrm{d}^6 \boldsymbol{\xi}' \left[\delta_{\gamma\mu} \nabla_\nu^r - \delta_{\gamma\nu} \nabla_\mu^r \right] , \tag{A.18c}$$

$$\tilde{\mathcal{M}}^{(Tp)} = \frac{1}{2} \left(\frac{\delta S}{\delta T} \right)^{-1} \left(\nabla_\nu^{R'} R_\mu' \, p' \right) \left[(\nabla_\nu^r v_\mu) - (\nabla_\mu^r v_\nu) \right] , \tag{A.18d}$$

$$\tilde{\mathcal{M}}_\gamma^{(pm)}(\boldsymbol{r}, \boldsymbol{\xi}) = \frac{1}{2} \, \Theta \left(\nabla_\nu^R R_\mu \, p \right) \left[\delta_{\gamma\mu} \nabla_\nu^r - \delta_{\gamma\nu} \nabla_\mu^r \right] , \tag{A.18e}$$

$$\tilde{\mathcal{M}}^{(pT)}(\boldsymbol{r}, \boldsymbol{\xi}) = -\frac{1}{2} \left(\frac{\delta S}{\delta T} \right)^{-1} \left(\nabla_\nu^R R_\mu \, p \right) \left[(\nabla_\nu^r v_\mu) - (\nabla_\mu^r v_\nu) \right] . \tag{A.18f}$$

A.3   Configurational entropy

In this Appendix, the expression for the entropy functional S in terms of the structural variable p is discussed. While the use of the $p \ln p$-expression is commonly accepted for the case that p is the 1- or N-particle distribution function of an N-particle system, the situation is less obvious for the model discussed in this study. In our case, p depends on two vectors, namely $\boldsymbol{R}$ and $\boldsymbol{Q}$, where both of them are difference vectors between two particles. However, due to translation invariance, in terms of degrees of freedom the pair $(\boldsymbol{R}, \boldsymbol{Q})$ can be seen as representing the absolute positions of two particles. The question

---

For analogous procedures to reduce from particle positions to difference vectors in polymer kinetic theory, the reader is referred to p. 108 in [38] and Sec. 4.3 in [29].

is thus how the entropy can be represented in terms of the 2-particle distribution function, for which we closely follow the developments in [113] in the following.

Consider a system wit N interacting particles with phase space coordinates $\Gamma = (\mathbf{x}_1, \mathbf{x}_2, \ldots, \mathbf{x}_N) \equiv (\mathbf{x}^N)$. The probability density for N particles to be at point Γ (at time t) is denoted by $f^{(N)}(\Gamma)$ and satisfies the normalization condition [113],

$$\int \cdots \int f^{(N)}(\Gamma) \mathrm{d}\mathbf{x}^N = 1 . \tag{A.19}$$

Based on (A.19), one can introduce the reduced 1- and 2-particle distributions, respectively, as

$$f^{(1)}(\mathbf{x}_1) = N \int \cdots \int f^{(N)}(\mathbf{x}^N)\, \mathrm{d}\mathbf{x}_2 \ldots \mathrm{d}\mathbf{x}_N , \tag{A.20a}$$

$$f^{(2)}(\mathbf{x}_1, \mathbf{x}_2) = N(N-1) \int \cdots \int f^{(N)}(\mathbf{x}^N)\, \mathrm{d}\mathbf{x}_3 \ldots \mathrm{d}\mathbf{x}_N . \tag{A.20b}$$

In [113], the entropy has been calculated neglecting higher than 2-particle correlations. The result can be written in the form (see [113] for details),

$$
\begin{aligned}
\frac{S - S_{\mathrm{eq}}}{k_{\mathrm{B}}} &= (N-2) \int f^{(1)}(\mathbf{x}_1) \ln \frac{f^{(1)}(\mathbf{x}_1)}{f_{\mathrm{eq}}^{(1)}(\mathbf{x}_1)} \mathrm{d}\mathbf{x}_1 \\
&\quad - \frac{1}{2} \iint f^{(2)}(\mathbf{x}_1, \mathbf{x}_2) \ln \frac{f^{(2)}(\mathbf{x}_1, \mathbf{x}_2)}{f_{\mathrm{eq}}^{(2)}(\mathbf{x}_1, \mathbf{x}_2)} \mathrm{d}\mathbf{x}_1 \mathrm{d}\mathbf{x}_2 .
\end{aligned}
\tag{A.21}
$$

with k_{B} the Boltzmann constant, and "eq" denoting the equilibrium quantities. It was noticed by Wallace earlier that entropy expressions of this type are well-convergent for dense fluids (see p. 2283 in [114]). Moreover, using computer simulations, it was shown in [115] that the 3-particle (and higher-order) terms are small in comparison to the 1-particle and 2-particle terms. Relations closely related to (A.21) are often used in the literature, e.g. [115–118].

Taking into account that

$$f^{(1)}(\mathbf{x}_1) = (N-1)^{-1} \int f^{(2)}(\mathbf{x}_1, \mathbf{x}_2)\, \mathrm{d}\mathbf{x}_2 \tag{A.22}$$

based on (A.20), it is manifest that the 2-particle distribution contains also the 1-particle distribution. Therefore, choosing the 2-particle distribution function as the modeling quantity automatically allows to also account for the 1-particle contributions in (A.21). However, when seeking to describe the dynamics of such a $f^{(2)}$-model that involves the maximization of entropy, the driving force

$$
\begin{aligned}
\frac{\delta(S/k_{\mathrm{B}})}{\delta f^{(2)}(\mathbf{x}_1, \mathbf{x}_2)} &= \frac{1}{2} \frac{N-2}{N-1} \left(\ln \frac{f^{(1)}(\mathbf{x}_1)}{f_{\mathrm{eq}}^{(1)}(\mathbf{x}_1)} + 1 + \ln \frac{f^{(1)}(\mathbf{x}_2)}{f_{\mathrm{eq}}^{(1)}(\mathbf{x}_2)} + 1 \right) \\
&\quad - \frac{1}{2} \left(\ln \frac{f^{(2)}(\mathbf{x}_1, \mathbf{x}_2)}{f_{\mathrm{eq}}^{(2)}(\mathbf{x}_1, \mathbf{x}_2)} + 1 \right)
\end{aligned}
\tag{A.23}
$$

contains mean-field type effects in the form of $f^{(1)}$ being an integral of $f^{(2)}$. One can anticipate that the final evolution equation for $f^{(2)}$ will contain these mean-field contributions as well, and it can be shown that one deals effectly with a Fokker-Planck equation for $f^{(2)}$ with mean-field effects. Since the purpose of Sec. 2.4 is to only give an illustrative example of the general model, the above issues of the entropy expression are not examined any further in this work, but rather left as a topic for further studies. It is pointed out that Fokker-Planck equations with mean-field effects need special care in their interpretation, and the reader is also referred to [119] for more details.

A.4   Spring constant and representative particle - pair number density

First, an estimate is given for the value of the number density of particle pairs, n, which has been introduced in Sec. 2.3.1, Eq. (2.10). We begin with the relationship between pair number density, n, and the particle number density m (both are considered per unit volume)

$$n = \frac{mp}{2} \ ,$$

(A.24)

with p the average number of neighboring particles per particle. In the following, both m and p, and thus n, will be related to the volume fraction ϕ.

For the particle number density m of spherical particles of diameter d, one finds readily

$$m = \frac{6\phi}{\pi d^3} \ .$$

(A.25)

For the pair number density n, we proceed as follows. A particle 1 is considered to be a neighbor of another particle 2 if any fraction of particle 1 is located closer than a certain distance $l/2$ from the center-of-mass of particle 2. Considering a sphere of radius $l/2$ of volume V_l, the (given) volume fraction can be expressed in the form $\phi = N_l V_p / V_l$, with V_p the volume of a single particle and N_l the number (including fractions) of particles contained in the sphere volume V_l. Using $V_p/V_l = (d/l)^3$, one obtains $N_l = \phi \, (l/d)^3$, and thus the number of neighboring particles is given by $p = N_l - 1$,

$$p = \phi \left(\frac{l}{d} \right)^3 - 1 \ .$$

(A.26)

Combining the particle number density (A.25) with the average number of neighboring particles (A.26), the average number density of particle pairs becomes

$$n = \frac{3}{\pi} \frac{\phi}{d^3} \left(\phi \left(\frac{l}{d} \right)^3 - 1 \right) \ ,$$

(A.27)

which is complete once a choice for the length l has been made.

Knowing the number density of particle pairs, n, we are able to calculate the value of spring constant k, as follows. As it was discussed in Sec. 2.3.1, the spring constant depends on the connectivity, and thus on n. Let us consider the stress tensor at equilibrium. For

simplicity, only the glassy-bridge contribution to the stress tensor is considered, and since the force on each particle in mechanical equilibrium vanishes, one obtains

$$\sigma_{\alpha\beta,\mathrm{eq}} = \int_{\mathcal{Q}^2} p \left[R_\alpha \left(\nabla_\beta^R \Phi(\boldsymbol{\xi}) \right) \right]^{\mathrm{sym}} \mathrm{d}^6 \boldsymbol{\xi} \bigg|_{\mathrm{eq}} \equiv 0. \tag{A.28}$$

Perturbing the equilibrium position $\boldsymbol{R}$ by a small amount $\delta\boldsymbol{R}$, the first order change in the stress tensor takes the form

$$\delta\,\sigma_{\alpha\beta} = \int_{\mathcal{Q}^2} p \left[R_\alpha \left(\nabla_\mu^R \nabla_\beta^R \Phi(\boldsymbol{\xi}) \right)_{\mathrm{eq}} \delta R_\mu \right]^{\mathrm{sym}} \mathrm{d}^6 \boldsymbol{\xi} \bigg|_{\mathrm{eq}}. \tag{A.29}$$

Using a (shear) perturbation of the form $\delta\boldsymbol{R} = \boldsymbol{\epsilon} \cdot \boldsymbol{R}$ with $\boldsymbol{\epsilon}$ the linear strain tensor, and in view of the form (2.38) of the potential Φ, (A.29) becomes

$$\delta\,\sigma_{\alpha\beta} = \frac{k\,n}{3} \langle |\boldsymbol{R}|^2 \rangle_{\mathrm{eq}} \epsilon_{\alpha\beta}. \tag{A.30}$$

where we have used the split (2.9), and $\langle R_\alpha R_\nu \rangle_{\mathrm{eq}} = (1/3)\langle |\boldsymbol{R}|^2 \rangle_{\mathrm{eq}} \delta_{\alpha\nu}$. Relation (A.30) can be set equal to $\delta\,\sigma_{\alpha\beta} = G_{\mathrm{comp}}\,\epsilon_{\alpha\beta}$, with G_{comp} strictly speaking the shear modulus of the glassy-bridge network. However, since the modulus of the "underlying" matrix material in the rubbery state is much smaller than that of the glassy material [48], one may approximate the modulus of the glassy-bridge network by that of the entire composite. One thus obtains the following relation for the spring constant,

$$k = \frac{3\,G_{\mathrm{comp}}}{n\langle |\boldsymbol{R}|^2 \rangle_{\mathrm{eq}}} = \frac{\pi d}{\sqrt[3]{\phi} \left(\phi \left(\frac{l}{d} \right)^3 - 1 \right)}\,G_{\mathrm{comp}}\,, \tag{A.31}$$

where in the second equality the relation (A.27) and the estimate $\langle |\boldsymbol{R}|^2 \rangle_{\mathrm{eq}} \simeq d^2/\phi^{2/3}$ for the square of the average neighbour distance has been used. For the case that two particles are called neighbors if their surface-to-surface distance is smaller than $d/2$ (meaning $l/2 = d$), one obtains

$$k = \frac{\pi d}{\sqrt[3]{\phi}\,(8\phi - 1)}\,G_{\mathrm{comp}}\,. \tag{A.32}$$

Bibliography

[1] T. A. Vilgis, G. Heinrich, and M. Klüppel. *Reinforcement of Polymer Nano-Composites: Theory, Experiments, and Applications*. Cambridge University Press, Cambridge, 2009.

[2] A. R. Payne. The dynamic properties of carbon black-loaded natural rubber vulcanizates – Part 1. *J. Appl. Polym. Sci.*, 6(19):57–63, 1962.

[3] L. Mullins. Effect of stretching on the properties of rubber. *J. Rubber Res.*, 16:275–282, 1948.

[4] L. Mullins. Softening of rubber by deformation. *Rubber Chem. Technol.*, 42:339–362, 1969.

[5] J. Diani, B. Fayolle, and P. Gilormini. A review on the Mullins effect. *Eur. Polym. J.*, 45(3):601–612, 2009.

[6] S. Cantournet, R. Desmorat, and J. Besson. Mullins effect and cyclic stress softening of filled elastomers by internal sliding and friction thermodynamics model. *Int. J. Solids Struct.*, 46(11-12):2255–2264, 2009.

[7] M. Semkiv, D. R. Long, and M. Hütter. Concurrent two-scale model for the viscoelastic behavior of elastomers filled with hard nanoparticles. *Continuum Mech. Thermodyn.*, 2016. in press.

[8] S. Kaufman, W. P. Slichter, and D. D. Davis. Nuclear magnetic resonance study of rubber-carbon black interactions. *J. Polym. Sci. A2*, 9(5):829–839, 1971.

[9] J. Berriot, H. Montès, F. Lequeux, D. R. Long, and P. Sotta. Evidence for the shift of the glass transition near the particles in silica-filled elastomers. *Macromolecules*, 35(26):9756–9762, 2002.

[10] J. Berriot, H. Montès, F. Lequeux, D. R. Long, and P. Sotta. Gradient of glass transition temperature in filled elastomers. *Eur. Phys. Lett.*, 64(1):50–56, 2003.

[11] M. C. Boyce, D. M. Parks, and A. S. Argon. Large inelastic deformation of glassy polymers. Part 1: Rate dependent constitutive model. *Mech. Mater.*, 7(1):15–33, 1988.

[12] R. B. Dupaix and M. C. Boyce. Constitutive modeling of the finite strain behavior of amorphous polymers in and above the glass transition. *Mech. Mater.*, 39(1):39–52, 2007.

[13] H. E. H. Meijer and L. E. Govaert. Mechanical performance of polymer systems: the relation between structure and properties. *Prog. Polym. Sci.*, 30(89):915–938, 2005.

[14] D. V. Guseva, P. V. Komarov, and A. V. Lyulin. Molecular-dynamics simulations of thin polyisoprene films confined between amorphous silica substrates. *J. Chem. Phys.*, 140(11):114903, 2014.

[15] C. Batistakis, M. A. J. Michels, and A. V. Lyulin. Confinement-induced stiffening of thin elastomer films: Linear and nonlinear mechanics vs. local dynamics. *Macromolecules*, 47(14):4690–4703, 2014.

[16] D. R. Long and P. Sotta. Nonlinear and plastic behavior of soft thermoplastic and filled elastomers studied by dissipative particle dynamics. *Macromolecules*, 39(18):6282–6297, 2006.

[17] S. Merabia, P. Sotta, and D. R. Long. A microscopic model for the reinforcement and the nonlinear behavior of filled elastomers and thermoplastic elastomers (Payne and Mullins effects). *Macromolecules*, 41(21):8252–8266, 2008.

[18] S. Merabia, P. Sotta, and D. R. Long. Unique plastic and recovery behavior of nanofilled elastomers and thermoplastic elastomers (Payne and Mullins effects). *J. Polym. Sci. Pol. Phys.*, 48(13):1495–1508, 2010.

[19] A. Papon, S. Merabia, L. Guy, F. Lequeux, H. Montès, P. Sotta, and D. R. Long. Unique nonlinear behavior of nano-filled elastomers: From the onset of strain softening to large amplitude shear deformations. *Macromolecules*, 45(6):2891–2904, 2012.

[20] R. J. M. Smit, W. A. M. Brekelmans, and H. E. H. Meijer. Prediction of the mechanical behavior of nonlinear heterogeneous systems by multi-level finite element modeling. *Comput. Method Appl. Mech. Eng.*, 155(1-2):181–192, 1998.

[21] R. J. M. Smit, W. A. M. Brekelmans, and H. E. H. Meijer. Prediction of the large-strain mechanical response of heterogeneous polymer systems: Local and global deformation behaviour of a representative volume element of voided polycarbonate. *J. Mech. Phys. Solids*, 47(2):201–221, 1999.

[22] R. J. M. Smit, W. A. M. Brekelmans, and H. E. H. Meijer. Predictive modelling of the properties and toughness of polymeric materials - Part II - Effect of microstructural properties on the macroscopic response of rubber-modified polymers. *J. Mater. Sci.*, 35(11):2869–2879, 2000.

[23] R. J. M. Smit, W. A. M. Brekelmans, and H. E. H. Meijer. Predictive modelling of the properties and toughness of polymeric materials - Part III - Simultaneous prediction of micro- and macrostructural deformation of rubber-modified polymers. *J. Mater. Sci.*, 35(11):2881–2892, 2000.

[24] T. A. Witten, M. Rubinstein, and R. H. Colby. Reinforcement of rubber by fractal aggregates. *J. Phys. II*, 3(3):367–383, 1993.

[25] G. Heinrich and M. Klüppel. *Recent Advances in the Theory of Filler Networking in Elastomers*. Springer, Berlin, 2002.

[26] M. Klüppel. *The Role of Disorder in Filler Reinforcement of Elastomers on Various Length Scales*. Springer, Berlin, 2003.

[27] M. Grmela and H. C. Öttinger. Dynamics and thermodynamics of complex fluids. I. Development of a general formalism. *Phys. Rev. E*, 56(6):6620–6632, 1997.

[28] H. C. Öttinger and M. Grmela. Dynamics and thermodynamics of complex fluids. II. Illustrations of a general formalism. *Phys. Rev. E*, 56(6):6633–6655, 1997.

[29] H. C. Öttinger. *Beyond Equilibrium Thermodynamics*. Wiley, Hobroken, 2005.

[30] L. R. G. Treloar. *The Physics of Rubber Elasticity*. Clarendon, Oxford, 3rd edition, 1975.

[31] C. Truesdell and W. Noll. *The Non-Linear Field Theories of Mechanics*. Springer, Berlin, 3rd edition, 2004.

[32] M. Hütter and T. A. Tervoort. Finite anisotropic elasticity and material frame indifference from a nonequilibrium thermodynamics perspective. *J. Non-Newtonian Fluid Mech.*, 152(1-3):45–52, 2008.

[33] G. G. Vogiatzis, E. Voyiatzis, and D. N. Theodorou. Monte Carlo simulations of a coarse grained model for an athermal all-polystyrene nanocomposite system. *Eur. Polym. J.*, 47(4):699–712, 2011.

[34] M. Hütter and T. A. Tervoort. Thermodynamic considerations on non-isothermal finite anisotropic elasto-viscoplasticity. *J. Non-Newtonian Fluid Mech.*, 152(1-3):53–65, 2008.

[35] H. C. Öttinger. Nonequilibrium thermodynamics for open systems. *Phys. Rev. E*, 73(3):036126, 2006.

[36] H. C. Öttinger. Bracket formulation of nonequilibrium thermodynamics for systems interacting with the environment. *J. Non-Newtonian Fluid Mech.*, 152(1):2–11, 2008.

[37] E. H. Lee. Elasticplastic deformation at finite strains. *J. Appl. Mech.*, 36(1):1–6, 1969.

[38] R. B. Bird, C. F. Curtiss, R. C. Armstrong, and O. Hassager. *Dynamics of Polymeric Liquids, volume 2: Kinetic Theory*. Wiley, New York, 2nd edition, 1987.

[39] H. C. Öttinger. *Stochastic Processes in Polymeric Fluids*. Springer, Berlin, 1996.

[40] M. Hütter and B. Svendsen. On the formulation of continuum thermodynamic models for solids as General Equations for Non-Equilibrium Reversible-Irreversible Coupling. *J. Elast.*, 104:357–368, 2011.

[41] B. J. Edwards. An analysis of single and double generator thermodynamic formalisms for the macroscopic description of complex fluids. *J. Non-Equilib. Thermodyn.*, 23(4):301–333, 1998.

[42] S. R. de Groot and P. Mazur. *Non-equilibrium Thermodynamics*. North Holland, Amsterdam, 1962.

[43] M. Hütter and B. Svendsen. Quasi-linear versus potential-based formulations of force-flux relations and the GENERIC for irreversible processes: Comparisons and examples. *Continuum. Mech. Therm.*, 25(6):803–816, 2013.

[44] R. J. Gordon and W. R. Schowalter. Anisotropic fluid theory - Different approach to dumbbell theory of dilute polymer-solutions. *Trans. Soc. Rheol.*, 16(1):79–97, 1972.

[45] L. F. Rossi, G. McKinley, and L. P. Cook. Slippage and migration in Taylor-Couette flow of a model for dilute wormlike micellar solutions. *J. Non-Newton. Fluid. Mech.*, 136(2-3):79–92, 2006.

[46] E. T. J. Klompen, T. A. P. Engels, L. E. Govaert, and H. E. H. Meijer. Modelling of the post-yield response of glassy polymers: Influence of thermomechanical history. *Macromolecules*, 38(16):6997–7008, 2005.

[47] T. A. P. Engels, L. E. Govaert, and H. E. H. Meijer. 2.29 - mechanical characterization of glassy polymers: Quantitative prediction of their short- and long-term responses. In *Polymer Science: A Comprehensive Reference*, pages 723 – 747. Elsevier, Amsterdam, 2012.

[48] D. W. Van Krevelen and K. Te Nijenhuis. *Properties of Polymers*. Elsevier, Amsterdam, 4th edition, 2009.

[49] E. M. Lifshitz and L. Pitaevskii. *Landau and Lifshitz: Course of Theoretical Physics, Vol. 5: Statistical Physics I*. Pergamon, Oxford, 3rd edition, 1980.

[50] M. Le Bellac, F. Mortessagne, and G. G. Batrouni. *Equilibrium and Non-Equilibrium Statistical Thermodynamics*. Cambridge University Press, Cambridge, 2004.

[51] R. W. Ogden. *Nonlinear Elastic Deformations*. Dover, Mineola (N.Y.), 1997.

[52] H. J. Kreuzer. *Nonequilibrium Thermodynamics and Its Statistical Foundations*. Clarendon Press, Oxford, 1981.

[53] D. J. Evans and G. P. Morriss. *Statistical Mechanics of Nonequilibrium Liquids*. Academic Press, London, 1990.

[54] J. H. Irving and J. G. Kirkwood. The statistical mechanical theory of transport processes. IV. The equations of hydrodynamics. *J. Chem. Phys.*, 18(6):817–829, 1950.

[55] D. R. Long and F. Lequeux. Heterogeneous dynamics at the glass transition in van der waals liquids, in the bulk and in thin films. *Eur. Phys. J. E*, 4(3):371–387, 2001.

[56] A. Dequidt, D. R. Long, P. Sotta, and O. Sanseau. Mechanical properties of thin confined polymer films close to the glass transition in the linear regime of deformation: Theory and simulations. *Eur. Phys. J. E*, 35(7):61, 2012.

[57] A. Papon, K. Saalwächter, K. Schäler, L. Guy, F. Lequeux, and H. Montès. Low-field NMR investigations of nanocomposites: Polymer dynamics and network effects. *Macromolecules*, 44(4):913–922, 2011.

[58] A. Papon, H. Montès, M. Hanafi, F. Lequeux, L. Guy, and K. Saalwächter. Glass-transition temperature gradient in nanocomposites: Evidence from nuclear magnetic resonance and differential scanning calorimetry. *Phys. Rev. Lett.*, 108(6):065702, 2012.

[59] A. Papon, H. Montès, F. Lequeux, J. Oberdisse, K. Saalwächter, and L. Guy. Solid particles in an elastomer matrix: Impact of colloid dispersion and polymer mobility modification on the mechanical properties. *Soft Matter*, 8(15):4090–4096, 2012.

[60] I. M. Ward. *Mechanical Properties of Solid Polymers*. Wiley, Chichester, 2nd edition, 1990.

[61] A. S. Krausz and H. Eyring. *Deformation Kinetics*. Wiley-Interscience, London, 1975.

[62] R. von Mises. Mechanik der festen Körper im plastisch deformablen Zustand. *Nachr. Kgl. Ges. Wiss. Göttingen Math.-phys. Klasse*, 1:582–592, 1913.

[63] R. Hill. A theory of the yielding and plastic flow of anisotropic materials. *Proc. R. Soc. Lond. Ser. A*, A195:281–297, 1948.

[64] T. A. Tervoort, E. T. J. Klompen, and L. E. Govaert. A multi-mode approach to finite, three-dimensional, nonlinear viscoelastic behavior of polymer glasses. *J. Rheol.*, 40(5):779797, 1996.

[65] K. S. Cho, K. Hyun, K. H. Ahn, and S. J. Lee. A geometrical interpretation of large amplitude oscillatory shear response. *J. Rheol.*, 49(3):747–758, 2005.

[66] R. H. Ewoldt, A. E. Hosoi, and G. H. McKinley. New measures for characterizing nonlinear viscoelasticity in large amplitude oscillatory shear. *J. Rheol.*, 52(6):1427–1458, 2008.

[67] K. Hyun, M. Wilhelm, C. O. Klein, K. S. Cho, J. G. Nam, K. H. Ahn, S. J. Lee, R. H. Ewoldt, and G. H. McKinley. A review of nonlinear oscillatory shear tests: Analysis and application of large amplitude oscillatory shear (LAOS). *Prog. Polym. Sci.*, 36(12):1697–1753, 2011.

[68] L. C. E. Struik. Physical aging in amorphous glassy polymers. *Ann. NY Acad. Sci.*, 279:78–85, 1976.

[69] J. M. Hutchinson. Physical aging of polymers. *Prog. Polym. Sci.*, 20(4):703–760, 1995.

[70] C. G'Sell and G. B. McKenna. Influence of physical ageing on the yield response of model DGEBA/poly(propylene oxide) epoxy glasses. *Polymer*, 33(10):2103–2113, 1992.

[71] O. A. Hasan and M. C. Boyce. Energy-storage during inelastic deformation of glassy polymers. *Polymer*, 34(24):5085–5092, 1993.

[72] L. C. E. Struik. On the rejuvenation of physically aged polymers by mechanical deformation. *Polymer*, 38:4053–4057, 1997.

[73] O. A. Hasan and M. C. Boyce. A constitutive model for the nonlinear viscoelastic viscoplastic behavior of glassy polymers. *Polym. Eng. Sci.*, 35(4):331–344, 1995.

[74] A. Q. Tool. Relaxation of stresses in annealing glass. *J. Res. Natl. Bur. Stand.(US)*, 34:199–211, 1945.

[75] C. P. Buckley, P. J. Dooling, J. Harding, and C. Ruiz. Deformation of thermosetting resins at impact rates of strain. Part 2: Constitutive model with rejuvenation. *J. Mech. Phys. Solids*, 52(10):2355–2377, 2004.

[76] T. D. Nguyen, H. J. Qi, F. Castro, and K. N. Long. A thermoviscoelastic model for amorphous shape memory polymers: Incorporating structural and stress relaxation. *J. Mech. Phys. Solids*, 56(9):2792–2814, 2008.

[77] E. Bouchbinder and J. S. Langer. Nonequilibrium thermodynamics of driven amorphous materials. II. Effective-temperature theory. *Phys. Rev. E*, 80(3):031132, 2009.

[78] T. D. Nguyen, C. M. Yakacki, P. D. Brahmbhatt, and M. L. Chambers. Modeling the relaxation mechanisms of amorphous shape memory polymers. *Adv. Mater.*, 22(31):3411–3423, 2010.

[79] K. Kamrin and E. Bouchbinder. Two-temperature continuum thermomechanics of deforming amorphous solids. *J. Mech. Phys. Solids*, 73:269–288, 2014.

[80] R. Xiao and T. D. Nguyen. An effective temperature theory for the nonequilibrium behavior of amorphous polymers. *J. Mech. Phys. Solids*, 82:62–81, 2015.

[81] T. M. Nieuwenhuizen. Thermodynamic description of a dynamical glassy transition. *J. Phys. A-Math. Gen.*, 31:L201–L207, 1998.

[82] T. M. Nieuwenhuizen. Thermodynamics of the glassy state: Effective temperature as an additional system parameter. *Phys. Rev. Lett.*, 80(25):5580–5583, 1998.

[83] T. M. Nieuwenhuizen. Formulation of thermodynamics for the glassy state: configurational energy as a modest source of energy. *J. Chem. Phys.*, 115(17):8083–8088, 2001.

[84] L. F. Cugliandolo, J. Kurchan, and L. Peliti. Energy flow, partial equilibration, and effective temperatures in systems with slow dynamics. *Phys. Rev. E*, 55(4):3898–3914, 1997.

[85] F. Sciortino, W. Kob, and P. Tartaglia. Inherent structure entropy of supercooled liquids. *Phys. Rev. Lett.*, 83:3214–3217, 1999.

[86] L. Berthier, J. L. Barrat, and J. Kurchan. A two-time-scale, two-temperature scenario for nonlinear rheology. *Phys. Rev. E*, 61(5B):5464–5472, 2000.

[87] H. C. Öttinger. Nonequilibrium thermodynamics of glasses. *Phys. Rev. E*, 74:011113, 2006.

[88] L. Leuzzi. A stroll among effective temperatures in aging systems: Limits and perspectives. *J. Non-Cryst. Solids*, 355(10-12):686–693, 2009.

[89] M. Utz, P. G. Debenedetti, and F. H. Stillinger. Atomistic simulation of aging and rejuvenation in glasses. *Phys. Rev. Lett.*, 84:1471–1474, 2000.

[90] T. A. P. Engels, L. E. Govaert, G. W. M. Peters, and H. E. H. Meijer. Processing-induced properties in glassy polymers: Application of structural relaxation to yield stress development. *J. Polym. Sci. Pol. Phys.*, 44(8):1212–1225, 2006.

[91] M. Hütter and T. A. Tervoort. Coarse graining in elasto-viscoplasticity: Bridging the gap from microscopic fluctuations to dissipation. *Adv. Appl. Mech.*, 42:253–317, 2008.

[92] I. Doghri. *Mechanics of Deformable Solids*. Springer, Berlin, 2000.

[93] M. Hütter and T. A. Tervoort. Statistical-mechanics based modeling of anisotropic viscoplastic deformation. *Mech. Mater.*, 80:37–51, 2015.

[94] R. B. Bird, R. C. Armstrong, and O. Hassager. *Dynamics of Polymeric Liquids*, volume 1. Wiley, New York, 1987.

[95] C. A. Angell. In K. Ngai and G. B. Wright, editors, *Relaxations in Complex Systems*, pages 1–11. National Technical Information Service, US Department of Commerce, Springfield, VA, 1985.

[96] C. A. Angell. Relaxation in liquids, polymers and plastic crystals - strong/fragile patterns and problems. *J. Non-Cryst. Solids*, 131–133:13–31, 1991.

[97] M. Semkiv and M. Hütter. Modeling aging and mechanical rejuvenation of amorphous solids. *J. Non-Equilib. Thermodyn.*, 41(2):7988, 2016.

[98] H. C. Öttinger. Modeling complex fluids with a tensor and a scalar as structural variables. *Rev. Mex. Fís.*, 48 Suppl. 1:220–229, 2002.

[99] I. Kolvin and E. Bouchbinder. Simple nonlinear equation for structural relaxation in glasses. *Phys. Rev. E*, 86:010501(R), 2012.

[100] A. N. Beris and B. J. Edwards. *Thermodynamics of Flowing Systems: with Internal Microstructure*. Oxford University Press, New York, 1994.

[101] L. Mullins. Permanent set in vulcanized rubber. *India Rubber World*, 120:63–66, 1949.

[102] M. Semkiv, P. D. Anderson, and M. Hütter. Two-subsystem thermodynamics for the mechanics of aging amorphous solids. *Continuum Mech. Thermodyn.*, 2016. paper is submitted.

[103] J. W. Gibbs. *On the Fundamental Formula of Statistical Mechanics, with Applications to Astronomy and Thermodynamics*. Salem Press, 1885.

[104] H. J. Kreuzer. *Nonequilibrium Thermodynamics and its Statistical Foundations*. Clarendon Press, Oxford, 1981.

[105] D. J. Evans and G. P. Morriss. *Statistical Mechanics of Nonequilibrium Liquids*. Academic Press, London, 1990.

[106] G. Adam and J. H. Gibbs. On the temperature dependence of cooperative relaxation properties in glass-forming liquids. *J. Chem. Phys.*, 43:139–146, 1965.

[107] I. M. Hodge. Effects of annealing and prior history on enthalpy relaxation in glassy polymers. 6. Adam-Gibbs formulation of nonlinearity. *Macromolecules*, 20(11):2897–2908, 1987.

[108] J. D. Ferry. *Viscoelastic Properties of Polymers*. John Wiley and Sons, 1980.

[109] M. Laso and H. C. Öttinger. Calculation of viscoelastic flow using molecular models: the CONNFFESSIT approach. *J. Non-Newtonian Fluid Mech.*, 47:1–20, 1993.

[110] C. W. Macosko. *Rheology: Principles, Measurements, and Applications*. VCH, 1994.

[111] M. Hütter, T. J. Faber, and H. M. Wyss. Kinetic model for the mechanical response of suspensions of sponge-like particles. *Faraday Discuss.*, 158:407–424, 2012.

[112] M. Kröger and M. Hütter. Automated symbolic calculations in nonequilibrium thermodynamics. *Comput. Phys. Commun.*, 181(12):2149–2157, 2010.

[113] M. Mayorga, L. Romero-Salazar, and J. M. Rubi. Stochastic model for the dynamics of interacting brownian particles. *Physica A*, 307(3-4):297–314, 2002.

[114] D. C. Wallace. On the role of density fluctuations in the entropy of a fluid. *J. Chem. Phys.*, 87(4):2282–2284, 1987.

[115] A. Baranyai and D. J. Evans. Direct entropy calculation from computer simulation of liquids. *Phys. Rev. A*, 40(7):3817–3822, 1989.

[116] B. B. Laird and A. D. J. Haymet. Calculation of the entropy from multiparticle correlation-functions. *Phys. Rev. A*, 45(8):5680–5689, 1992.

[117] L. Romero-Salazar, M. Mayorga, and R. M. Velasco. Maximum entropy formalism for a dense gas. *Physica A*, 237:150–168, 1997.

[118] M. Mayorga, L. Romero-Salazar, and R. M. Velasco. Entropy balance equation for a dense gas. *Physica A*, 237:169–188, 1997.

[119] T. D. Frank. *Nonlinear Fokker-Planck Equations*. Springer Series in Synergetics. Springer, Berlin, 2005.

Samenvatting voor algemeen publiek

Tweeschalige modellering van gevulde - elastomeermechanica

In de productie van banden worden harde nanodeeltjes verspreid in een elastomeermatrix ter verbetering van de mechanische eigenschappen van de band. Door de aanwezigheid van de vullerdeeltjes vertoont de resulterende nanocomposiet gedrag dat onbekend is voor het ongevuld elastomeer, namelijk het prominente Payne effect (een significante afname van de elasticiteitsmodulus onder oscillerende afschuiving met grote amplitude), het Mullins effect (na het stoppen van een grote opgelegde deformatie, neemt de elasticiteitsmodulus weer toe met de wachttijd), en een significant toegenomen breukenergie. Deze fenomenen vinden hun oorsprong in het bestaan van geïmmobiliseerd matrixmateriaal rondom de vullerdeeltjes, i.e. zogenaamde glasachtige lagen, zoals ondersteund wordt door experimentele (bijv. Nuclear Magnetic Resonance) en numerieke (Molecular Dynamics en Monte Carlo simulaties) studies. In het bijzonder kunnen de glasachtige lagen van verschillende deeltjes overlappen voor een voldoende hoge volumefractie van de vullerdeeltjes, wat resulteert in zogenaamde glasachtige bruggen en daarmee in de formatie van een glasachtig netwerk. Dit netwerk strekt zich uit over de rubberachtige matrix en leidt uiteindelijk tot nanocomposiet-specifiek mechanisch gedrag. Verscheidene modelleerbenaderingen in de literatuur berusten grotendeels op representatieve volume-elementen met grote aantallen deeltjes, wat deze benaderingen buitensporig duur maakt voor macroscopisch inhomogene deformaties. Ter verlichting van dit probleem is het doel van deze thesis:

"Formulering van een zeer efficiënt tweeschalig model dat het transiënt niet-lineair mechanisch gedrag van silica-gevulde elastomeren effectief beschrijft in termen van microstructuren processen".

Ter formulering van een dynamisch model dat twee niveaus van beschrijving in rekening brengt, evenals de wederzijdse koppeling ertussen, is er een abstracte procedure nodig. In deze thesis wordt niet-evenwichtsthermodynamica gebruikt voor dat doeleinde, in het bijzonder het "General Equation for the Non-Equilibrium Reversible-Irreversible Coupling (GENERIC)" framework. Dit resulteert in een set evolutievergelijkingen die de macroscopische vrijheidsgraden (de impulsdichtheid, de temperatuur of de entropie, en de deformatiegradiënt) koppelen aan de evolutie van de microstructuur. Dat laatste wordt vertegenwoordigd door slechts één representatief (naburig) deeltjespaar, aangezien de meest essentiële bijdrage van de dynamica op deeltjesniveau aan de macroscopische respons haar oorsprong vindt in de interactie van naburige deeltjes. De voornaamste vo-

ordelen van het gebruik van het GENERIC framework zijn de formulering van het effect van de macroscopische deformatie op de dynamica van de microstructuur (macro → micro koppeling), evenals de specificatie van de constitutieve relatie voor de macroscopische spanningstensor die beïnvloed wordt door de rangschikking van de vullerdeeltjes (micro → macro koppeling).

Hoewel het bovengenoemd model voor het beschrijven van het niet-lineair visco-elastisch materiaalgedrag goed werkt gedurende relatief korte tijdsperiodes, heeft het echter beperkte validiteit gedurende lange tijdsperiodes. Dit komt doordat het matrixmateriaal rondom de vullerdeeltjes, die in een glasachtige staat zijn, fysieke veroudering vertoont in de tijd, wat resulteert in een toenemende waarde van de elasticiteitsmodulus en uiteindelijk het Mullins effect. Voordat de fysieke veroudering van de glasachtige bruggen in rekening gebracht wordt in het tweeschalig model, wordt eerst de veroudering van glasachtige polymeren bestudeerd vanuit het perspectief van niet-evenwichtsthermodynamica. Voor dat doeleinde wordt het concept van kinetische en configuratie subsystemen uit de literatuur toegepast en uitgebreid, wat het beschrijven van relaxatie/equilibratie van verschillende structurele eigenschappen op verschillende tijdschalen mogelijk maakt. Op deze manier worden zowel fysieke veroudering als mechanische verjonging beschreven. Daarnaast wordt er gevonden dat de spanningstensor in dit soort systemen van hypo- in plaats van hyperelastische aard is. Na het bestuderen van de fysieke veroudering van glasachtige polymeren wordt het tweeschalig nanocomposietmodel uitgebreid om de fysieke veroudering van de glasachtige bruggen in rekening te brengen.

Tenslotte wordt de microschaalcomponent (deeltjesniveau) van het tweeschalig nanocomposietmodel vertaald van een Fokker-Planck vergelijking naar stochastische differentiaalvergelijkingen, en daarna geïmplementeerd in een Brownian Dynamics type simulatieschema. Onder een opgelegde oscillerende afschuiving met grote amplitude wordt de niet-lineariteit van het visco-elastisch mechanisch gedrag numeriek beschouwd. In het bijzonder wordt er gevonden dat (i) het voorgesteld tweeschalig model de bekende Payne en Mullins effecten vertoont, en dat (ii) het 'representatief-paar' concept een adequate representatie is van het systeem met grote aantallen deeltjes bij kleine en gematigde deformatieamplitudes.

Ter conclusie kunnen de voornaamste prestaties van deze PhD studie als volgt samengevat worden:

- Een zeer efficiënt en thermodynamisch kloppend tweeschalig model is ontwikkeld voor het beschrijven van het niet-lineair visco-elastisch gedrag van elastomeren die gevuld zijn met harde nanodeeltjes, die leiden tot de bekende Payne en Mullins effecten, die gebaseerd zijn op microscopische principes.

- Vergelijking met simulaties met grote aantallen deeltjes in de literatuur toont dat het 'representatief-paar' concept dat ontwikkeld is in deze thesis een adequate vereenvoudiging vertegenwoordigd, met name voor kleine en gematigde rek.

- Het voordeel van het gebruik van het voorgesteld 'representatief-paar' model in plaats van de tegenhanger met grote aantallen deeltjes ligt in de significante verlaging van de rekentijd met meerdere ordegroottes. Dit maakt het 'representatief-paar'

model geschikt voor berekeningen die gebaseerd zijn op RVE in macroscopisch in-homogene FEM-berekeningen.

Acknowledgments

With this thesis an important state in my life has been reached. Looking back at the past four years, an exciting, challenging and truly enjoyable period, many people have supported and helped me to reach this state. It is my pleasure to express my deepest appreciation and gratitude to all of them.

Particularly, I would like to gratefully thank dr. sc. nat. Markus Hütter, my daily supervisor, for teaching and inspiring me with very valuable opinions and bright ideas, which really helped me to grow not only professionally but also as a person. I remember our first meeting, it was an interview, where you introduced me the concept of nonequilibrium thermodynamics, and especially GENERIC. After this meeting, on the way back to a hotel I thought: "...it is a great concept, very similar to Lagrangian and Hamiltonian mechanics; I will continue analytical work...", but I did not understand yet its power and beauty. During the past four years I have learned from you how to be persistent in order to be an independent academic researcher.

I would like to thank my promoter, prof. dr. ir. Patrick Anderson for his support and guidance, especially during my thesis preparation. We started to work together almost two years ago. During this period, I have truly enjoyed our mathematical discussions. It is a pleasure to work with you.

I would also like to gratefully acknowledge prof. Didier Long, dr. ir. Tom Engels, prof. dr. Hans Christian Öttinger and prof. Jay D. Schieber for their stimulating discussions, crucial ideas and suggestions.

My special gratitude to my room mates and all friends from the Polymer Technology Group. In particular, our Fruit-Times, RPK-courses, and other activities have been wonderful. I would also like to thank all my Ukrainian friends for creating the nice Ukrainian atmosphere here in The Netherlands.

I wish to extend my deep thanks to my parents for their constant support and believing in me. I am also grateful to my sister Sophia and brother Volodymyr, who truly love me.

Finally, last but not least, I want to express my gratitude to my lovely Natalia. Thank you very much for listening to my presentations, reading the manuscripts, as well as for all your support, trust and patience.

Mykhailo Semkiv
Eindhoven, July, 2016

Curriculum Vitae

Mykhailo Semkiv was born on 22nd of October 1985 in Velyka-Turia, Ivano-Frankivsk region, Ukraine. After graduating from high school, in September 2003 he started his university education in the department of Mechanics and Mathematics at National Taras Shevchenko University of Kyiv, Ukraine. In June 2007, he defended his bachelor thesis in Mechanics entitled "Detecting the source of earthquakes by a standard grid method" in the group of Theoretical and Applied Mechanics, headed by Prof. V. Meleshko. He continued his education in the same group as a master student, and in 2009 he defended the master thesis "Dynamic crack propagation along material interfaces". From 2009 till 2012, he had been working on "Diffraction of elastic waves on local inhomogeneity in a waveguide" in the group of Theoretical and Applied Mechanics, and received the degree of Candidate of Science. Being interested in non-equilibrium thermodynamics and elasto-viscoplasticity, in June 2012 he started his PhD studies at the Eindhoven University of Technology, where under the supervision of dr. sc. nat. M. Hütter and prof. dr. ir. P.D. Anderson, he has been working on the analytical and numerical modeling of the mechanical behavior of elastomers filled with hard nanoparticles. The results of this research are presented in this dissertation.